A SAILWING VERTICAL AXIS WIND TURBINE FOR SMALL SCALE APPLICATIONS

Philip Scott Revell

A thesis submitted for the degree of Ph.D.
at the University of Warwick

Dept. of Engineering Science March 1983

CONTENTS

page no.

page no.

****

LIST OF ILLUSTRATIONS AND TABLES

following page no.

following page no.

following page no.

NOMENCLATURE

a Slope C_L/α_{eff} prior to stall

a_o Slope C_L/α prior to stall

A Turbine swept area

A_B Blade plan area

A_i Cross-sectional area of inertia pipe

A_p Piston area of reciprocating pump

AR Aspect ratio of aerofoil = b/c

b Length of aerofoil blade

c Blade chord or strut chord

C_D Drag coefficient = Drag force/$\frac{1}{2}\rho A_B V_R^2$

C_F' Thrust coefficient = Retarding force on airstream/$\frac{1}{2}\rho A V^2$

C_L Lift coefficient = Lift force/$\frac{1}{2}\rho A_B V_R^2$

C_{id} Induced drag coefficient = $C_L^2/\pi AR$

C_P Power coefficient = $P/\frac{1}{2}\rho A V_w^3$

C_P' Power coefficient = $P/\frac{1}{2}\rho A V^3$

C_{P_T} Membrane tension coefficient = $P_T/\frac{1}{2}\rho V_R^2 c$

C_Q Torque coefficient = Turbine torque/$\frac{1}{2}\rho A V_w^2 R$

C_R Radial force coefficient = $C_L\cos\alpha + C_D\sin\alpha$

C_S' Mean torque coefficient = $\frac{1}{2\pi}\int_0^{2\pi} C_T q^2 \, d\theta$

C_T Tangential force coefficient = $C_L\sin\alpha - C_D\cos\alpha$

$(C_T q^2)$ Instantaneous torque coefficient for a blade = $T/\frac{1}{2}\rho A_B V^2 R$

C_{T_T} Trailing edge tension coefficient = $T_T/\frac{1}{2}\rho A_B V_R^2$

C_x Induced tension coefficient

= chordwise component of tension induced/$\frac{1}{2}\rho V_R^2 c$

d Diameter of leading edge

dD Elemental drag force

dL Elemental lift force

D_i Diameter of the inertia pipe

e Ratio: force per unit width/strain, for membrane or base of natural logs.

E_T Ratio: force/strain, for trailing edge line

f Frequency

F Retarding force on windstream

g Acceleration due to gravity

h_L Head loss

H Head of water

J Moment of inertia

k Constant = a/a_o

K non-dimensional head loss coefficient = $h_L / \frac{u^2}{2g}$

l Suspension length

L_i Length of inertia pipe

m Turbine mass

$\dot{m}$ Water mass flow rate

n Number of turbine blades

p Dynamic pressure or axis co-ordinate

P Power produced by turbine

P_T Membrane pre-tension per unit width

P_w Power in the wind

q Ratio: V_R/V

Q Volumetric water flow rate

r_B Blockage ratio in wind tunnel = $\frac{c \sin\alpha}{1.3 \text{ metres}}$

R Rotor radius

R_p Pump crank length

R_{ii} Auto-correlation function

R_s Suspension radius

Re Reynolds number = $\rho V_R c / \mu_{air}$ or $\bar{u} D_i / \nu$

T Torque

T_T Pre-tension in trailing edge

u Water flow velocity, or a length

v Fluctuating component of windspeed

V Induced windspeed

V_R Relative windspeed

V_w Free windspeed

ω A length

W Work done

x Maximum hollow in trailing edge curve

y Ratio: $z/R\tan\gamma$

z Vertical distance along turbine axis

α Angle of incidence of relative wind to blade chord

α_{eff} Effective angle of incidence, with finite apsect ratio

β Virtual pitch angle

γ Angle of inclination of turbine blade to the vertical, or piston angular position

δ Dimensionless speed

ε Blockage factor

η_{VOL} Volumetric efficiency

ϑ Azimuthal angle (blade angular position)

λ Piston angular postion

μ Tip speed ratio = $R\Omega/V_w$

μ' Tip speed ratio = $R\Omega/V$

μ_{air} Viscosity of air $\simeq 1.82.10^{-5}$ kg/ms

ν Virtual camber ratio or kinematic viscosity of water

ξ Dimensionless flow = $\eta_{VOL}\delta$

ρ Air density $\simeq 1.2$ kg/m^3

ρ_F Mass of membrane per unit area

ρ_w Water density $\simeq 10^3$ kg/m^3

σ Turbine solidity $=\Sigma A_B/2A$

τ Time interval

$\phi(\omega)$ Power spectral density

Ω Angular velocity

ω Frequency

SUMMARY

The use of sailwing aerofoils in vertical axis wind turbines has been investigated. It was anticipated that this could make vertical axis turbines more suitable for water pumping and that this might help to meet the need for a cheap pump for irrigation existing in many parts of the world.

A numerical analysis of the theoretical performance of such a turbine, using existing aerodynamic data for simply constructed sailwings, has been made. This gave an improved understanding of the operation of such turbines but showed a need for further aerodynamic data. Some new wind tunnel tests of sailwings are described in which the effect of pre-tension was investigated and four different fabrics were tested. The results are presented for angles of incidence up to 180 degrees and compared with previous data.

With the fresh data, new performance predictions were made which led to the design of a two metre diameter prototype turbine. This used an inclined blade configuration with a guyed top bearing. Canvas was used for the sails. It was predicted that the turbine performance would be significantly affected by windspeed.

The turbine was built and later tested in the open air. An acceleration test method was used and the tests generally confirmed the predictions. The averaged starting torque coefficient was about 0.07; the averaged peak power coefficient was about 0.1 at a tip speed ratio of 1.4.

Consideration has been given to improving windpump system efficiency by improving the gust energy utilisation. Some tests of a diaphragm pump are described in which inertia flow effects were used. A pair of such pumps were later connected to the prototype turbine. A number of problems were encountered and satisfactory operation was not achieved in the time available. The main problem was the cyclic driving torque produced by the three bladed turbine.

INTRODUCTION

This thesis is the result of some research into the potential for using sailwing aerofoils in vertical axis wind turbines. It was anticipated that such a turbine could be suited to low lift water pumping, particularly for irrigation, in Third World countries.

There would not seem to be any doubt about the considerable potential of renewable energy technologies in meeting the energy needs of development. The people of the Third World, in fact, already meet the majority of their energy needs from solar energy and, when wood, food, crop residues etc. are included, the energy use is much higher than might be supposed. However, as shown by Makhijani (1976), the efficiency of energy usage is generally very low and it is probably by increasing the efficiency of energy use that some of the most pressing energy needs of the poor may best be met in a short time.

Basic in an increase in the energy use efficiency, is an increase in the productivity of agriculture. Properly managed, an increased energy input to agriculture, in the form of fertiliser, irrigation and machinery, may increase the net energy output per unit of land; i.e. crops may capture more solar energy. Hence, subsistance agriculture may be transformed into one producing surplus energy, in the form of food and crop residues, to other parts of the economy.

If irrigation is available then it may be possible to harvest several crops a year where rainfall may be largely confined to one season and crop failure due to erratic rains may be avoided. For widespread irrigation a source of energy other than that of human labour or draught animals is necessary, particularly if the land is to be productively cultivated in the dry season. The use of windpumps seems an obvious solution in areas where a suitable wind regime exists.

Makhijani suggests some criteria for windmill design in the rural Third World:

"1. Low cost; the total cost should be less than $200 and preferably less than $100 so that small farmers and others who may need a source of power for cottage industries would be able to afford it, (1976 prices)

2. It should have sufficient power to enable irrigation of a small plot ($\frac{1}{4}$ to $\frac{1}{2}$ a hectare) and a power take off to enable it to perform other functions such as sugar cane crushing. The size of the windmill therefore depends on the source and quantity of water needed,

3. It should be made of local materials as far as possible and with local skills (i.e. those available in a small village). Among the reasons for establishing this criterion are: i. low capital input and high labour intensity,

ii. accessibility of the technology to the poor,

iii. ease and quickness of maintenance and repair when required,

iv. high job quality in terms of job

satisfaction in ones work and control of it,

v. high labour productivity,

4. It should be stable under adverse weather conditions,

5. It should have a high starting torque so that auxilary starting devices are not needed."

The quantity of water required for irrigation depends on the climate, the crop and its stage of growth and the efficiency of the water distribution system. Average requirements seem to lie between 40 and 100 m^3/ha per day (Stern,1979; United Nations,1981). With a lift of 4m and an average of six hours pumping per day, this would require a power in the range 100 to 200 W/ha.

In recent years there have been a number of attempts to produce cheap windpump designs suitable for irrigation. In India, the Madurai Windmill Committee have produced a Cretan design suitable for irrigation in low winds (Sherman, 1976) and work on a similar design has recently been done at the National Aeronautical Laboratory at Bangalore (Tewari,1978). Another irrigation project using a Cretan windpump design, in Ethiopia, has been described by Fraenkel (1976). The Dutch Steering Committee for Wind Energy for Developing Countries(SWD) have some promising designs in operation in Sri-Lanka and elsewhere of the multi-blade type. (TOOL,1982). The Intermediate Technology Development Group (ITDG) have designed a low maintenance multi-blade windpump which is now in use in several countries (Fraenkel,1978). Fraenkel (1982) has pointed out a tendency to underestimate the technical requirements of windpumps, leading to the

failure of many wind power projects; he also mentions a tendency for research to concentrate on the aerodynamics at the expense of system optimisation. Dixon (1979) has drawn attention to the low system efficiency of most windpumps.

Wind power is hardly a new technology; Golding(1976) mentions a reference to a wind powered irrigation scheme in Babylon in the 17th century BC, and certainly windmills were in common use in Persia in the 4th century AD. These windmills had a vertical axis of rotation and relied on drag forces for their operation, shield walls protecting the blades as they moved upwind. It may have been from these designs that the Chinese windmill described by Needham (1965) derives. This design, still in widespread use, removes the need for shield walls, as the rectangular, 'junk' type sails luff automatically when moving into the wind.

Wind power developed in Europe in the 12th century AD and became an important source of power, particularly for grain milling but also for water pumping. These machines had an horizontal axis of rotation, with blades formed by spreading sails over a light wooden lattice. In the Mediterranean region, a design of mono-directional, stone tower windmill developed, with triangular cloth sails. It was from this design that the Cretan windmill was adapted for irrigating small intensively cultivated plots, early in the 20th century.

Multi-blade windpumps were originally developed in France in the 19th century and played an important part in

developing parts of America and Australia. This is now the most common and widely distributed type of windmill. Multi-blade windpumps tend to be optimised for high lift applications and their high cost, all metal construction has restricted their use in the Third World. Their need for regular skilled maintenance has meant that those machines which have been installed have often fallen into dis-repair.

The Savonius type of vertical axis windmill was developed in the 1920's (Savonius,1930) and has found widespread application for ventilation. It has also been used for water pumping but it has a high material requirement and is vulnerable in storms.

Developments in aerodynamics have led to very efficient designs of propellor turbines and there is now a sizeable effort directed towards the large scale generation of electricity by wind power. The Darrieus type of vertical axis wind turbine has undergone rapid development since 1971. It has a comparable efficiency to propellor type designs and has the advantages of a vertical axis turbine of not requiring orientation into the wind and of a smaller support tower.

Darrieus, a French engineer, filed a patent application for his turbine in 1925. The design utilised a number of blades of aerofoil cross-section and was intended to operate with " the peripheral speed of the blades much exceeding the speed of the current". It was not until 1971 that Rangi and South developed the design as a vertical axis wind turbine (Rangi and South,1971). They used a curved blade configuration

so as to minimise the blade stresses arising from the rotation. The design was found to combine the advantages of a vertical axis with the performance of propellor type turbines. For small machines, for stand alone applications, the design has the drawback of not being reliably self-starting.

It is not essential to use a curved blade arrangement. If the blades are set vertically and parallel to the axis then more power is produced near the blade tips, although this is likely to be offset by induced drag losses and the drag incurred by struts. Straight blades are easier to manufacture and, by allowing the blades to incline at high speeds it is possible to arrange for self-regulation of the power output in high winds. Straight blades also make possible several methods of introducing a self starting capability. One method is to arrange for a cyclic pitch variation, as described by Grylls et al (1978), another method is the use of very low aspect ratio blades (Mays and Musgrove,1978). Another possibility would be to use sailwing rather than solid aerofoils; the camber then changes automatically depending on the relative wind direction and it may offer a cheap method of aerofoil construction.

The sailwing concept was developed at Princeton University in 1948 (Ormiston,1971). A sailwing is constructed from a leading edge spar to which ribs are attached to form a framework which supports a trailing edge cable. A membrane is wrapped around the leading edge and attached to the trailing edge so as to form the upper and lower aerofoil surfaces. The trailing edge is tensioned and curved, imposing a chordwise pre-tension in the membrane and so minimising

deflections due to aerodynamic loads. A horizontal axis windmill using sailwings was developed at Princeton in 1960 (Sherman,1976) and has been adapted for water pumping in India (Sherman,1973).

Attempts to use sailwing type aerofoils in vertical axis wind turbines appear to date to have had only limited success. Hurley (1979) has developed a vertical axis sail rotor which appears to have a maximum tip speed ratio of less than one but which he reports develops a high torque at slow speeds. New Age Access (PO Box 4, Hexham, UK) have experimented with a similar design intended for electricity generation but abandoned development after mechanical problems. Newman and Ngabo (1978) describe some wind tunnel tests on a design using sailwings and report a peak power coefficient of 0.15 at a tip speed ratio of 1.5.

Initially, the present research sought to ascertain whether the apparently rather poor performance of vertical axis sailwing turbines was inherent in the use of sailwings or could be improved by suitable design. A numerical analysis of the theoretical performance has been made, using a single streamtube model of the induced flow through the turbine. Existing aerodynamic data for sailwing aerofoils from wind tunnel tests by Roberts and Newman (1979) was used. A description of the analysis and the results obtained are given in the first two chapters.

It was apparent that there were a number of shortcomings in the aerofoil data that was used and so it was decided to undertake new wind tunnel tests of sailwings to collect further

aerodynamic data. In particular these tests sought to investigate the effect of pre-tension in the fabric and the performance with different fabrics. The design of suitable measuring apparatus and the subsequent tests and results are described in Chapter Three. The new data is compared with the previous data and also with some limited data by Buehring (1977).

The fresh aerodynamic data allowed a fresh assessment of the performance to be expected from such a turbine. This suggested that the performance would inevitably be quite low but the suitability, for pumping applications, of the predicted torque characteristics encouraged the design and construction of a 2m diameter turbine. This is described in Chapters Four and Five.

To obtain data on the actual performance of the turbine in a natural wind, a series of performance tests were made with the turbine unloaded. Details of the tests and the results obtained are in Chapter Six. The results gave reasonable agreement with predictions. The average peak power coefficient obtained was about 0.1 with a starting torque coefficient of about 0.07.

The application of the prototype turbine as a windpump was then considered with a view to low lift applications. A large amount of energy was shown to be contained in the gusts occurring in the wind. Consideration was given to improving the utilisation of this energy by modifying the pump torque characteristics; hence increasing the system efficiency. Tests were made on a diaphragm pump in which

inertia flow effects were investigated. A pair of diaphragm pumps were later connected to the turbine. A number of problems were encountered and for various reasons, satisfactory operation was not achieved in the time available. Some possible modifications to the arrangement are discussed. This is contained in Chapter Seven. Some general conclusions concerning the future potential for such turbines have been made.

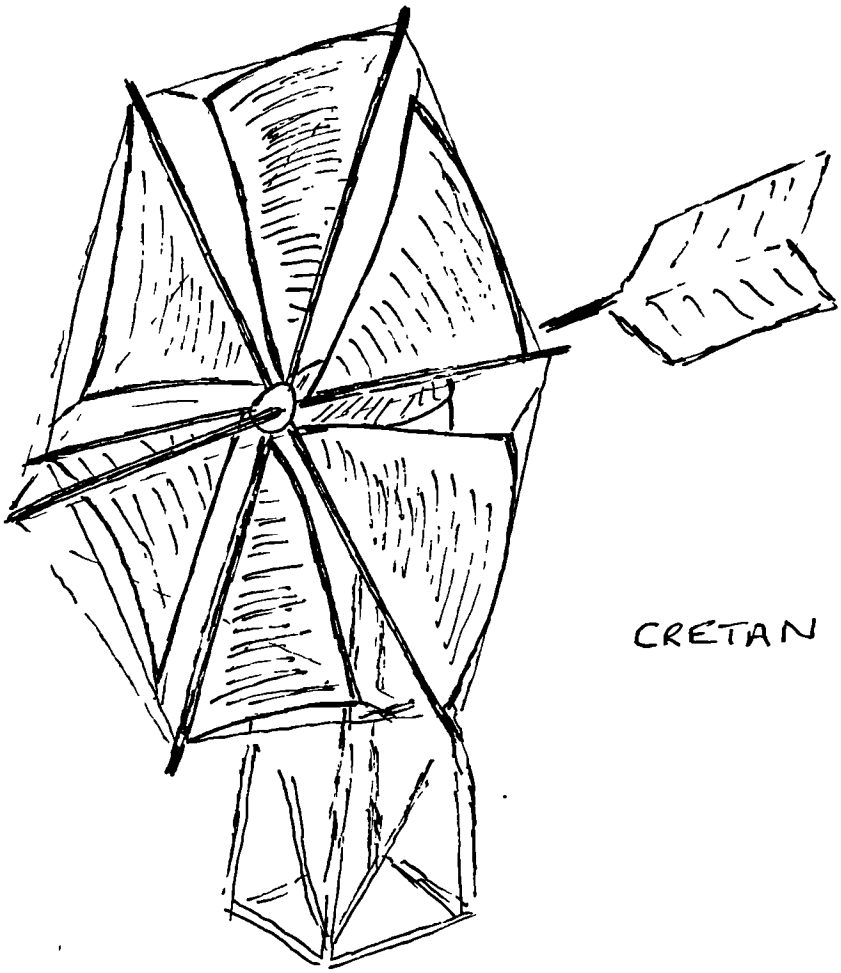

CRETAN

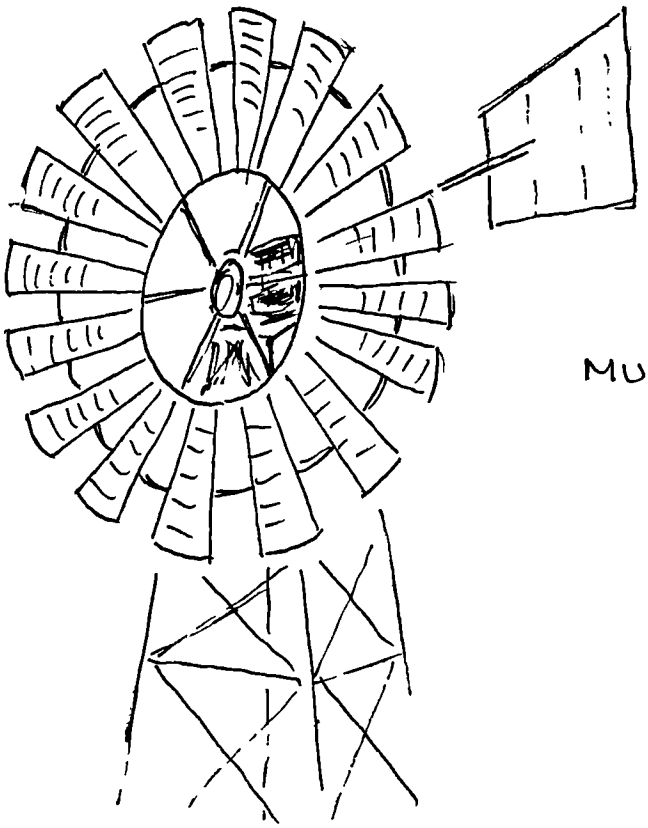

MULTI-BLADE

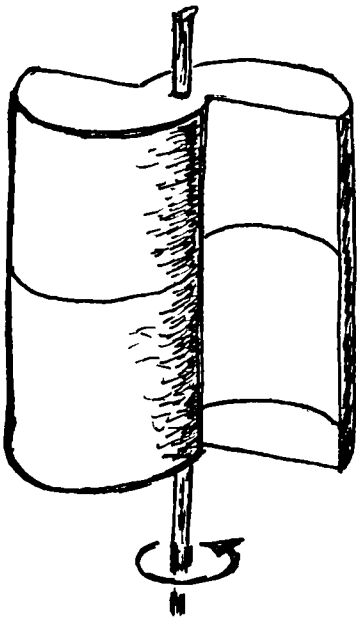

SAVONIUS

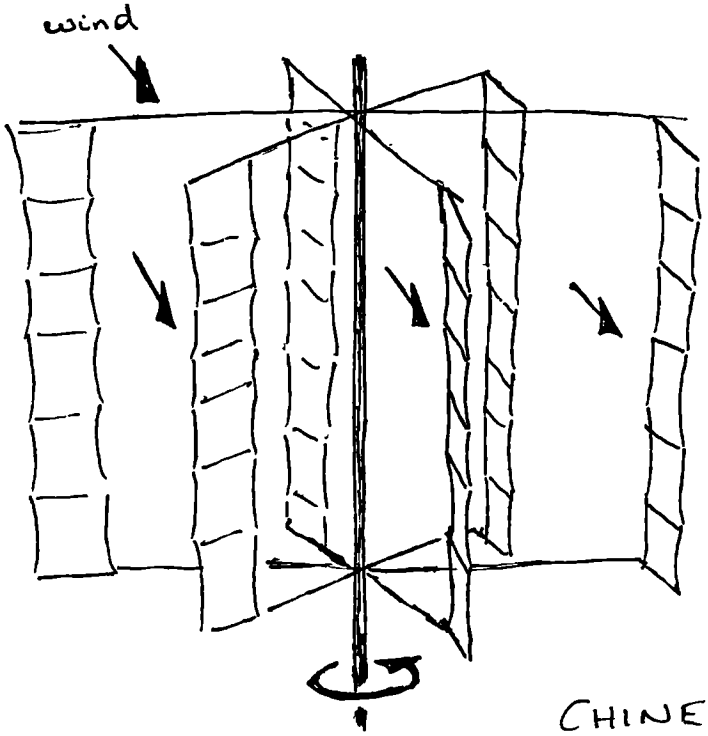

CHINESE

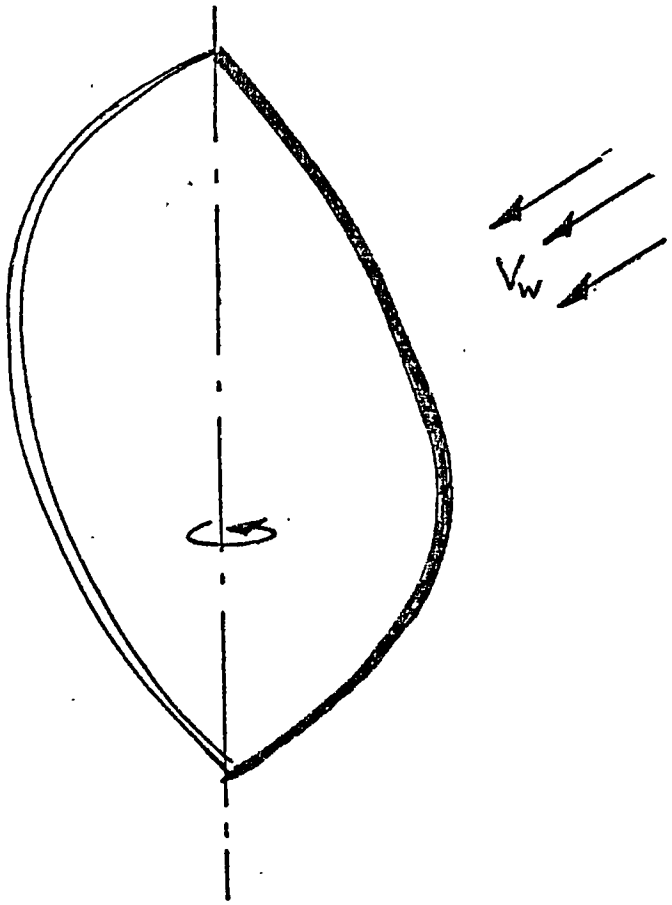

Darrieus Rotor - curved blade arrangement.

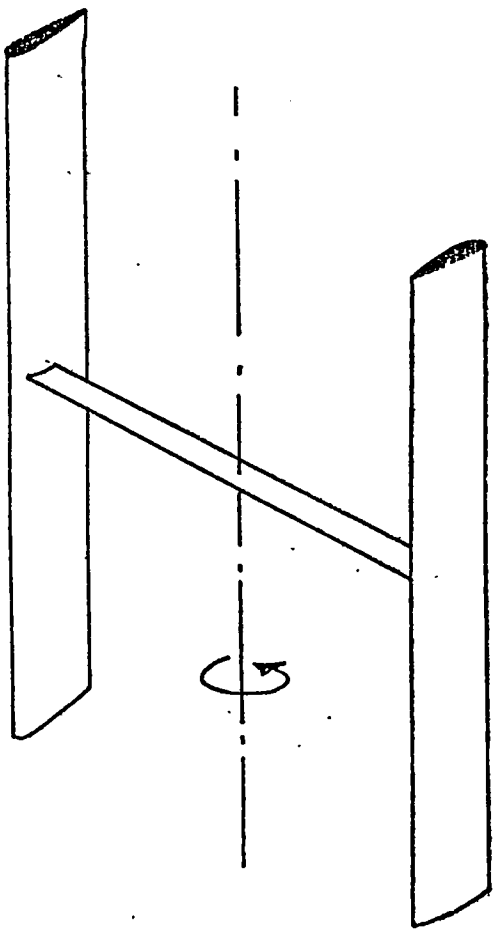

Darrieus Rotor - straight blade arrangement.

CHAPTER ONE

PERFORMANCE THEORY FOR DARRIEUS TURBINES

1.1. Introduction

This chapter describes the method used to analyse the performance of a sailwing vertical axis turbine. The 'single streamtube' model is described together with the methods used to allow for the variation of Reynolds number and the effect of a finite aspect ratio. Some limitations of the method are discussed and in particular, flow curvature and unsteady flow, which are not accounted for in the theory, are mentioned.

A qualitative understanding of the operation of a vertical axis wind turbine may be gained from a study of Fig.1.1. This shows a blade element at various azimuthal positions for a particular windspeed and a given blade angular speed. If the local azimuthal speed $R\Omega$ is large compared to the local windspeed V (Fig.1.1b), the blade element remains unstalled for all azimuthal positions; the lift force dL contributes a positive driving torque while the drag force dD detracts from it. When $R\Omega < V$ on the other hand (Fig.1.1c), the angle of incidence α varies widely and the blade is in reversed flow for part of the time. Then it is the drag force which provides the driving torque.

It should be clear that the actual flow through the rotor will be extremely complex. The earliest attempt at a performance prediction model was made by Templin(1974) using a 'single streamtube' approximation to the induced flow. This combines one dimensional momentum theory with blade element analysis. The turbine is modelled as an actuator disc enclosed in a single streamtube and momentum theory is then used to calculate the induced windspeed at the turbine. The

induced wind flow is thus modelled as being uniform at all points in the rotor, whereas in reality, both the speed and direction of the induced flow will vary throughout the rotor. Using this approximation to the induced flow, integration of the blade forces gives an estimate of the mean power output. The blade forces are calculated as if the blades are always in quasi-steady flow. Since the induced flow is assumed uniform, the power output from the upwind pass of the blade ($0>\theta>\pi$) is assumed to be the same as the power output from the downwind pass ($\pi>\theta>2\pi$), so long as the blade chord is set on a tangent to the circle which the blade describes. The angle of incidence α, at an azimuthal angle $\theta=2\pi-\phi$, is the same magnitude, though of different sign, as the angle of incidence at $\theta=2\pi+\phi$.

Considering Fig.1.2., in which the turbine is replaced by an actuator disc exerting a decelerating thrust F on the windstream, and applying the continuity, momentum and energy equations to a large control volume, gives the result:

$$V = \frac{V_w}{1+\frac{1}{4}C_F'} \qquad [1.1]$$

where C_F' is a thrust coefficient based on the local velocity V :

$$C_F' = \frac{F}{\frac{1}{2}\rho A V^2} \qquad [1.2]$$

and A is the frontal area of the turbine.

The power output is then given by $P=VF$ and it is easy to show, by the Betz analysis (Appendix1) ,that the maximum fraction of the power in the wind that may be extracted is $\frac{16}{27}$.

When the turbine is stationary, and at low tip speed ratios this model of the induced flow may be simplified still further by assuming that the induced wind velocity is actually equal to the free wind velocity i.e. $V=V_w$, the flow blockage is

assumed to be negligable.

Some improvement in the model of the induced flow may be made by replacing the single streamtube enclosing the actuator disc by a bundle of stream filaments. Such a multiple streamtube model was originally proposed by Strickland(1976) and has since been refined by Read and Sharpe(1980), among others. This small refinement does give some improvement in the flow model but also adds greatly to the complexity of the performance calculations.

Several attempts have been made to develop a vortex model of the flow. Duremberg(1979) appears to have had some success in applying the method developed by Fanucci(1976) and improved by Migliore(1978) but was only able to obtain convergent solutions with low turbine solidities and over a limited range of tip speed ratios. This method would seem to have considerable possibilities but is unable to handle stalled blades.

The crudeness of the approximations used in the single streamtube model of the induced flow are obvious but use of this model here is justified by its simplicity, and hence economical use of computer time, and by the previous success with which it has been used in predicting the overall performance of Darrieus turbines (see for example Shankar,1976). Although it has been shown to produce slightly optimistic predictions of the peak power coefficient it seems quite adequate for use here where, as will be seen, the main uncertainties in the predictions arise from uncertainties in the behaviour of the sailwings.

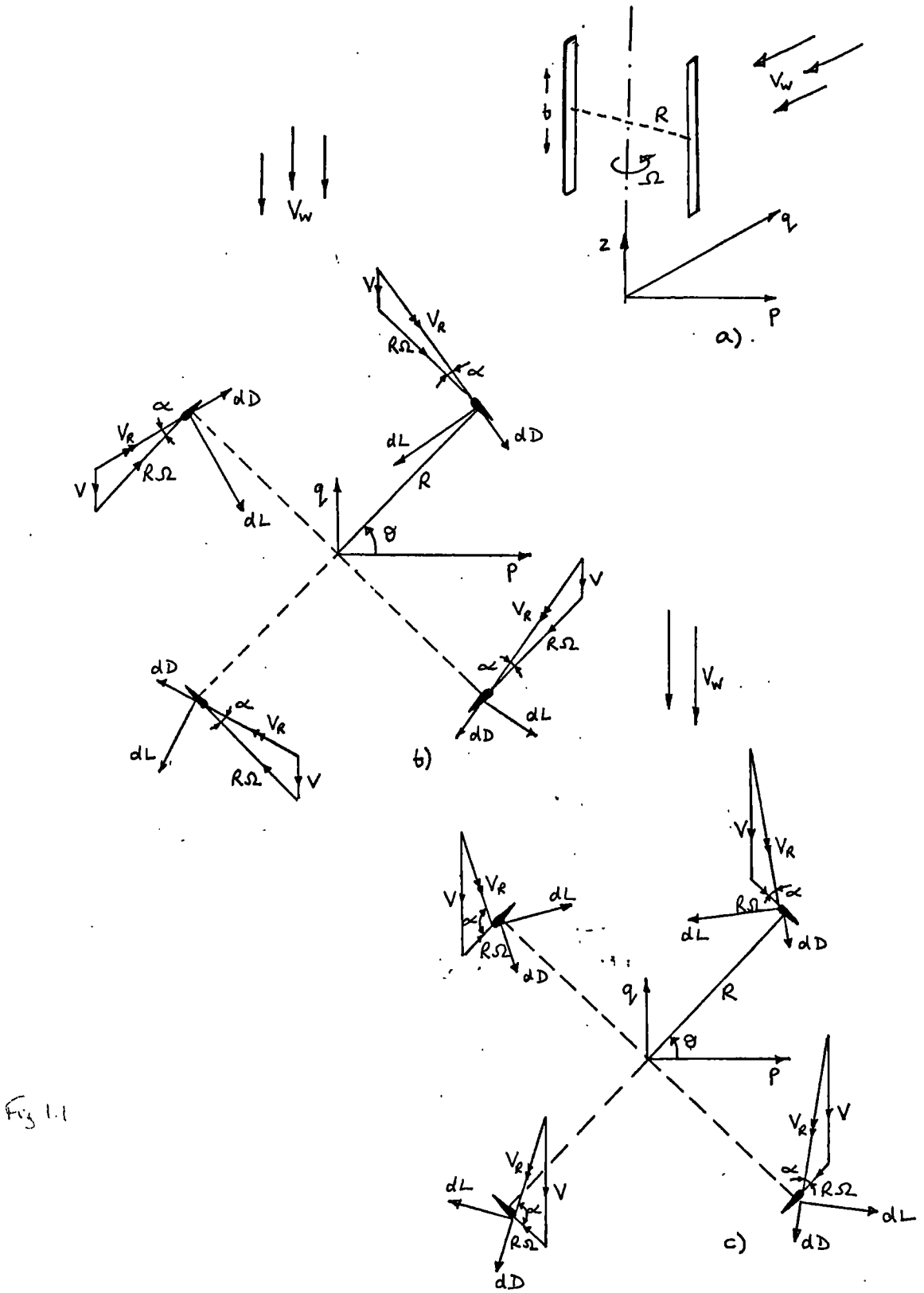

Fig 1.1

Fig.1.1. Section through a Darrieus turbine showing a blade element at various positions.

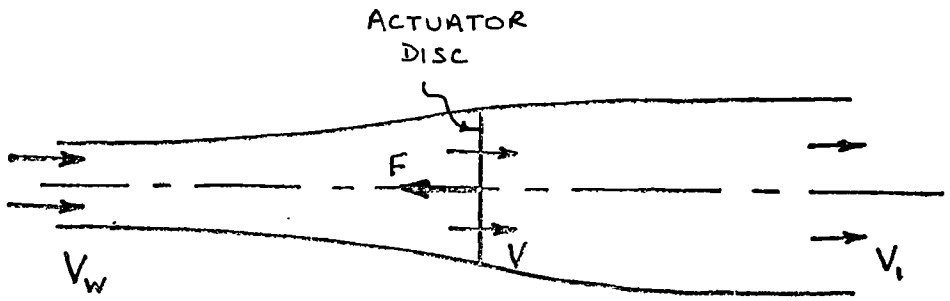

Fig.1.2. Actuator disc model of the turbine.

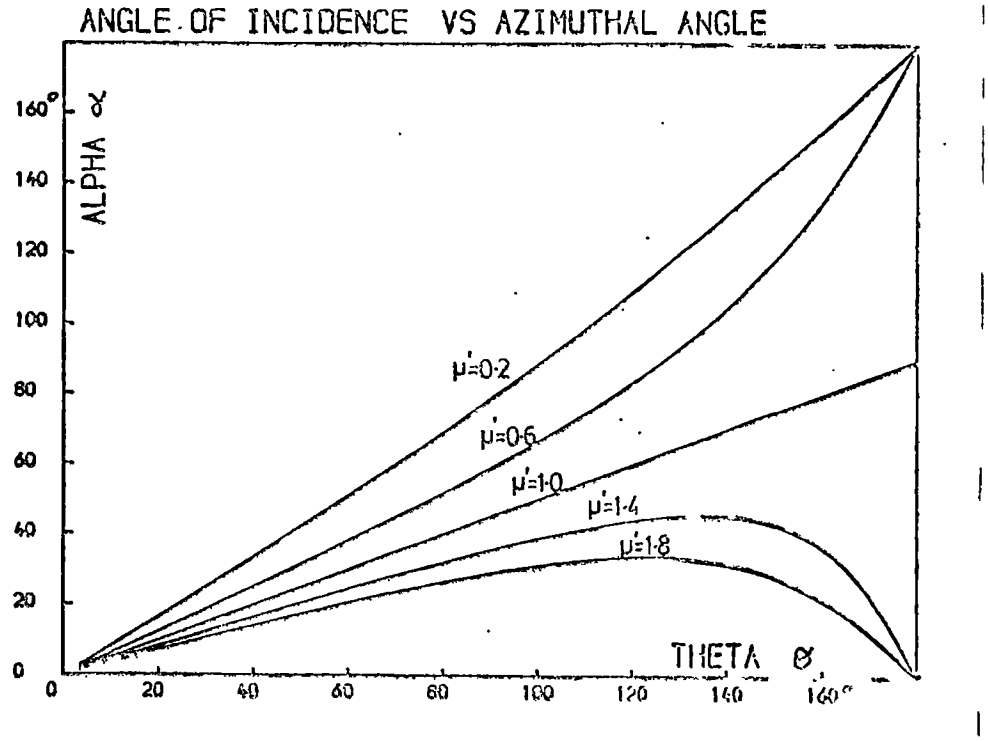

Fig.1.3. Variation of angle of incidence with azimuthal angle at low tip speed ratios.

1.2. Analysis

The basic method of analysis used in the next chapter is outlined below. Some more detail may be found in Appendix1. The method follows that described by Shankar(1976).

To avoid any need for iteration, the calculations are performed at chosen values of the tip speed ratio μ', based on the induced wind speed i.e. $\mu' = \frac{R\Omega}{V}$ [1.3]

As is described below, this allows calculation of a power coefficient C_p': $C_p' = \frac{Power}{\frac{1}{2}\rho A V^3}$ [1.4]

and the thrust coefficient C_F' defined above(eqn.[1.2]).

Use of eqn.[1.1] enables calculation of the true tip speed ratio μ: $\mu = \frac{R\Omega}{V_w}$ [1.5]

and the power coefficient C_p: $C_p = \frac{Power}{\frac{1}{2}\rho A V_w^3}$ [1.6]

as: $\mu = \frac{\mu'}{(1+\frac{1}{4}C_F')}$ [1.7]

and: $C_p = \frac{C_p'}{(1+\frac{1}{4}C_F')^3}$ [1.8]

At low tip speed ratios, when $V \simeq V_w$ and hence $\mu \simeq \mu'$ this problem is obviously avoided.

The analysis presented here is slightly simplified as it is assumed that the blades are straight and parallelto the axis of the turbine rotation.

The angle of incidence made by the relative wind to the blade chord varies with azimuthal position and thetip speed

ratio: $$\alpha = \text{atan}\frac{\sin\theta}{\mu' + \cos\theta} \qquad [1.9]$$

The way in which the angle of incidence varies with azimuthal position at low tip speed ratios (i.e. $\mu \simeq \mu'$) is shown in Fig.1.3.

The instantaneous contribution of the forces acting on a blade to the driving torque, depends on the net force component acting on the tangent to the circle described by the blade. The tangential force coefficient C_T, is related to the lift and drag coefficients C_L and C_D :

$$C_T = C_L \sin\alpha - C_D \cos\alpha \qquad [1.10]$$

The instantaneous driving torque per blade T_B, is therefore: $$T_B = C_T \cdot \tfrac{1}{2}\rho V_R^2 . R . b . c \qquad [1.11]$$

where b is the blade length, c the blade chord and R the turbine radius.

Now, substituting $q = \frac{V_R}{V}$ [1.12] gives: $T_B = C_T q^2 \cdot \frac{1}{2}\rho V^2 . R . b . c$ [1.13]

in which the term $C_T q^2$ may be considered as an instantaneous torque coefficient for the blade.

The ratio q is given by: $$q = \frac{\sin\theta}{\sin\alpha} \qquad [1.14]$$

Integrating for all azimuthal positions gives the mean torque: $$T = \frac{n}{2\pi}\int_0^{2\pi} C_T q^2 \cdot \tfrac{1}{2}\rho V^2 R\, b\, c \; d\theta \qquad [1.15]$$

where n is the total number of turbine blades.

The term $\frac{1}{2\pi}\int_0^{2\pi} C_T q^2 \, d\theta$ is a mean torque coefficient C_S', based on the total blade area ΣA_B ($\Sigma A_B = n.c.b$), rather than on the turbine frontal area A : $$C_S' = \frac{\text{Torque}}{\frac{1}{2}\rho \Sigma A_B V^2 R} \qquad [1.16]$$

Since : Power = Torque x Angular Velocity [1.17]

and as angular velocity $\Omega = \frac{V\mu'}{R}$ [1.18]

eqn.[1.15] becomes: Power= $C_s' n \frac{1}{2} \rho V^2 R b c \frac{V\mu'}{R}$

$$= C_s' \cdot \tfrac{1}{2} \rho \Sigma A_B V^3 \mu' \qquad [1.19]$$

Now the power coefficient C_p' is: $C_p' = C_s' \cdot \mu' \cdot \frac{\Sigma A_B}{A}$ [1.20]

The torque coefficient C_Q is defined as: $C_Q = \frac{\text{Torque}}{\frac{1}{2}\rho A V_w^2 R}$ [1.21]

and from eqns. [1.5] & [1.17] $C_p = \mu . C_Q$ [1.22]

therefore when $\mu \simeq \mu'$: $C_Q \simeq C_s' \frac{\Sigma A_B}{A}$ [1.23]

The coefficient of thrust C_F' is given by:

$$C_F' = \frac{1}{2\pi} \int_0^{2\pi} (C_L \sin(\theta-\alpha) + C_D \cos(\theta-\alpha)) d\theta \cdot \frac{\Sigma A_B}{A} \qquad [1.24]$$

The ratio $\frac{\Sigma A_B}{2A}$ will be defined as the turbine solidity σ .

A computer program has been written to perform the calculations. Numerical integration using the trapezium rule was used with an interval in θ of $\frac{\pi}{50}$ radians. At each blade position, the angle of incidence is calculated (eqn.[1.9]). The relevant values of lift and drag coefficient are selected from the aerofoil data, linear interpolation between data points being used.

1.2.1. The Effect of Reynolds Number

Blade Reynolds number is defined as:

$$Re = \frac{\rho V_R c}{\mu_{air}}$$

The performance of aerofoils is strongly dependent on the Reynolds number, particularly when the number is low as is likely in a small turbine. When operating at low tip

speed ratios, the variation of the relative windspeed V_R with azimuthal angle is large. It is therefore preferable that, if suitable data is available, the instantaneous blade Reynolds number be calculated and then the relevant data set used for each calculation position. Calculation of the blade Reynolds number requires specification of a value for the product of windspeed with blade chord ($V_w \times c$). At higher tip speed ratios the Reynolds number will be higher and will vary less.

1.2.2. The Effect of Blade Aspect Ratio

When straight blades are used, the blade aspect ratio may have an important influence on the aerodynamic properties. The blade aspect ratio AR is defined as the ratio of the blade length to the blade chord, b/c . At high values of AR the flow over the aerofoil is essentially two dimensional but as the ratio is reduced the effect of flow across the blade tips becomes significant. The effect is to induce a 'downwash' velocity, reducing the effective angle of incidence while additional drag arises from blade tip losses.

In the analysis of the next chapter, corrections given by Glauert(1959) for rectangular aerofoils have been used (Table 1.1.). The effective angle of incidence is calculated from: $\alpha_{eff} = \alpha . k$
where α is given by eqn.[1.9]. The value of k is taken from the table, depending on the value of the ratio $\frac{AR}{a_o}$ where a_o is the slope of the curve of lift coefficient vs. angle of incidence prior to stall. The lift and drag coefficients corresponding to this angle of incidence have then been used in the calculations, with the addition of an induced drag

coefficient, representing the tip losses, taken as:

$$C_{id} = \frac{C_L^2}{\pi AR}$$

$\frac{AR}{a_o}$	k
0.25	0.426
0.50	0.587
0.75	0.675
1.00	0.729
1.25	0.767
1.50	0.794
1.75	0.815

Table 1.1.

The corrections have only been applied where the aerofoil was unstalled. Above stall any small change in the effective angle of incidence will have less effect as the lift curve is then much less steep.

1.3. Discussion

The crude nature of the approximations used for the induced flow through the turbine has already been mentioned. Clearly there is no reason to assume that the Betz limit should apply to a Darrieus turbine in which the energy is extracted from the wind over a distance in the stream rather than at a single position. Apart from this, two other factors which affect the validity of the predictions will be mentioned here. These are: the fact that the model assumes quasi-steady aerodynamic forces on the blades at each azimuthal position, whereas the angle of incidence may infact be varying rather rapidly; the possible flow curvature effect arising from the variation of the angle of incidence along the blade chord.

Differentiating the expression for the angle of

incidence (eqn. [1.9]): $\frac{d\alpha}{dt} = \frac{1}{1+\left(\frac{\sin\theta}{\mu'+\cos\theta}\right)^2} \frac{d}{dt}\left(\frac{\sin\theta}{\mu'+\cos\theta}\right)$

This reduces to: $\frac{d\alpha}{dt} = \frac{\Omega}{(\mu'+\cos\theta)^2+\sin^2\theta}\left[(\mu'+\cos\theta)\cos\theta+\sin\theta\cos\theta\right]$

For specified values of $\frac{V}{R}$ the variation of $\frac{d\alpha}{dt}$ with azimuthal angle may be plotted for various tip speed ratios. Typical curves are shown in Fig.1.4. Under certain conditions the variation may clearly be quite rapid; it is not clear what effect this may have. Further complications will arise in a real wind due to its varying speed and direction.

Migliore and Wolfe(1979) have drawn attention to the possible importance of flow curvature. When the ratio of the blade chord to the turbine radius increases, then the change in the angle of incidence made by the relative wind, between the leading and trailing edge, becomes more significant (Fig.1.5) e.g. if $\frac{c}{R}=0.2$ the difference is about 15°. The magnitude of the relative wind will also vary but this effect is small. The aerofoil is then effectively in curvilinear rather than rectilinear flow. Migliore and Wolfe suggest using conformal mapping techniques to transform the geometric aerofoil in curvilinear flow to a virtual aerofoil in rectilinear flow. The magnitudes of the camber and pitch of the virtual aerofoil will depend on the tip speed ratio, the azimuthal angle and the blade chord to turbine radius ratio. For sailwings, the problem is complicated by the varying natural profile.

Any quantitative assessment of either of these effects is beyond the scope of the present analysis which merely sought to assess, in a general way, the potential performance that could be expected from a Darrieus type turbine, employing sailwings instead of solid aerofoils.

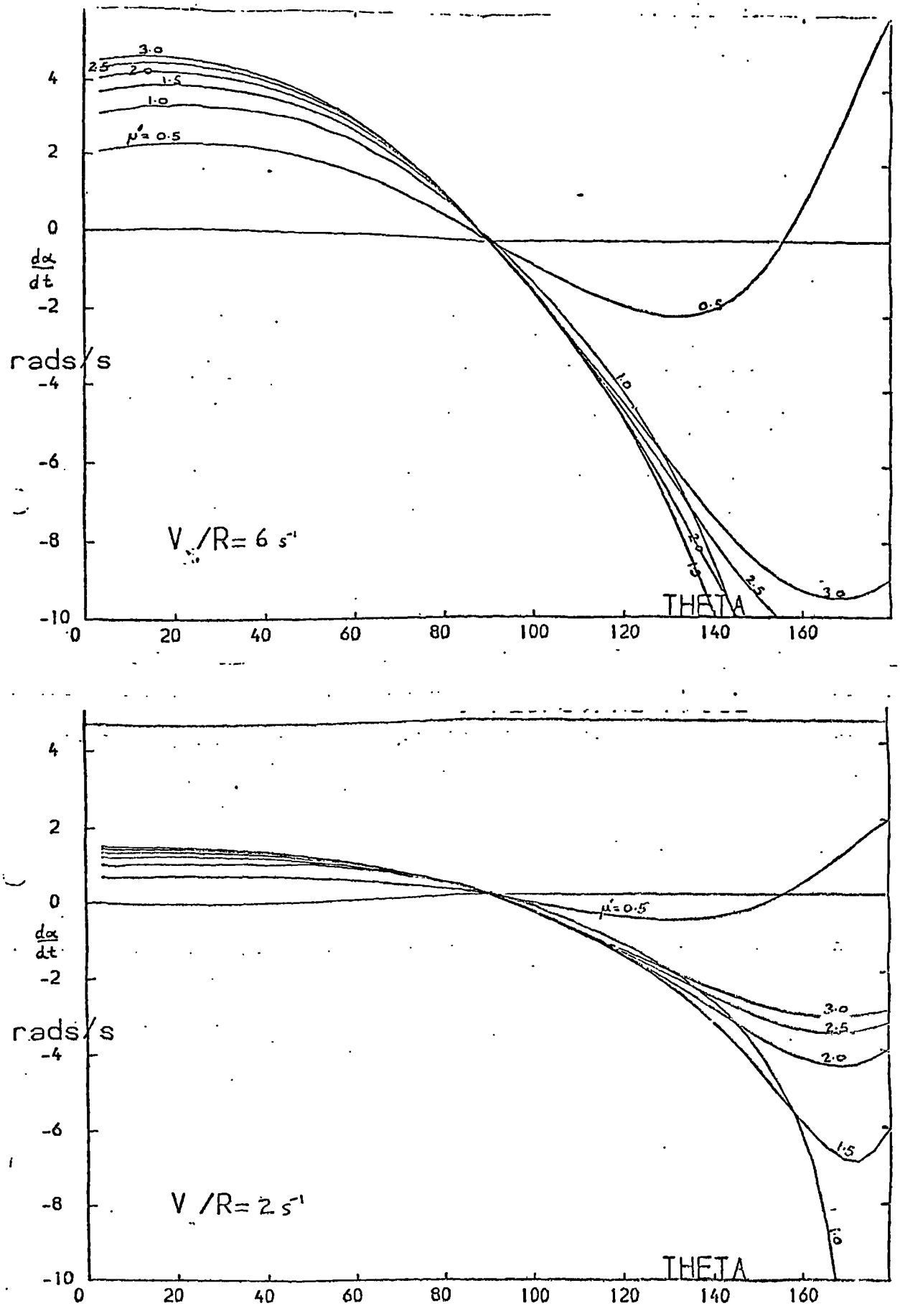

Fig.1.4. Rate of change of angle of incidence vs. azimuthal angle.

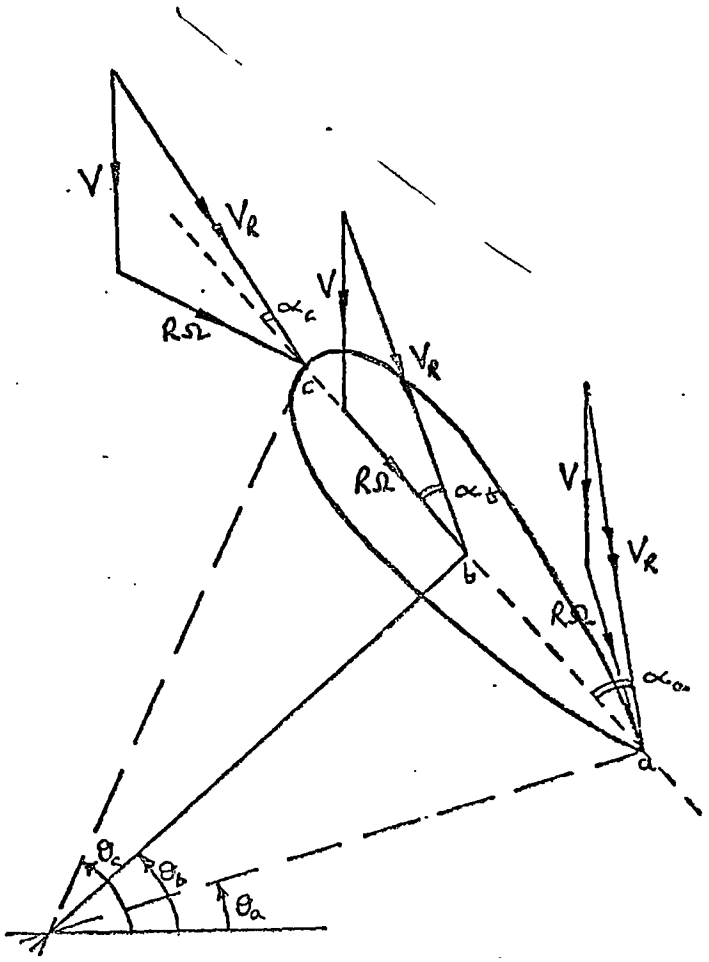

Fig.1.5. Variation of angle of incidence along blade chord.

CHAPTER TWO

THE PERFORMANCE OF SAILWINGS IN DARRIEUS TURBINES

2.1. Introduction

A numerical analysis has been performed, using the method described in the previous chapter, to examine the performance of vertical axis, sailwing turbines at both high and low tip speed ratios. The aerodynamic data for sailwings has been taken from Robert and Newman (1979).

To see how the aerofoil characteristics affect the torque at low tip speed ratios, the variation of the coefficient C_T (the tangential force coefficient) and of the product $C_T q^2$ (an instantaneous torque coefficient) with azimuthal position is plotted. Also plotted is the variation of the mean torque coefficient C_s' with tip speed ratio. The effects of a change of scale (and hence Reynolds number) and of low aspect ratio are examined.

At high tip speed ratios, plots of power coefficient vs. tip speed ratio have been derived for various solidities and the effect of low aspect ratio is again examined.

2.2. Data

In order to verify the analysis and to provide a comparison, the analysis was first performed using data for a standard solid aerofoil section. Data for the NACA0012 section, given by Shankar (1976) has been used. This was taken from Critzos et al (1955) and Jacobs and Sherman (1939) and is for a Reynolds number of the order of 300,000. This aerofoil section has been used in Darrieus turbines. The lift

and drag coefficients are shown in Fig.2.1.

Aerodynamic data for sailwings has been taken from the results reported by Robert and Newman (1979) which appear to provide the only existing data covering the full range of angles of incidence. They used a simple sailwing construction consisting of a circular rod over which was wrapped a membrane, the two sides of which met at a sharp trailing edge. The trailing edge was held fixed relative to the leading edge and was of a wedge shape, pivoted about its vertex so as to allow the sailwing to assume its natural camber. The sailwing had a nominal chord of 100mm and was mounted between endplates. lift and drag were measured with a nylon spinnaker fabric, having a weight of 41 g/m^2, at Reynolds numbers from 9.10^4 to 30.10^4 . The data used here is for two different leading edge rod diameters, 6.35mm and 9.53mm. They also reported some limited tests on a stiffer, polyester ('Dacron') fabric. The data employed is shown in Figs.2.2. to 2.4. In all cases, the fabric is described as being 'just taut' with the wind off.

Sailwing 1 : taut nylon, d=6.35mm, c=99.3mm
Sailwing 2 : taut nylon, d=9.53mm, c=98.4mm
Sailwing 3 : taut 'Dacron', d=9.53mm, c=97.7mm

Table 2.1.

It can be seen from the data that the natural camber of of the sailwings causes high lift coefficients at low incidence but also high drag coefficients. The very late stall apparent with the 'Dacron' material is surprising and Robert and Newman attribute this to the stiff nature of this fabric.

The purpose of using a wedge shaped trailing edge was to provide rigidity and so avoid twisting along the span. In a vertical axis turbine, such a trailing edge would not be practical; twisting would occur because of the centrifugal loads and this would prevent pivoting, if not causing breakage. In a practical turbine it would seem necessary to use a wire or cord trailing edge, curved and under tension. Such a trailing edge may be effectively rigid (depending on the tension, curvature and relative windspeed) but it will impart a chordwise pre-tension in the sail fabric. The pre-tension in the tests of Robert and Newman appears to be very low. It is not immediately clear how this may affect the validity of the results of the following analysis.

Another uncertainty in the analysis arises in the calculation of the tangential force coefficient from lift and drag data. The value of the coefficient is given by the sometimes rather small difference between two relatively large terms (eqn. [1.10]): $C_T = C_L \sin\alpha - C_D \cos\alpha$
Measurement errors on C_L, C_D and α are not given.

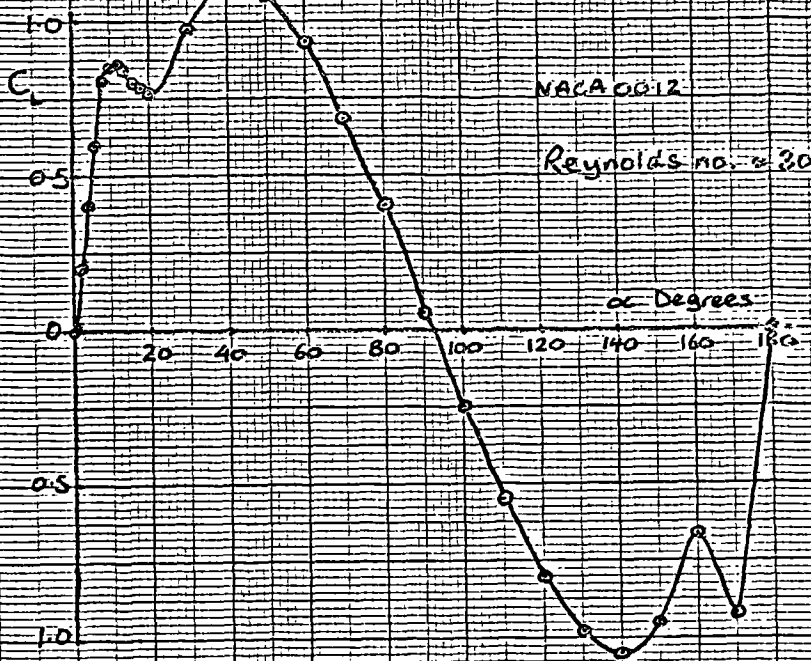

α	C_L	C_D
0	0·0	0·0100
2	0·200	0·0100
4	0·400	0·0110
6	0·600	0·0130
8	0·800	0·0220
10	0·850	0·0850
12	0·860	0·1800
14	0·810	0·2100
16	0·800	0·2300
18	0·780	0·2400
20	0·760	0·2400

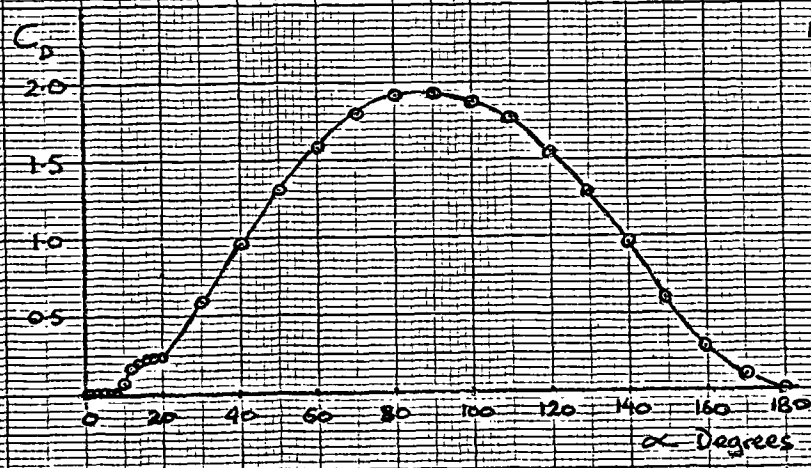

Data given by Shankar (1976), taken from Critzos et al (1955) and Jacobs and Sherman (1939)

Fig. 2.1. Lift and drag coefficients used for the solid aerofoil (NACA0012), taken from Shankar (1976)

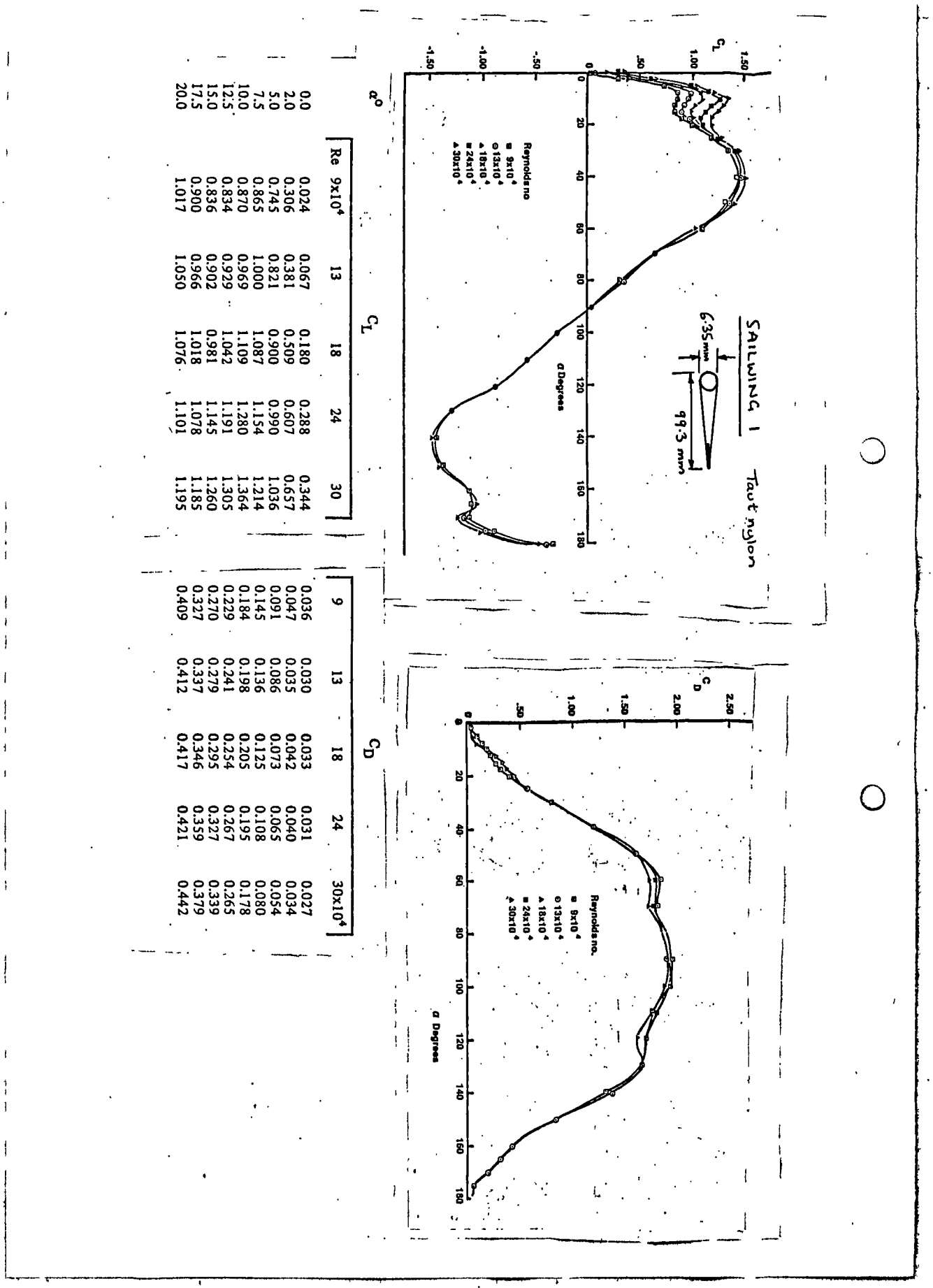

	C_L					
	Re 9×10^4	13	18	24	30
0.0	0.024	0.067	0.180	0.288	0.344
2.0	0.306	0.381	0.509	0.607	0.657
5.0	0.745	0.821	0.900	0.990	1.036
7.5	0.865	1.000	1.087	1.154	1.214
10.0	0.870	0.969	1.109	1.280	1.364
12.5	0.834	0.929	1.042	1.191	1.305
15.0	0.836	0.902	0.981	1.145	1.260
17.5	0.900	0.966	1.018	1.078	1.185
20.0	1.017	1.050	1.076	1.101	1.195

	C_D				
	9	13	18	24	30×10^4
0.0	0.036	0.030	0.033	0.031	0.027
2.0	0.047	0.035	0.042	0.040	0.034
5.0	0.091	0.086	0.073	0.065	0.054
7.5	0.145	0.136	0.125	0.108	0.080
10.0	0.184	0.198	0.205	0.195	0.178
12.5	0.229	0.241	0.254	0.267	0.265
15.0	0.270	0.279	0.295	0.327	0.339
17.5	0.327	0.337	0.346	0.359	0.379
20.0	0.409	0.412	0.417	0.421	0.442

Fig.2.2. Lift and Drag coefficients for Sailwing1,
(from Robert and Newman, 1979)

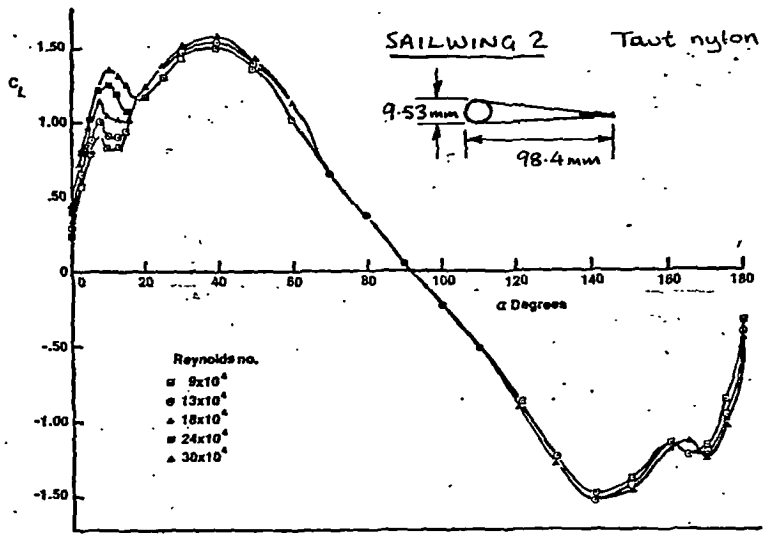

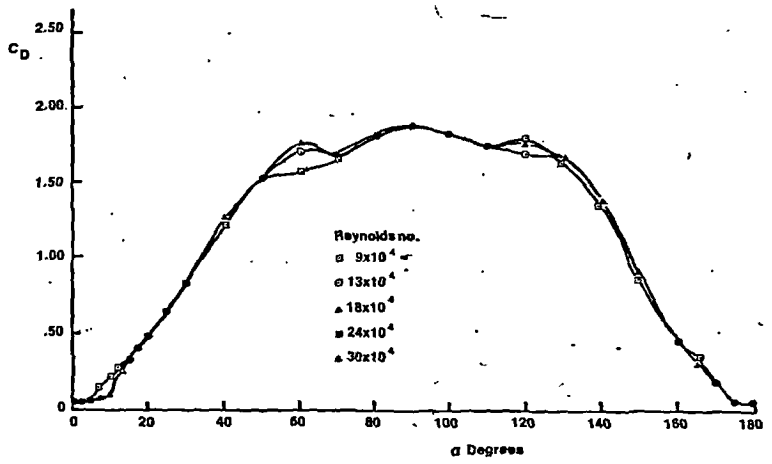

α°	C_L					C_D				
	Re 9x10⁴	13	18	24	30	9	13	18	24	30x10⁴
0.0	0.243	0.296	0.352	0.405	0.433	0.048	0.046	0.047	0.051	0.049
2.5	0.563	0.652	0.727	0.780	0.796	0.060	0.055	0.053	0.050	0.046
5.0	0.791	0.878	0.963	1.024	1.045	0.064	0.066	0.063	0.058	0.050
7.5	0.913	1.016	1.150	1.226	1.247	0.147	0.137	0.088	0.074	0.067
10.0	0.820	0.912	1.039	1.261	1.367	0.198	0.211	0.217	0.190	0.094
12.5	0.829	0.901	1.018	1.188	1.327	0.233	0.251	0.279	0.286	0.277
5.0	0.938	0.992	1.010	1.068	1.250	0.306	0.317	0.316	0.323	0.327
7.5	1.140	1.166	1.170	1.150	1.171	0.408	0.415	0.413	0.406	0.402
0.0	1.181	1.229	1.239	1.239	1.226	0.476	0.484	0.491	0.487	0.475

Fig.2.3. Lift and drag coefficients for Sailwing2, (from Roberts and Newman, 1979)

C_L					
α°	Re 9×10^4	13	18	24	30
0.0	0.174	0.180	0.169	0.150	0.135
2.5	0.495	0.487	0.439	0.384	0.343
5.0	0.866	0.854	0.847	0.843	0.837
7.5	1.060	1.061	1.029	1.002	0.987
10.0	1.268	1.261	1.235	1.211	1.185
12.5	1.344	1.341	1.318	1.298	1.271
15.0	1.391	1.400	1.369	1.356	1.340
17.5	0.971	1.053	1.155	1.222	1.440
20.0	1.148	1.108	1.087	1.112	1.147

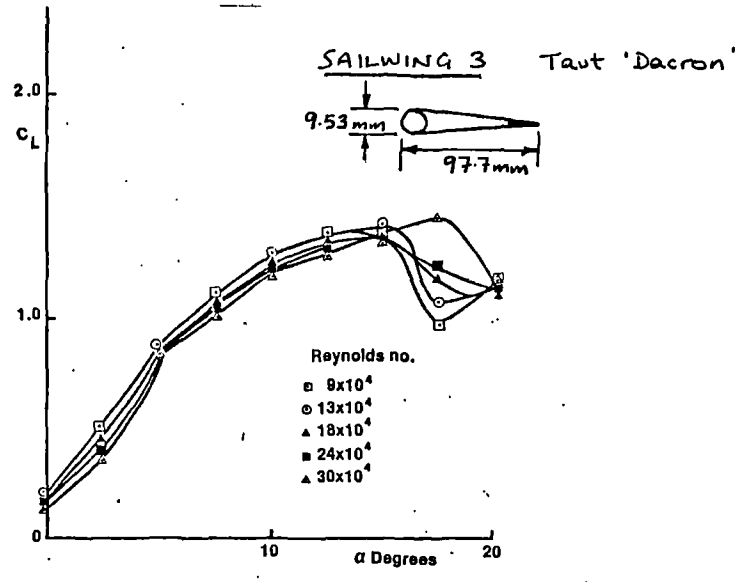

C_D					
α°	9	13	18	24	30×10^4
0.0	0.036	0.030	0.028	0.024	0.020
2.5	0.047	0.041	0.034	0.031	0.023
5.0	0.063	0.058	0.054	0.047	0.040
7.5	0.072	0.068	0.064	0.058	0.053
10.0	0.090	0.087	0.081	0.077	0.071
12.5	0.121	0.125	0.118	0.112	0.109
15.0	0.127	0.156	0.153	0.146	0.141
17.5	0.364	0.365	0.350	0.318	0.188
20.0	0.433	0.430	0.408	0.405	0.422

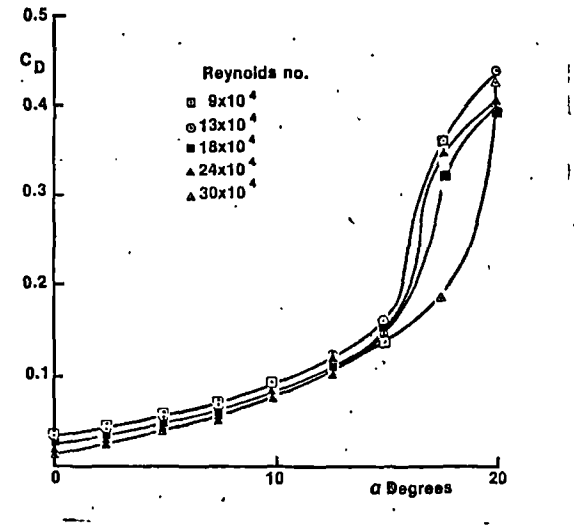

Fig.2.4. Lift and drag coefficients for Sailwing3, (from Roberts and Newman, 1979)

2.3. Results

All these results assume a turbine with straight blades, set parallel to the axis of rotation. Unless otherwise stated, aspect ratio effects are not considered and, for the sailwings, the product $V_w \times c$ has been taken as 3 m^2/s. This value was chosen so as to give blade Reynolds numbers in the range 24.10^4 to 30.10^4 at low angles of incidence. No allowance has been made for parasitic drag losses.

The variation in angle of incidence made by the relative wind with azimuthal angle, is shown in Fig.2.5. for several, low tip speed ratios. When the tip speed ratio is very low, it can be seen that the angle of incidence reaches 180 degrees. When the angle of incidence is greater than 90 degrees, and the aerofoil is in reversed flow, it is the drag forces which provide a driving torque. As the tip speed ratio increases above unity, the maximum angle of incidence occurring is reduced, until it is eventually below the stall angle of the aerofoil.

It is of interest to see how the ratio q^2 ($q = V_r/V$) varies with azimuthal angle, since this has a strong influence on the instantaneous torque coefficient $C_T q^2$. From Fig.2.6. it is evident that, at low tip speed ratios, the relative contribution made to driving torque at higher azimuthal angles, is increasingly reduced as the tip speed ratio increases.

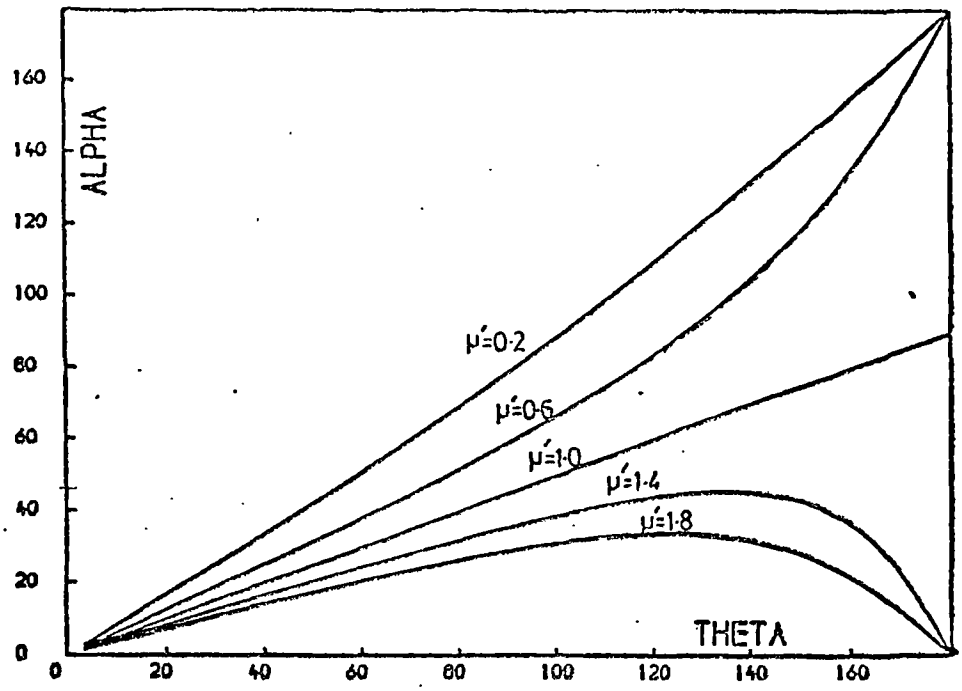

Fig.2.5. Angle of incidence vs. azimuthal angle at low tip-speed ratios.

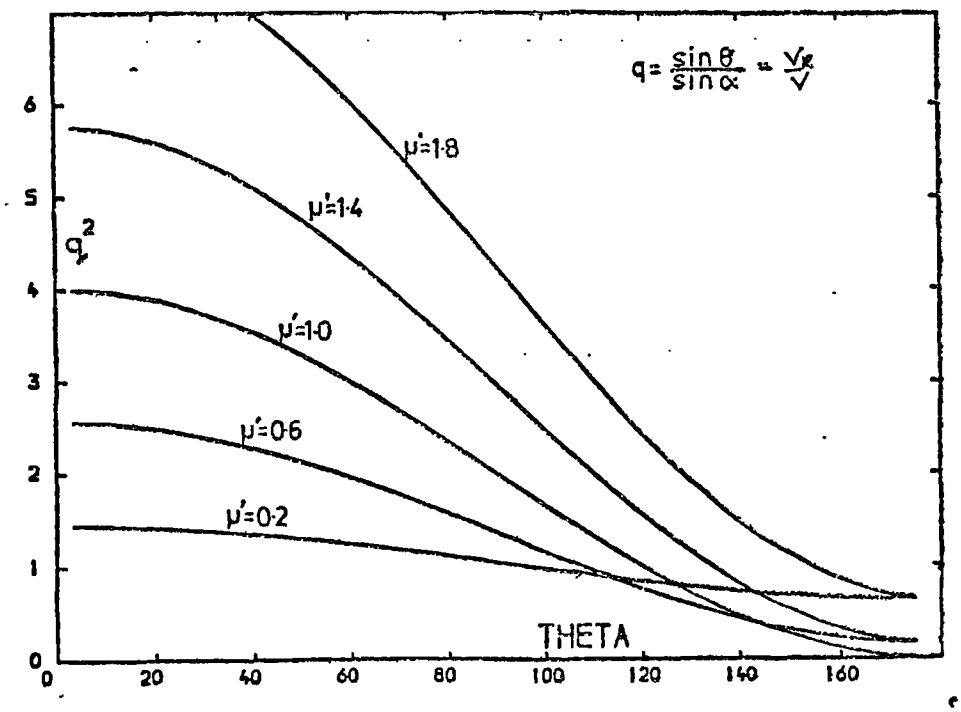

Fig.2.6. Ratio q^2 vs. azimuthal angle at low tip-speed ratios.

2.3.1. Low Speed Performance

The variation of the tangential force coefficient C_T and the instantaneous torque coefficient $C_T q^2$ with azimuthal angle θ, has been plotted for the various aerofoils, at tip speed ratios of 0.2, 0.8, and 1.4 (Figs.2.7. to 2.9.). The 'Dacron' aerofoil is not included here because of the limited data available. It is clear that at the lowest tip speed ratios, a large part of the driving torque is contributed by drag forces. But as the tip speed ratio increases to unity this contribution is progressively reduced by the effect of the q^2 term.

A significant difference between the solid aerofoil and the sailwings can be seen to be the positive torque contribution made by the sailwings when the angle of incidence is between about 30 degrees and 70 degrees (e.g. for $\sim 40° < \theta < 80°$ when $\mu = 0.7$). This difference is due to the higher lift coefficients of the sailwings. As the tip speed ratio increases, this contribution is also reduced by the effect of the q^2 term and at tip speed ratios of above about 1.8 such high angles of incidence no longer occur; driving torque then depending solely on azimuthal positions where the blade is unstalled.

From the plots of the mean torque coefficient C_s' in Fig.2.10, it can be seen how the low speed performance compares with the different aerofoils. With the solid aerofoil, the decreasing contribution from drag forces causes a drop in the mean torque until a minimum is reached at a tip speed ratio of about unity. This explains the poor starting characteristics of solid bladed vertical axis turbines. For the sailwings on the other hand, the loss in the drag contribution is more than made up for in the lift contribution from angles of incidence

between about 30 and 70 degrees.

The effect of low Reynolds number on the starting performance may be seen in Fig.2.11. in which the torque curves obtained with two different values of $V_w \times c$ are compared. It is clear that a low wind speed or a smaller blade chord may significantly affect the turbine starting characteristics.

2.3.2. High Speed Performance

Theoretical turbine performance curves at higher tip speed ratios and with several solidities are plotted in Figs. 2.12.to 2.15. The results for the solid aerofoil are as expected, predicting an optimum solidity of 0.2 and a peak power coefficient of 0.43, before allowing for parasitic drag and other losses, at a tip speed ratio of about 4.5. The predictions made using the data for Sailwing 1 and Sailwing 2 show maximum power coefficients of 0.24 and 0.28 respectively; an optimum tip speed ratio of between 4 and 5; and low optimum solidities of 0.15 to 0.2. Sailwing 3, the 'Dacron' sail, gives a rather higher peak power coefficient of about 0.34 at a tip speed ratio of 2.8 and with an optimum solidity of 0.3. The results show how an increased stall angle leads to a reduction in the optimum tip speed ratio and an increase in the optimum solidity.

2.3.3. The Influence of Aspect Ratio

The analysis was repeated with an allowance for low aspect ratio (as described in section 1.2.2.). For the solid aerofoil, at low tip speed ratios, the torque coefficient

appears to be little affected, provided that the aspect ratio is above about 8. (Fig.2.16). However, at higher tip speed ratios (Figs.2.17.and 2.18.), the peak power coefficient is considerably reduced; down to about 0.35 ($AR=8$) from 0.43 ($AR=\infty$). A lower aspect ratio can be seen to cause an increase in optimum solidity and reduction in optimum tip speed ratio, as would be expected from the effective increase in the stall angle.

With their higher lift coefficients, the sailwings suffer severely from the effects of a low aspect ratio. This is as the induced drag coefficient is assumed to be proportional to the square of the lift coefficient (Figs.2.19 to 2.23).

It should be noted that the reduction in the optimum tip speed ratio will lead to a reduction in the parasitic losses. Also, the increase in solidity will increase the actual torque produced, which may improve starting.

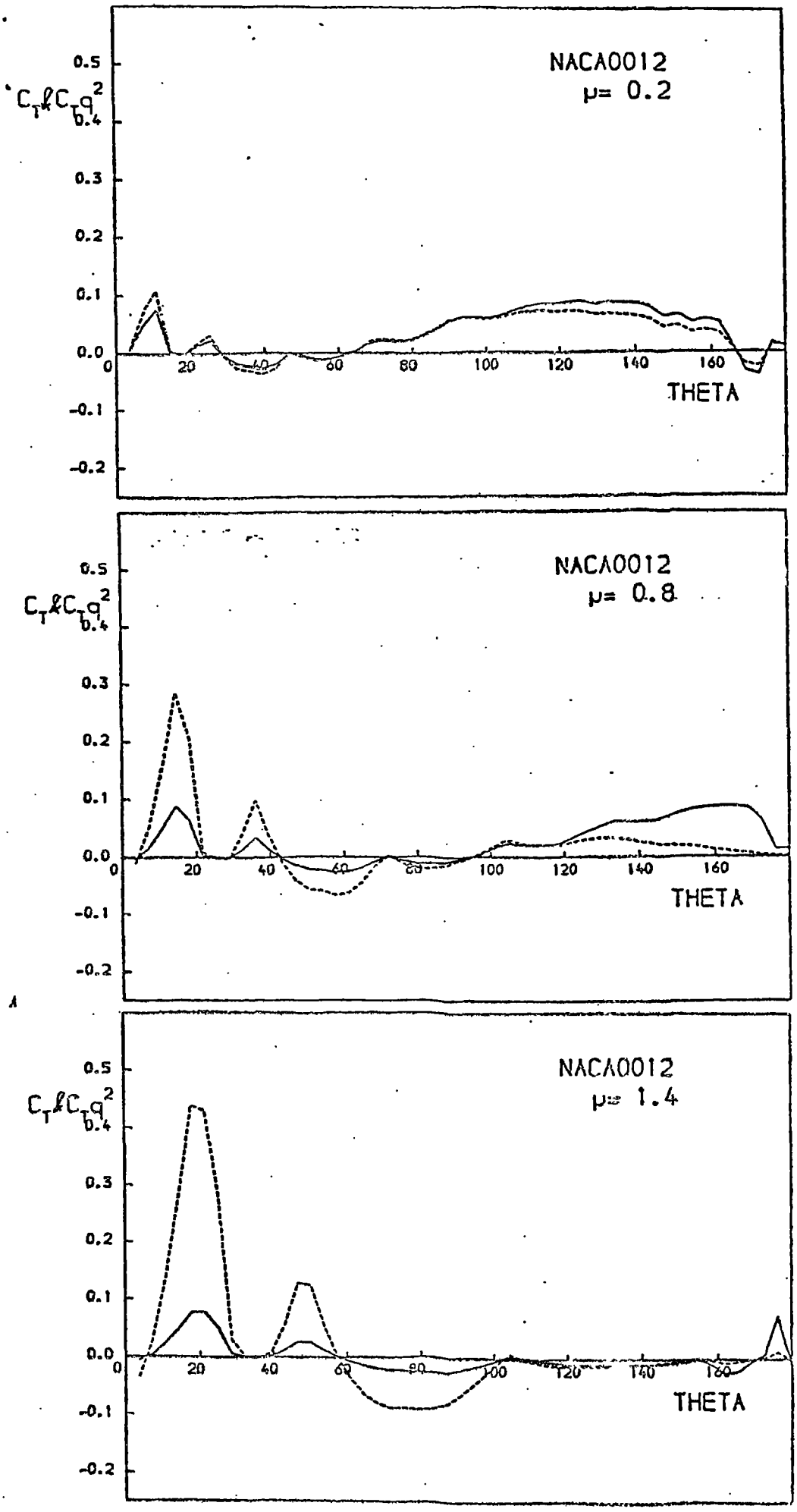

Fig.2.7. Tangential force (solid line) and torque coeffs. vs. azimuthal angle, solid aerofoil.

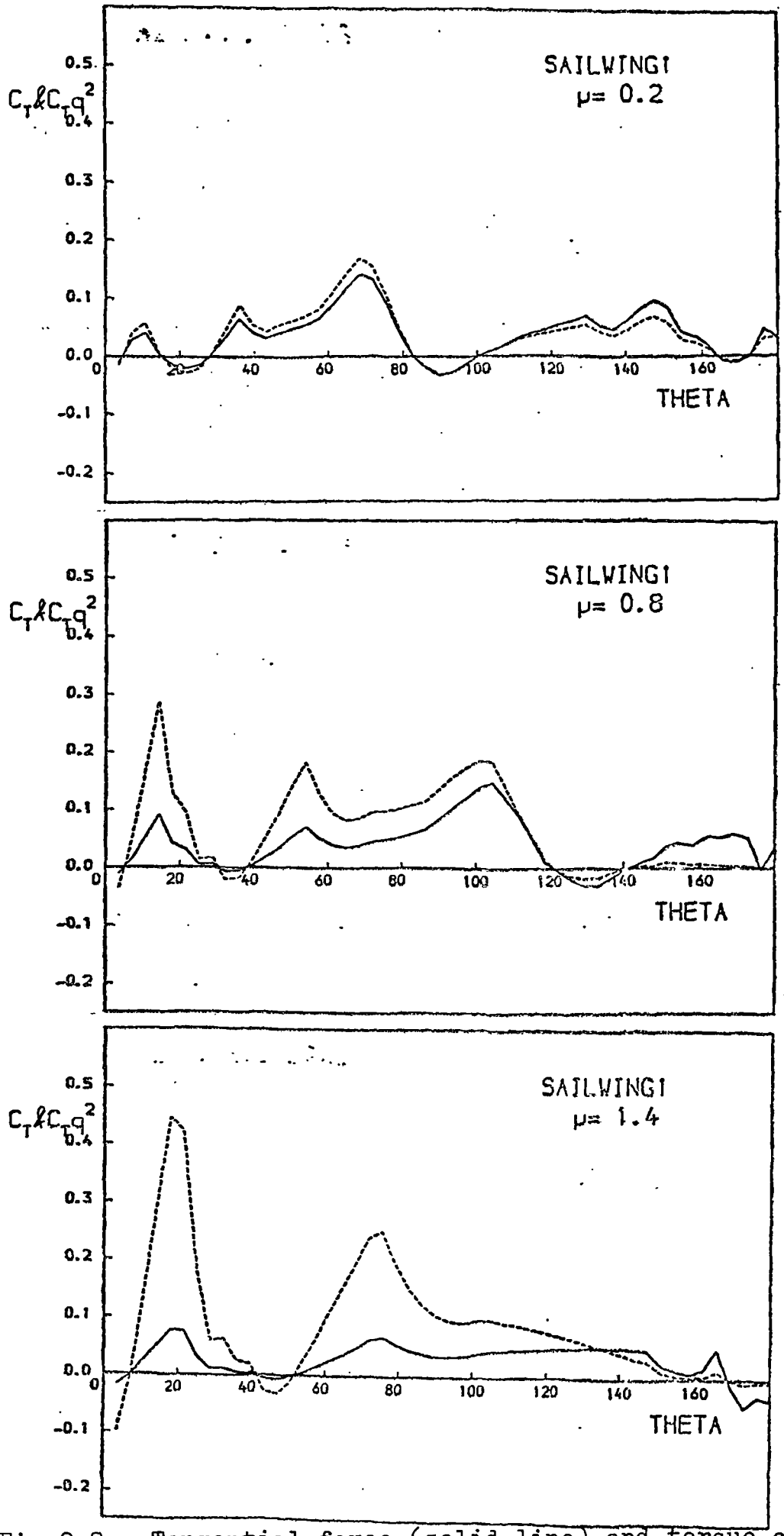

Fig.2.8. Tangential force (solid line) and torque coeffs. vs. azimuthal angle, Sailwing1.

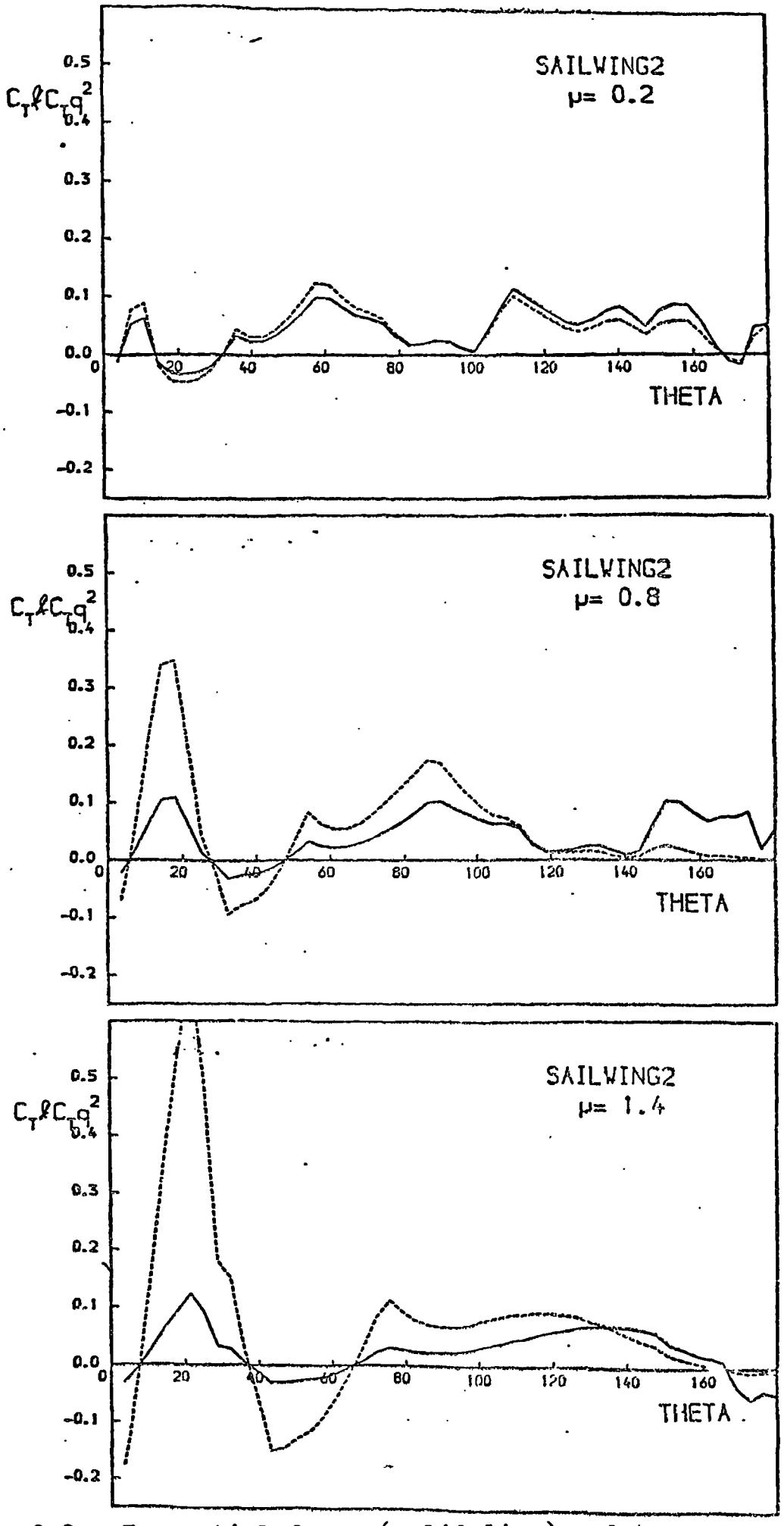

Fig.2.9. Tangential force (solid line) and torque coeffs. vs. azimuthal angle, Sailwing2.

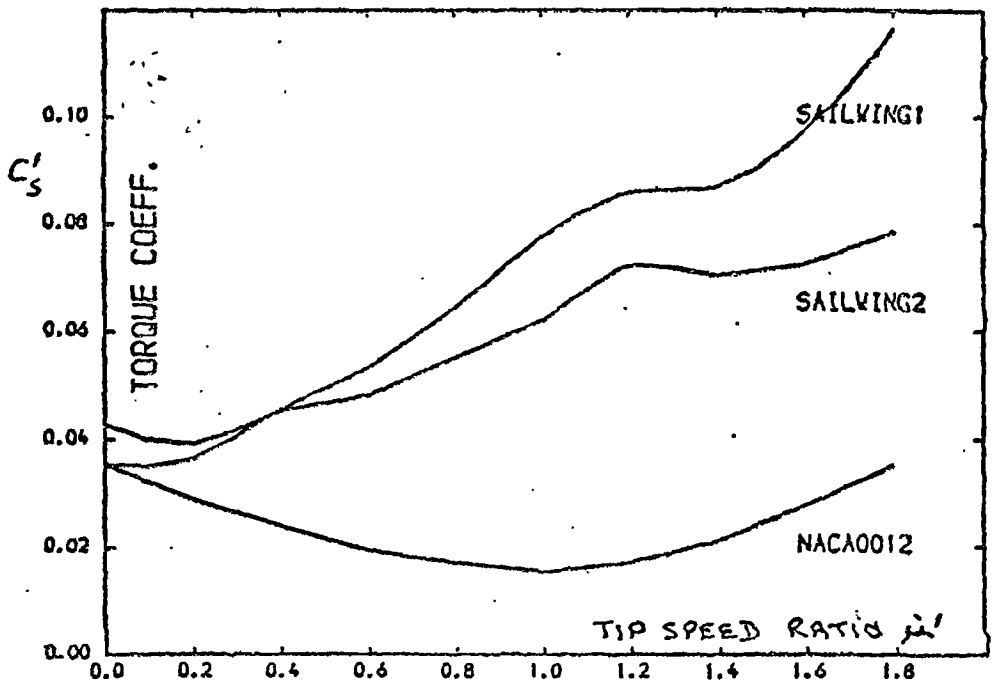

Fig.2.10. Mean torque coefficient vs. tip speed ratio

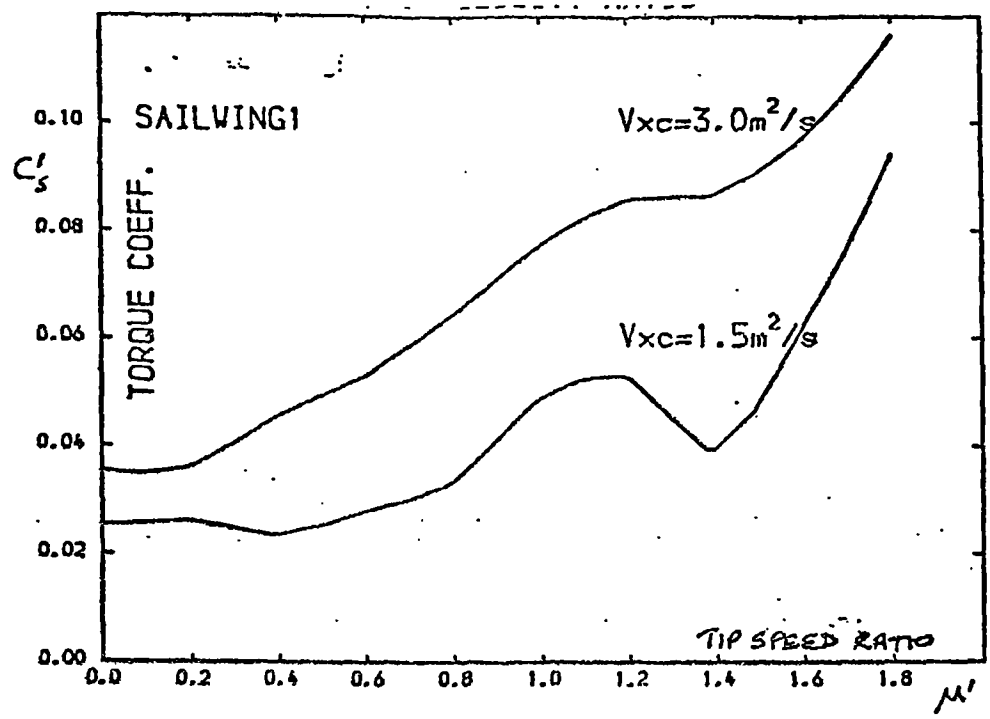

Fig.2.11. Mean torque coefficients vs. tip-speed ratio for sailwing1 with varying scale.

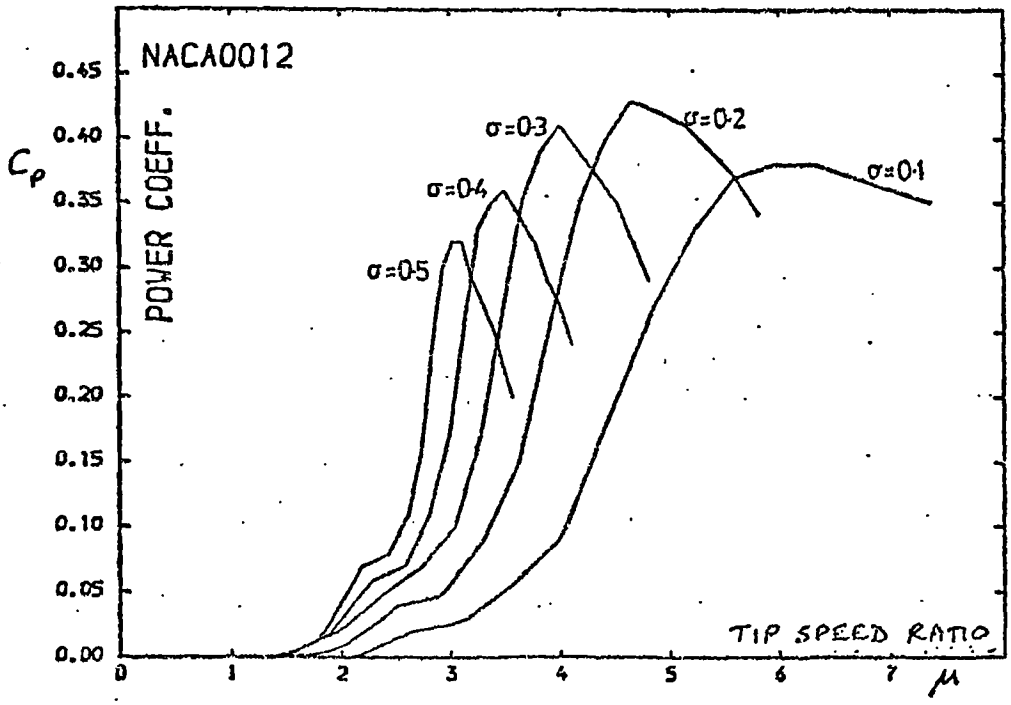

Fig.2.12. Power coefficient vs. tip-speed ratio.

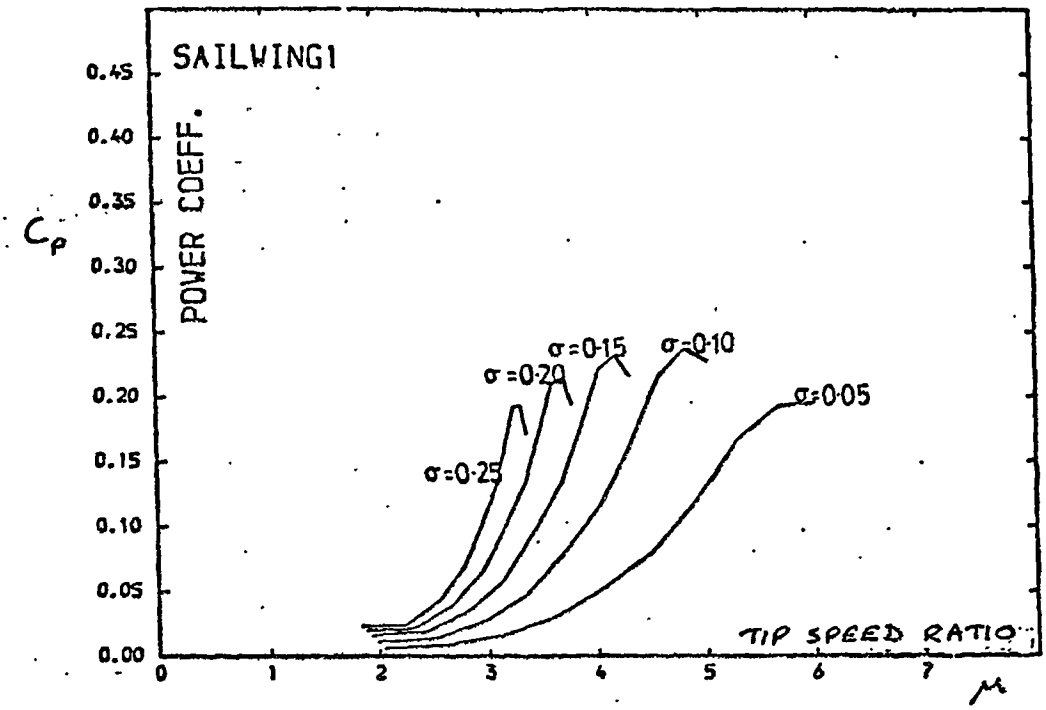

Fig.2.13. Power coefficient vs. tip-speed ratio.

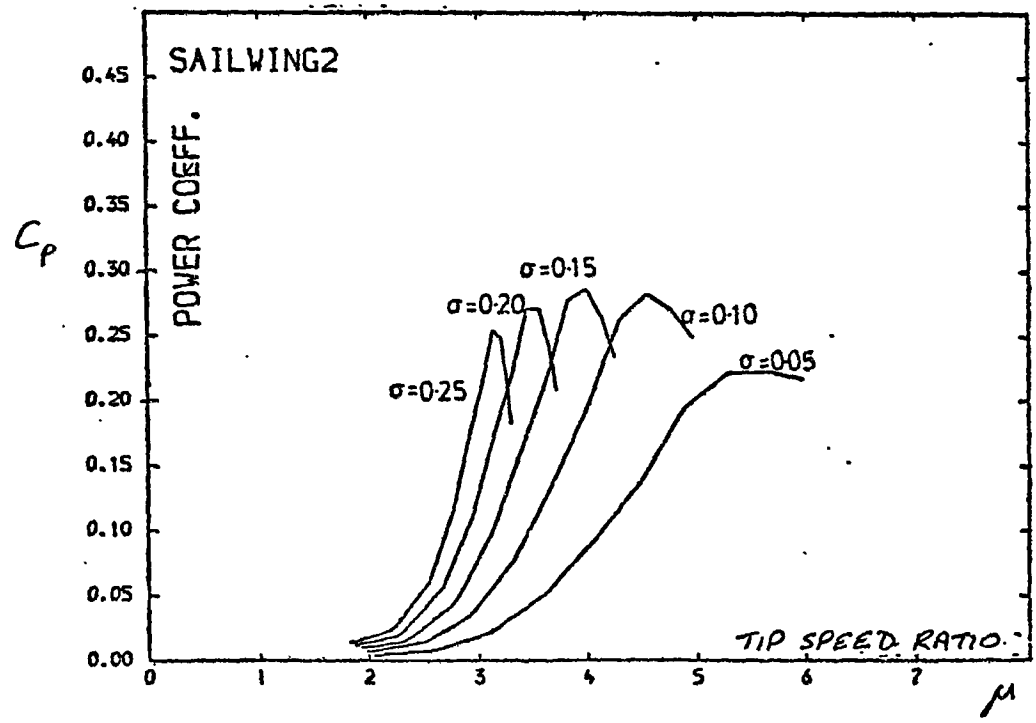

Fig.2.14. Power coefficient vs. tip-speed ratio.

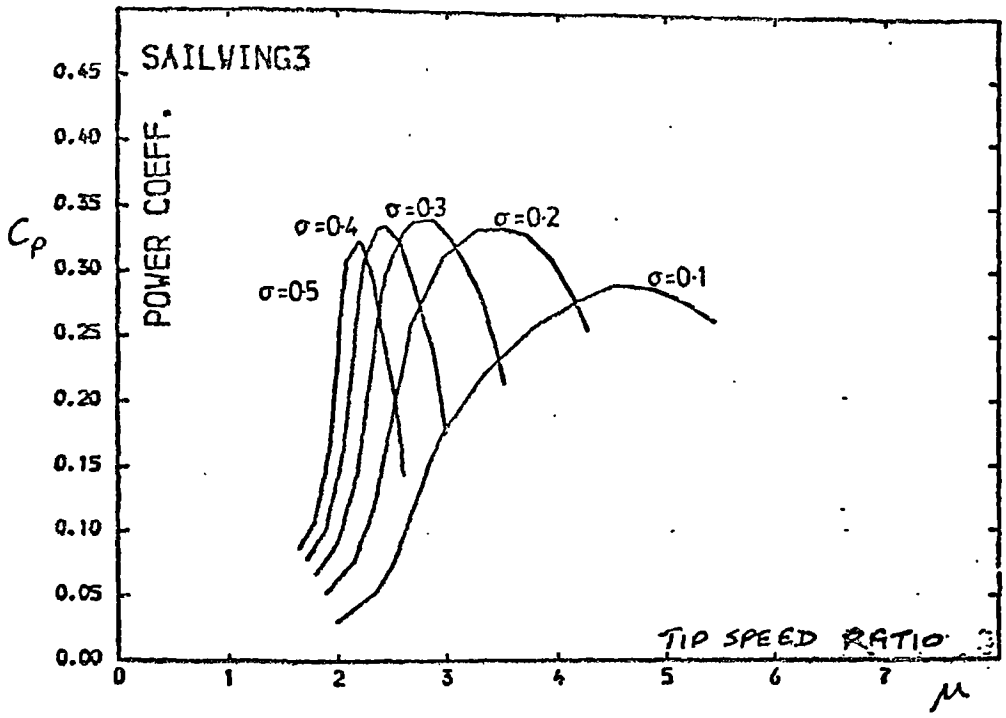

Fig.2.15 Power coefficient vs. tip-speed ratio.

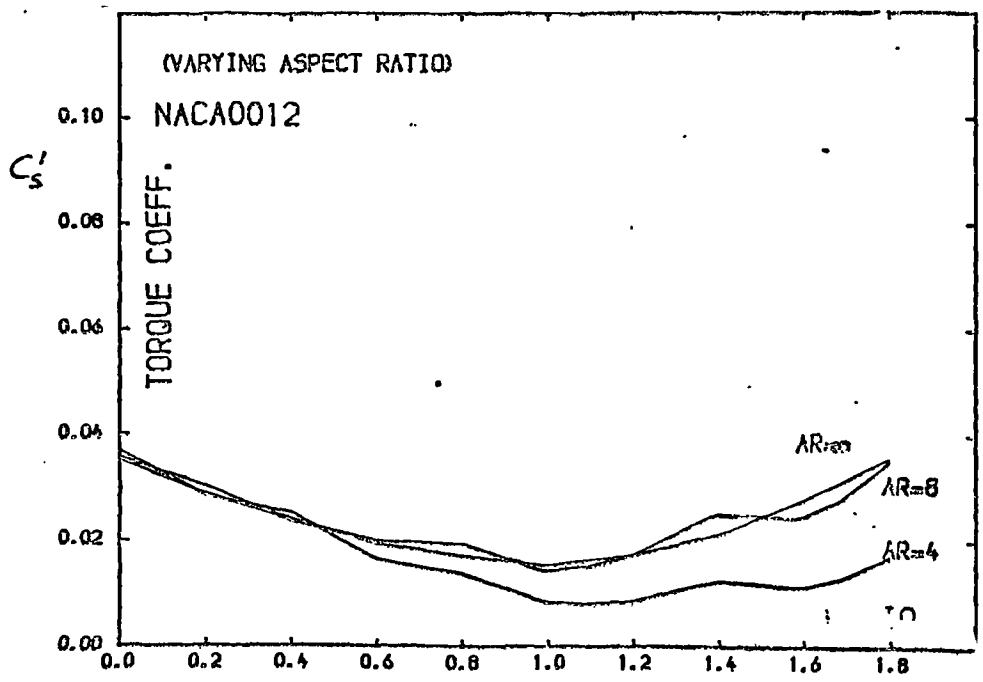

Fig.2.16. Mean torque coefficient vs. tip speed ratio. (solid aerofoil, varying aspect ratio)

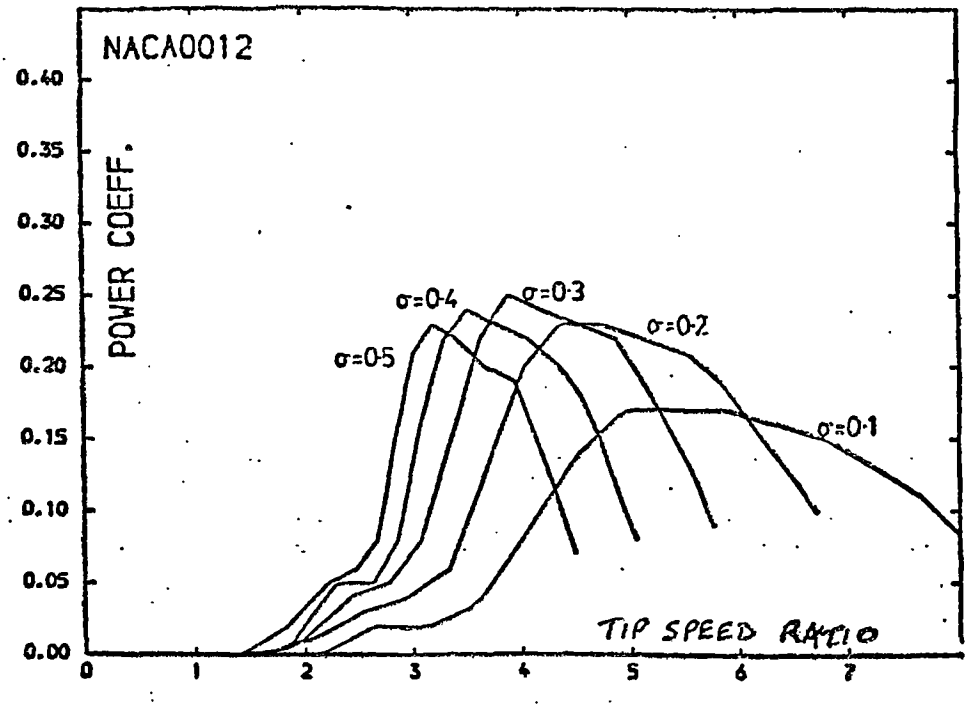

Fig.2.17. Power coefficient vs. tip-speed ratio for solid aerofoil with AR=4

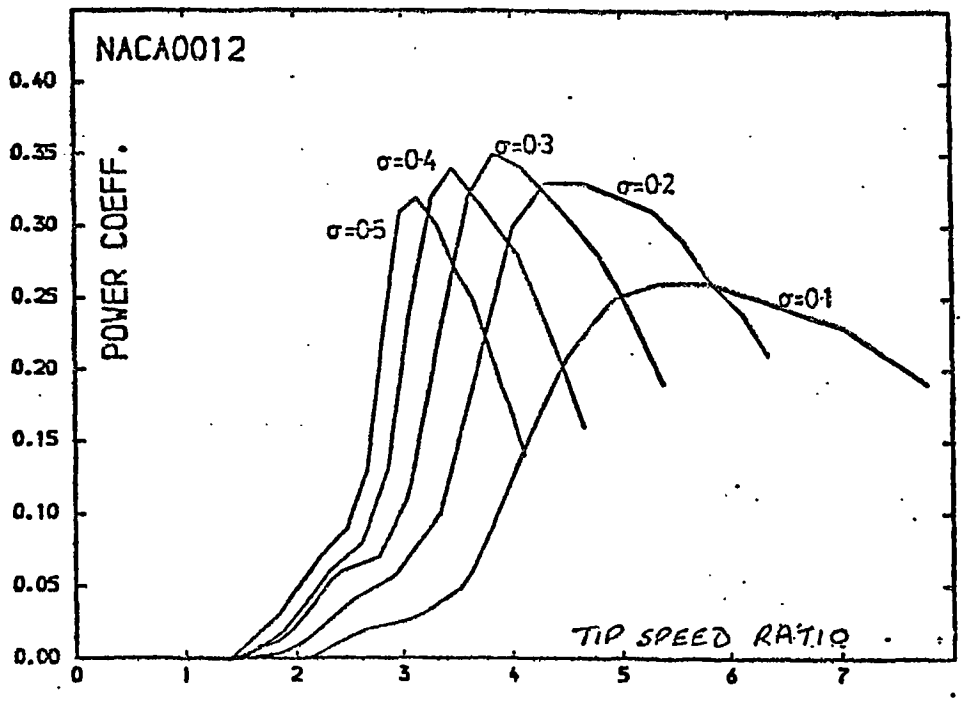

Fig.2.18. Power coefficient vs. tip-speed ratio for solid aerofoil with AR=8

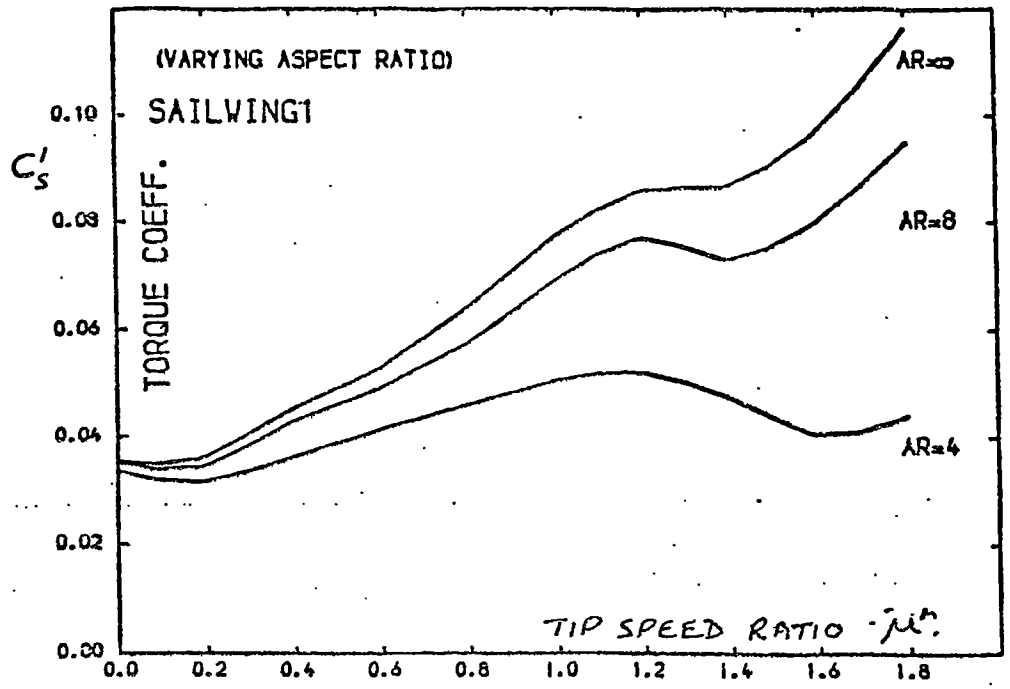

Fig.2.19. Mean torque coefficient vs. tip speed ratio Sailwing 1, varying aspect ratio.

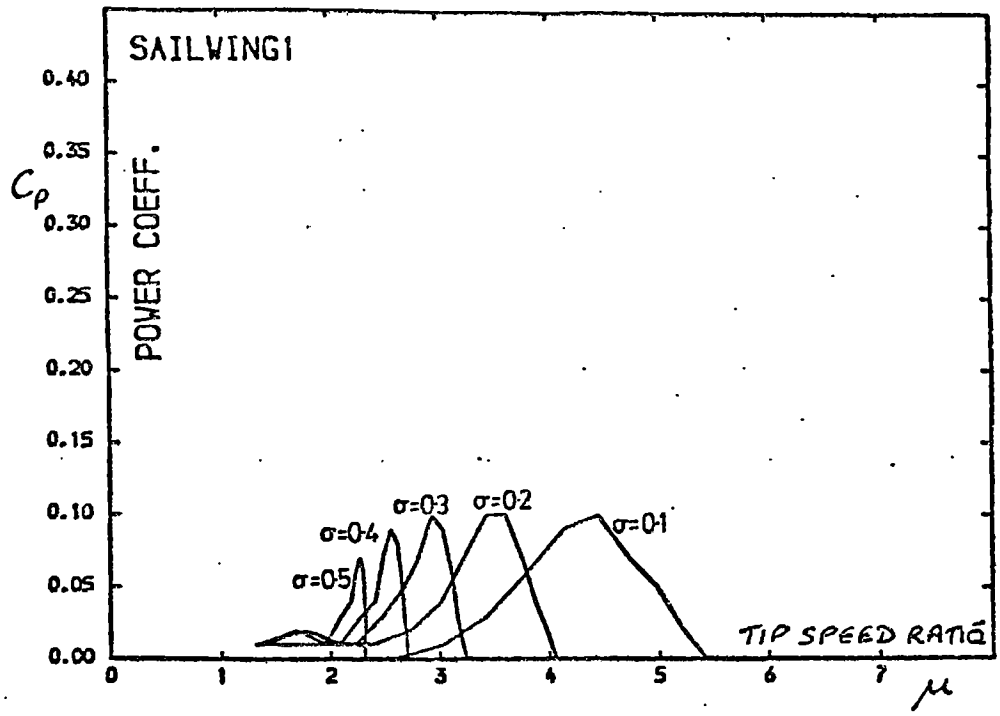

Fig.2.20. Power coefficient vs. tip-speed ratio for sailwing1 with AR=8

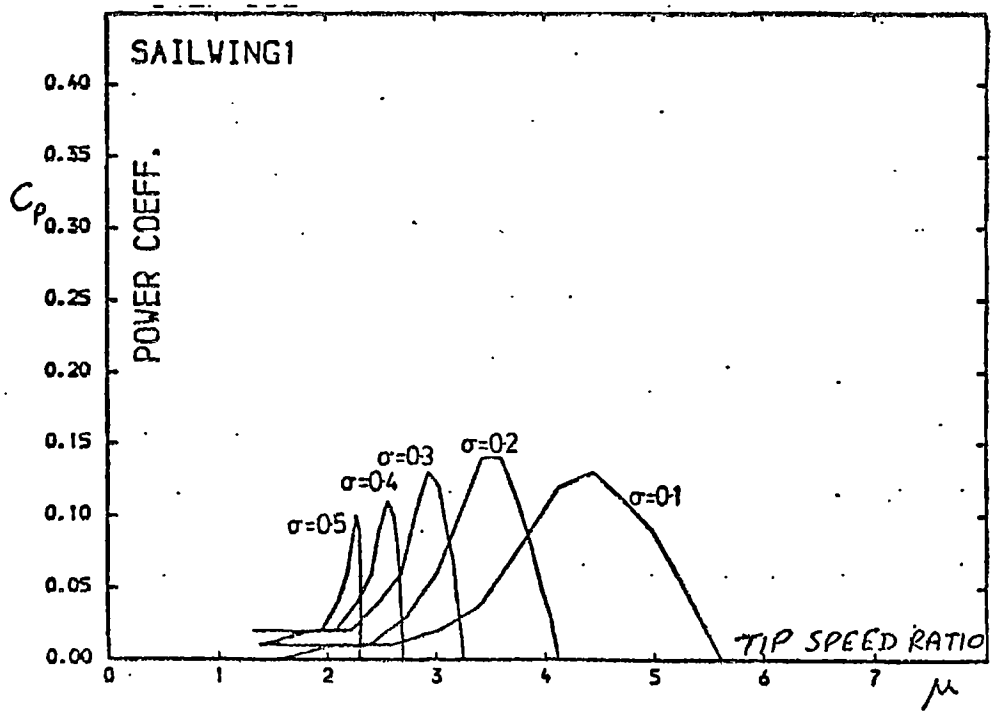

Fig.2.21. Power coefficient vs. tip-speed ratio for sailwing1 with AR=10

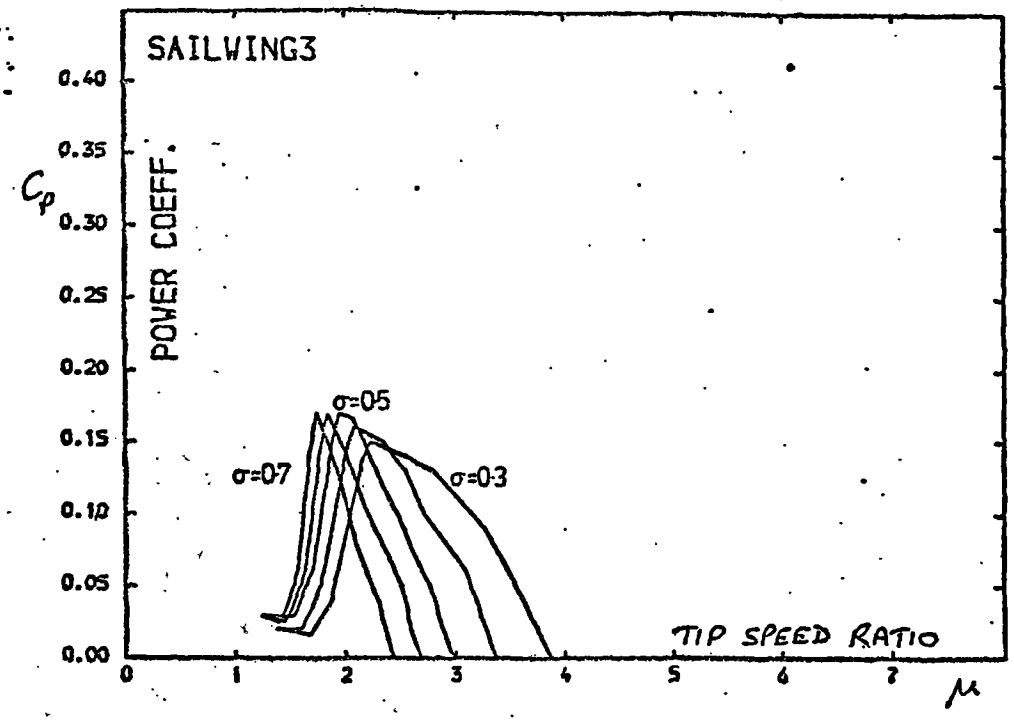

Fig.2.22. Power coefficient vs. tip-speed ratio for sailwing3 with $AR=4$

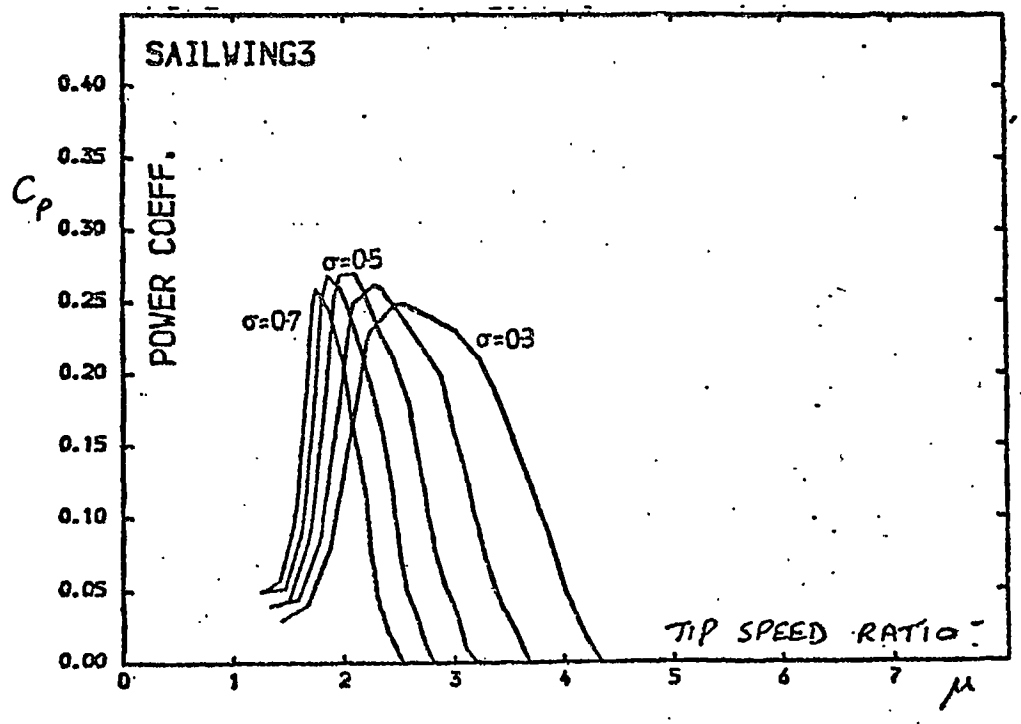

Fig.2.23. Power coefficient vs. tip-speed ratio for sailwing3 with $AR=8$

2.4. Discussion

From the results of this analysis, it would appear possible to achieve high tip speed operation of a sailwing vertical axis wind turbine. If this is the case then structural design may be rather difficult. A large load must be carried by the leading edge dowel of a sailwing in this application. It must transmit most of the aerodynamic load as well as resisting the membrane tension and centrifugal loads. If the solidity required is low, as with the nylon sailwing, then this problem is especially difficult and extensive bracing, with associated parasitic drag, may be necessary. The performance at the higher tip speed ratios does appear to be slightly better with the larger diameter leading edge dowel, but this improvement is unlikely to continue if the diameter were increased further. The need to keep the aspect ratio high adds to the problem. Clearly the design would be much easier with the 'Dacron' sailwing, the characteristics of which produce a lower optimum tip speed ratio, an increased optimum solidity and a reduced sensitivity to aspect ratio.

However, the results of the analysis are in particular doubt at the higher tip speed ratios. Then, the turbine performance depends on the value of the tangential force coefficient C_T prior to stall. The value of this coefficient is in some doubt, both because of the uncertain error in its calculation and because it is not known how sensitive it is to the pre-tension in the membrane. For the trailing edge to remain rigid at high tip speed ratios, when the relative windspeed is likely to be high, would require a high pre-tension. This is in contrast to the very low pre-tension

apparently used in arriving at the present data. It may be that some deflection of the trailing edge would not be detrimental to the turbine performance but too slack a sail could become unstable.

Before proceeding further, there would seem to be a need to investigate the effect of pre-tension on the sailwing performance, to investigate the effect of trailing edge deflections and to try to ascertain what the important fabric properties determining sailwing behaviour really are. It seems strange that the stiffness of the 'Dacron' can make such a difference to its aerodynamic performance.

It is clear that the low tip speed ratio performance of vertical axis wind turbines should be much improved if sailwings rather than solid aerofoils are used. The performance seems likely to be adversely affected if the scale is too small. For the small scale applications envisaged for such a rotor the blade chord will inevitably be rather less than one metre and so the product $V_w \times c$ is unlikely to be above about 1.5 m^2/s in low winds. The starting torque coefficients will therefore be lowest in light winds, which is unfortunate but presumably not unique to this type of turbine. From this analysis it also seems that too low an aspect ratio will adversely affect the low tip speed ratio performance. Whether this is actually the case will depend on how the aerofoil performance after stall is changed by a low aspect ratio. In this analysis, no change has been assumed but from the observations of Mays and Musgrove (1978) it seems possible that there is actually some benificial effect on the tangential force coefficient after stall. They reported

much improved starting with a Darrieus turbine when low aspect ratio blades were used in a high solidity design. This would not seem to be explained entirely by the increased solidity.

No clear optimum has emerged for the ratio of leading edge diameter to blade chord. The smaller diameter appears to give a marginal improvement at low tip speed ratios and the larger diameter at higher tip speed ratios. However, the differences hardly seem significant in view of the uncertainties in the analysis.

2.5. Conclusions

It is clear that a theoretical analysis of the performance of Darrieus type turbines becomes more difficult when sailwings rather than solid aerofoils are employed. This is because of the number of variables which could affect the sailwing behaviour.

Before constructing a sailwing turbine, it appears desirable to have more extensive data on the aerodynamic performance of sailwings, in particular with concern to the effect of pre-tension in the sail fabric and to the effect of different fabric properties.

Some firm conclusions may be drawn from the analysis:

1. Sailwing vertical axis wind turbines should have much better starting characteristics than solid bladed turbines, due to the high lift coefficients of sailwings at angles of incidence between about 30 and 70 degrees.

2. The starting performance will be adversely affected if the product of windspeed with blade chord is too low (less than about 3 m^2/s).

3. If high tip speed ratio operation is reached, then a high aspect ratio will be necessary to obtain reasonable power coefficients. This is due to the high lift coefficients of sailwings, and hence the high induced drag losses of a low aspect ratio blade.

CHAPTER THREE

WIND TUNNEL TESTS OF SAILWINGS

3.1. Introduction

A series of wind tunnel tests on sailwings has been made. The main purpose of these tests was to investigate the effect of pre-tension in the fabric and the performance of different sail fabrics. It was also hoped to investigate the effect of trailing edge deflection on the aerodynamic characteristics. The tests that were carried out are detailed in Table 3.1. All the tests were made at a Reynolds number of about 20.10^4.

The data obtained in the tests has been compared with that of Robert and Newman (1979), used in the analysis of the previous chapter and also with data for a limited range of angles of incidence by Buehring (1977).

To perform the tests, a measuring balance had to be designed for the blowdown wind tunnel in the Dept. of Engineering at the University of Warwick. The calibration of this was checked by testing a standard aerofoil section (NACA0012).

To make the data as useful as possible for predicting the performance of a vertical axis wind turbine, the measuring balance was designed to give direct measurement of the force acting along the aerofoil chord, to give values of the tangential force coefficient C_T, and of the force normal to this. However, the lift and drag coefficients have also

been derived, so that the data is also presented in standard form. A few tests were made using a pre-tensioned and curved, elastic trailing edge line, in place of the rigid trailing edge otherwise used.

The application of the data obtained from tests on sailwings is not entirely straight-foward because of the large number of variables which may be involved. Apart from the Reynolds number; the elastic properties, stiffness, density, porosity and pre-tension of the sail fabric may have to be considered. If deflection of the trailing edge occurs, then the elasticity, pre-tension and curvature of this, and also the blade geometry, are further variables. In the following tests, a number of dimensionless parameters have been used:

$\frac{\rho_F}{\rho c}$ the non-dimensional density of the fabric, where ρ_F is its mass per unit area, ρ the air density and c is the blade chord.

$C_{P_T} = \frac{P_T}{\frac{1}{2}\rho V_R^2 c}$ the tension coefficient for the membrane, where P_T is the pre-tension per unit length and V_R is the relative windspeed.

$Re = \frac{\rho V_R c}{\mu_{air}}$ the Reynolds number, based on blade chord.

$\frac{E_T}{T_T}$ where E_T is the ratio of force/strain for the trailing edge line and T_T is its pre-tension.

$C_{T_T} = \frac{T_T}{\frac{1}{2}\rho A_B V_R^2}$ the tension coefficient for the trailing edge line, where A_B is the area of one blade ($A_B = bc$).

$\frac{b}{c}$ the blade length to chord ratio.

$\frac{b}{x}$ the ratio of blade length to maximum hollow in the trailing edge.

The membrane and trailing edge tension coefficients are related by the blade geometry. When the trailing edge hollow is small, the relationship is: $C_{p_T} = C_{T_T} \cdot \frac{x}{b} \cdot \beta$ (Appendix3)

By performing a number of tests with various materials and pre-tensions and with both a rigid and elastic trailing edge, it was hoped that it would be possible to assess the relative importance of the various factors involved.

Measurements were also made of the chordwise component of the membrane tension; the value of this is required for the structural design.

3.2. Experimental Apparatus

The blowdown wind tunnel used for the tests has a working cross-section of about 1.3m x1.1m. The aerofoils were mounted horizontally and supported in a bearing at each end (Figs.3.1 and 3.2). A flexure element was conneeted between the aerofoil and one of the bearings. This flexure element was machined from an aluminium block and strain-gauged to provide measurement of the chordwise and normal force components on the aerofoil. The strain-gauges are connected in such a way as to eliminate interference from pitching moments (Fig.3.3). The universal joints on each side serve to accomodate slight misalignment between the bearings, without the flexure element being stressed and also, to ensure that the strains in the flexure are dependent solely on the shear forces and so independent of the flexural stiffness of the aerofoils. There was a small clearance between the ends of the aerofoils and the tunnel walls of about 3mm maximum.

The windspeed in the tunnel is about 25m/s and not easily variable; all the tests were therefore made at a Reynolds number of about 20.10^4, using a blade chord of 0.13m. For the sailwing leading edge, an aluminium rod of 13 mm diameter was used. For strength reasons, it was necessary to have a rib at mid-span. This gave; $\frac{t}{c} \approx 4$ and $\frac{d}{c} = \frac{1}{10}$.

Most of the tests were made using a rigid trailing edge. This was made of sheet metal, formed as in Fig.3.4. The pins at either end allowed it to swivel and so not interfere with the natural profile assumed by the sail. Tensioners on the endplates allowed a crude adjustment of the pre-tension

applied to the membrane. This tension was measured by the strain-gauges on the leading edge rod.

For those tests in which a pre-tensioned, elastic trailing edge was used, the trailing edge was given a curve in the form of a circular arc, with the maximum hollow equal to 3% of the blade length (Fig.3.5.). The tension in the trailing edge was set using a torque wrench.

The apparatus was calibrated using weights. This showed that there was negligable interference between the measurements of the force components and no discernable effect from pitching moments. To check the calibration and the behaviour of the apparatus, measurements were made using a NACA0012 aerofoil section. The lift and drag coefficients have been calculated from the measurements and are plotted in Fig.3.6. The results have been corrected for wake blockage using Maskells correction (see below). The results are compared with the data given by Shankar(1976) for this section and with data reported by Pope (1949) for the slightly thicker NACA0015 section. The lift curve slope prior to stall was 0.093 per degree and stall occurred at an angle of incidence of 7.5 degrees. The drag coefficient at zero incidence was measured as 0.008. Above stall, agreement is better with Pope than with the data given by Shankar. The data given by Shankar was derived from results reported by Critzos et al (1955), who seem to suggest that the disagreement between their data and that of Pope, might be due to some flow past the blade tips in Pope's tests, at angles of incidence around 90 degrees. This seems a possible explanation for the rather low peak drag coefficient measured here; for a flat

plate of infinite aspect ratio, Massey (1970) gives a drag coefficient of 2.01, but this is very sensitive to aspect ratio, being reduced to e.g. 1.40 at an aspect ratio of 18. This would actually make the data more valid for application to a straight bladed, Darrieus type turbine.

Generally, the results give confidence in the functioning and calibration of the balance. The calibration was repeated at regular intervals during the tests and showed no significant variation.

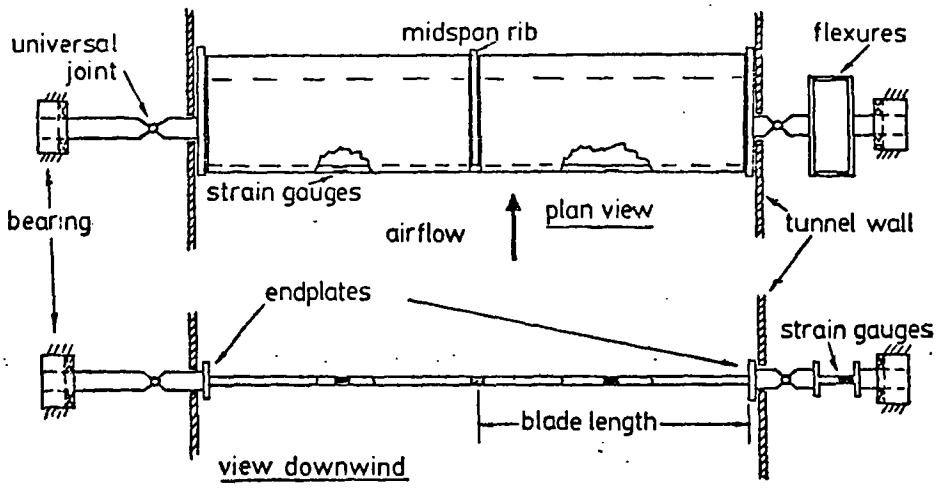

Fig.3.1. Experimental set-up.

Test	Membrane	Density ρ_F g/m²	Proofing	Pre-tension P_T N/m	Trailing Edge	ϵ_T/T_T	C_{TT}	C_{PT}	$\frac{\rho_F}{\rho.c}$
Ca1	Canvas	134	none	110	Rigid			2.2	0.9
Ca1p	Canvas	134	wax	110	Rigid			2.2	0.9
Ca2p	Canvas	134	wax	10	Rigid			0.2	0.9
Ny1	Spinnaker Nylon	72	none	140	Rigid			3.0	0.5
Ny2	Spinnaker Nylon	72	none	20	Rigid			0.4	0.5
Ny1p	Nylon	67	Polyurethane	100	Rigid			2.0	0.4
Ny2p	Nylon	67	Polyurethane	30	Rigid			0.6	0.4
Dac1	Dacron	180	none	140	Rigid			3.0	1.2
Dac2	Dacron	180	none	80	Rigid			1.6	1.2
Dac3	Dacron	180	none	30	Rigid			0.6	1.2
Ny1w	Spinnaker Nylon	72	none	80	Wire	320	6.5	1.6	0.5
Ny2w	Spinnaker Nylon	72	none	50	Wire	510	4.1	1.0	0.5
Ny1n	Spinnaker Nylon	72	none	80	Nylon	20	6.5	1.6	0.5
Ny2n	Spinnaker Nylon	72	none	50	Nylon	31	4.1	1.0	0.5

Table 3.1.

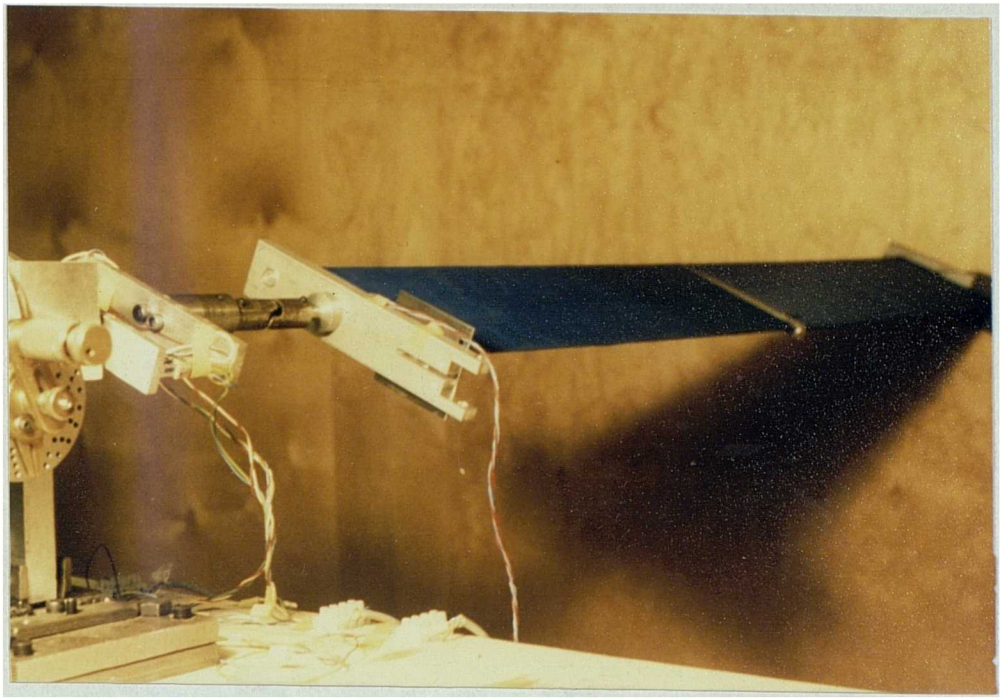

Fig.3.2. View of experimental set-up with the tunnel wall removed.

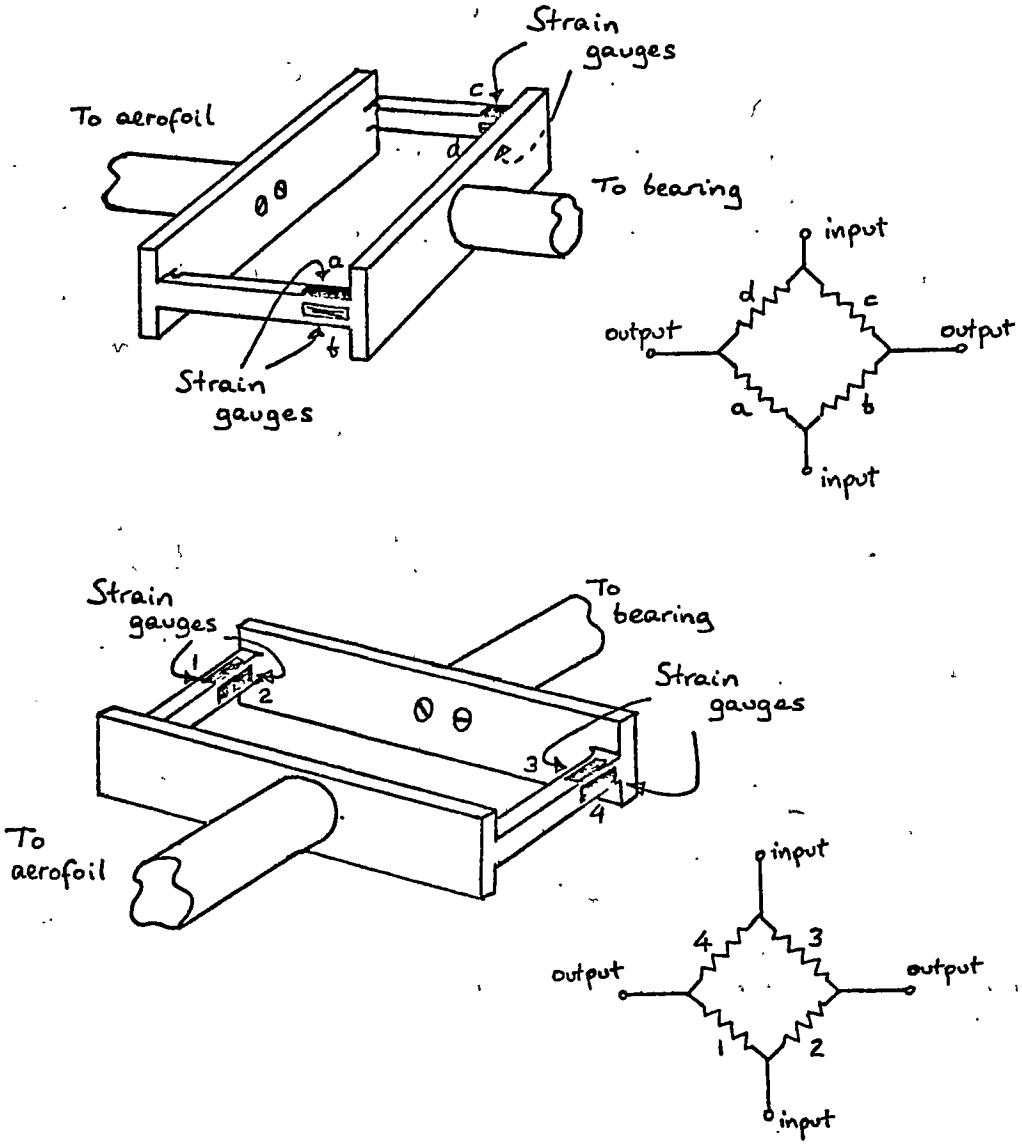

Fig.3.3. Arrangement of the flexures and strain gauge bridges.

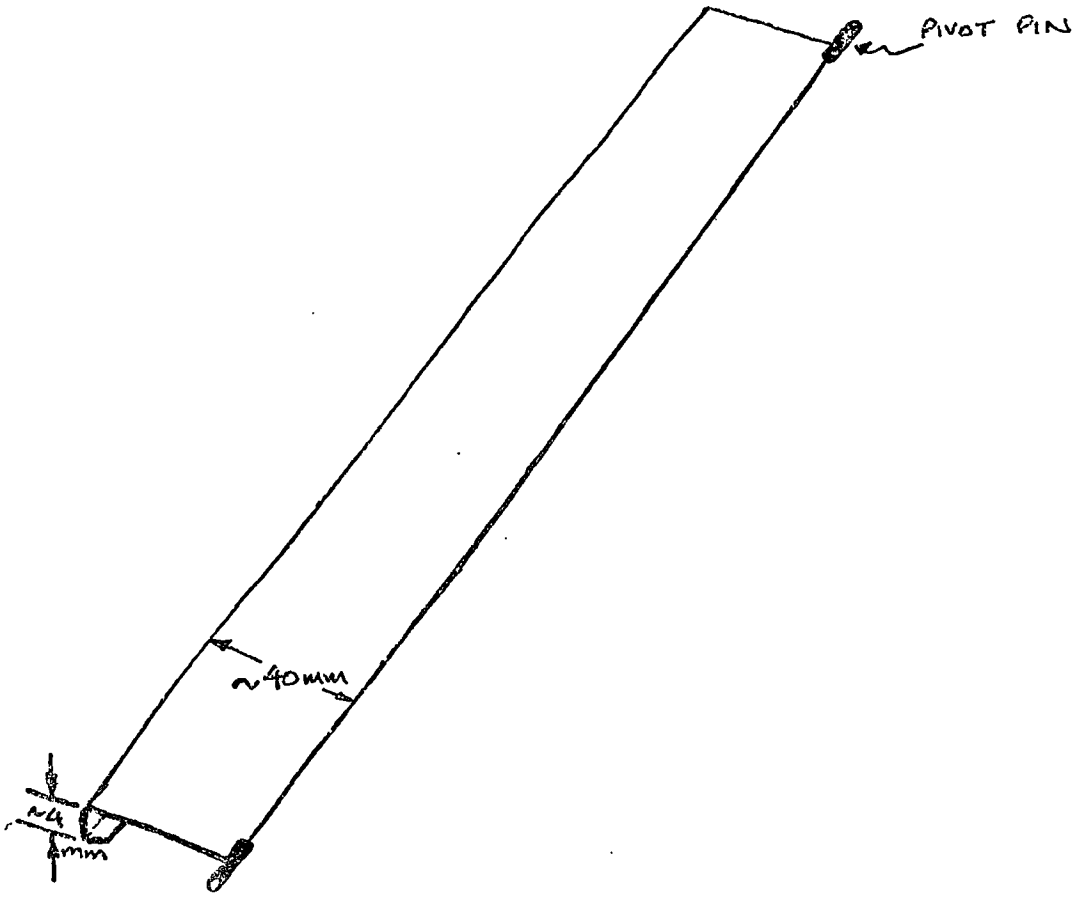

Fig.3.4. Rigid trailing edge.

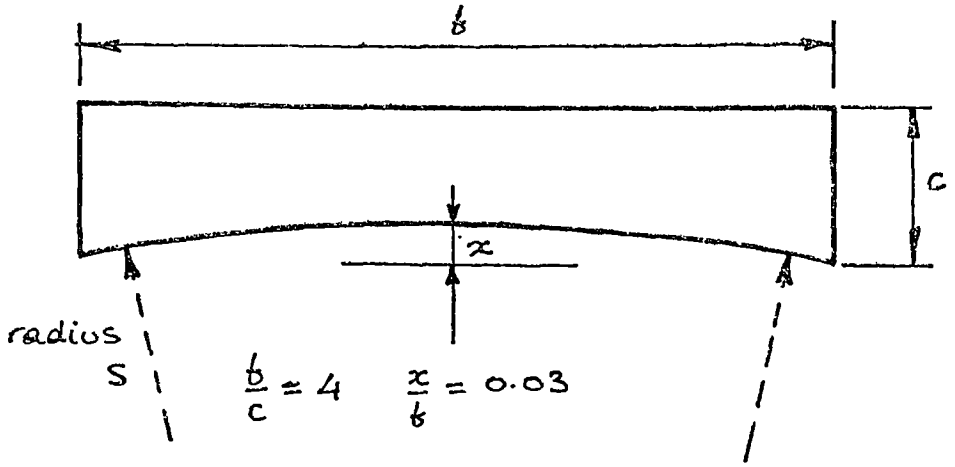

Fig.3.5. Blade geometry for elastic trailing edge tests.

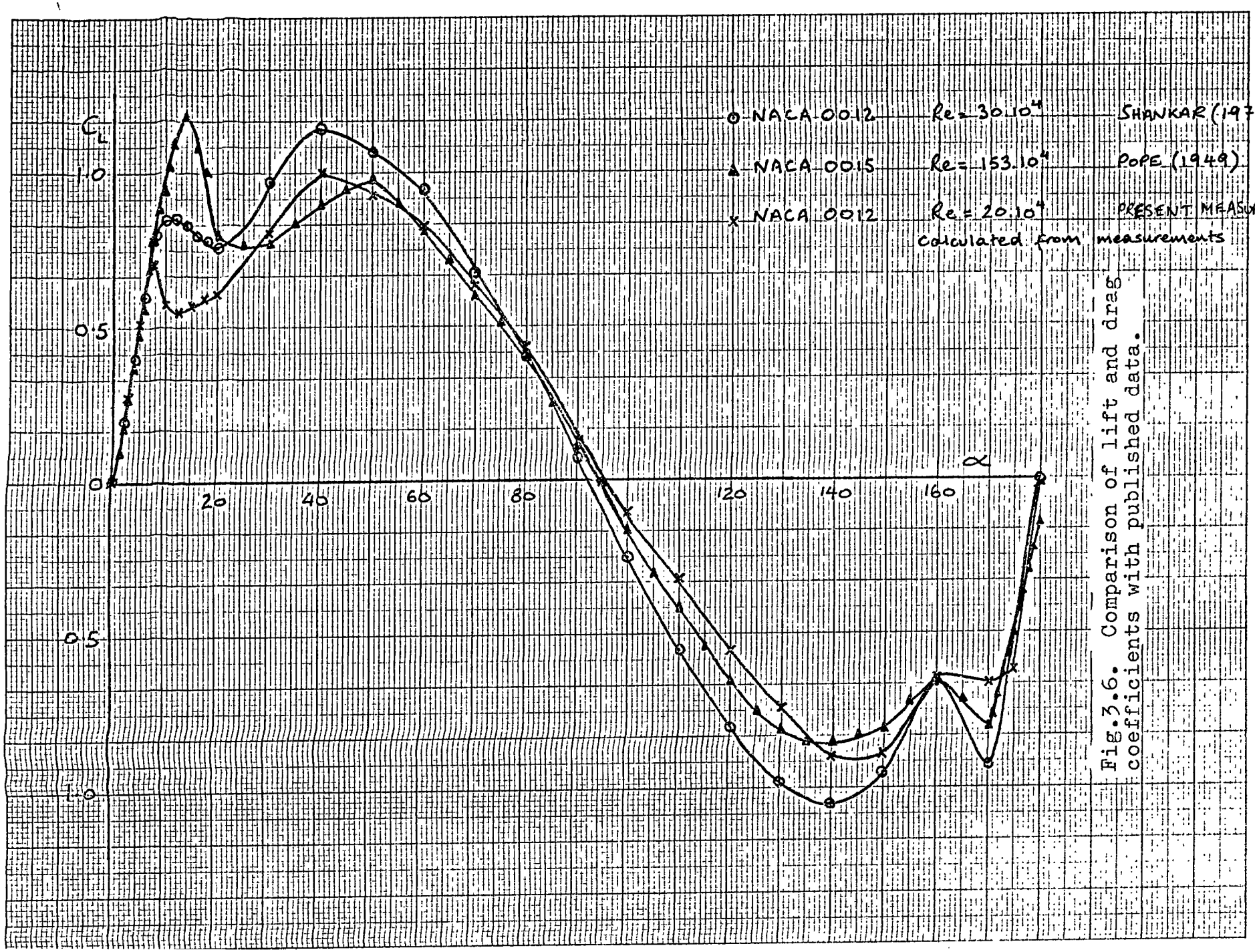

Fig.3.6. Comparison of lift and drag coefficients with published data.

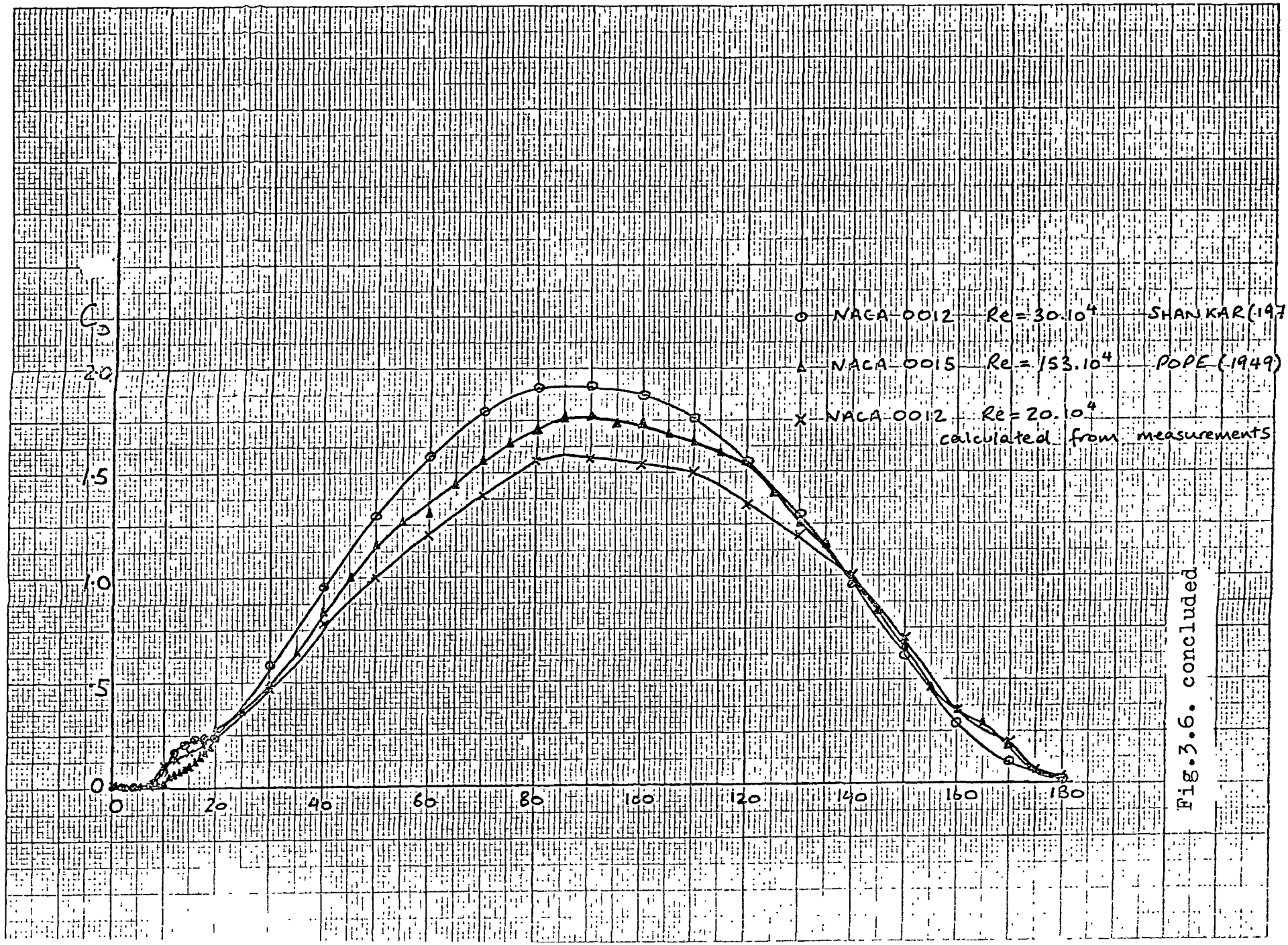

Fig.3.6. concluded

3.3. Test Details and Procedure

Four different sailwing fabrics were tested. These were: canvas, spinnaker nylon, polyurethane coated nylon and 'Dacron' - a polyester material. The choice of fabrics was mainly determined by what it was possible to obtain. The canvas was tested both unproofed and proofed with a wax solution - 'Mesowax'. The elasticity of the fabrics was measured in a tensile test machine with specimens 16mm wide and 150mm long. This gave the values given in Table 3.2. These values should be regarded as approximate as the extension was slightly non-linear at low loads, particularly with the canvas.

Specimens 16mm wide x 150mm long	
Canvas	0.3 mm/N
Spinnaker Nylon	0.3 mm/N
Coated Nylon	0.5 mm/N
'Dacron'	0.08 mm/N

Table 3.2.

The fabrics were oriented with the thread directions running chordwise and spanwise. No attempt was made to measure the porosity or stiffness of the fabrics. The unproofed canvas was quite porous, the spinnaker nylon slightly so and the other fabrics effectively non-porous. The 'Dacron' was very much stiffer than any of the other fabrics.

All the fabrics were tested with the rigid trailing edge at both high and low pre-tensions. The possible error in the measurement of pre-tension may be about $\pm$10% (Appendix 3). For the tests with an elastic trailing edge, the spinnaker nylon was used. Two different trailing edge lines were used:

1mm diameter stranded steel wire and 2mm diameter nylon cord (E_T=50.7 kN/unit strain and E_T =3.1 kN/unit strain respectively). These tests were only done for low angles of incidence.

All the measurements were corrected for wake blockage using Maskells correction for a closed tunnel (Maskell,1963). This gives a simple expression for the change in dynamic pressure due to the flow blockage caused by the wake:

$$\Delta p = \rho \varepsilon C_D' r_B$$

The dynamic pressure ρ was measured by pitot-static tube while there was no obstruction in the tunnel. The blockage factor ε was taken from Maskell as 0.96. The drag coefficient C_D' was calculated from the measured drag force using the uncorrected dynamic pressure. The blockage ratio r_B is simply: $r_B = \frac{c \sin\alpha}{1.3}$, 1.3m being the tunnel height. The maximum blockage ratio was therefore equal to 0.1 and the maximum blockage correction was nearly 15% at angles of incidence near 90 degrees.

Other tunnel interference effects were assumed to be negligable but corrections were applied for the tare drag of the sailwing endplates. This drag was measured directly, with just the endplate nearest the flexure in position, the universal joint being replaced by a rigid connection. The tare drag corrections to the radial force coefficient C_R were negligable but reached 0.005 for the tangential force coefficient C_T at angles of incidence of 30 and 150 degrees.

The voltage outputs from the strain gauge bridges were amplified and measured using a digital voltmeter. Readings were taken at intervals of 2.5 degrees in the angle of incidence up to 20 degrees and at 10 degree intervals thereafter. Reading errors were minimised by doing repeat tests so that at least three readings were taken at each position. The accuracy of the coefficients C_T and C_R is thought to better than $\pm$ 0.004 and $\pm$ 0.01 respectively, except for angles of incidence between about 60 and 100 degrees where vibration of the apparatus occurred and accurate measurement was more difficult. Then the accuracy is thought to be better than about $\pm$ 0.03 and $\pm$ 0.1 respectively.

Apart from measuring the pre-tension, the strain gauges on the leading edge provided readings of the induced tension in the membrane. The induced tension coefficient is defined as:

$$C_x = \frac{\text{chordwise component of induced membrane tension}}{\frac{1}{2}\rho V_R^2 c}$$

The accuracy of this measurement is probably only $\pm$ 20%.

3.4. Results

The vibration of the apparatus, found to occur with angles of incidence between about 60 and 100 degrees, was not caused by any flapping of the sail itself, which proved to be stable at all angles of incidence when a rigid trailing edge was used. With an elastic trailing edge, some flapping of the sail did occur near zero incidence, particularly with the nylon cord, which was unstable up to $\alpha = 5^\circ$, with the lower tension.

3.4.1. Solid Aerofoil and Rigid Trailing Edge Tests

The measured results are presented in terms of the force coefficients C_T and C_R :

The tangential force coeff. C_T = Force acting along aerofoil chord/$\frac{1}{2}\rho A_B V_R^2$

The radial force coeff. C_R = Force acting normal to aerofoil chord/$\frac{1}{2}\rho A_B V_R^2$

These results are plotted in Figs.3.7 to 3.14 It can be seen that the pre-stall performance of the sailwings was generally very poor compared to the solid aerofoil. Positive values of C_T were only obtained with low pre-tension and strongly negative values occurred at and near zero incidence. Stall occurred at an angle of incidence of about 8 degrees. After stall, the values of C_T measured with the solid aerofoil are higher than those previously calculated from the lift and drag data (chapter 2).

The curves of C_T values for the sailwings have a rather different shape to that of the solid aerofoil. In particular, the peak value occurs at a lower angle of incidence, which may be attributed to the induced camber of the sailwings. The difference is most marked with the canvas sailwings; these gave rather higher peak values than the other fabrics and also appear to be more sensitive to the pre-tension, particularly at around 120 degrees incidence.

Lift and drag coefficients have been calclulated from the measurements and are plotted in Figs.3.15 to 3.23. Seperate curves have been drawn for angles of incidence up to 20 degrees (Fig.3.21 to 3.23). These curves allow a comparison with previous data and also show why it was considered important to measure the tangential force coefficient directly as significant changes in the value of C_T with pre-tension are not readily apparent from the lift and drag coefficient curves. In Figs.3.16 3.19 and 3.22, the data from Robert and Newman (1979) for a nylon sailwing (sailwing 2 in the previous chapter) is included for comparison. The lift slope, the stall angle and the drag coefficient at zero incidence agree well but otherwise the agreement is not good. At high angles of incidence the discrepancy may be due to some flow over the blade tips in the present tests. In Fig.3.23 the results for the 'Dacron' sailwings are compared. The high lift coefficients and very late stall reported by Robert and Newman were not repeated in the present tests. It should be noted that at zero incidence the sailwings were stable with either camber and that there was a small area of hysteresis at very low incidence. Fig.3.24 shows the results reported by Buehring (1977). The pre-tension was not measured and nor is the sail material specified but the results seem to support the present measurements.

It is difficult to assess the influence of the various fabric properties on the sailwing performance. The 'Dacron' sail was stiff and quite inelastic in comparison to the coated nylon, yet the results for these two materials, with similar pre-tensions, show no distinct differences. From the results for the nylon and canvas sailwings, porosity* seems to have an effect on the tangential force coefficient prior to stall. The reason for the different behaviour of the canvas sails at high angles of incidence is not evident. It is speculated that perhaps it is due to the rather non- linear elasticity of the canvas.

Before stall the pre-tension is clearly a dominant factor, with reduced tension giving higher tangential force and lift coefficients. Above stall, an increase in pre-tension generally increases the tangential force coefficient, and this is particularly so with the canvas. With a much higher pre-tension coefficient, a sailwing would, presumably, tend to behave more as a solid aerofoil.

* note: there was no significant change in surface roughness between the proofed and unproofed nylon.

3.4.2. Elastic Trailing Edge Tests

Measured force coefficients for the tests with an elastic trailing edge are shown in Figs.3.25 and 3.26. Lift and drag coefficients have also been calculated (Fig.3.27 & 3.28). The results for the rigid trailing edge test Ny2 are included for comparison.

When deflection of the trailing edge occurs, the aerofoil camber will increase and twisting of the sail will increase the mean pitch. The two effects are not separable but depend on the pre-tension and elasticity of both the sail fabric and the trailing edge line.

The effect of trailing edge deflection on the tangential force coefficient, in particular, is clearly considerable. Above about 7.5 degrees incidence C_T becomes positive and remains so. However, at low incidence, when instability occurs, the magnitude of the negative values becomes greater. The increase in drag coefficient at very low incidence is clear in tests Ny1n and Ny2n in Fig.3.28. From the lift curve, it can be seen how the change in pitch reduces the slope of the curve and how a later and more gradual stall occurs. With a wire trailing edge, it can be seen that a small reduction in tension gives a small increase in the maximum lift coefficient, due to an increase in camber, but also causes an increase in the drag coefficient, so the net effect is to reduce the value of C_T. With the much more elastic, nylon trailing edge, the effect of reducing the tension is to allow a change of pitch, increasing the sail twist, so that stall becomes even more gradual; the maximum lift coefficient is reduced and the drag appears unchanged. The net effect is again to reduce the value of C_T.

With the blade geometry used here, and over the small range of tensions tested, it seems that a higher tension in the trailing edge leads to a general improvement in the tangential force coefficient. However, a much larger increase in the pre-tension would presumably give an opposite effect; the trailing edge tending to become rigid.

3.4.3. The Induced Tension Coefficient

The measurements of the induced tension coefficient C_x, are plotted in Fig.3.29 & 3.30. It can be seen that an increase in the pre-tension reduces the maximum coefficient value. The maximum value measured for the nylon sailwings agrees well with the value of 'between 3 and 4' reported by Robert and Newman (1979) for a nylon sailwing (Sailwing 2).

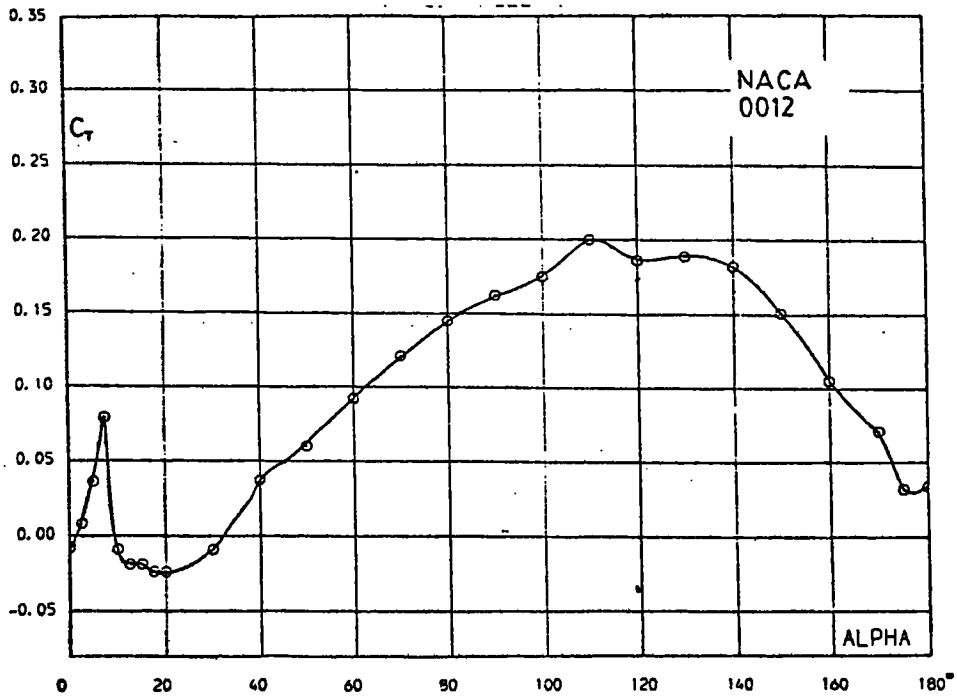

Fig.3.7. Tangential force coefficient vs. angle of incidence for NACA0012 aerofoil.

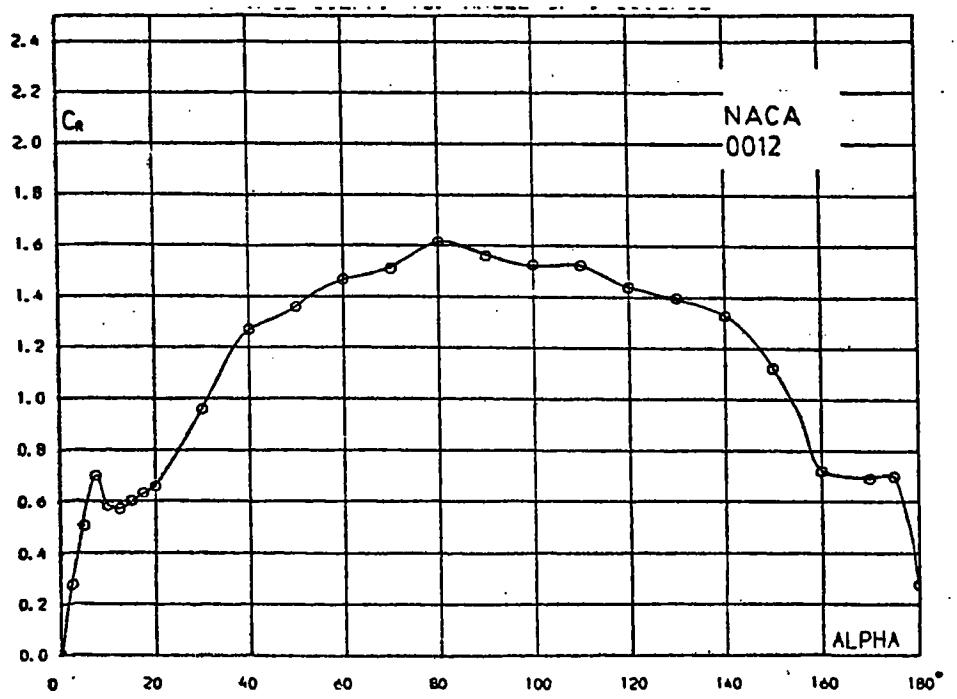

Fig.3.8. Radial force coefficient vs. angle of incidence for NACA0012 aerofoil.

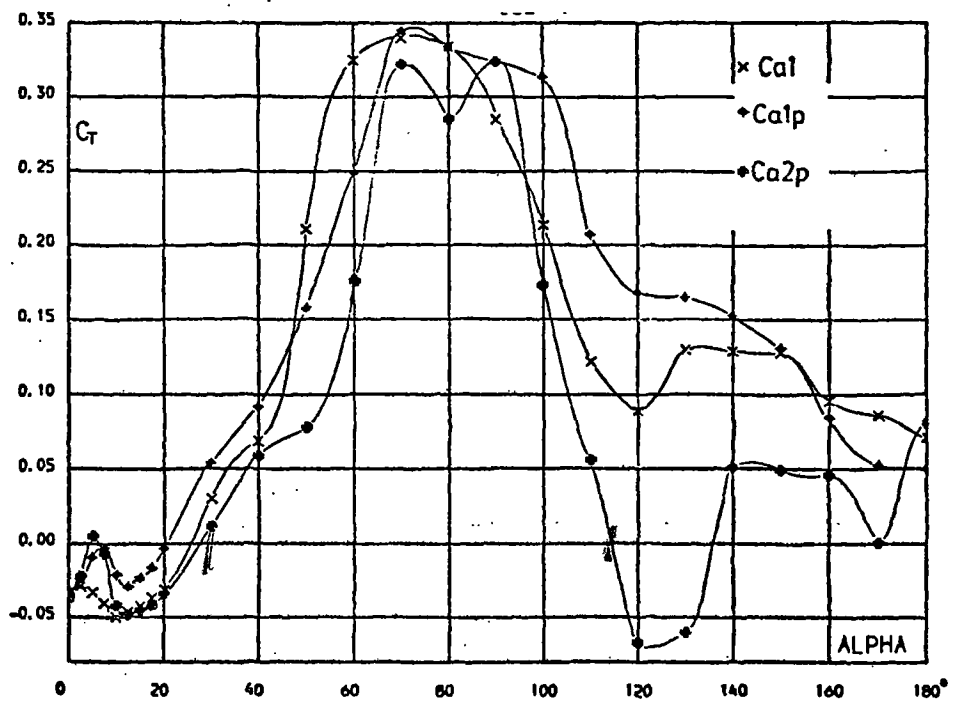

Fig.3.9. Tangential force coefficient vs. angle of incidence for canvas sailwings.

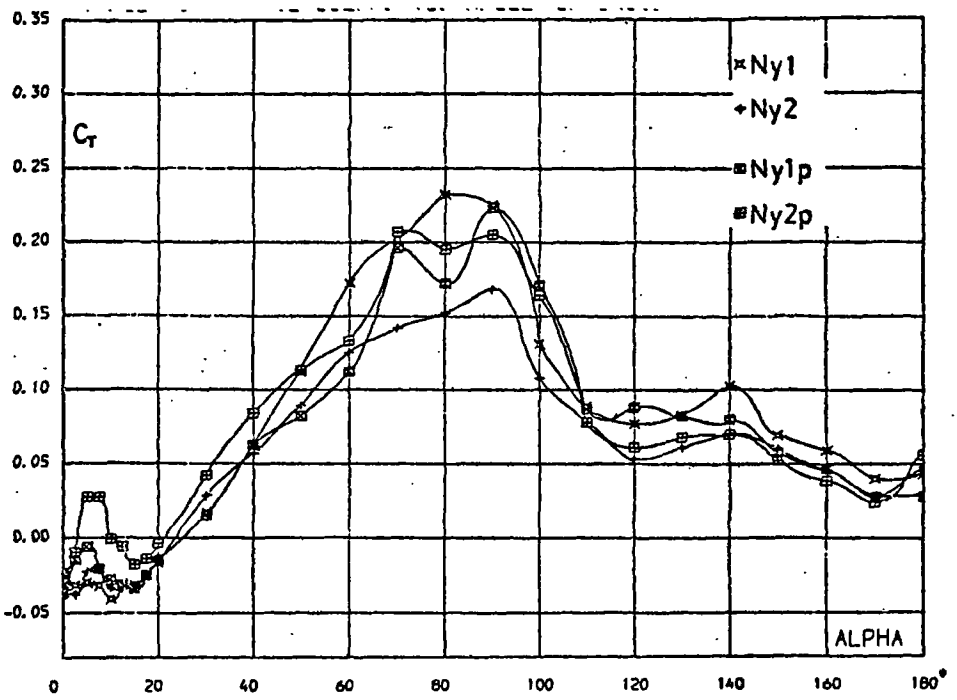

Fig.3.10. Tangential force coefficient vs. angle of incidence for nylon sailwings.

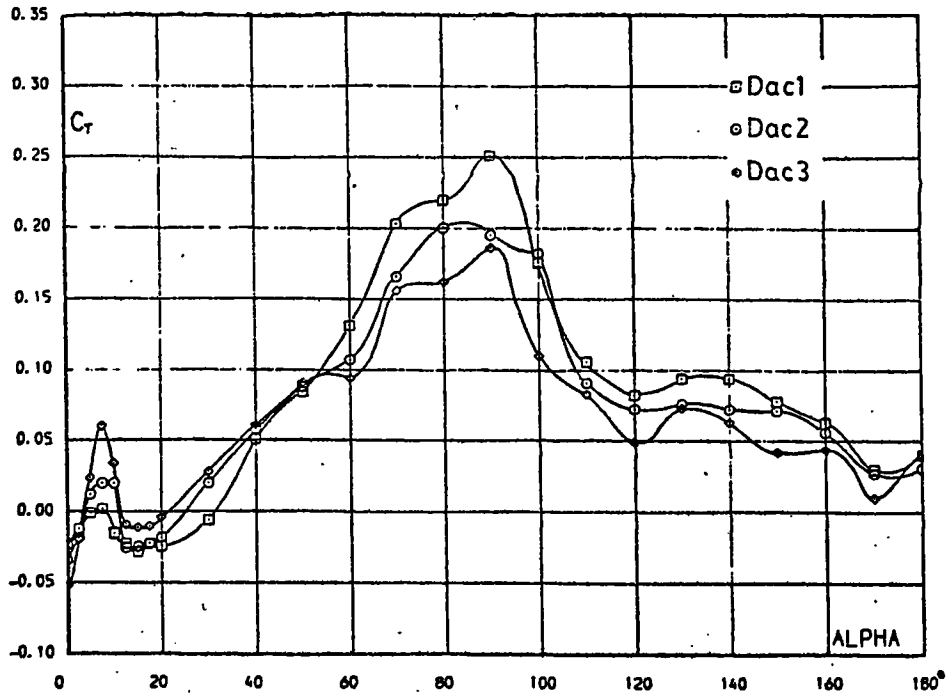

Fig.3.11. Tangential force coefficient vs. angle of incidence for 'Dacron' sailwings.

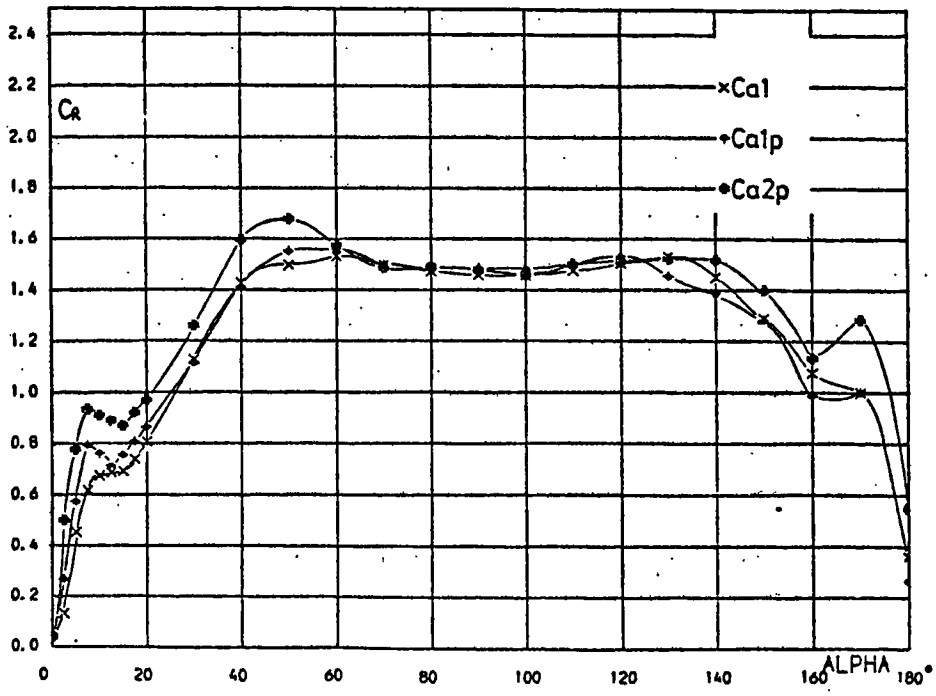

Fig.3.12. Radial force coefficient vs. angle of incidence for canvas sailwings.

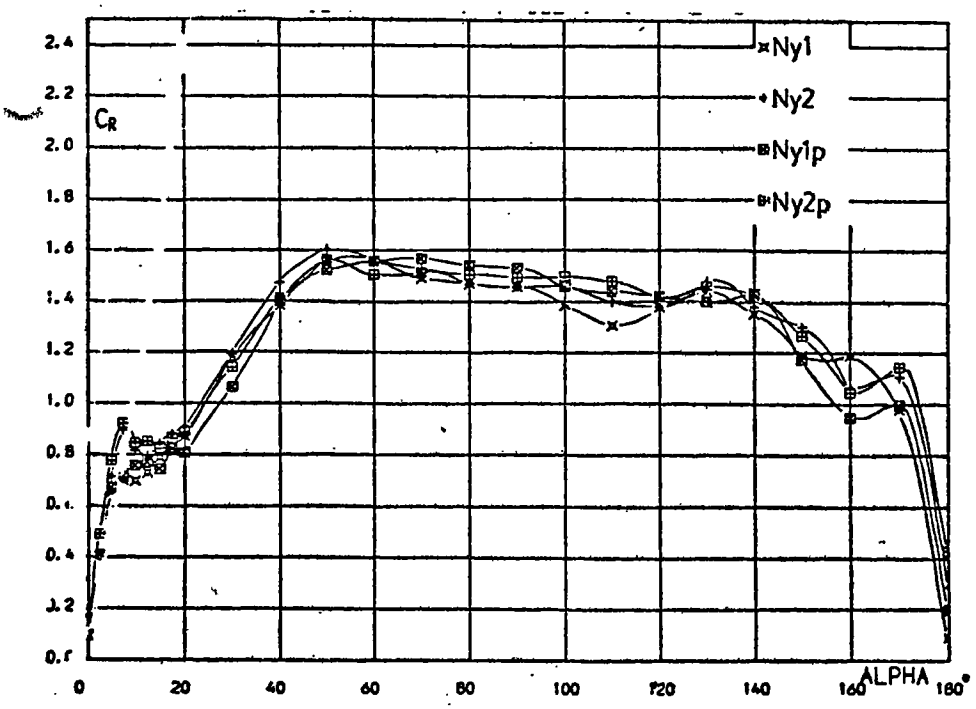

Fig.3.13. Radial force coefficient vs. angle of incidence for nylon sailwings.

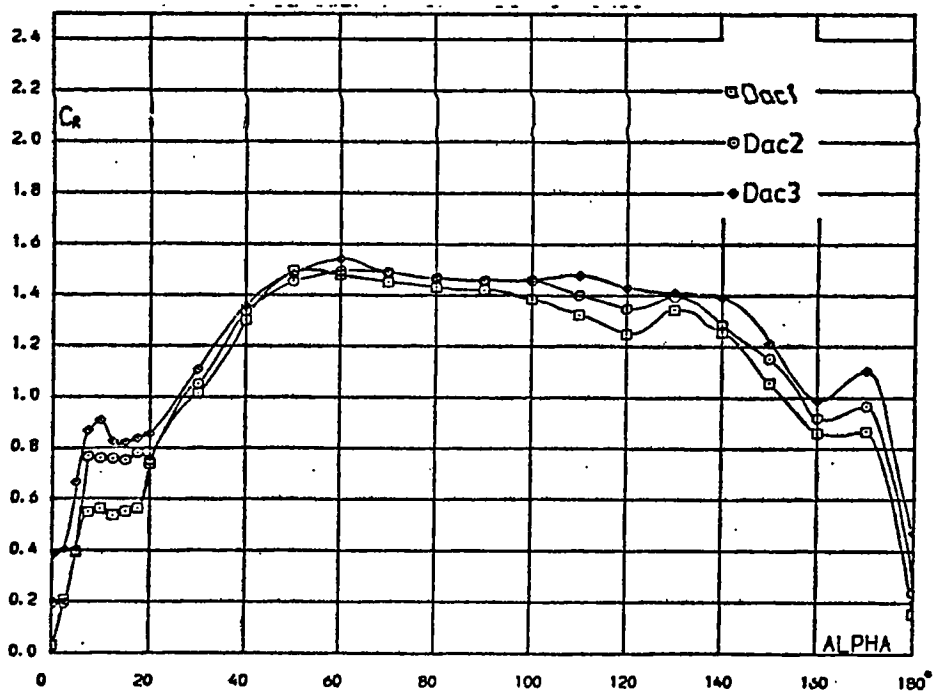

Fig.3.14. Radial force coefficient vs. angle of incidence for 'Dacron' sailwings.

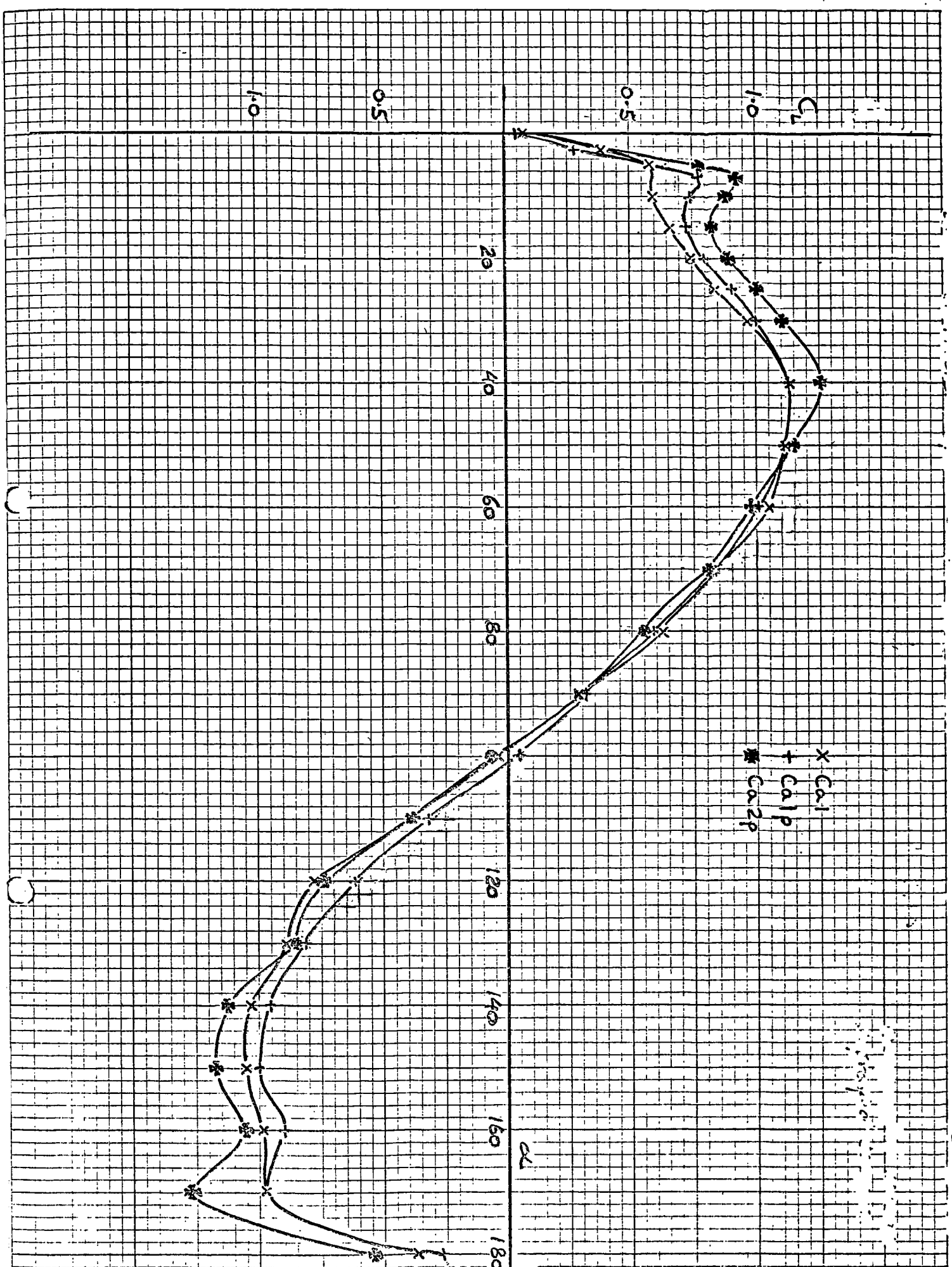

Fig.3.15. Lift coefficients for canvas sailwings

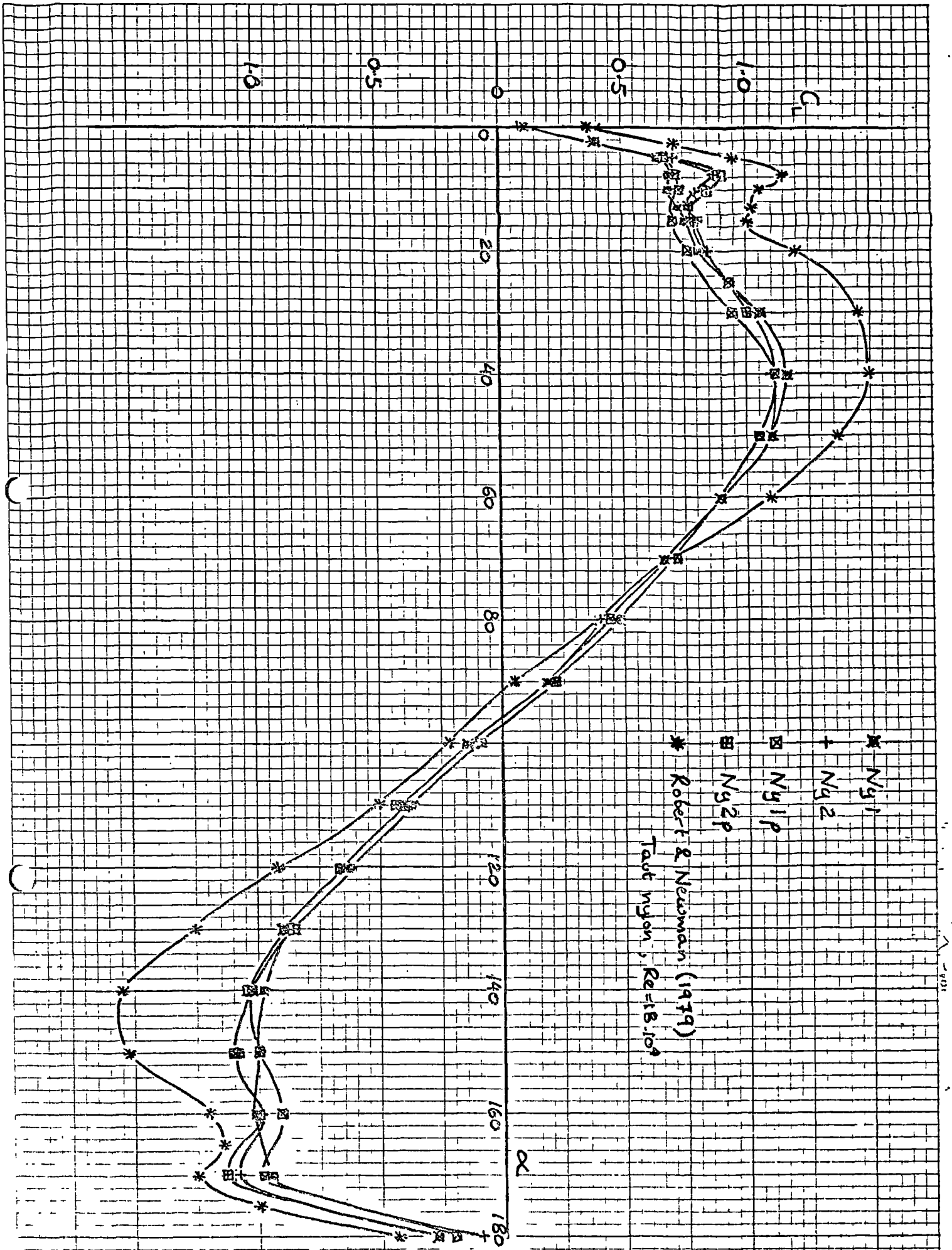

Fig.3.16. Lift coefficients for nylon sailwings.

Fig.3.17. Lift coefficients for Dacron sailwings

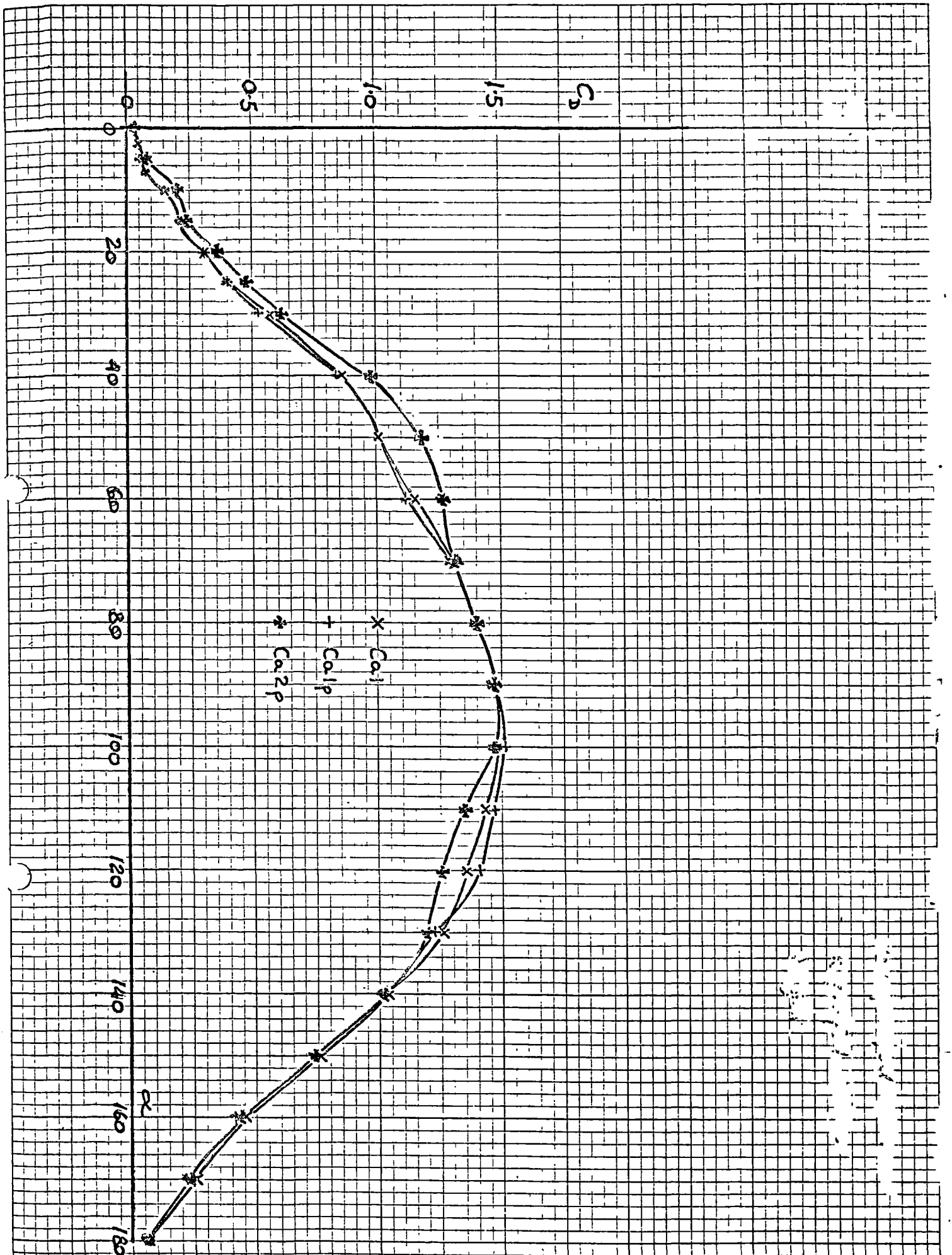

Fig.3.18. Drag coefficients for canvas sailwings.

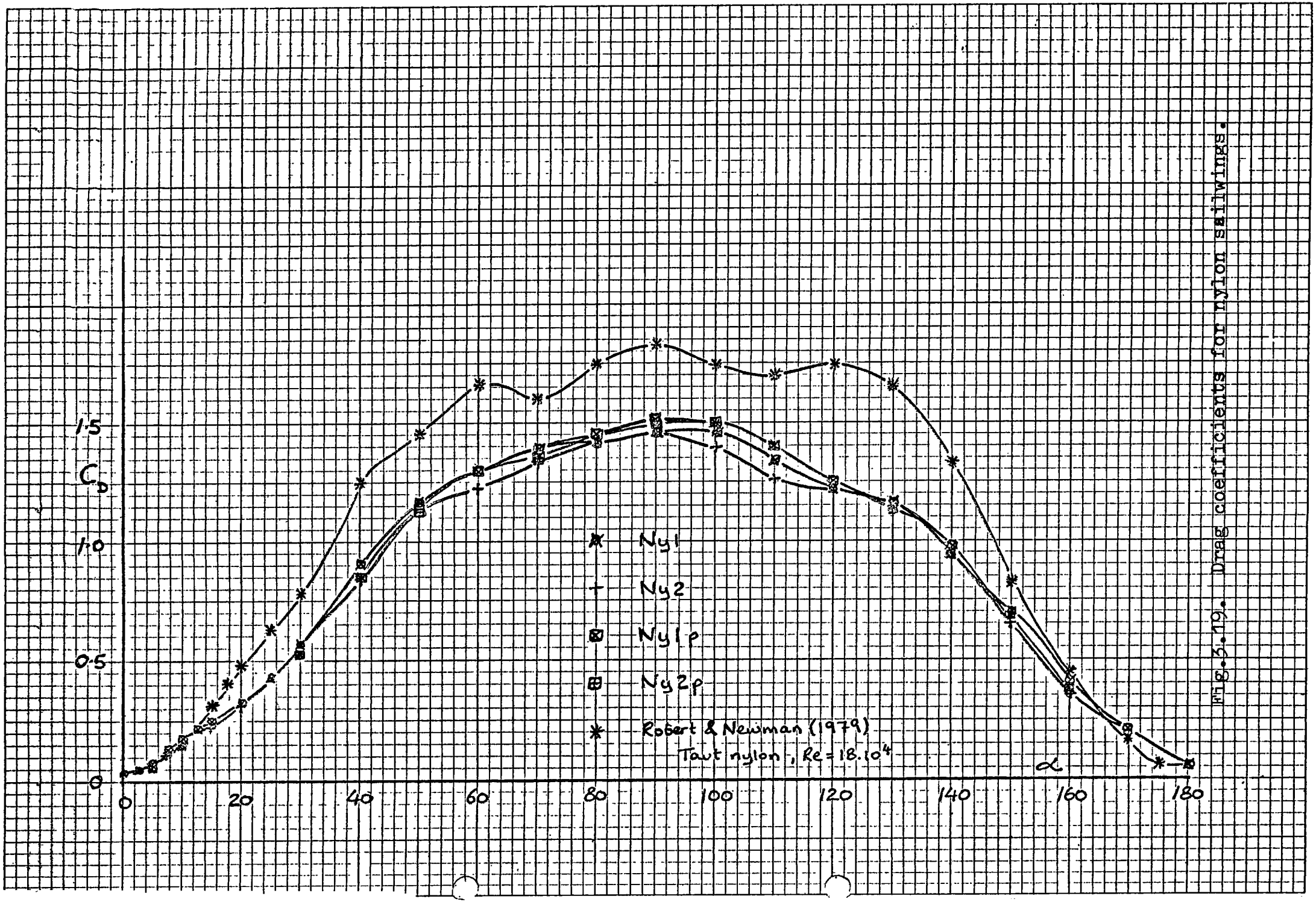

Fig 3.19. Drag coefficients for nylon sailwings.

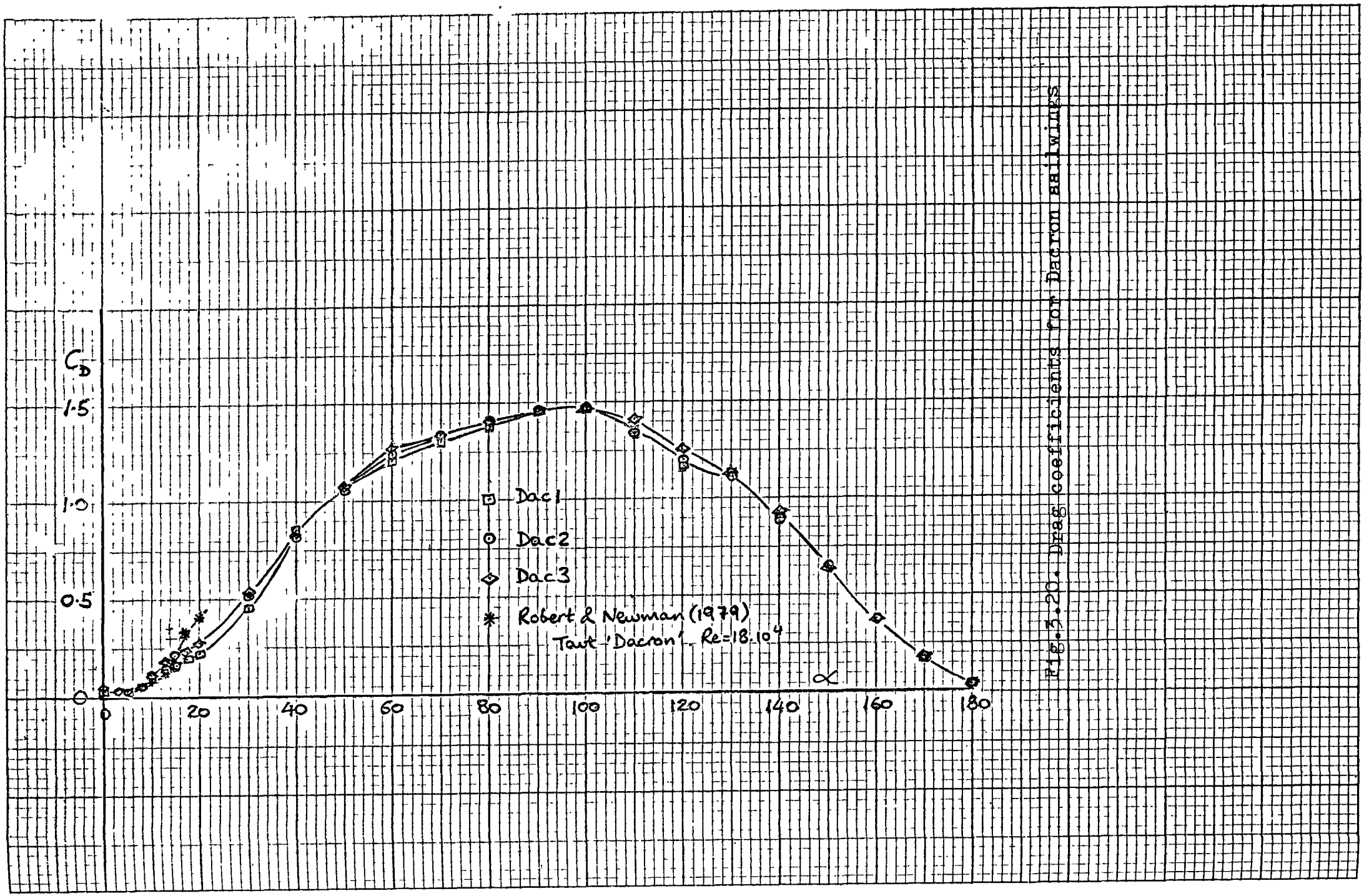

Fig. 3.20. Drag coefficients for Dacron sailwings

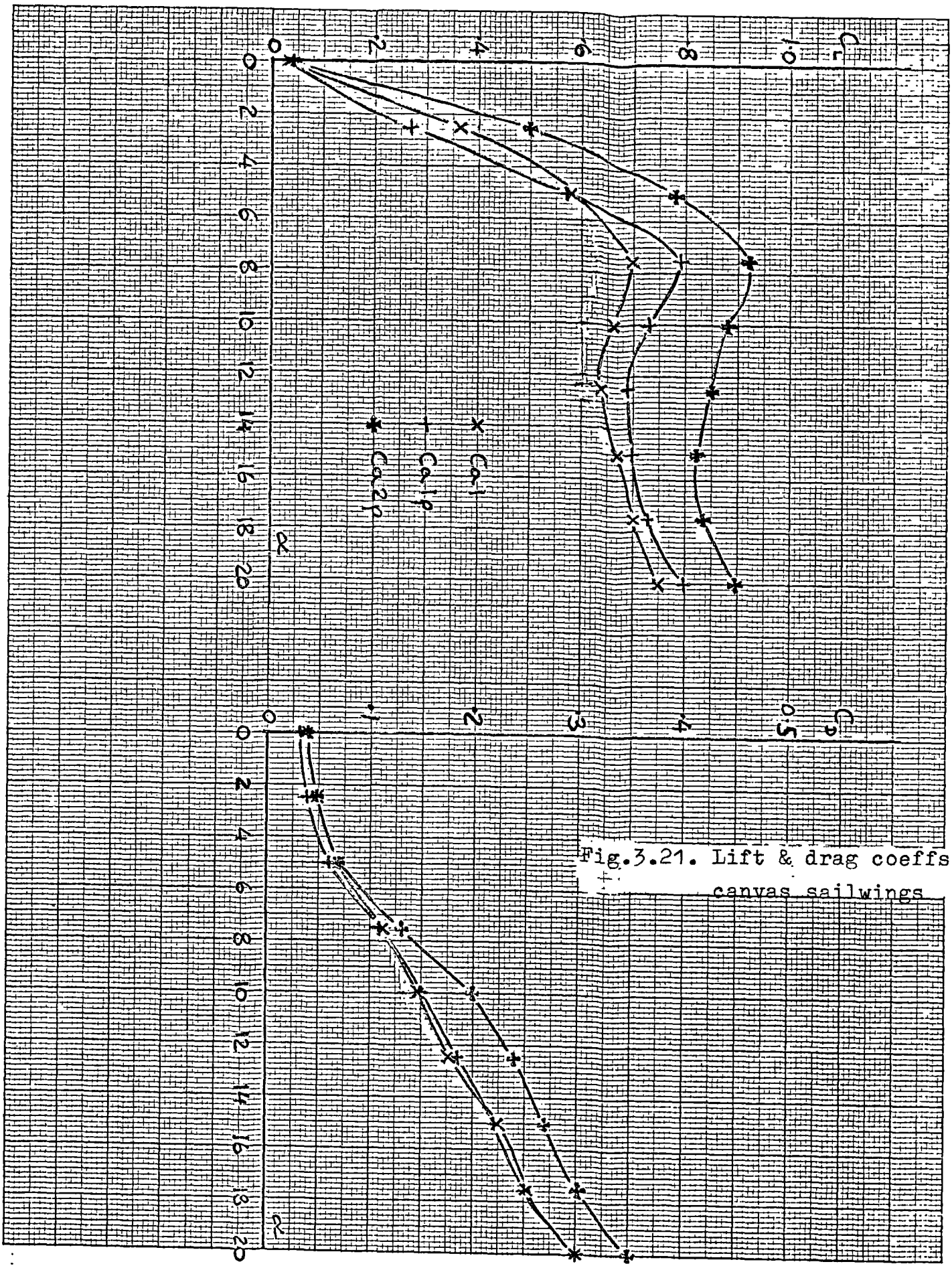

Fig.3.21. Lift & drag coeffs.
canvas sailwings

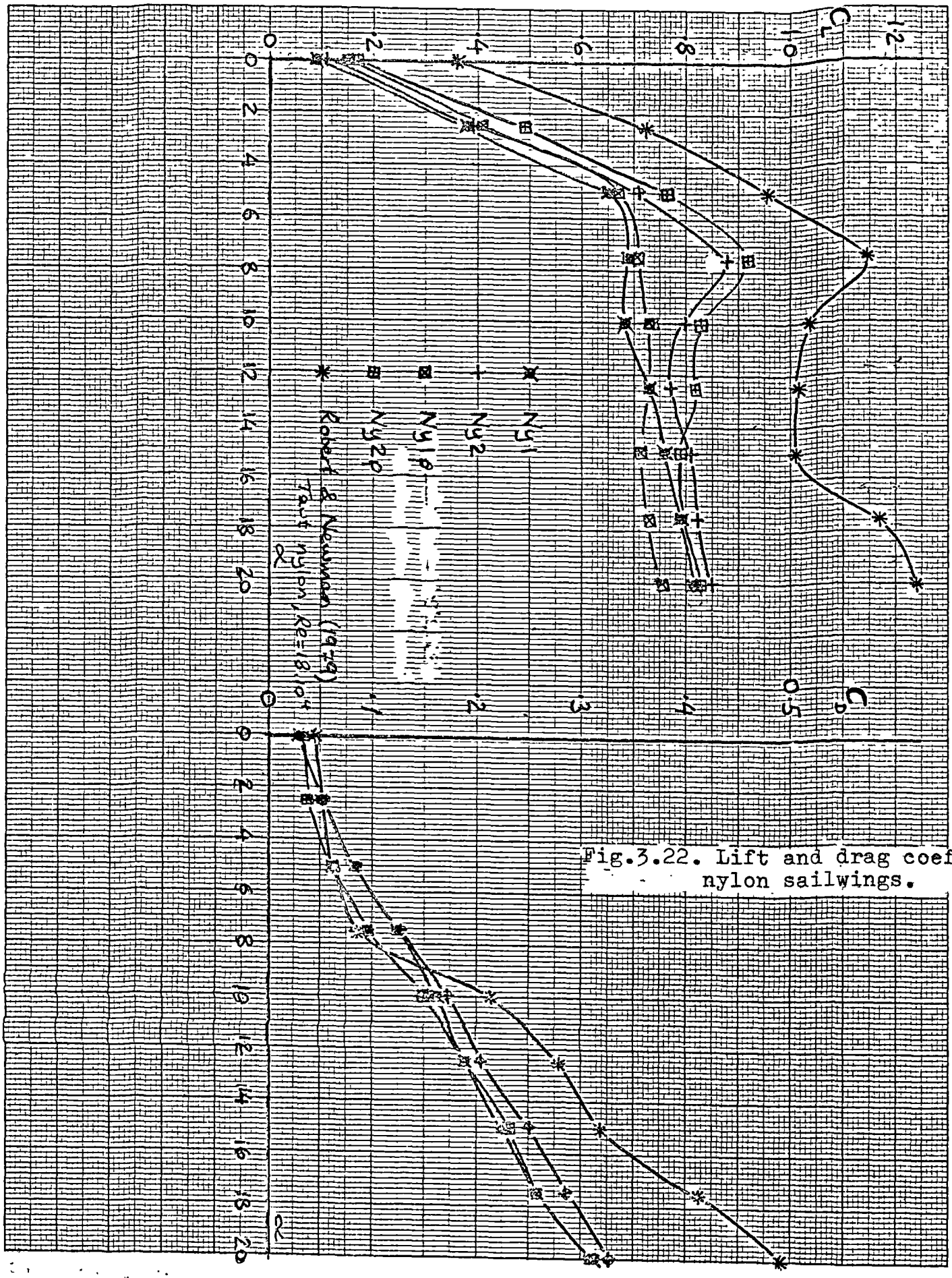

Fig.3.22. Lift and drag coeffs nylon sailwings.

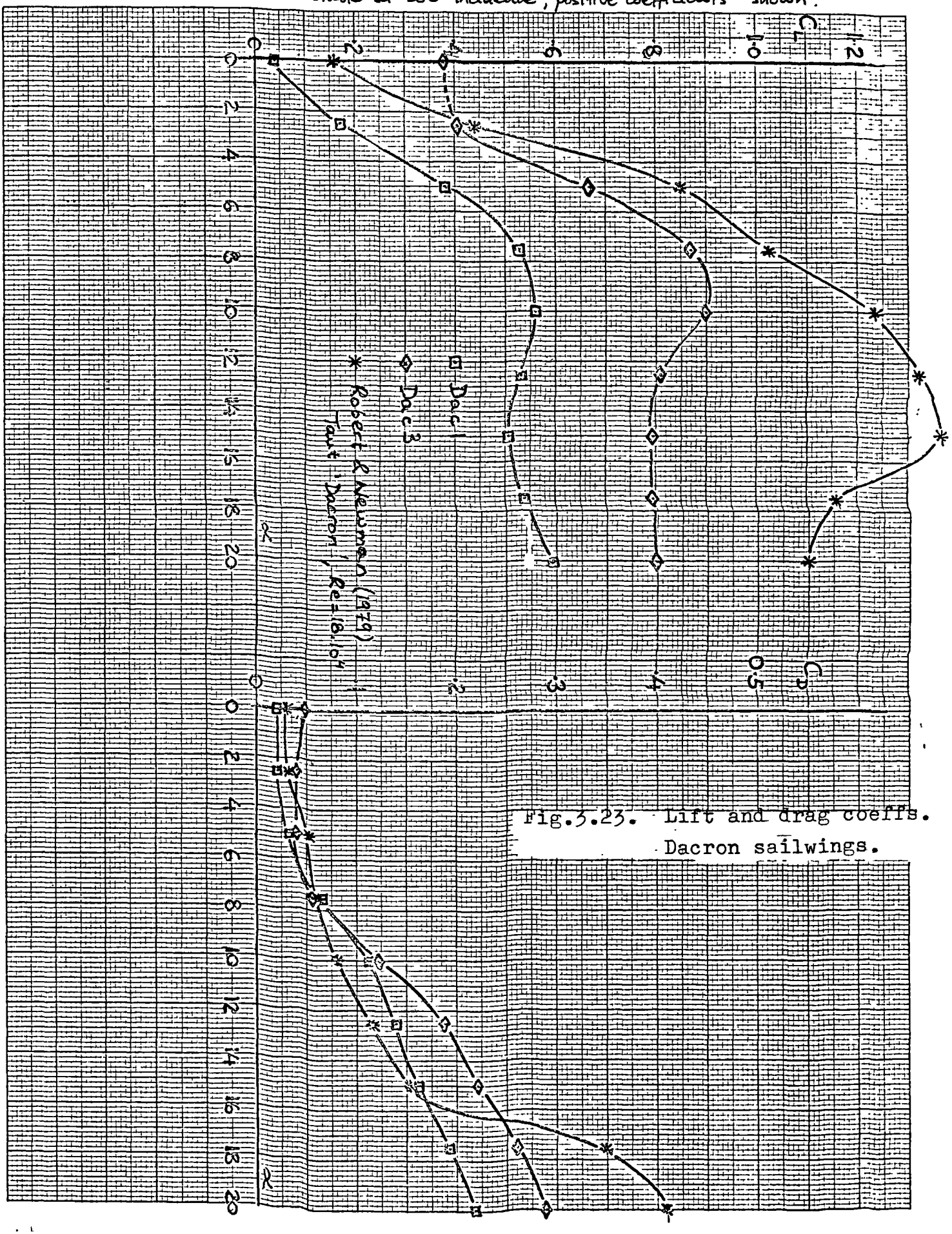

Fig.3.23. Lift and drag coeffs. Dacron sailwings.

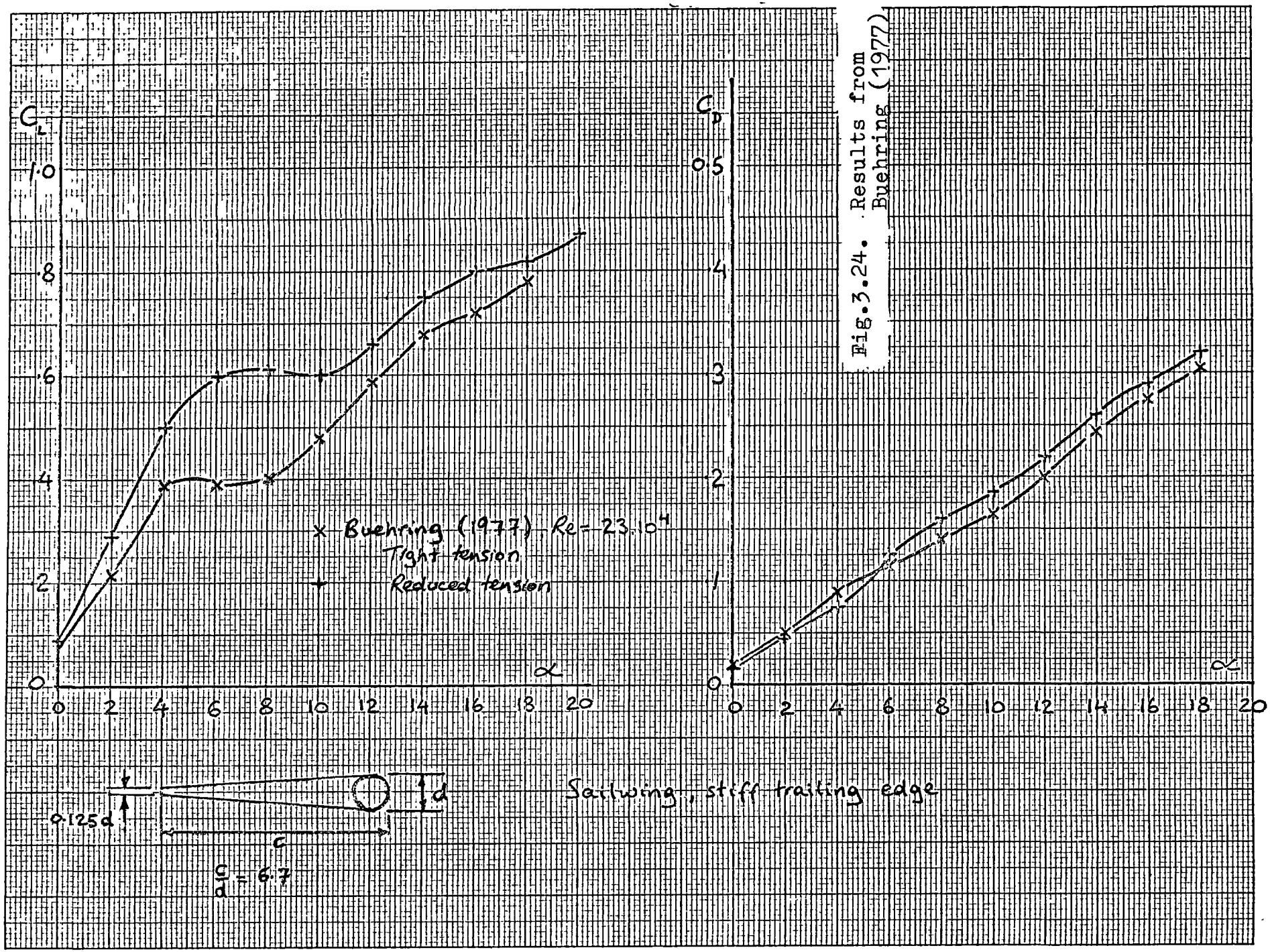

Fig.3.24. Results from Buehring (1977).

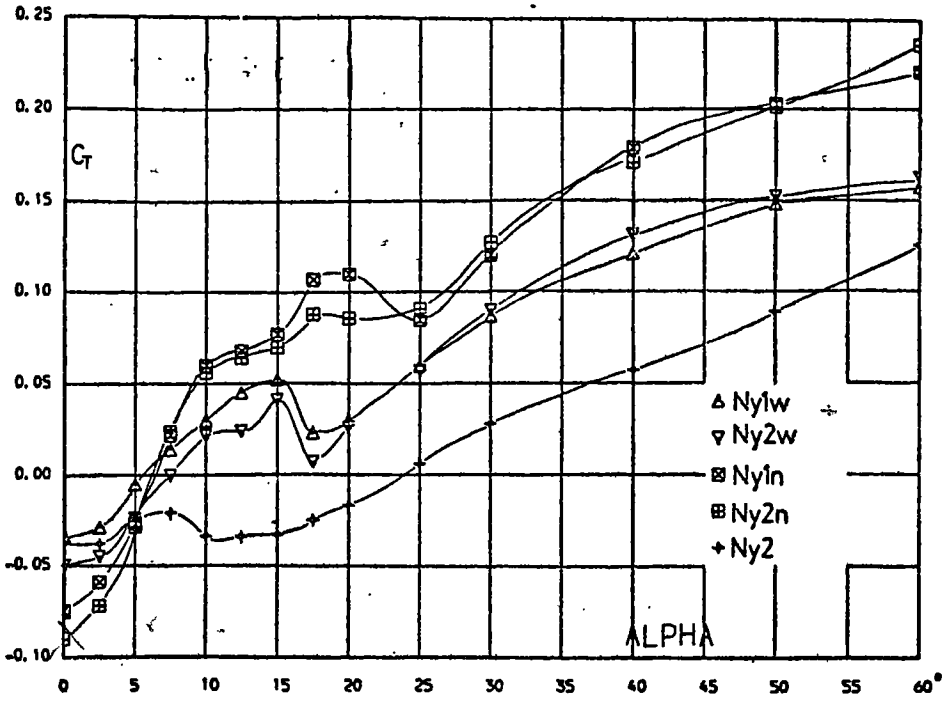

Fig.3.25. Tangential force coefficient vs. angle of incidence for sailwings with an elastic trailing edge.

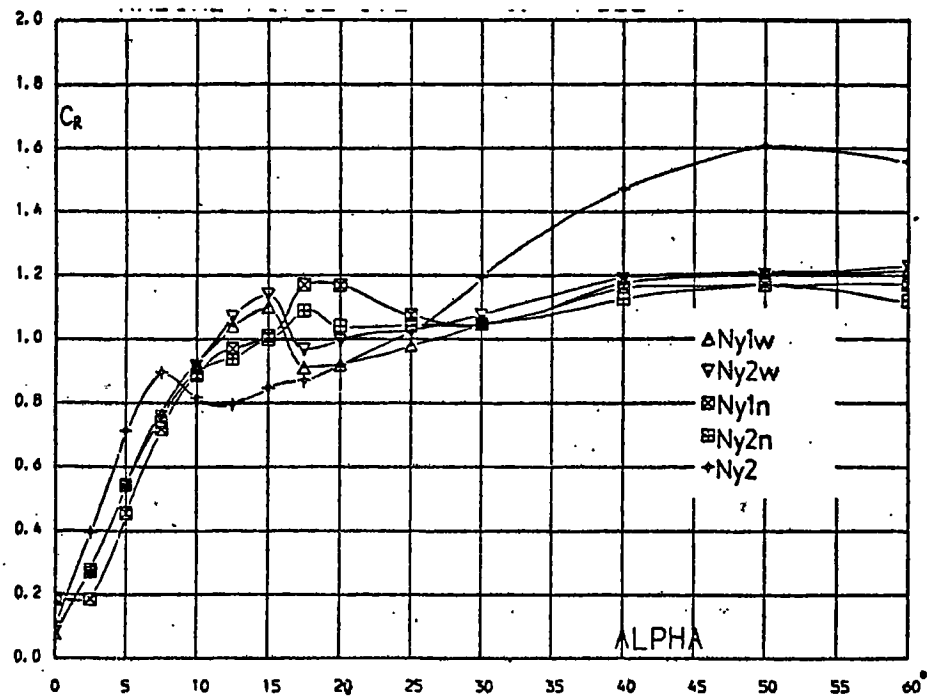

Fig.3.26. Radial force coefficient vs. angle of incidence for sailwings with an elastic trailing edge.

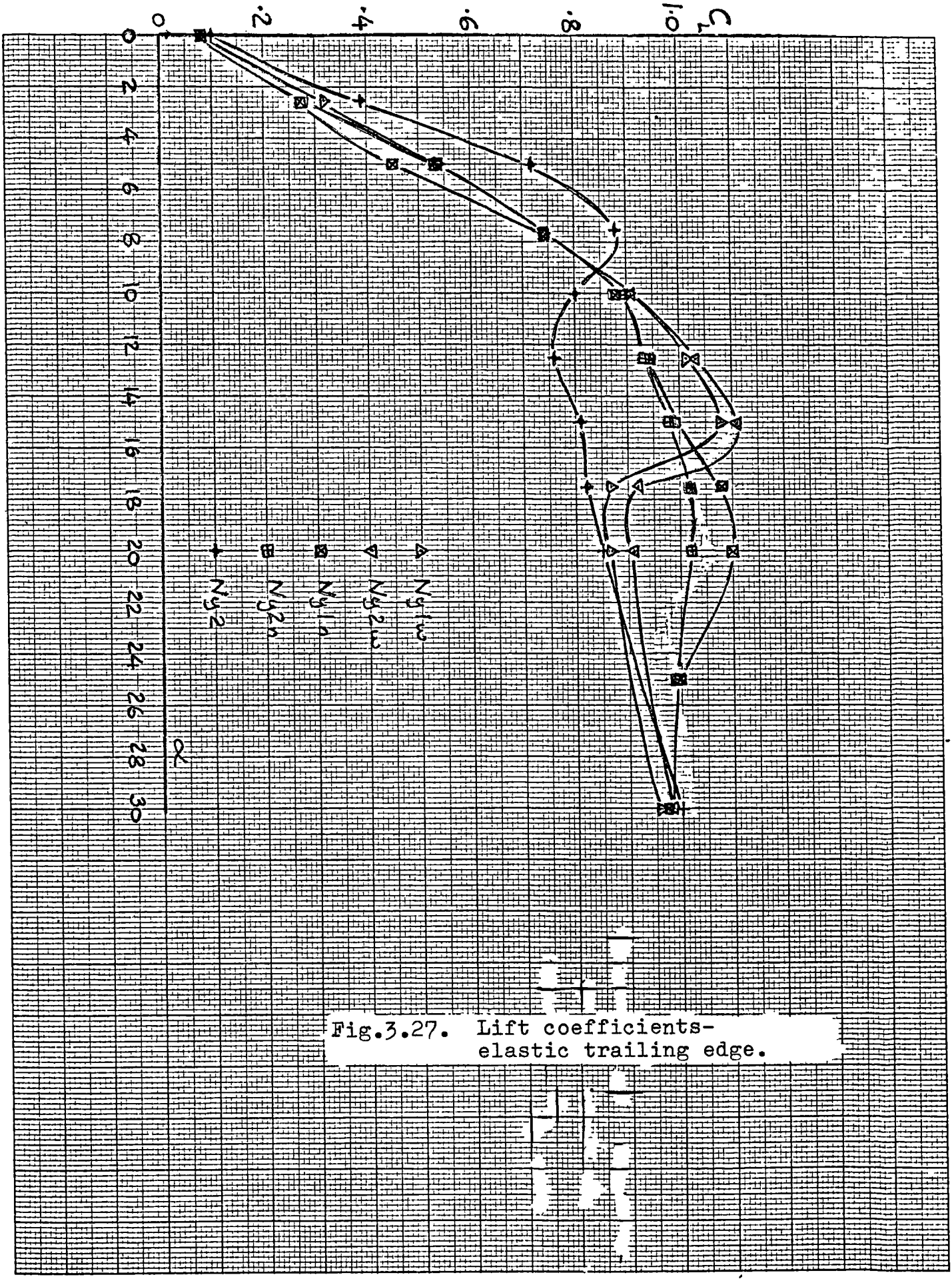

Fig.3.27. Lift coefficients-
elastic trailing edge.

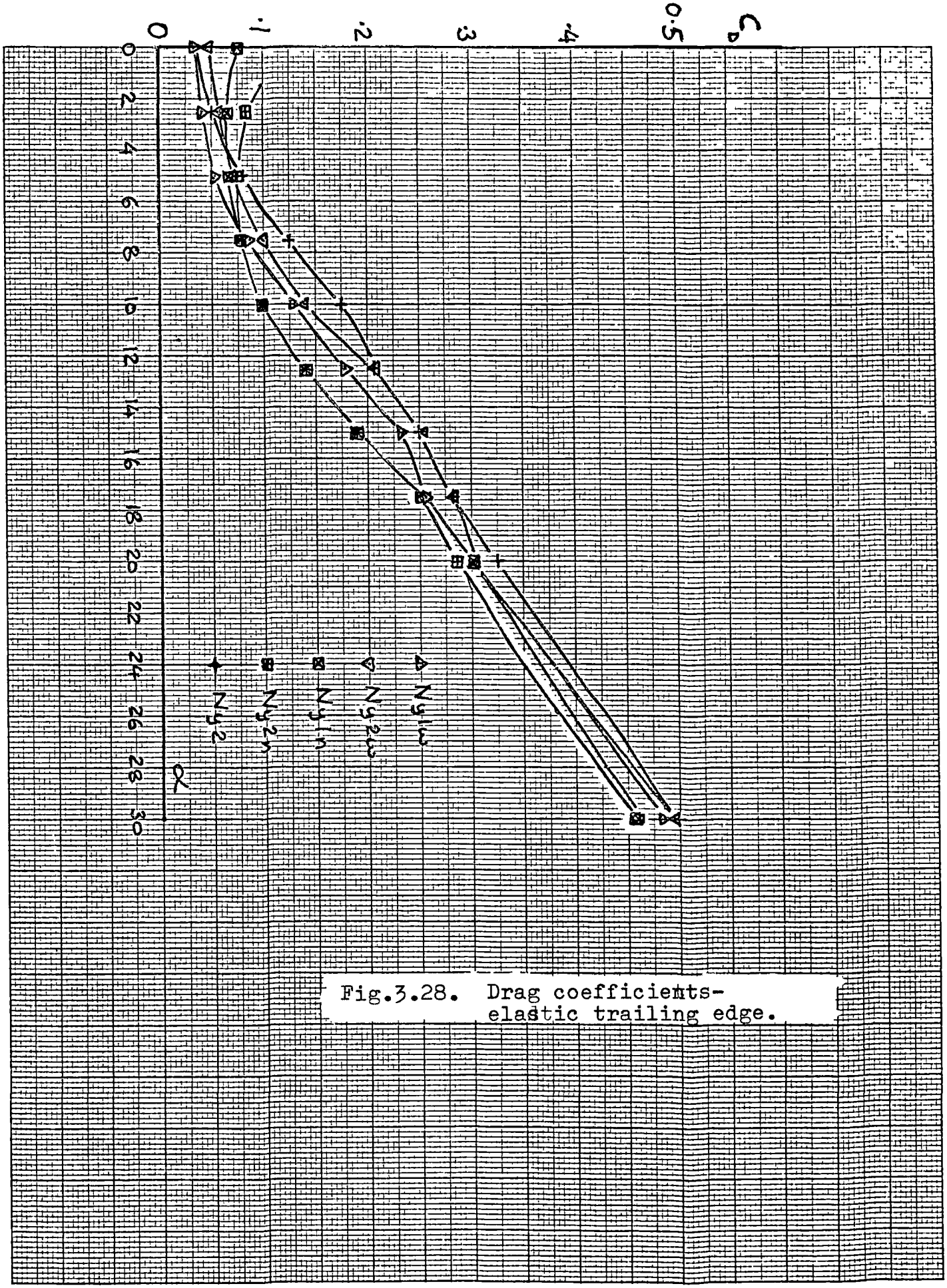

Fig.3.28. Drag coefficients- elastic trailing edge.

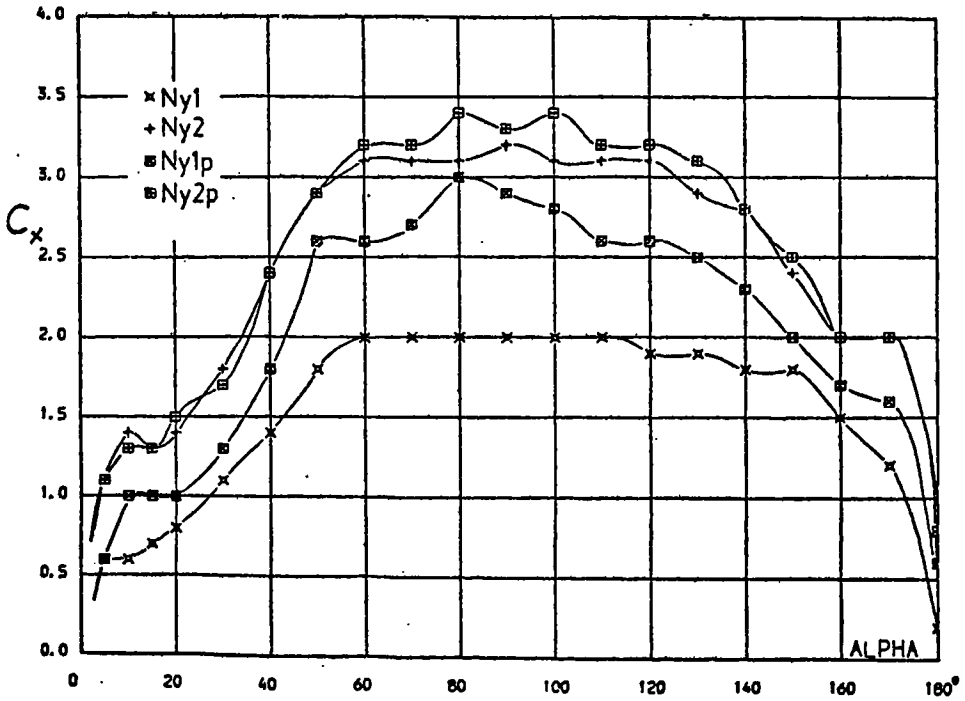

Fig.3.29. Induced tension coefficient (chordwise component of induced tension/$\frac{1}{2}\rho V_R^2 c$) vs. angle of incidence.

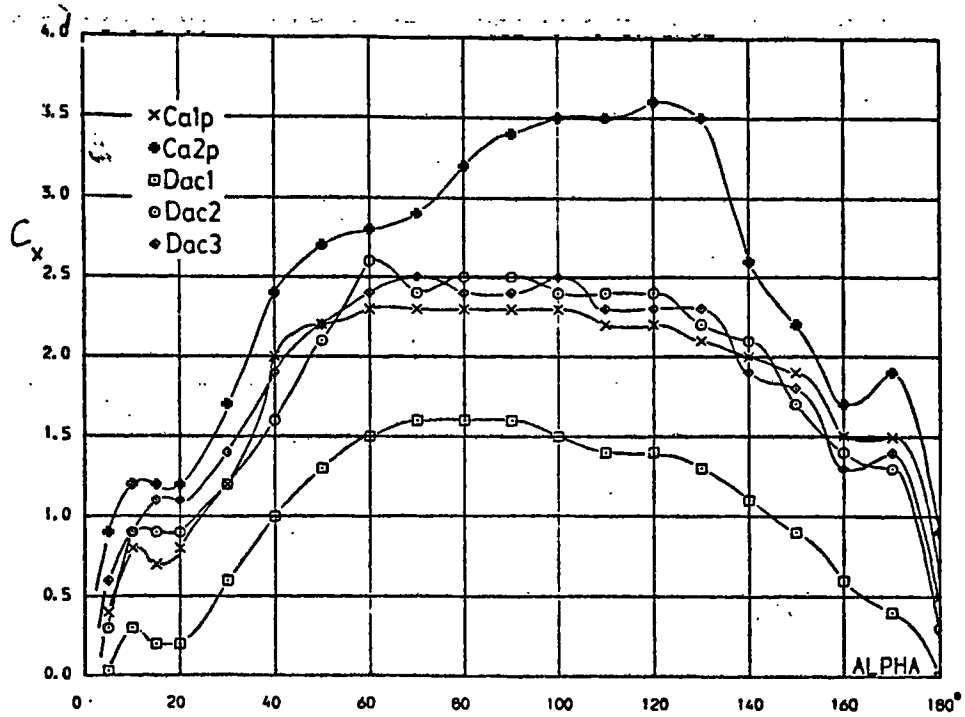

Fig.3.30. Induced tension coefficient vs. angle of incidence.

3.5. Conclusions

A measuring balance has been designed and used in a series of wind tunnel tests to produce some new data on the aerodynamic performance of sailwings at all angles of incidence. Direct measurement of the chordwise component of force, to give values of the tangential force coefficient, has shown significant differences from values previously calculated from lift and drag data.

Sailwing performance was very poor prior to stall. The dominant influence was found to be the pre-tension applied to the fabric; a low pre-tension giving a better performance. The elasticity and stiffness of the fabric were not found to have any clear effect, while porosity appeared detrimental.

After stall, canvas sailwings were found to give rather higher tangential force coefficients than other fabrics. Increased pre-tension gave a general increase in tangential force coefficient with the canvas being the most sensitive.

The measurements do not give very good agreement with the results reported by Robert and Newman (1979) and the late stall they observed with a 'Dacron' fabric was not repeated. The present measurements are supported, at low angles of incidence, by the data of Buehring (1977). (Fig 3.24)

If deflection of the trailing edge is allowed to occur, then there is a significant effect on the force coefficients. A more elastic trailing edge gave a greater improvement in tangential force coefficients but became unstable easily at low angles of incidence, causing high drag.

CHAPTER FOUR

THE PERFORMANCE OF SAILWINGS IN DARRIEUS TURBINES -- A RE-ASSESSMENT

4.1. Introduction

The performance to be expected from a vertical axis, sailwing turbine has been re-assessed, in light of the fresh aerodynamic data reported in the previous chapter.

The analysis follows that used in Chapter Two for low speed performance. The influence of pre-tension and sail fabric is discussed. Starting torque coefficients are predicted but it was not found possible to produce meaningful power coefficient predictions because of the lack of a flow model for the induced flow through a low tip speed ratio, high solidity turbine and the limited range of pre-tension coefficients covered by the data.

4.2. Results and Discussion

The variation of the tangential force coefficient C_T, and of the instantaneous torque coefficient $C_T q^2$, with azimuthal angle, has been calculated at several tip speed ratios, using the data from test Ca1p.(Fig.4.1). Curves of the mean torque coefficient C_S', have been computed for all the aerofoils tested (Figs.4.2 to 4.5). For the solid (NACA0012 aerofoil, it is seen that the starting torque coefficient

is higher than previously predicted and , also, that the 'deadband' is wider. This latter difference is not significant as it is caused by the low Reynolds number, and consequent low stall angle of the data; in practice the Reynolds number would increase with tip speed ratio. For the sailwings, higher starting torque coefficients are also predicted. However, it is clear that turbine operation is limited by the poor sailwing performance at low angles of incidence and that only low tip speed ratio operation can be expected; except perhaps, from the coated nylon and 'Dacron' sails with low pre-tension(tests Ny2p and Dac3) or if trailing edge deflections occur.

Now, in a turbine, the values of the tension coefficients for the sailwings are not constant. The coefficients were defined as follows:

$$C_{pT} = \frac{P_T}{\frac{1}{2}\rho V_R^2 c} \qquad \text{and} \qquad C_{TT} = \frac{T_T}{\frac{1}{2}\rho V_R^2 A_s}$$

The relative windspeed is related to the induced windspeed by equation [1.12]: $q = \frac{V_R}{V}$

At low tip speed ratios it has been assumed that the induced windspeed may be approximated by the free windspeed. In this case, the tension coefficients are proportional to $1/q^2 V_w^2$. If the turbine operates in windspeeds of between, say, 3 m/s and 10 m/s, then the coefficients will change by a factor of about eleven. The variation of q^2 with azimuthal angle has already been plotted (Fig.2.6) and the variation of $1/q^2$ is plotted here.(Fig.4.6). The tension coefficients clearly have a large range of variation during each turbine

revolution, quite apart from the effect of windspeed fluctuations. In fact, the range over which the tension coefficients may vary, makes it obvious that the data is not adequate for an accurate performance prediction. Considering Fig.4.6, the performance is likely to be rather more affected by the reduction in coefficient that occurs at lower azimuthal angles, than by the increase that occurs at high azimuthal angles. This is as the contribution made to driving torque at azimuthal angles above about 130 degrees is relatively small (Fig.4.1). The effect of a reduction in pre-tension coefficient may be seen from the curves of torque coefficient C_s' (Figs.4.3 to 4.5) and it varies for each fabric. The starting torque coefficient is little affected, except in the case of the canvas sailwings.

When the turbine is stationary in a low wind, the trailing edge tension coefficient C_{T+}, must be high if sail instability when operating, perhaps in a higher wind, is to be avoided. Instability would detract from the turbine performance and, perhaps more importantly, reduce sail life.

Since in high winds there is an excess of energy available, it seems necessary that a turbine be optimised for operation in low winds. Then the tension coefficients will be high and the trailing edge effectively rigid. The curves of the torque coefficient C_s', show that only low tip speed ratio operation can then be expected, and so a high solidity σ ($\sigma = \frac{\Sigma A_B}{2A}$) will be required. Thus, even if the effect of trailing edge deflections in high winds was to allow higher tip speed ratio operation, this would not occur because of the high solidity. In fact, use of the data from tests

Ny1w and Ny1n, in the single streamtube program (assuming a constant value of the trailing edge tension coefficient), shows that high power coefficients would not be obtained (Figs.4.7 and 4.8). This does not say that some trailing edge deflection may not give some benefit at lower tip speed ratios.

If a high solidity is used, then it is not possible to use the single streamtube program as the assumptions made, concerning the induced flow, break down at low tip speed ratios. Similarly, the approximation used before, that at low tip speed ratios, the induced windspeed was almost equal to the free windspeed, is of limited use. It does therefore not seem to be possible to produce meaningful curves of predicted power coefficients.

What may be predicted is the starting torque produced, as the induced windspeed is then equal to the free windspeed. From equation [1.16] :

$$\text{Starting torque} = C_s' \tfrac{1}{2} \rho \Sigma A_B R V_w^2$$

From Figs. 4.3 to 4.5 :

$$\text{Starting torque} \geq 0.06 . \tfrac{1}{2} \rho \Sigma A_B R V_w^2$$

In terms of the torque coefficient C_Q:

$$C_Q = \frac{\text{Torque}}{\frac{1}{2} \rho A V_w^2 R}$$

it is predicted that, on starting : $C_Q \geq 0.06 \frac{\Sigma A_B}{A}$

while for the canvas sailwing, this may reach, $C_Q = 0.15 \frac{\Sigma A_B}{A}$

Canvas would seem to have several advantages over the other fabrics tested as a material for sailwings for this application. It seems that the starting torque coefficient will be higher and will be at its highest in low winds, when the pre-tension coefficient C_{P_T} is high. Also it is a fabric which is likely to be readily obtainable in most places and, if proofed, should be reasonably durable. Nylon and 'Dacron' are less likely to be easily available, nylon may be affected by sunlight and 'Dacron' is difficult to stitch.

Although it has not been found possible to make accurate theoretical performance predictions for vertical axis sailwing turbines, it is clear that the rather poor performance obtained by previous workers is inherent in the use of simple sailwing aerofoils. However, if such a turbine can achieve power coefficients of 0·15, as reported by Newman and Ngabo (1978), and high starting torque coefficients, as predicted here, then it could have some advantages over other designs because of its vertical axis of rotation and low cost construction.

It may be that higher power coefficients could be obtained by the use of more sophisticated sailwing aerofoils, with a D-shaped leading edge spar and ribs to maintain a better aerofoil shape. But structural design would be difficult, parasitic losses might be high due to the bracing required and the simplicity of the design could be lost.

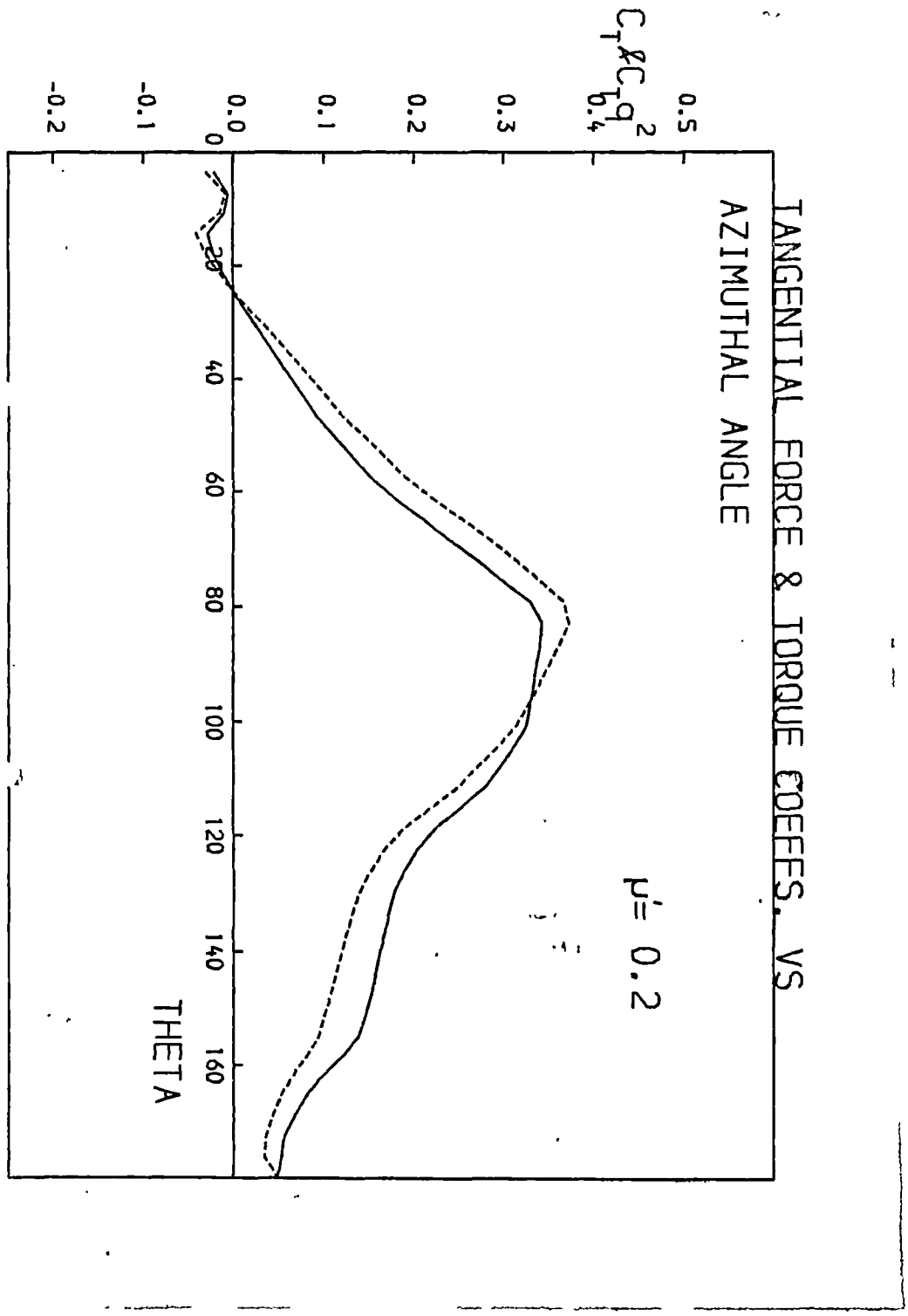

Fig.4.1. Tangential force (solid line) and torque coeffs. vs. azimuthal angle - Ca1p

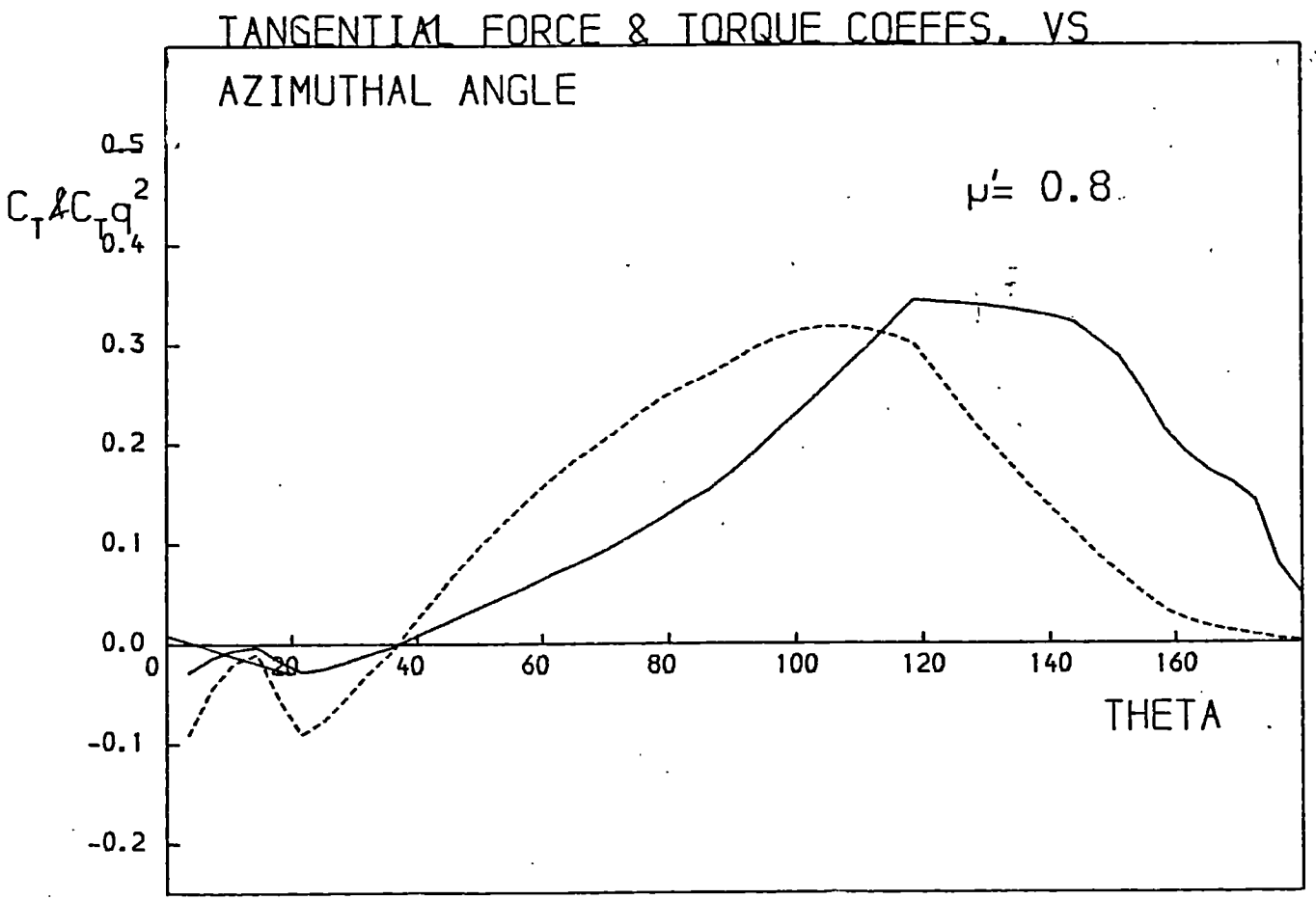
TANGENTIAL FORCE & TORQUE COEFFS. VS
AZIMUTHAL ANGLE
C_T & C_{TQ}
μ'= 0.8
0.5
0.4
0.3
0.2
0.1
0.0
-0.1
-0.2
0
20
40
60
80
100
120
140
160
THETA

Fig.4.1. cont.

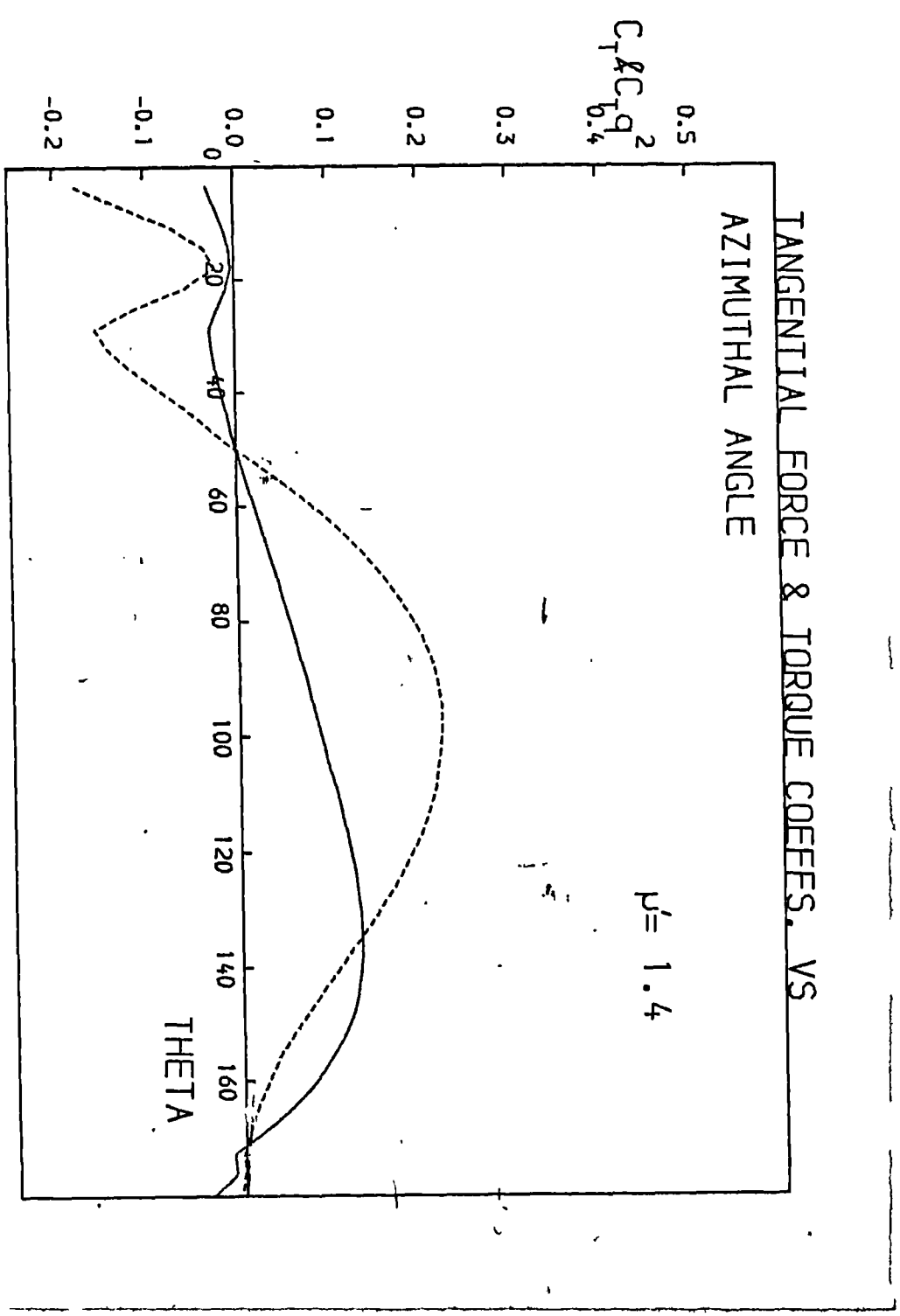

Fig.4.1. concluded

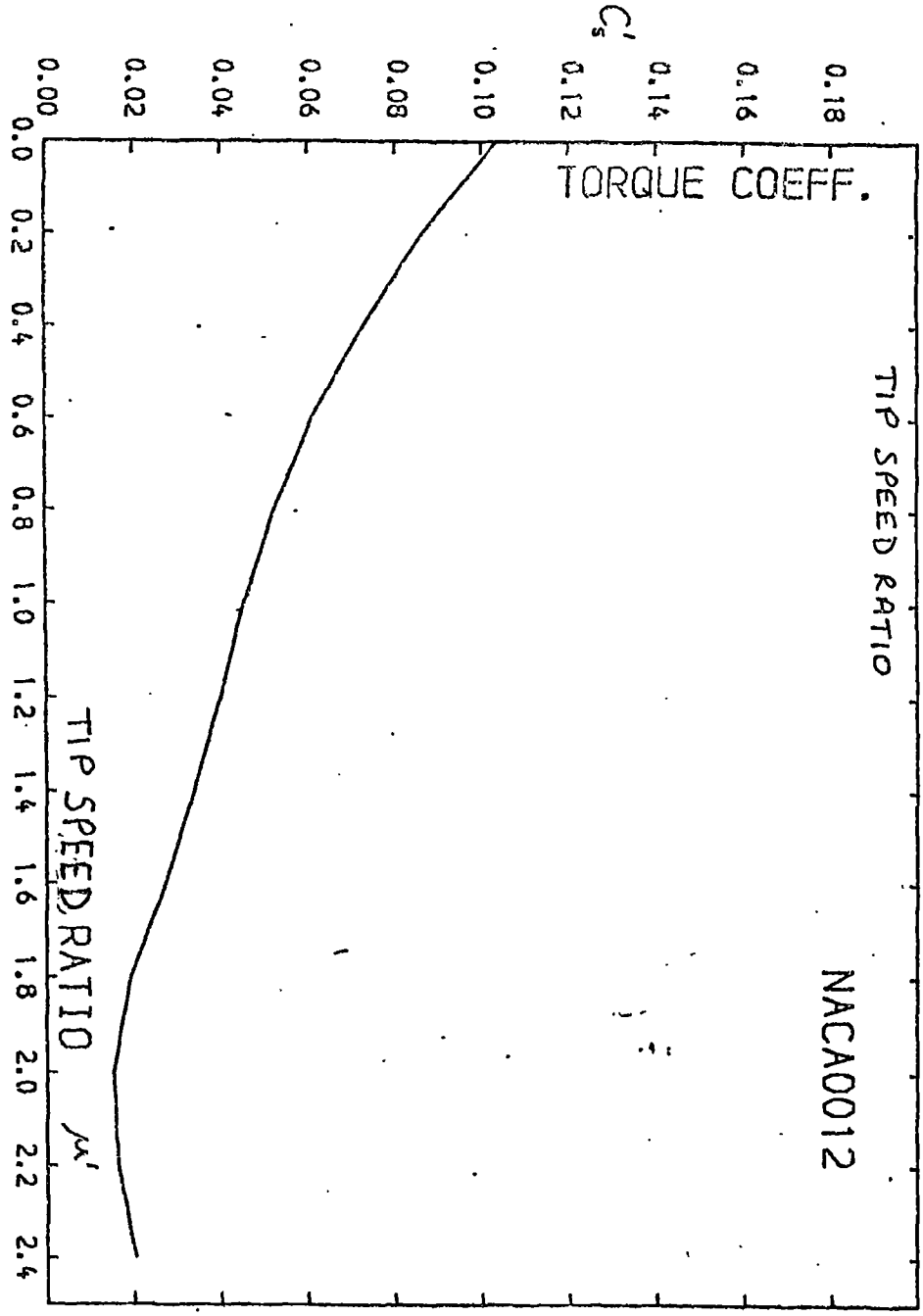

Fig.4.2. Torque coefficient vs. tip speed ratio -solid aerofoil.

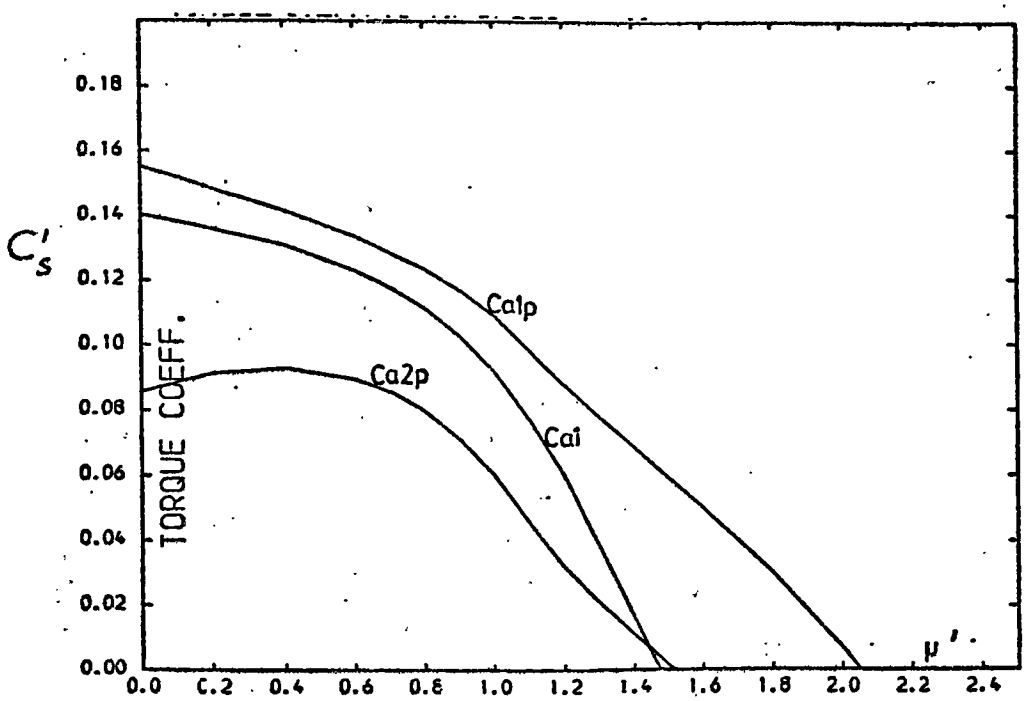

Fig. 4.3. 4.3 Torque coefficient vs. tip-speed ratio from data for canvas sailwings.

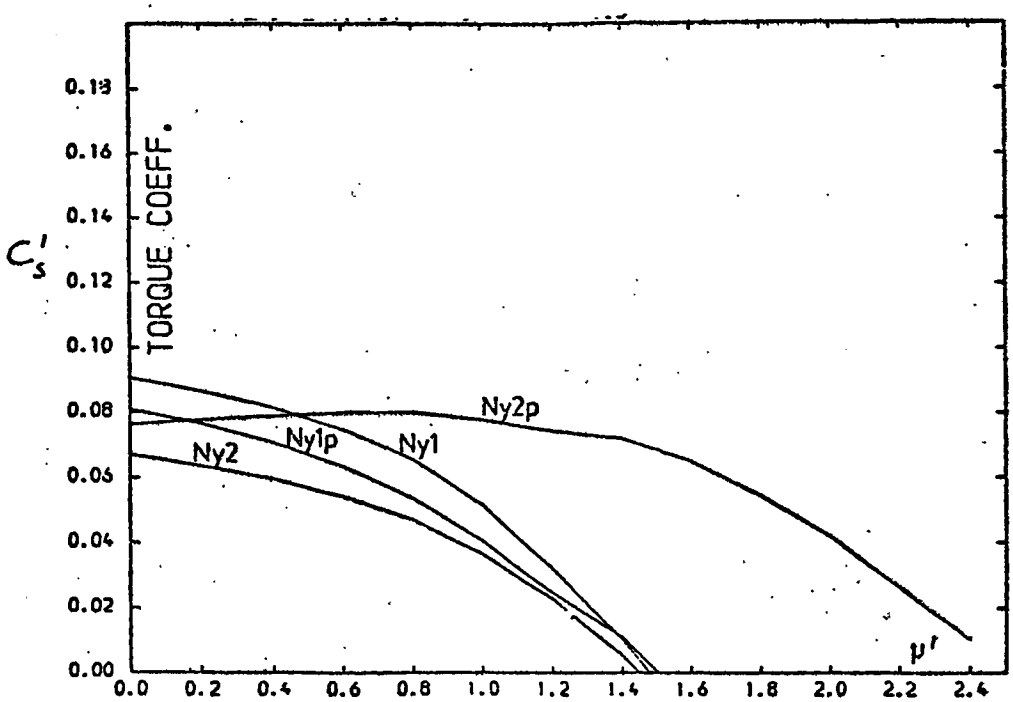

Fig. 4.4. 4.4 Torque coefficient vs. tip-speed ratio from data for nylon sailwings.

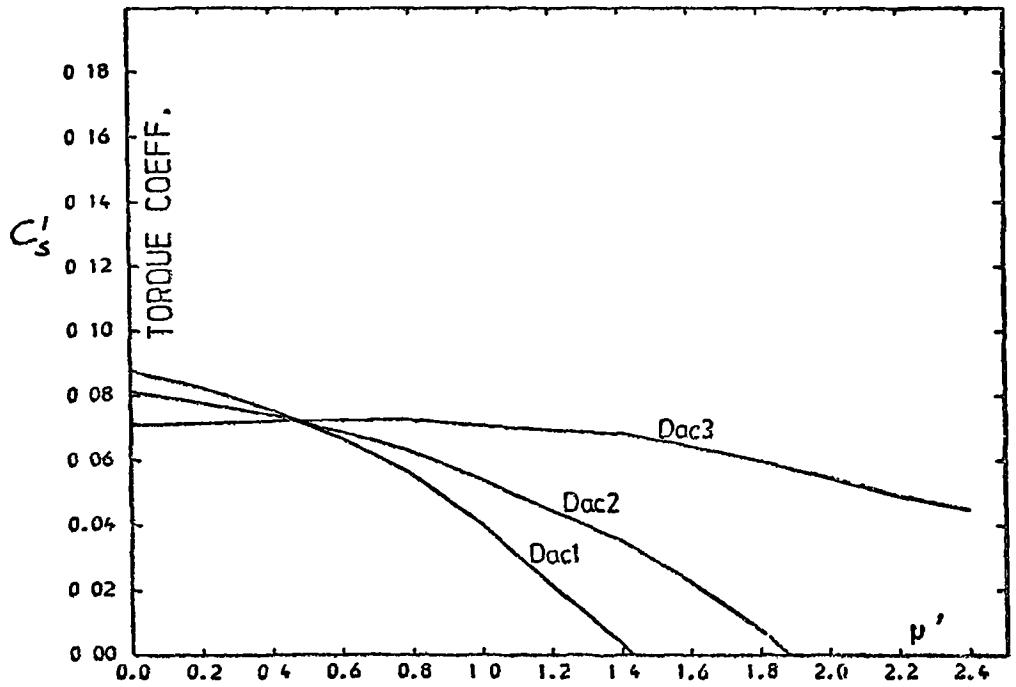

Fig.4.5. Torque coefficient vs. tip-speed ratio from data for 'Dacron' sailwings.

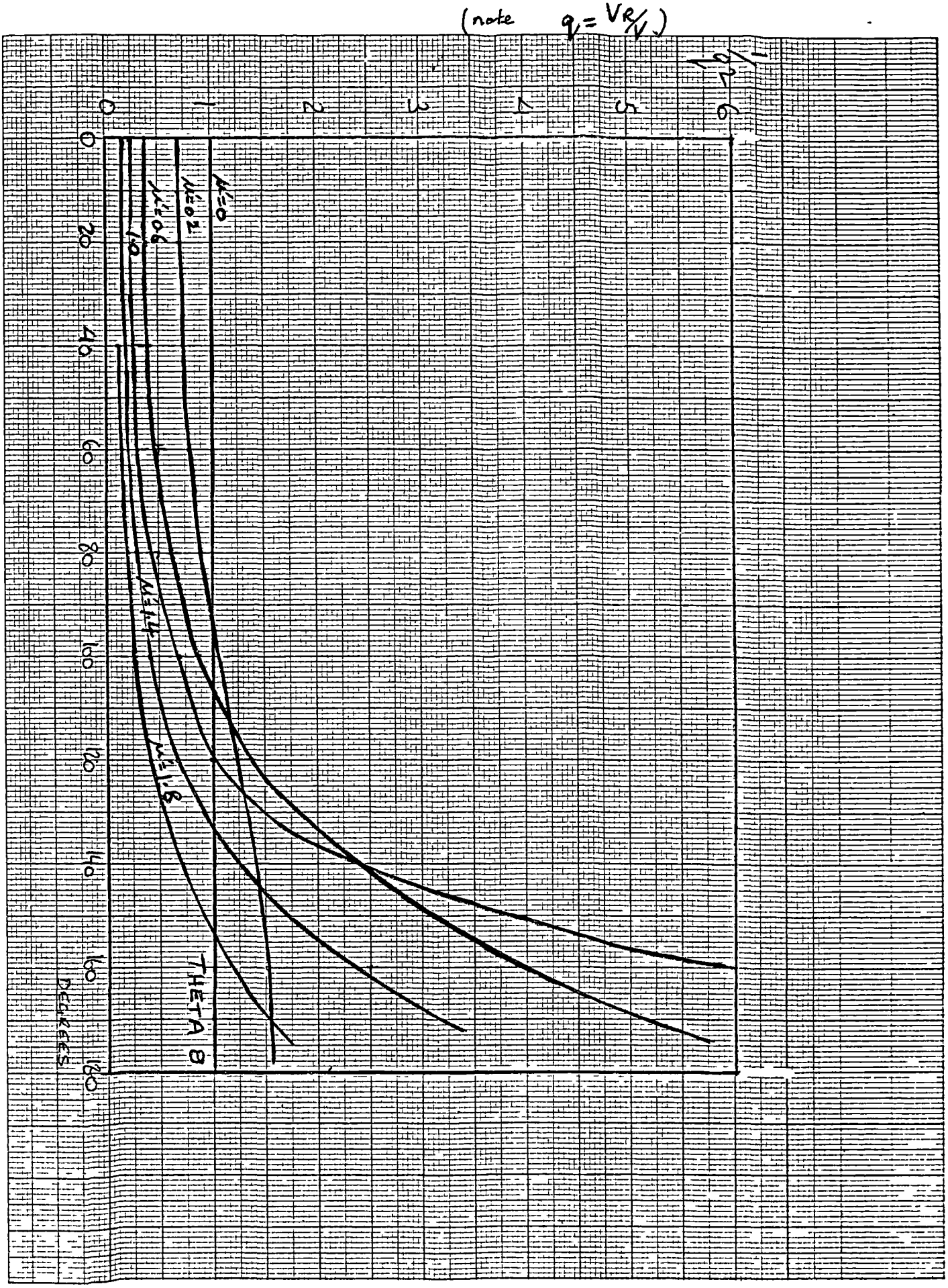

Fig.4.6. Variation of the ratio $1/q_2^2$ with azimuthal angle.

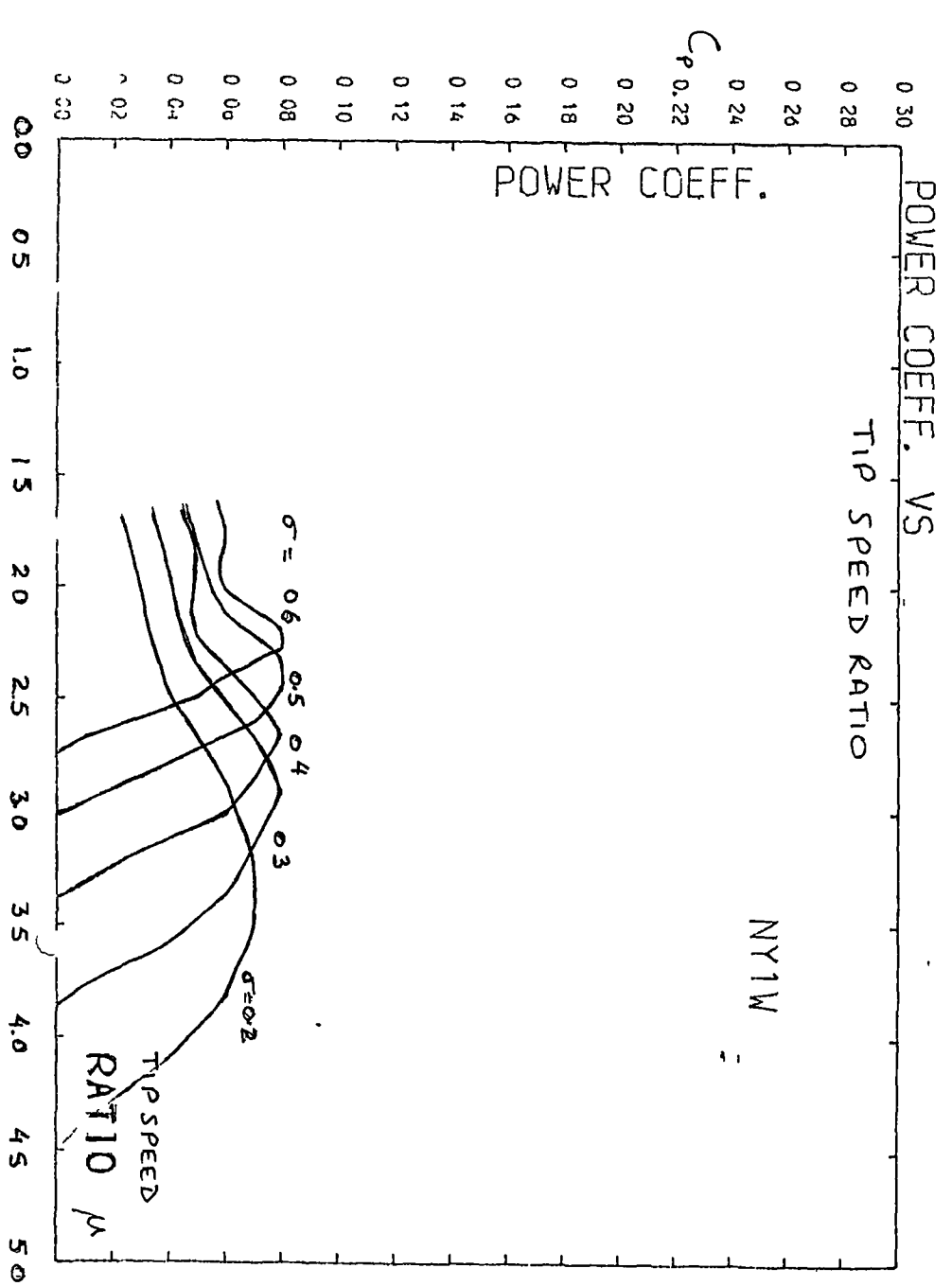

Fig.4.7. Power coefficient vs tip speed ratio

single streamtube program, data from test Ny1w

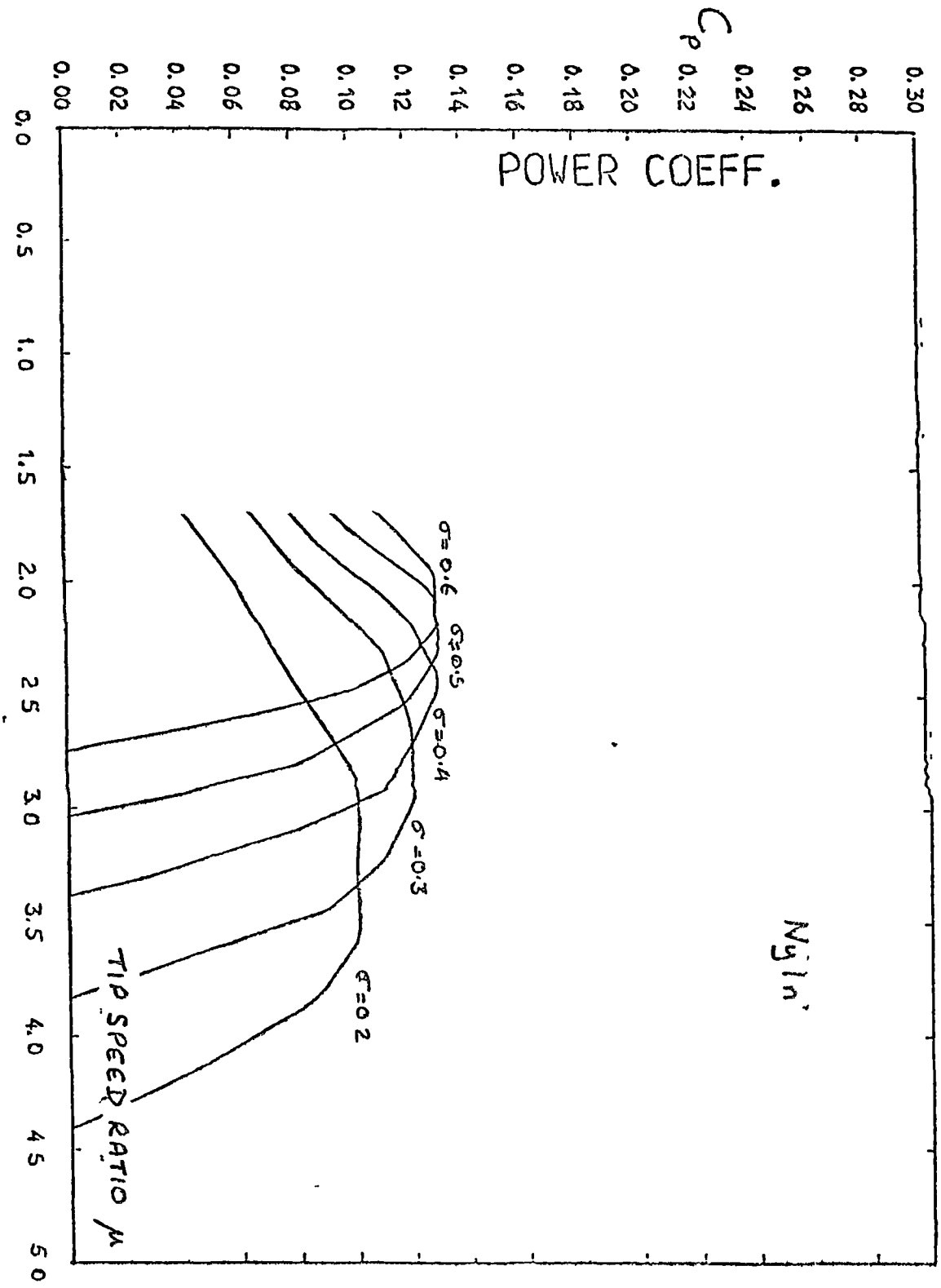

Fig. 4.8. Power coefficient vs. tip-speed ratio from data from test Nylon.

4.3. Conclusions

The new data for sailwings, obtained in the wind tunnel tests, has been used in the same low speed performance analysis as was performed in Chapter Two. It is clear that high tip speed ratio operation of a vertical axis turbine will not occur with these sailwings and so the maximum power coefficient will be quite low and a high solidity will be required.

It is not possible to make accurate theoretical predictions of turbine performance, for two reasons: firstly, the large range of variation in the pre-tension coefficients, shown to occur over the operating range, makes the data inadequate; secondly, with a high solidity turbine, operating at a low tip speed ratio, the single streamtube model of the flow cannot be applied and approximating the induced windspeed by the free windspeed is only valid at the lowest tip speed ratios.

It is however possible to predict the starting torque coefficient. In all cases, the torque coefficient C_Q on starting should be greater than $0.06 \frac{\Sigma A_e}{A}$ and for canvas sailwings it may reach $0.15 \frac{\Sigma A_e}{A}$.

Canvas appears to be the most suitable fabric of those tested. The starting torque coefficient may be higher than with the other materials and performance will be highest in low winds, when least energy is available.

CHAPTER FIVE

A PROTOTYPE TURBINE

5.1. Introduction

From the re-appraisal of the performance that could be expected from a vertical axis sailwing turbine, it was clear that a low speed, high solidity design was necessary. Such a design will inevitably have a quite low performance but its possible advantages over other designs, due to its vertical axis of rotation and low cost construction, seemed to make further investigation worthwile, especially since the torque characteristics appeared to be well suited to pumping applications. It was therefore decided to build a prototype and to undertake performance measurements on an open air test site, so as to provide reliable performance data.

Some of the factors arising in the design of such a turbine, and the design choices to be made, are discussed. Details of the two metre diameter prototype design are given and some predictions for the turbine performance are presented.

5.2. Discussion

The use of sailwings in a vertical axis wind turbine introduces structural problems when compared to solid bladed designs. The leading edge member must carry most of the aerodynamic load, must resist the loading applied by the

tension in the sail membrane and is also subject to centrifugal loads due to the rotation. All these loads increase with windspeed and tip speed ratio. The stresses arising in the leading edge member limit the length of blade which may be used without some form of bracing. Bracing inevitably incurs drag which, although not important at the lowest tip speed ratios, increases rapidly at tip speed ratios above one.

Several configurations for a vertical axis turbine may be considered (Fig.5.1). With arrangements a) and b), the leading edge member is additionally stressed by having to react all or part of the trailing edge tension. The struts must be large enough to support the weight of the blades, they must also transmit the driving torque to the axis and have to restrain the blade in position. It should be realized that the struts ma y come under a substantial compressive load. In arrangement c), the leading edge member is not so highly loaded but a longer blade length is required for a given swept area. The struts must still be large enough to withstand the compressive load now applied by the trailing edge tension. The central shaft also comes under a compressive load, applied by the cables supporting the top bearing; which also means that the bearings must both withstand an axial thrust.

Eventually the choice of design configuration should come down to the cost for a given useful output. However, the cost will depend on the local availability of materials and the useful output is difficult to predict as it will depend on the load matching and the performance of each

turbine configuration. With vertical blades, flexing of the leading edge member will allow increased deflection of the trailing edge; this may limit the tip speed ratio. The use of inclined blades will reduce the starting torque coefficient but may increase the peak power coefficient as the optimum tip speed ratio is increased; this may also allow improved load matching. Less deflection of the trailing edge will occur and deflections will have less effect as most of the power is then produced near the outer ends of the blades.

In the event, the inclined blade configuration was chosen for the prototype turbine and the design was very similar to that tested in a wind tunnel by Newman and Ngabo (1978). The main differences in the present design were the use of canvas sails rather than 'Dacron' and the use of individual blade struts instead of a central supporting disc.

5.3. Design Details

A diameter of two metres was chosen for the turbine. The size was determined mainly by cost restrictions and practical considerations of ease of construction and installation. It was decided to use three sets of blades so as to give strucural stability and as this should be sufficient to ensure self-starting. The blades were two metres long and were inclined at an angle of 30 degrees to the vertical. This gave a swept area of 3.5 m^2. The design is shown in Fig.5.2.

The choice of sail dimensions was fairly arbitrary as no clear guidelines had emerged from the theoretical work. However, the peak power coefficient of a low tip speed ratio turbine is unlikely to be very sensitive to small changes in the solidity. The sail dimensions are shown in Fig.5.3 and gave a ratio of total sail area to swept area of 1.1. Canvas was chosen for the sails for the reasons discussed in section 4.2; i.e. because it seemed that the starting torque was likely to be higher and that the performance should be best in low winds. Tent fabric, with a density of 250 g/m^2 was used and was treated with 'Mesowax' waterproofer and preserver.

The trailing edge was curved in a circular arc with a maximum hollow equal to 3% of the blade length. Two different materials were used for the trailing edge line; 3mm stranded steel rope ($\epsilon_T \simeq$ 83 kN/unit strain) and 3mm nylon cord ($\epsilon_T \simeq$ 0.82 kN/unit strain). The lines were secured at the bottom endplate to tensioners which allowed setting of the pre-tension by means of a torque wrench. The leading edge was a 40mm diameter wooden dowel (mopstick), painted for weather protection. Wood was chosen for its high strength to weight ratio. The central struts and leading edge mounts were made from 20mm and 25mm conduit respectively. At their inner end, the struts were bolted to a plywood triangle which was connected to the central shaft by aluminium flanges. Although the struts were probably stronger than necessary a significant reduction in the parasitic drag would require a streamlined section. A solid supporting disc would result in less drag but seems very wasteful of material.

The central shaft was in two sections of 1" galvanised steel pipe, secured at each end by aluminium flanges. This shaft was stiffened by wires, as can be seen in Fig.5.2. These served to both stiffen the shaft and to assist in alignment during construction. Between each endplate and bearing, the pipe was replaced by 25mm solid steel shaft. This was necessary to withstand the bending stresses in the top shaft. This shaft must be quite long, since the bearing needs to be mounted such that the lines of action of the guy wires pass through its centre. This avoids the bearing swiveling in its housing due to uneven guy wire tension arising from wind loads. The bearings used were 25mm internal diameter deep groove ball bearings with sealed races and spherically machined outer surfaces. These are able to swivel in their housings and so could accomodate small shaft deflections.

For the guys, 3mm stranded steel cable was used, attached by barrel strainers to 1.5m long angle iron stakes. Five guy wires were used do as to provide redundancy. The support tower was fabricated from 1" square section steel tubing. It was clamped to a foundation block, sunk into the ground. This was a 0.6m sided concrete cube, which happened to be available and which provided ample ballast.

The turbine was constructed by the author. The main difficulty was found to be in accurately aligning the top and bottom shafts. Otherwise the individual components were quite easy to manufacture and no particular skill was required. The turbine was balanced statically.

It was found that three people could install the turbine without difficulty. The tower was clamped to the foundation, the turbine was then lifted, with its axis horizontal, and pins on the bottom bearing plate located into slots on the top of the tower. Using a rope and gin pole arrangement, the turbine was simply pulled upright. A back rope maintained the turbine vertical while the guy wires were attached to their stakes and tensioned.

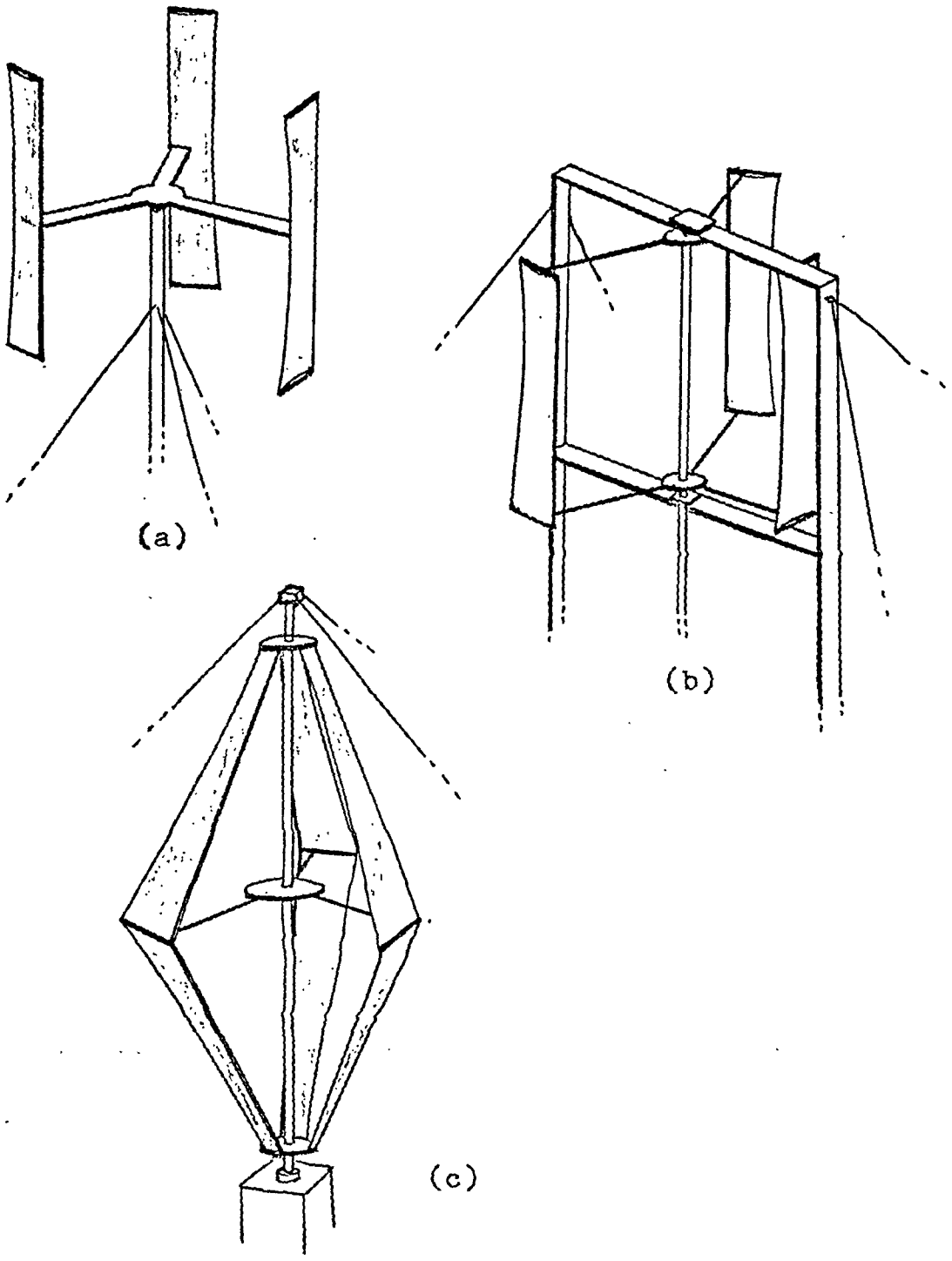

Fig.5.1. Some possible arrangements for a sailwing turbine.

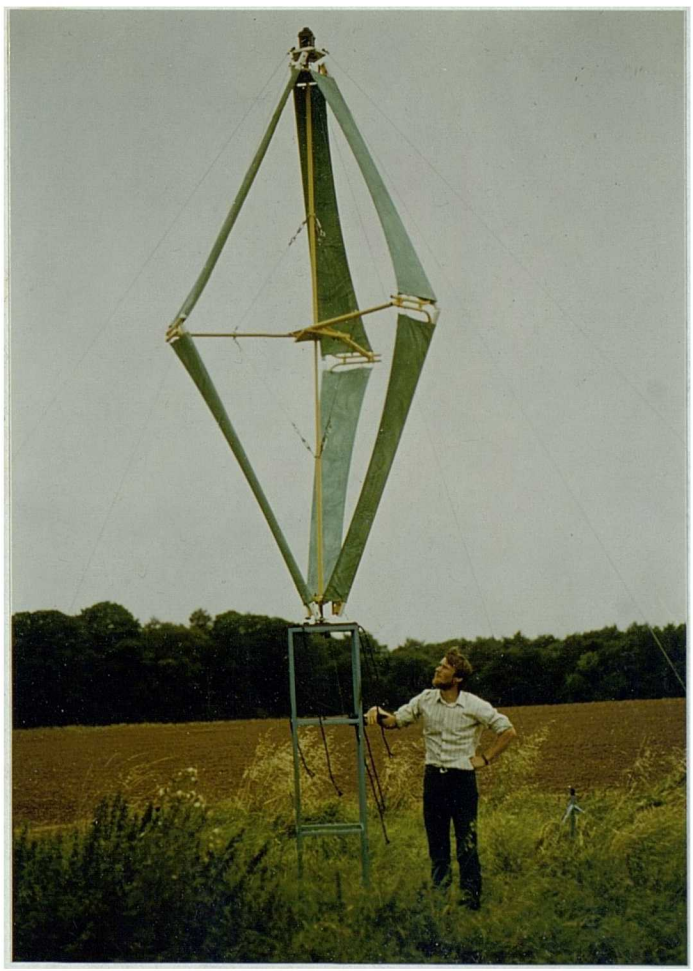

Fig.5.2. View of the prototype turbine.

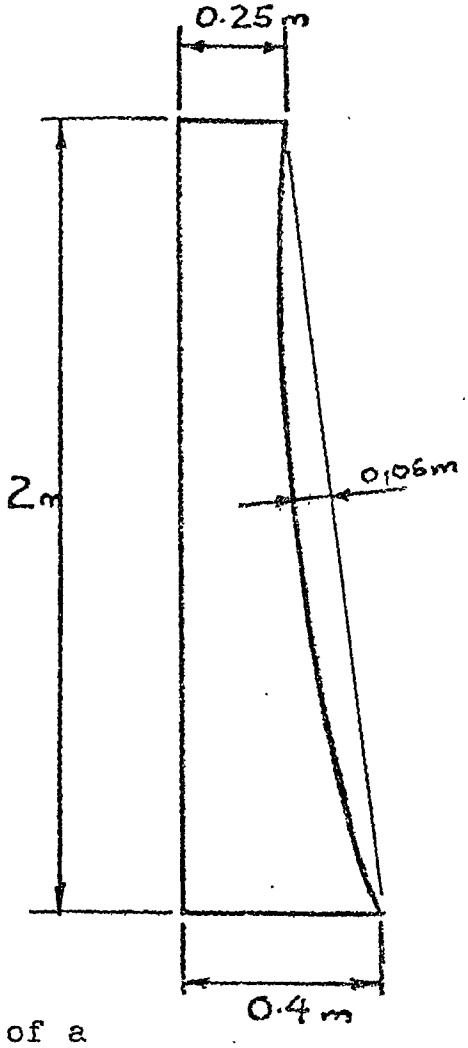

Fig.5.3. Dimensions of a single sail

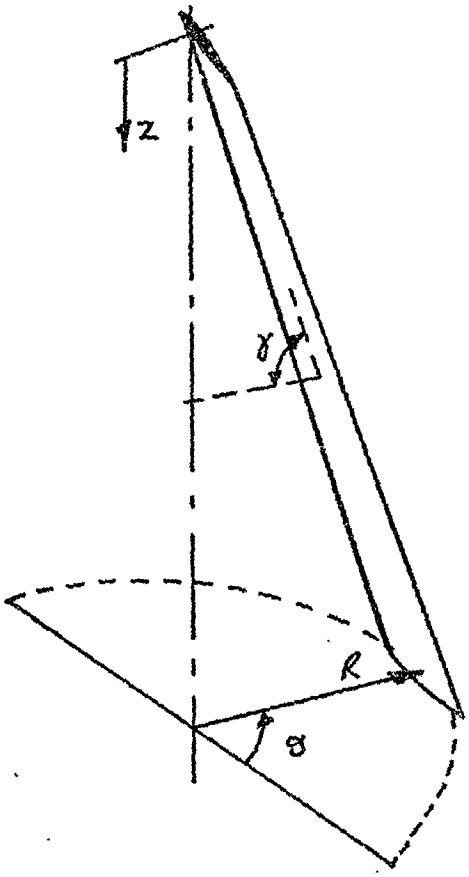

Fig.5.4. An inclined turbine blade.

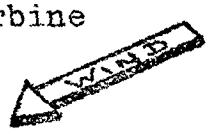

$$y = \frac{z}{R \tan \gamma}$$

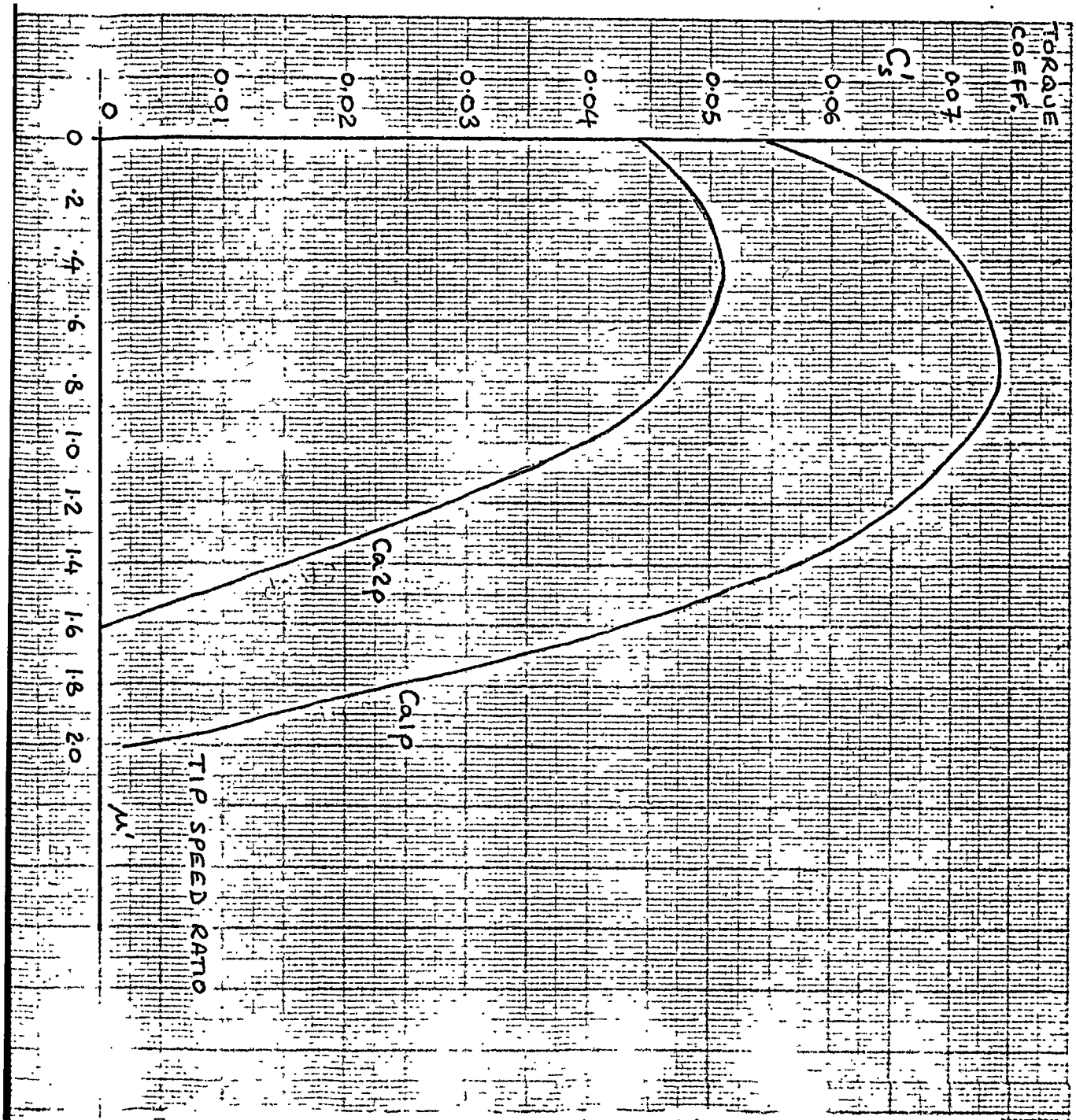

Fig.5.5. Torque coefficient vs. tip speed ratio
-prototype turbine —prediction

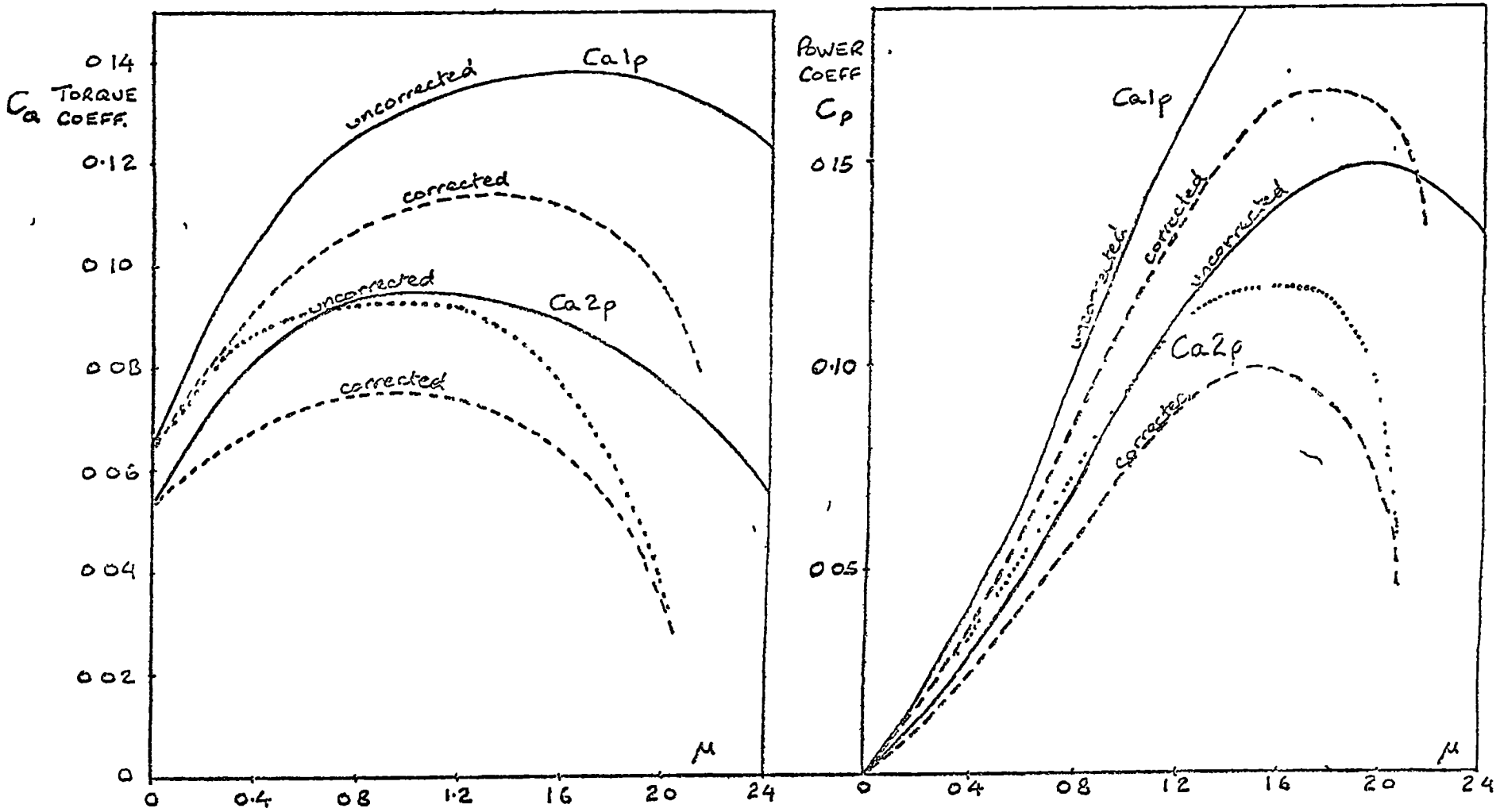

Fig. 5.6. Predicted torque and power coefficient curves for the prototype turbine.

——— prediction

– – – – – corrected for parasitic drag

..... assumed average performance

proofed canvas sailwing

pre-tension coefficients.

Ca1p $C_{p_T} = 2.2$

Ca2p $C_{p_T} = 0.2$

5.4. Prototype Theoretical Performance

To allow for the inclined blades of the prototype, it is necessary to slightly modify the theory presented in Chapter One and used to produce the torque curves of the previous chapter.

The expression for angle of incidence α (eqn. [1.9]) becomes:

$$\alpha = \text{atan}\left(\frac{\sin\gamma\sin\theta}{\mu' y + \cos\theta}\right) \qquad [5.1]$$

where $y = \frac{z}{R\tan\gamma}$ [5.2] (Fig.5.4)

and the expression for the ratio q (eqn. [1.14]) becomes:

$$q = \sqrt{(y\mu' + \cos\theta)^2 + (\sin\theta\sin\gamma)^2}$$

The derivation of these equations may be found in Appendix 5.

Now, it is possible to repeat the analysis, except that it is necessary to integrate along the z-axis at each azimuthal blade position. Doing this analysis using the data from tests Ca1p and Ca2p for the canvas sailwings, produces the curves of torque coefficient C_s' vs. μ' shown in Fig.5.5. Lacking a better alternative, these curves have been converted to curves of true torque coefficient C_Q and power coefficient C_P vs. true tip speed ratio, by assuming that the solidity is still small enough for the approximation for the induced flow, $V \simeq V_w$ to be reasonably valid. Hence, it is assumed that:

$$C_Q \simeq C_s' \cdot \frac{\Sigma A_B}{A} \quad ; \quad C_P \simeq C_Q \cdot \mu' \quad ; \quad \mu \simeq \mu'$$

Obviously, these approximations become less valid as tip speed ratio increases. This gives the curves, shown by solid lines, in Fig.5.6. The parasitic drag caused by the struts has been estimated, as shown in Appendix 5. Allowance for this drag gives the modified predictions for the torque and power coefficients shown by the dashed curves. Since the tension coefficient is generally lower at the higher tip speed ratios, it is possible to draw in the dotted curve as a speculative prediction of the probable average performance. This assumes that, in the average windspeed, the value of the pre-tension coefficient C_{ρ_T} when the turbine is stationary, is as it was in the wind tunnel test Ca1p (i.e. $C_{\rho_T} = 2.2$).

It is clear from these predictions that the effect of using inclined blades has been to significantly affect the starting torque coefficient expected. Surprisingly, the predicted starting torque coefficient is now little affected by the pre-tension coefficient.

5.5 Conclusions

A prototype vertical axis sailwing turbine has been designed and constructed. The diameter was two metres and three sets of blades were used inclined at an angle of 30 degrees to the vertical, the top bearing being held by guy wires. The swept area was 3.5 m^2 and the ratio of total blade area to swept area was 1.1. Canvas tent fabric was used for the sails.

The turbine was quite easy to construct except for some difficulty experienced in aligning the top and bottom shafts accurately. Some theoretical predictions for the performance indicate a torque coefficient C_Q of about 0.06 on starting. The predictions are less reliable at higher tip speed ratios but indicate a maximum power coefficient of between about 0.1 and 0.15 at a tip speed ratio of 1.6 to 1.8. The torque and power coefficients are expected to be significantly affected by the windspeed at higher tip speed ratios.

CHAPTER SIX

PERFORMANCE TESTS ON THE PROTOTYPE TURBINE

6.1. Introduction

Having built a prototype turbine, it was tested in the open air, to obtain data on its actual performance characteristics in a natural wind and so allow assessment of its suitability as a source of power.

Because of the variable nature of the natural wind, measurement of the performance characteristics of a turbine is not easy. There are basically two possible approaches. Either the turbine may be loaded by some form of dynamometer and run at constant speed, a series of tests at different speeds providing a complete picture of the performance. Or, the turbine may be left unloaded and be allowed to accelerate to its free wheeling speed, continuous measurement of its acceleration enabling calculation of the power output throughout the speed range. The first method has been used in open air testing of small turbines; as described, for example, by Herepath and Woollard (1980); but with a small turbine, it would seem difficult to maintain constant speed operation. Herepath and Woollard in fact found it necessary to allow for the power absorbed by fluctuations in the turbine speed. The second method has the advantage of simplicity, no sophisticated loading device being required. This method was originally used by Sharpe (1977) in wind tunnel tests and its use in open air testing has been described by, for example, Stacey and Musgrove (1981).

In both methods, considerable scatter in the results is inevitable and it is usual to sort the results into intervals of tip speed ratio and to average the data collected in each 'bin '. The main cause of scatter is the uncertainty with which the free windspeed experienced by the turbine may be estimated. Because of turbulence, this windspeed may be quite different to that measured by anemometers which must inevitably be some distance away.

Work was delayed several months by difficulty in obtaining permission to install the turbine on a test site on the university campus. The site eventually obtained was situated near the top of a slight hill with farmland to the south and south-west; the prevailing wind direction. The north-easterly direction was blocked by a single storey barn about ten metres distant (Fig.6.1).

6.2. Test Equipment and Measurements

6.2.1. Measurement of the Turbine Inertia

The acceleration test method relies on a knowledge of the moment of inertia of the turbine in order to calculate the power absorbed in accelerating. The turbine inertia was measured by arranging for it to be suspended as a torsional pendulum; allowing calculation of the inertia from

$$J = \frac{mgR_s^2}{(2\pi f)^2 l}$$

where J is the moment of inertia of the turbine about the axis of rotation, m is the turbine mass, R_s is the radius at

which the suspension ropes were attached, l is the length of the suspension ropes and f is the frequency of oscillation.

The turbine was assembled in the laboratory and suspended by ropes attached to each of the blade struts so that its axis was vertical. Values were recorded as follows: m =38 kg $\pm$0.2, R_s =0.56 m $\pm$0.005, f =0.318 Hz $\pm$0.002, l =2.00 m $\pm$0.01. These give a value of J =14.4 kg.m^2 $\pm$4%.

6.2.2. Measurement of Turbine Speed

The turbine speed must be measured to allow calculation of the instantaneous tip speed ratio and acceleration. The speed was measured using a tachometer, consisting of a disc with slots cut in the periphery and running through a slotted opto-isolator connected in an electronic circuit. The circuit contained a tachometer chip and produces a d.c. voltage output proportional to input pulse frequency (Fig.6.2). Details of the circuit are contained in Appendix 6. Calibration of the circuit showed a linear output up to about 300 Hz, corresponding to more than twice the maximum operating frequency.

6.2.3. Measurement of Windspeed

Measurement of windspeed enables values of instantaneous turbine speed and power to be converted to values of tip speed ratio, torque and power coefficient. The windspeed was measured using two anemometers, positioned slightly upstream of the turbine, at the turbine mid-height (Fig.6.3). It was

considered that this positioning allowed the anemometers to be as close as possible to the turbine while still measuring the free windspeed, undisturbed by the presence of the turbine. The free windspeed experienced by the turbine was estimated as the mean of the values recorded by the two anemometers. While this estimates the free windspeed a short time before the turbine speed was measured, the time difference was normally rather less than the time interval used in sampling the continuous recordings of wind and turbine speed that were made. Also, it should be realized that the wind direction may vary markedly during a short period and that the anemometers had a finite response time.

The anemometers and masts were constructed in the engineering workshops and calibrated in the wind tunnel. The anemometers used slotted discs and identical electronic circuits as the tachometer, producing a d.c. output proportional to windspeed (Appendix 6).

6.2.4. Measurement of the Trailing Edge Tension

The pre-tension in the trailing edge line was set using a torque wrench on the tensioning bolts. Because of friction in the bolts and the large rangecovered by the wrench, measurement was not very accurate. The accuracy was probably no better than $\pm$ 50 N. The tensions set were: wire trailing edge, 130 N and 250 N; nylon trailing edge, 400 N. In a 5m/s wind the pre-tension coefficients C_{PT}, based on mean chord, were thus: 3, 6 and 9 respectively with the turbine stationary.

6.2.5. Test Method

The voltage signals from the tachometer and the two anemometers were recorded on three channels of a multi-channel analoque cassette recorder in FM mode. The turbine was allowed to accelerate from rest to free wheeling speed before being braked and the cycle repeated. Recordings made during a typical test run are shown in Fig.6.4. It can be seen that the correlation between the windspeed readings was not particularly good. This method gave recordings covering the full range of tip speed ratio. A total of 180 minutes of recordings were made with the wire trailing edge and 130 minutes with the nylon cord.

6.3. Data Processing and Analysis

The recorded cassettes were played back through digitising equipment and the resulting data transferred to the PR1ME computer in the department. A sampling interval of one second was chosen.

To reduce the scatter in the values of torque and power coefficients, calculated from the measurements, data for which the windspeed estimate was too uncertain was eliminated. The windspeed measurements from the two anemometers were considered at the beginning and end of each sampling interval. The mean and standard deviation of the four values were calculated and if the coefficient of variation (standard deviation / mean) was greater than 0.08, then the data was rejected. A total of 88% of the data was eliminated in this

way.

With the remaining data, instantaneous values were estimated as follows: Considering the time interval (t) to (t+1);

free windspeed= $V_w(t) = \frac{1}{4}\left(V_{w_1}(t) + V_{w_2}(t) + V_{w_1}(t+1) + V_{w_2}(t+1)\right)$

turbine speed= $\dot{\theta}(t) = \frac{1}{2}\left(\Omega(t) + \Omega(t+1)\right)$

turbine acceleration= $\ddot{\theta}(t) = \Omega(t+1) - \Omega(t)$

torque= $T(t) = J\,\ddot{\theta}(t)$

power= $P(t) = T(t)\,\dot{\theta}(t)$

tip speed ratio= $\mu(t) = \dfrac{\dot{\theta}(t)R}{V_w(t)}$

torque coefficient= $C_Q(t) = \dfrac{T(t)}{\frac{1}{2}\rho A V_w(t)^2 R}$

power coefficient= $C_P(t) = C_Q(t)\,\mu(t)$

The sampling interval used and the coefficient of variation selected, were found to be acceptable compromises. A more rigorous rejection criterion could have increased the certainty of the windspeed estimate but would have reduced the amount of usable data. A shorter sampling interval would have increased the amount of data but, in fact, this was found to increase the scatter in the results, even when the windspeed data was given a time delay.

Considerable scatter was still present in the results and to produce performance curves the values were sorted into 'bins', 0.2 wide intervals in tip speed ratio. From the values collected in each bin, the mean and standard deviation were calculated and are plotted in Figs. 6.5 and 6.6. The number of values collected in each bin is also shown. All the values for the tests with the wire trailing edge were binned together in view of the uncertainty in the measurement of the trailing edge tension and the large range of windspeed during each test run.

The main cause of scatter in the results, apart from the remaining uncertainty in the windspeed estimate, is probably the effect of windspeed on the turbine performance. At very low turbine speeds, the effect of ripple in the tachometer voltage output may also have been significant. A small systematic error in the results is mainly introduced by the possible error in the measurement of the turbine inertia. Maximum errors have been estimated as follows: μ, $\pm$1.5%; C_a, $\pm$6.5%; C_p, $\pm$8% (Appendix 6).

6.4. Results and Discussion

The turbine was found to self-start readily and accelerated to a free-wheeling tip speed ratio of about 1.6. The torque and power coefficient curves obtained with the wire and nylon trailing edge lines are shown in Figs.6.5 and 6.6 respectively. The error bars represent plus and minus one standard deviation of the data in each bin. The scatter is explained partly by the uncertainty in the estimate of the

free windspeed experienced by the turbine and partly by the expected variation in the turbine performance due to changes in windspeed. The windspeed during the tests ranged between 2 m/s and 12 m/s.

It can be seen that the average values produce reasonably smooth curves. The theoretical predictions (see section 5.4) are included in the figures. The agreement with the prediction of the probable average performance is quite good and the agreement in the measured and predicted starting torque coefficient in particular, gives encouraging support to the wind tunnel test data of canvas sailwings.

The differences observed between the results for the wire and, the much more elastic, nylon trailing edge lines are small and hardly significant but are consistent with the expected effect of trailing edge deflections; namely, an improvement in performance at low tip speed ratios and a detrimental effect at higher tip speed ratios. A problem with the nylon trailing edge line was the flapping of the sails which occurred when the turbine was parked.

No particular shortcomings in the mechanical design were apparent, except that the tower should have been stiffer. The turbine survived storm force winds (>25m/s) when parked, with only minor damage to one of the sails.

Fig.6.1. View of the wind turbine test site.

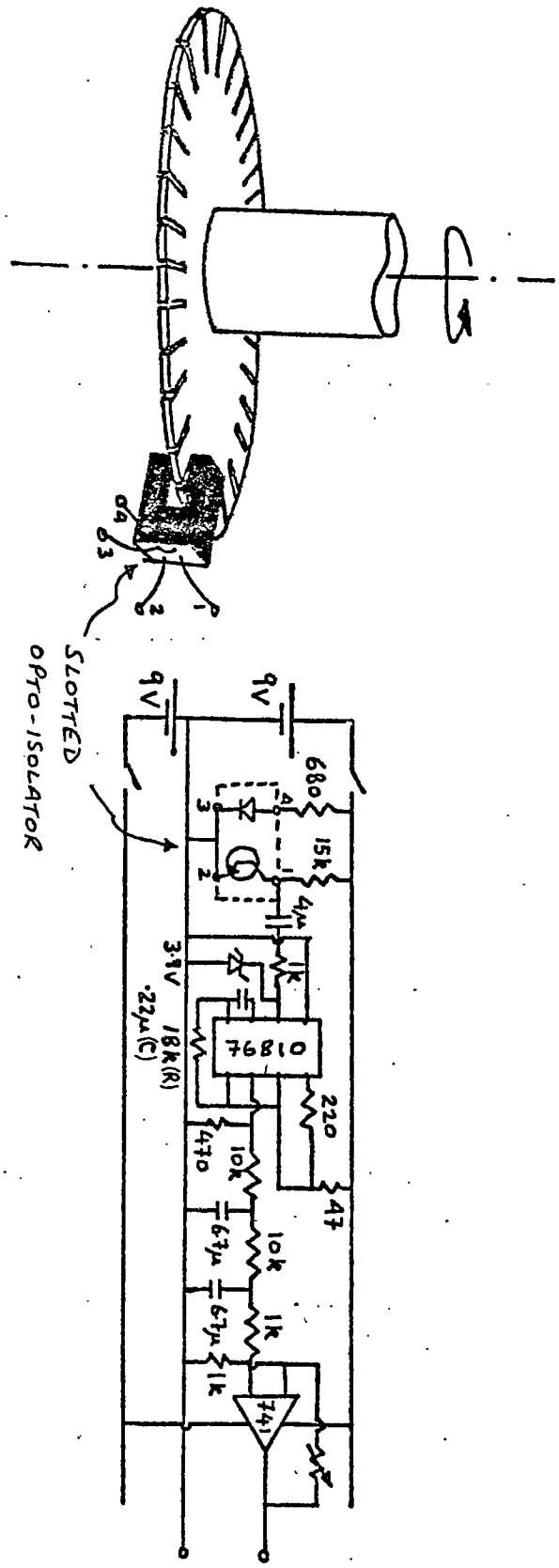

Fig. 6.2. Diagram of the tachometer arrangement.

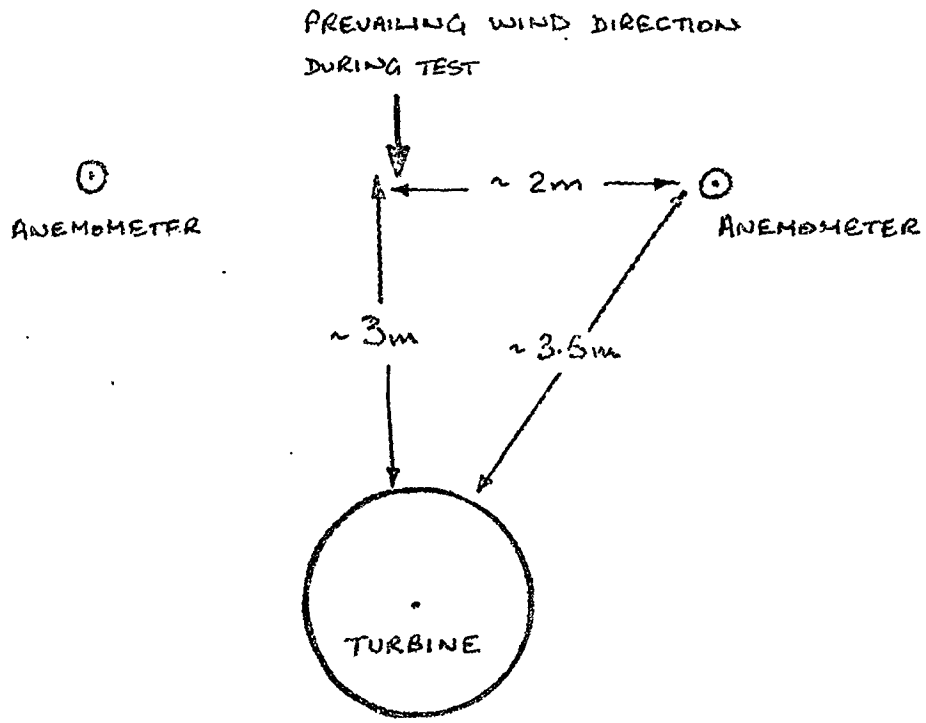

Fig.6.3. Schematic plan of the prototype turbine test arrangement

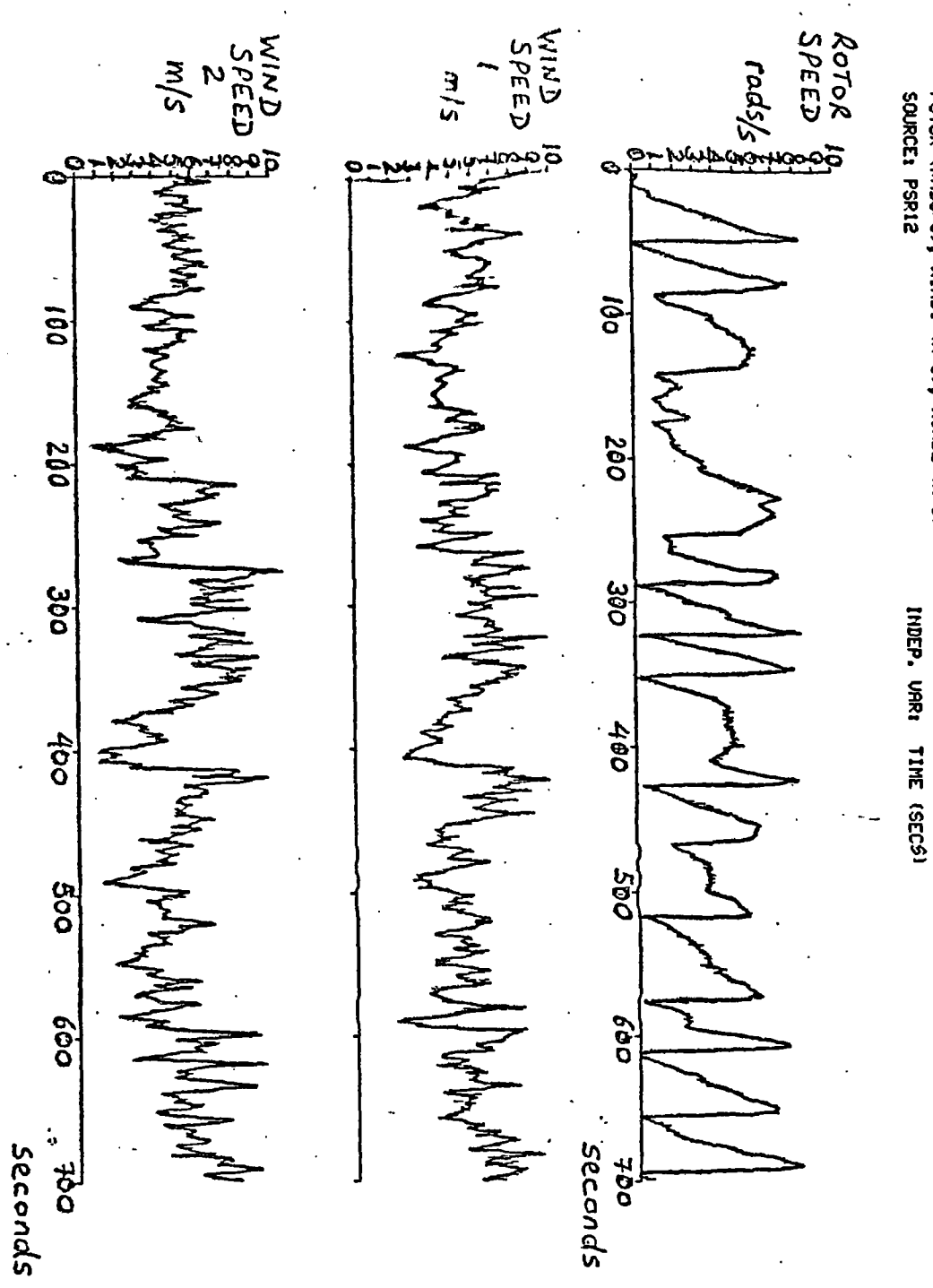

Fig.6.4. Rotor and windspeed vs. time during a typical test run

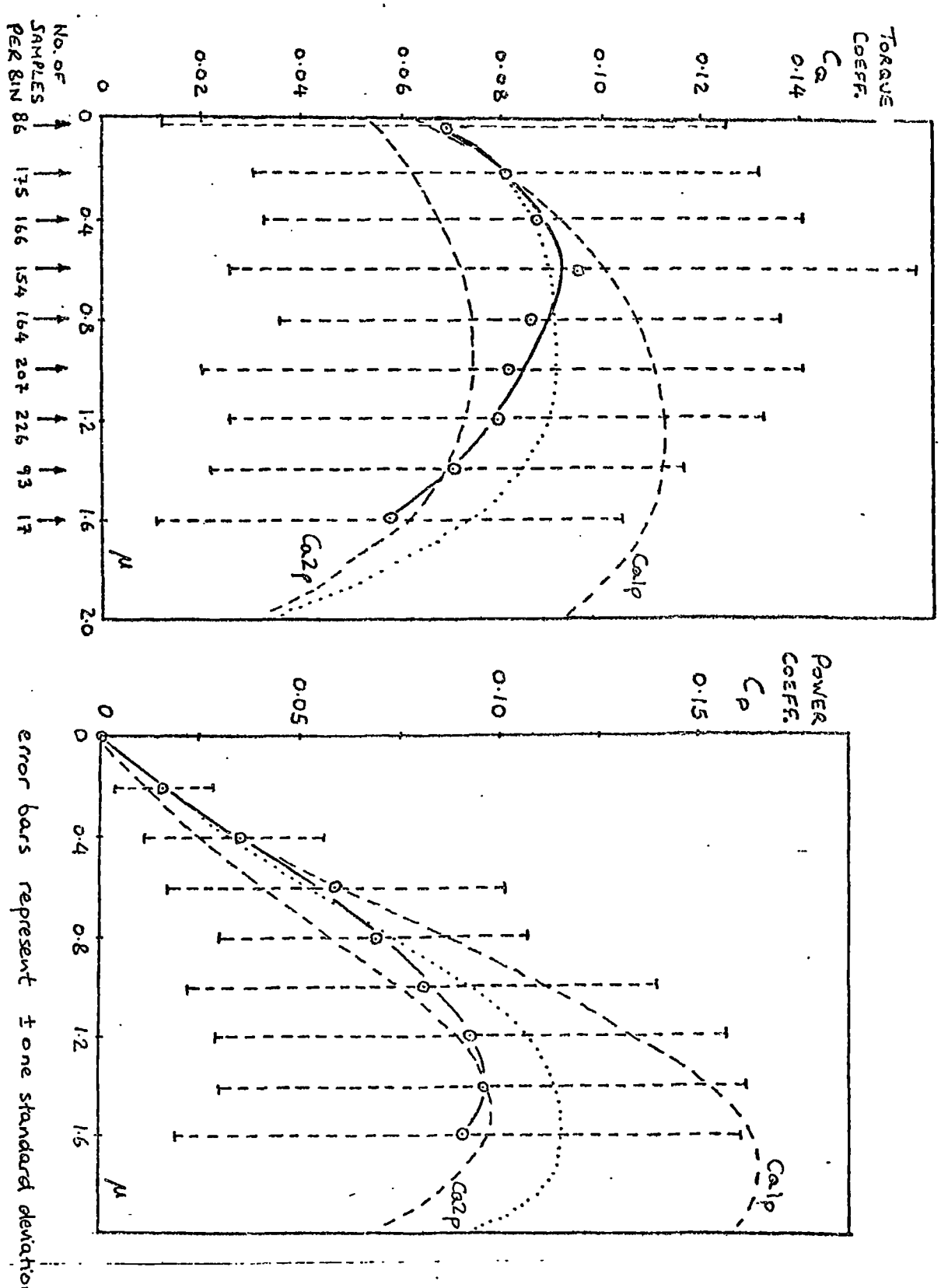

Fig. 6.5. Torque and power coefficients vs. tip-speed ratio with a nylon trailing edge.

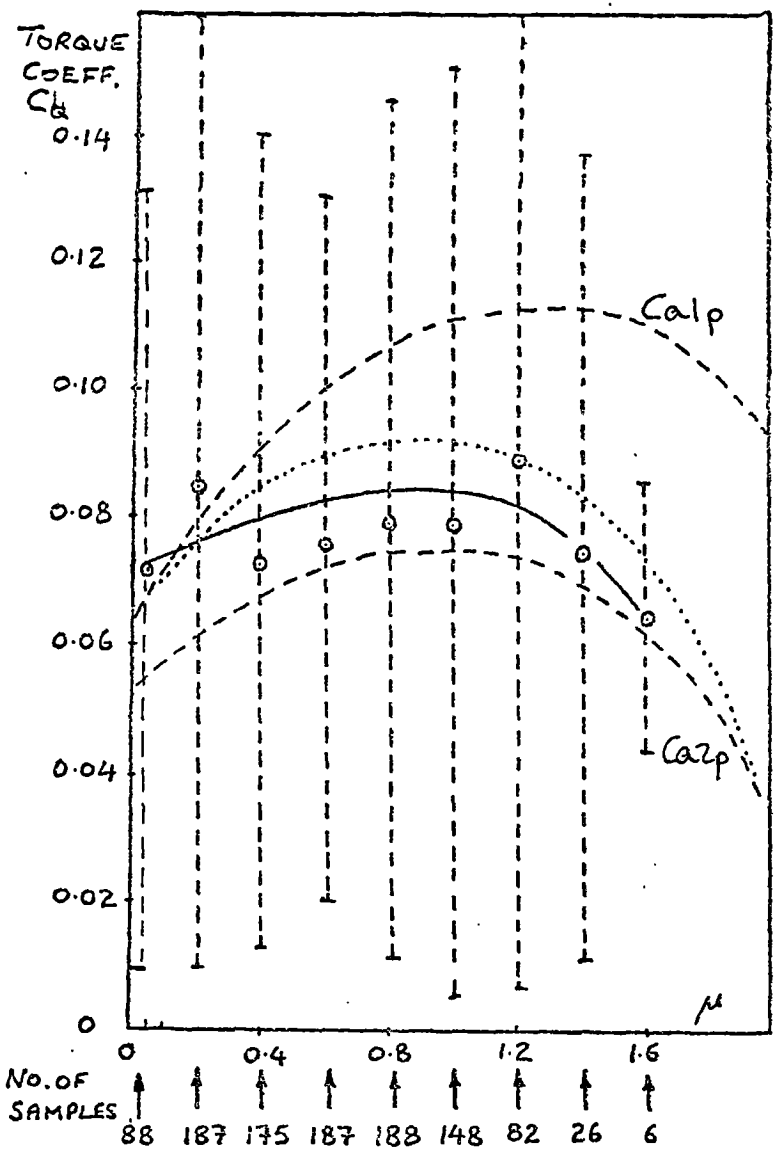

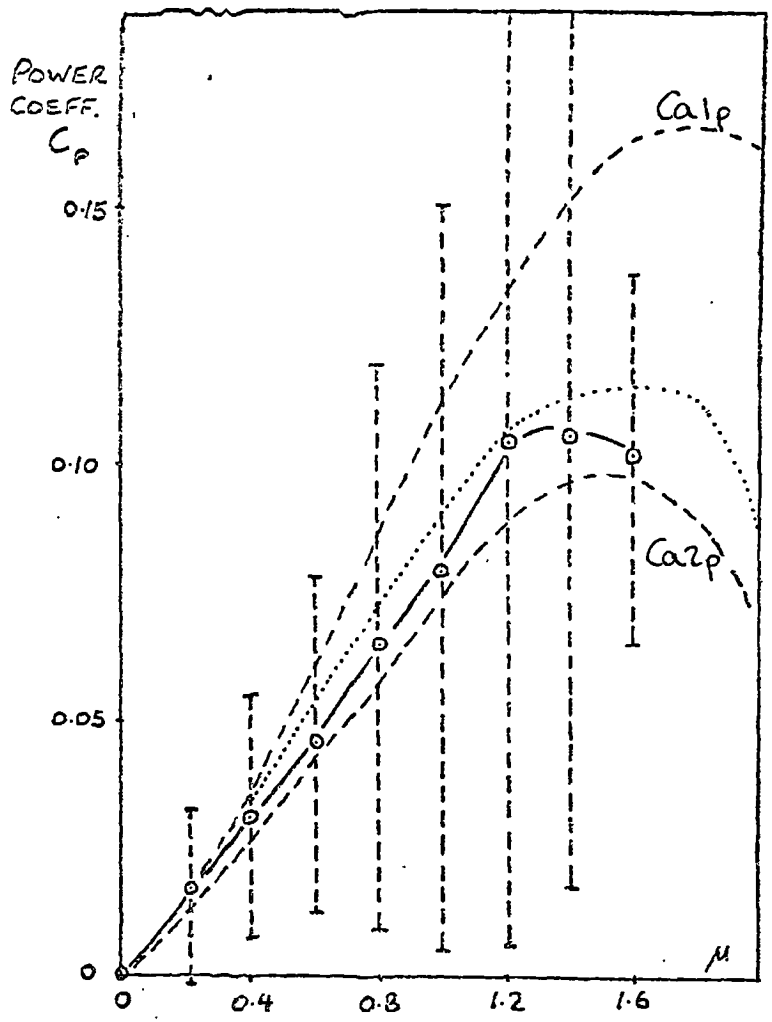

Fig.6.6. Torque and power coefficients vs. tip-speed ratio with a wire trailing edge

error bars represent ± one standard deviation

average windspeed = 5·0 m/s

—⊙— average measurements

– – – – predicted performance, corrected for parasitic drag } see Section 5.4.

····· assumed average performance

6.5. Comparison with other Turbines

The present prototype was of very similar design to the turbine tested in a wind tunnel by Newman and Ngabo (1978). The main differences were that they used 'Dacron' sails and a central supporting disc rather than individual blade struts. The ratio of blade area to swept area was 1.24, compared to 1.1 for the prototype. They found that the peak power coefficient varied slightly with trailing edge tension and elasticity. The test result shown (Fig.6.7), the best obtained, gave a power coefficient of 0.15 at a tip speed ratio of 1.3. They report a maximum starting torque coefficient C_Q, of 0.03.

The sail rotor described by Hurley (1979) has five blades, set vertically. The sails were of canvas and no trailing edge line was used, the trailing edge merely being cut in a V-shape. The ratio of blade area to swept area was 1.13. This rotor has been tested in the open air using a constant speed method (Hurley, 1980) and the results shown in Fig.6.8 were obtained. With the small number of measurements and the large scatter, the claimed peak power coefficient of 0.13 seems slightly optimistic. He does not report any measurements of starting torque. The low maximum tip speed ratio may be due to the lack of pre-tension in the trailing edge.

Stacey and Musgrove (1981) describe field tests of a high solidity, low aspect ratio, solid bladed Darrieus turbine. They obtained the results shown in Fig.6.9. As in the present measurements, the marked points are averages of a large

number of values and the error bars represent plus and minus one standard deviation. With the aerofoils set with their chord perpendicular to the cross-arm, the maximum power coefficient obtained was 0.09 at a tip speed ratio of 1.9. However, when they gave the blades an initial pitch offset of 3.5 degrees, nose out, they obtained a maximum power coefficient of 0.17. They attributed this to the effects of flow curvature.

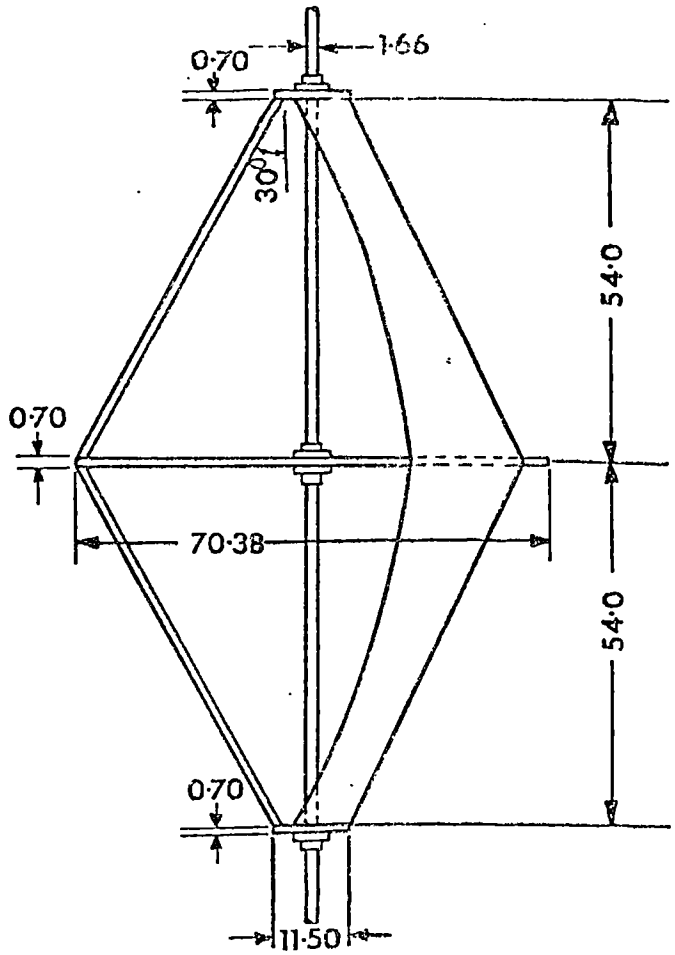

Side view of the wind turbine with the principal dimensions in inches.

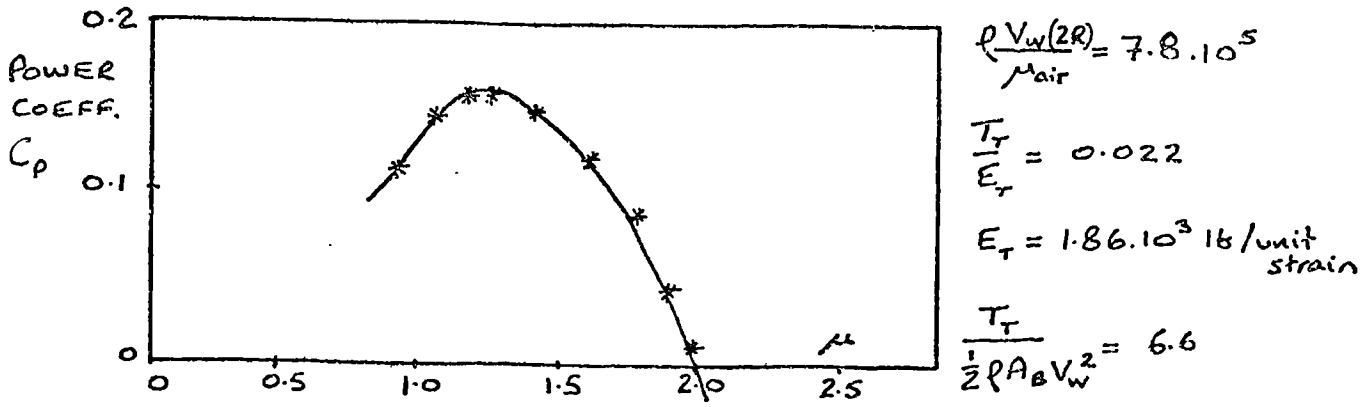

Fig.6.7. Power coefficient vs. tip-speed ratio

McGill sailwing turbine.

(Newman and Ngabo, 1978)

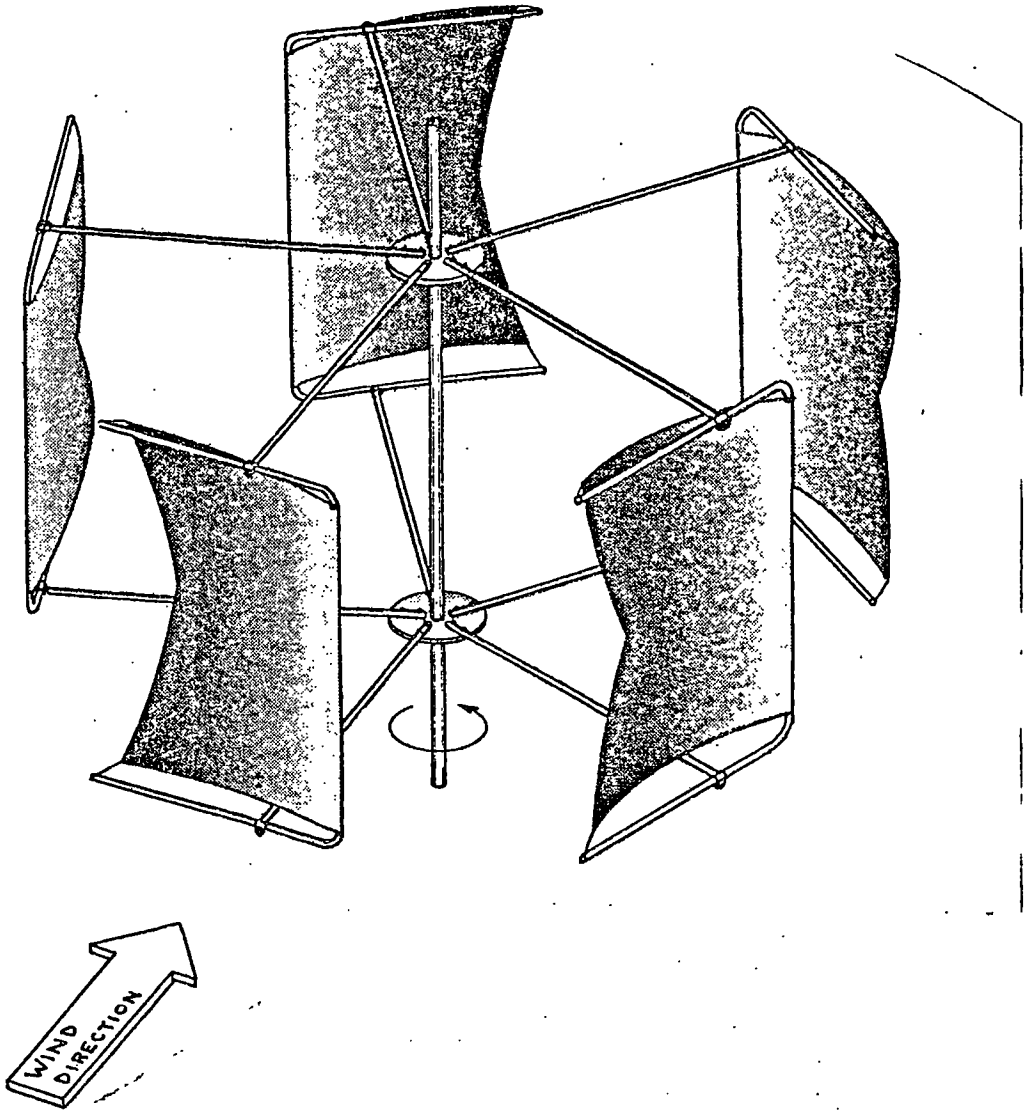

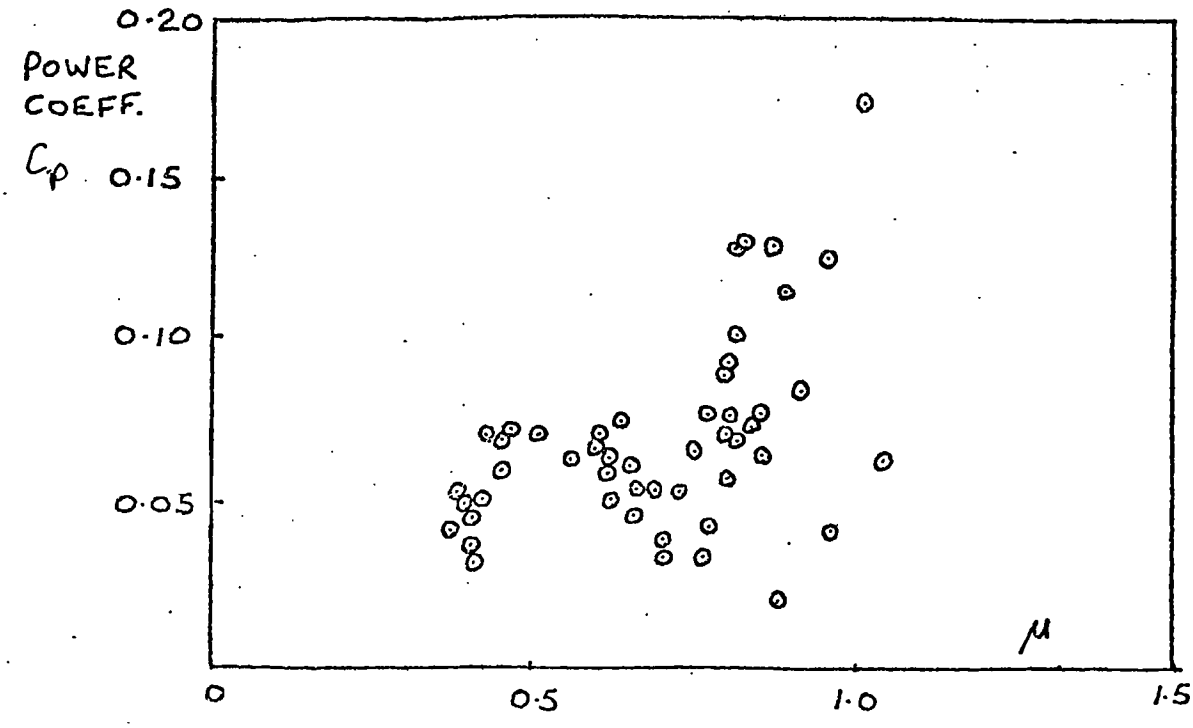

Fig.6.8. Power coefficient vs. tip speed ratio
Hurley sail rotor (Hurley, 1980)

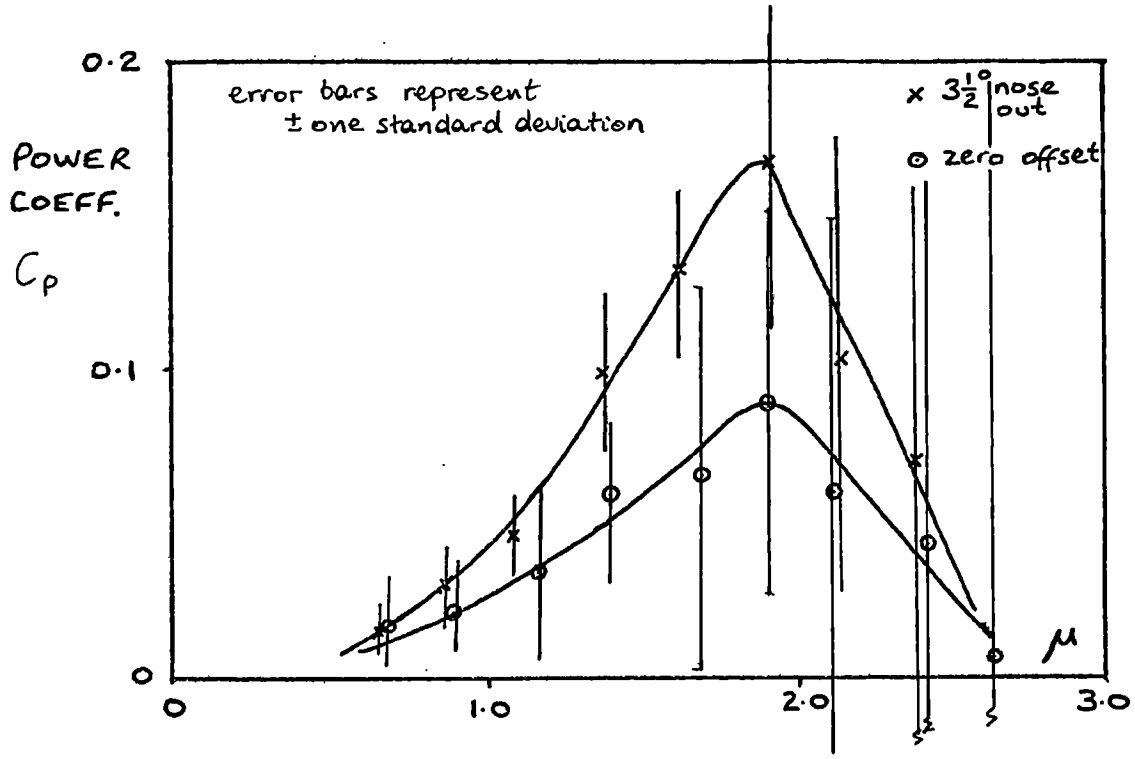

Fig. 6.9. Power coefficient vs. tip-speed ratio (NACA0015) solid-bladed, high solidity turbine. $\frac{\Sigma A_B}{A} = 0.53$ $AR = 3.125$ $\frac{c}{R} = 0.27$

(Stacey and Musgrove, 1981)

6.5.1. Flow Curvature and the Prototype Turbine

Flow curvature, and its effect on the 'virtual' blade profile and pitch, is explained in section 1.3. Its influence depends on the value of the blade chord to turbine radius ratio. For the prototype, this ratio was large; equal to 0.4 at the maximum radius position, comparing to the value of 0.27 in the solid bladed turbine of Stacey and Musgrove.

For a sailwing, it seems rather difficult to predict the virtual blade profile because of the continuously varying natural profile. However, to give an idea of the magnitude of the effect at low tip speed ratios, a simplified, approximate analysis has been performed to show the variation of virtual camber and pitch, assuming a non-varying natural profile. The method is explained in Fig.6.10. The angle of incidence is calculated at four positions along the blade chord; the following expressions for the virtual camber ratio ν and pitch β then give an approximation to the virtual blade profile:

$$\nu \simeq \tfrac{1}{6}\tan(\alpha_2-\alpha_1) + \tfrac{1}{3}\tan\beta$$

$$\beta \simeq \tfrac{1}{6}\operatorname{atan}\left(\tan(\alpha_2-\alpha_1) + 2\tan(\alpha_2-\alpha_3) + \tan(\alpha_2-\alpha_4)\right)$$

The results are plotted for several low tip speed ratios in Fig.6.11 ,for the maximum radius position.

Now, the operation of a solid bladed turbine is rather different to that of the sailwing prototype. At its optimum tip speed ratio, the solid bladed turbine derives all its driving torque from blade positions where the blade is unstalled. The tangential force coefficient is very sensitive to small

changes in angle of incidence in this, pre-stall region and so the effect of a change in incidence caused by flow curvature may be large. The sailwing turbine though, derives its driving torque from blade positions with a large range of incidence and so a small change in the effective incidence is less likely to have much effect. The effect of virtual pitch with the sailwing will be to generally give a slight increase in the camber on the upstream blade pass and a slight decrease on the downstream pass. This is the same effect as a small reduction in the pre-tension and a small increase respectively; this will not be affected by an initial pitch offset. It seems unlikely that an initial pitch offset will have any significant effect on the performance of the prototype turbine.

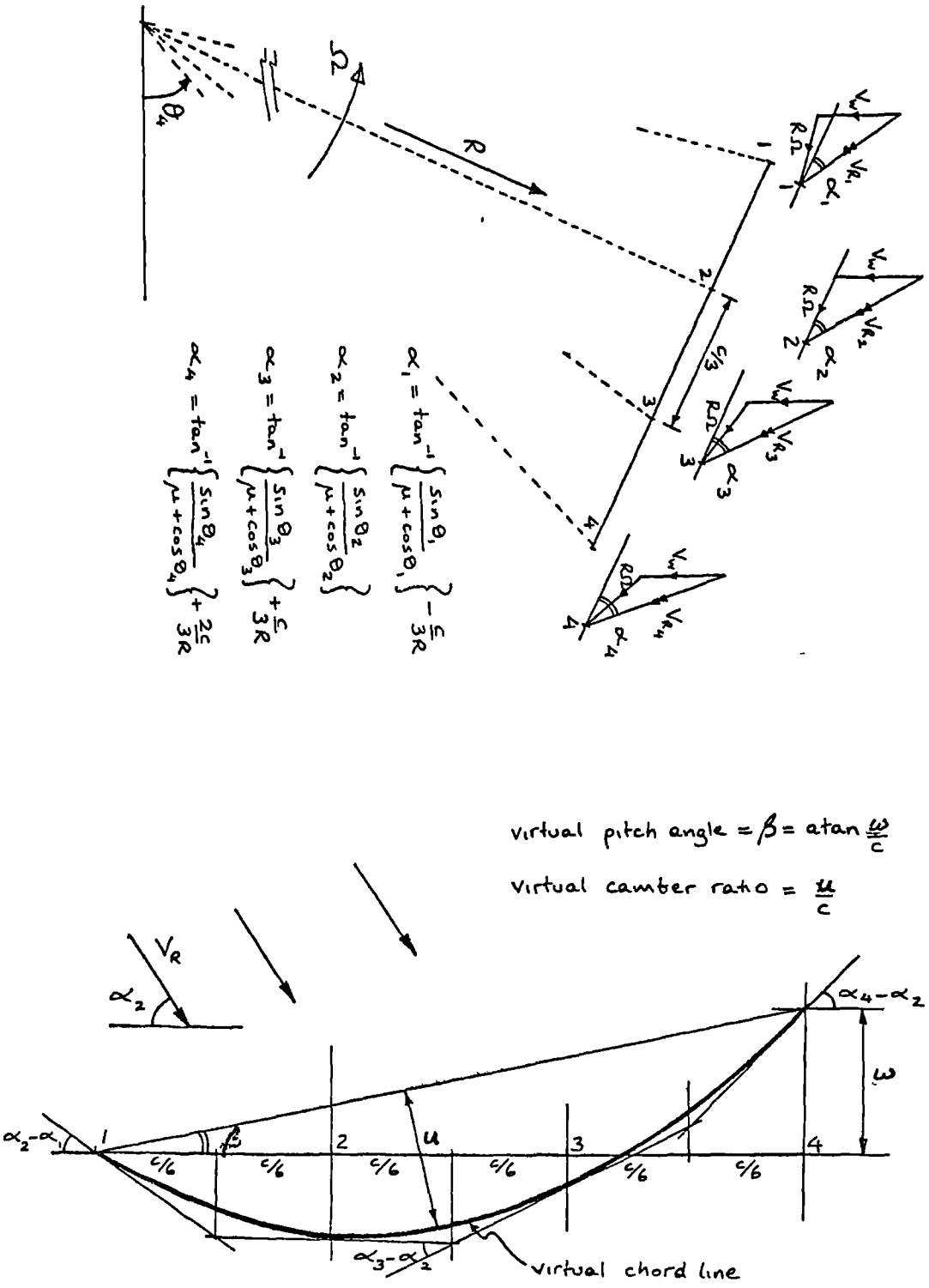

Fig.6.10. An approximation to the virtual blade profile.

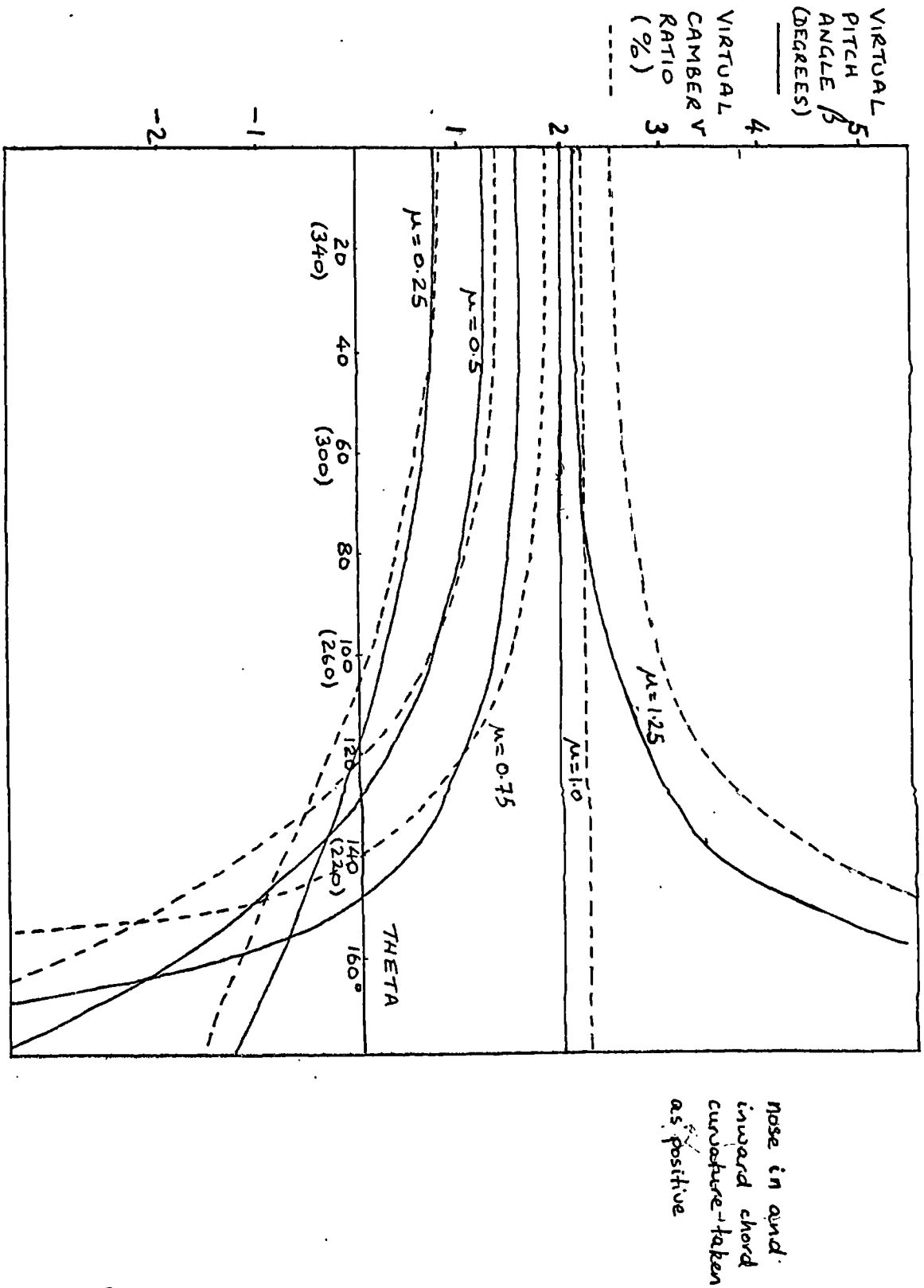

Fig.6.11. The variation of virtual pitch angle and virtual camber ratio with azimuthal angle at low tip-speed ratios. $c/R = 0.4$

6.6. Conclusions

The prototype vertical axis sailwing turbine has been tested in the open air using an acceleration test method to produce performance curves. Considerable scatter was present in the results but this was not significantly greater than obtained in field testing by other workers despite additional scatter probably introduced by variations in turbine performance with windspeed. The averaged values produced quite smooth curves for the torque and power coefficients which are in reasonable agreement with predictions, particularly at low tip speed ratios. Peak power coefficients of 0.11 and 0.095 ($\pm$0.009) were obtained with the wire and nylon trailing edge lines respectively and in both cases the starting torque coefficient was about 0.07 ($\pm$0.0045). The optimum tip speed ratio was about 1.4 and the free-wheeling tip speed ratio about 1.6.

CHAPTER SEVEN

THE PROTOTYPE TURBINE AS A WINDPUMP

7.1. Introduction

Although the performance of the prototype turbine is quite poor beside that of a good multi-blade design, which should produce power coefficients two or three times as high (Dunn, Eisa et al, 1979), it is probably quite similar to that of a Cretan windmill. From the tests, the torque characteristics appear to be well suited to pumping applications and it may be that, with its vertical axis and cheap construction, such a design could have advantages in some applications, particularly if good pump matching can be achieved.

The power in the wind depends on the cube of the windspeed. Most windpumps however, use a reciprocating pump with a constant torque requirement, the power absorbed therefore only rises in direct proportion to the windspeed and so , except in the lowest winds, most of the wind energy is wasted. The importance of improving the pump matching however, probably does not lie in increasing the output in high winds so much as in allowing better use of the energy in the gusts occurring in low winds. A windpump must generally be designed to produce sufficient output in the lowest wind likely to occur and so, increased output in high winds cannot be used, unless storage is available. But, increasing the system efficiency in low winds would enable the use of a smaller and hence cheaper windpump.

In this chapter, the amount of energy contained in gusts is demonstrated using the measurements of windspeed made during the performance tests and the factors limiting how much of this energy a wind turbine can use are discussed. A simple analysis has been used to show how the torque characteristics of the pump can affect the output.

The torque characteristics of reciprocating pumps may be altered by the effects of the inertia of the water in the pipes. Some tests have been made in which this effect was investigated, using a diaphragm pump. These tests were not very successful in obtaining high volumetric efficiencies but it did seem that a pair of such pumps would provide a suitable load for testing the prototype turbine. Subsequent tests of the prototype under load revealed a number of problems. Some possible modifications to the arrangement are discussed.

7.2. Turbulence in the Wind and Windpump Output

Van der Hoven (1957) has shown there to be two major peaks in the spectrum of horizontal windspeed (Fig.7.1). The peak occurring at a period of about 100 hours, corresponds with the passage of atmospheric pressure systems. The peak occurring at a period of about one minute (0.02 hrs.) with the gusts which are of interest here.

Because of the low viscosity of air, the wind near the ground is almost always turbulent. It may be visualized as a steady flow in which a random series of eddies are embedded. At a particular point, a series of gusts and lulls

occur as the eddy direction coincides with or goes against the general flow. The turbulence is of mechanical and convective origin and, close to the ground is dependent on: altitude, ground roughness, windspeed and temperature lapse rate (Lumley and Panofsky, 1964). It is assumed here that the turbulence experienced at the test site was typical.

At any instant, the windspeed can be considered as having steady and varying components; $V_w(t) = \bar{V}_w + v(t)$. The instantaneous power in the wind per unit area is thus:

$$P_w = \tfrac{1}{2}\rho\,(\bar{V}_w + v(t))^3$$

$$\text{i.e.} \quad P_w = \tfrac{1}{2}\rho\,(\bar{V}_w^3 + 3\bar{V}_w v(t)^2 + 3\bar{V}^2 v(t) + v(t)^3)$$

The average power is therefore:

$$\bar{P}_w = \tfrac{1}{2}\rho\,(\bar{V}_w^3 + 3\bar{V}_w\bar{v^2} + \bar{v^3}) \quad \text{per unit area}$$

(noting that $\bar{v} = o$), and as in practice the last term is small, the power in the wind may be determined from the mean windspeed $\bar{V}_w$ and its variance $\bar{v^2}$.

The mean and variance of the windspeed were calculated for each recording made in a low wind. The variance was found to lie between 1.0 and 1.6 m^2/s^2 and calculation of the average power showed it to lie between 1.2 and 1.3 times the value of $\frac{1}{2}\rho\bar{V}^3$. Some typical traces of windspeed recorded at the test site are shown in Fig.7.2. This additional 20 to 30% energy is only available to small turbines

as it is contained in small eddies; the turbine diameter must be rather less than the eddy diameter for a net energy gain. Another factor limiting the availability of this energy is the speed response of the turbine. This response will depend on the turbine inertia and the power/speed characteristics of the turbine and its load. The inertia of a vertical axis turbine is generally greater than that of a horizontal axis machine as the blades are on the circumference of the swept area. But this is a minor factor beside the energy that a horizontal axis turbine may lose in yawing. Gusts usually come from a different direction to the general flow and der Kinderen et al(1977) have estimated that at least 20% of the total energy is thereby lost to horizontal axis turbines.

This suggests that small, vertical axis wind turbines have perhaps 20% more energy available to them than other turbines. However, gust energy will be wasted unless it can be absorbed by the load. To demonstrate how the torque/speed characteristic of the load can affect the energy absorbed, a simple mumerical analysis has been used.

A typical ten minute recording of windspeed has been used in a computer program with performance data from the prototype tubine and idealised pump torque characteristics. The program calculated the rotor speed and the power absorbed by the pump at one second intervals, assuming quasi-steady operation at each point. Only positive displacement pumps were considered and idealised characteristics with no cyclic torque variations were assumed. Starting problems,

due to the difference between starting and mean rumning torque, were not considered as the time interval was too short for meaningful consideration of this. The assumed torque characteristics, and those of the prototype turbine are shown in Fig.7.3. The results of the analysis are given in Figs.7.4 and 7.5. These show the variation of turbine speed and power absorption by the load with time, together with the windspeed and wind power traces. It can be seen that the best matched constant torque pump absorbs only 70% of the energy absorbed by the variable torque pump.

Clearly, a better matched pump can significantly increase the system efficiency of a windpump and hence, development of such a pump would seem a promising way of reducing the capital cost of a windpump installation.

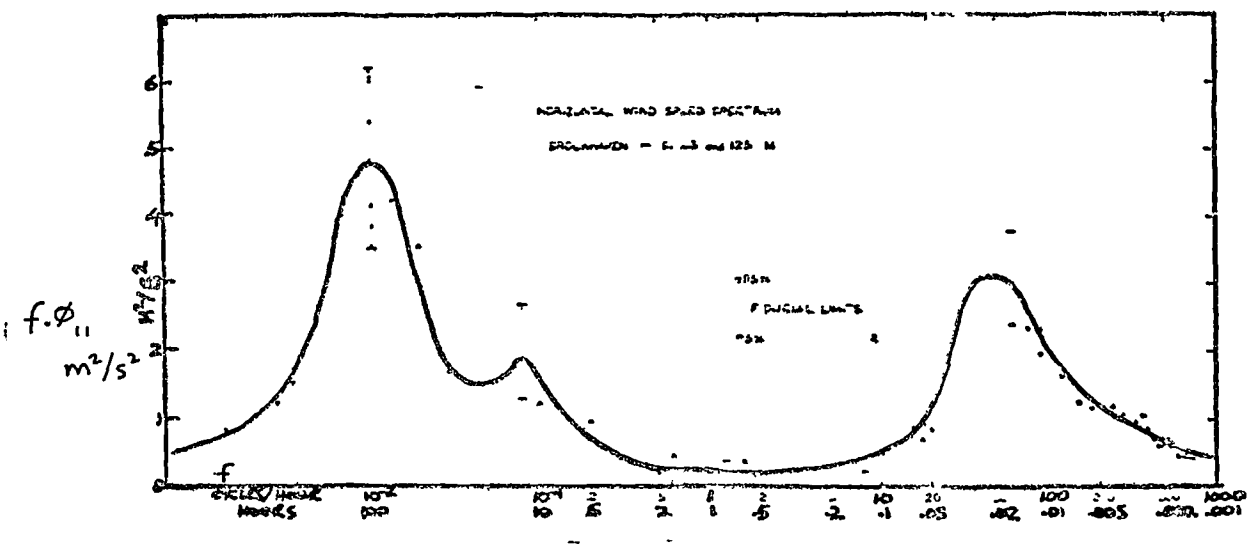

Fig.7.1. A Spectrum of the Horizontal Windspeed (van der Hoven, 1957)

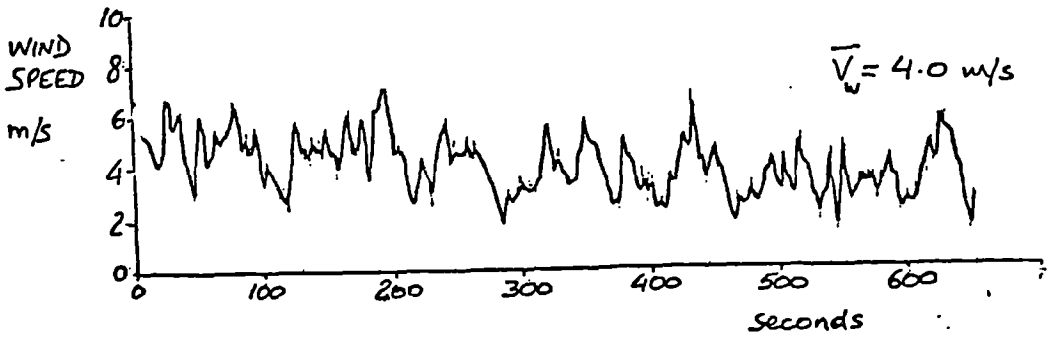

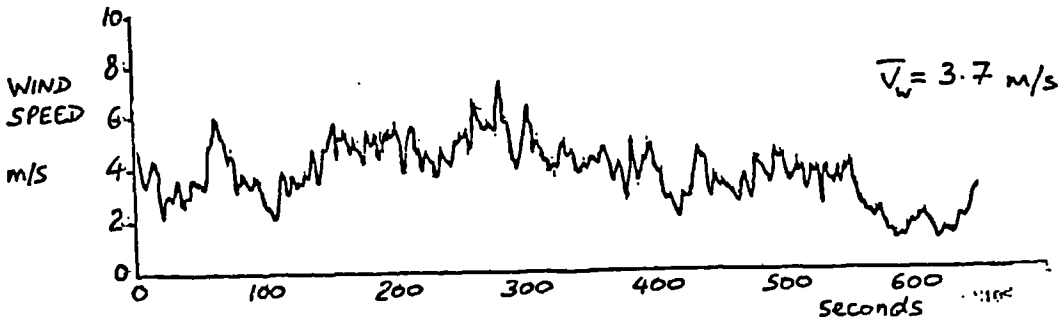

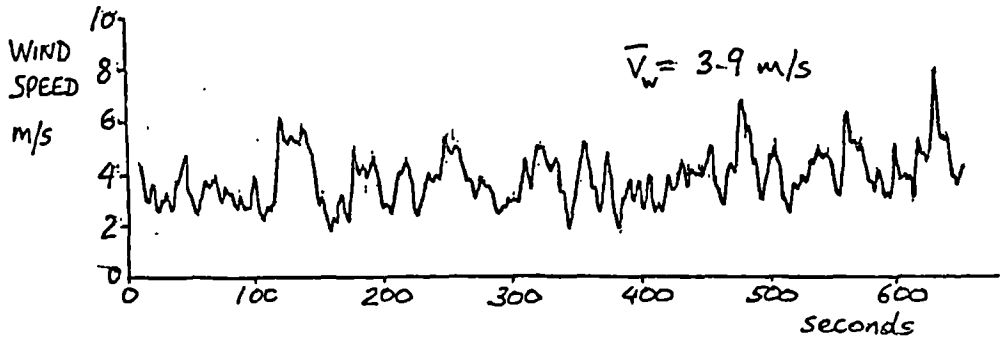

Fig.7.2. Some typical recordings of windspeed at the test site.

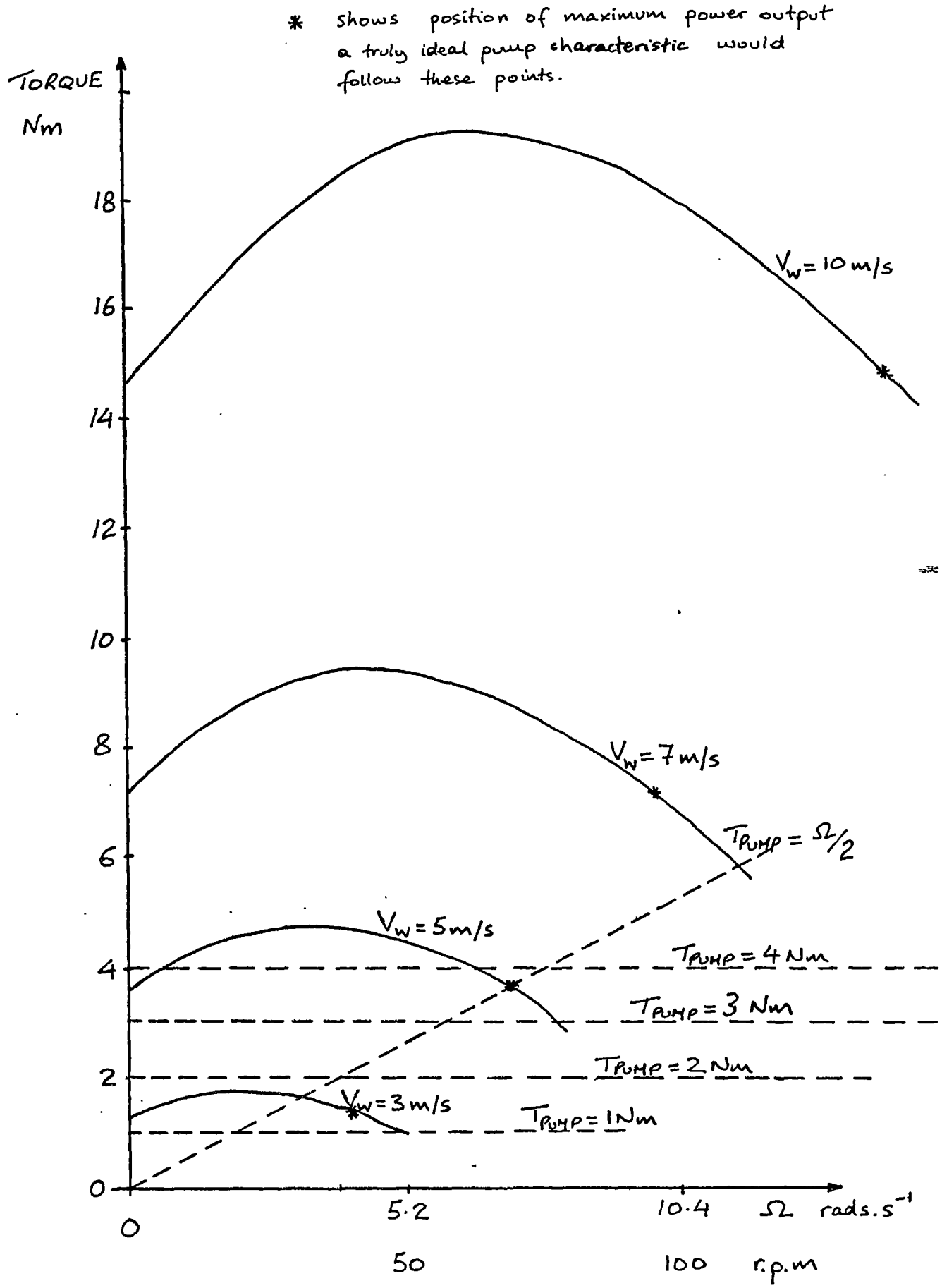

Fig.7.3. Turbine and load torque curves.

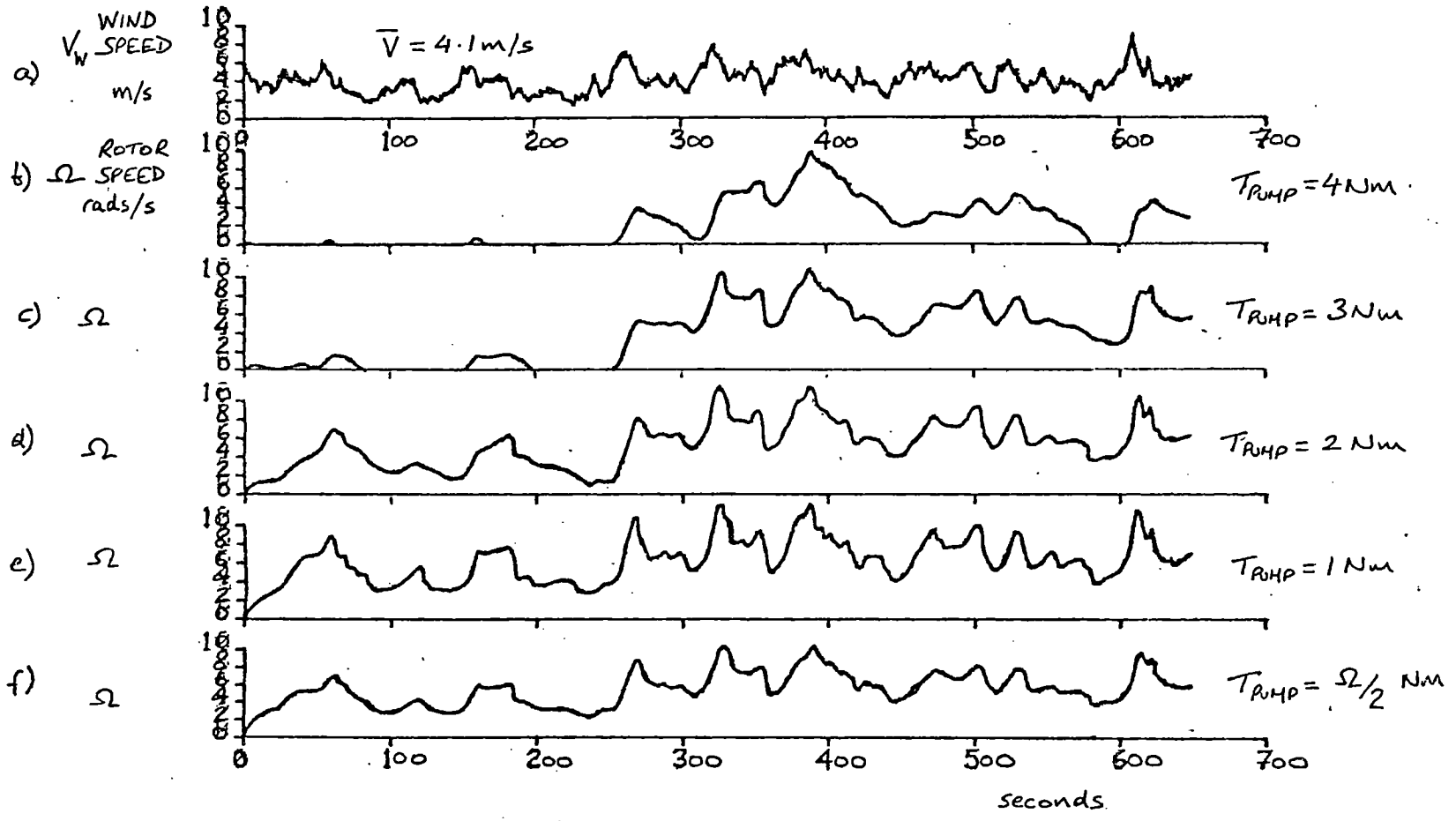

Fig.7.4. Wind speed and rotor speed vs. time with various load torques.

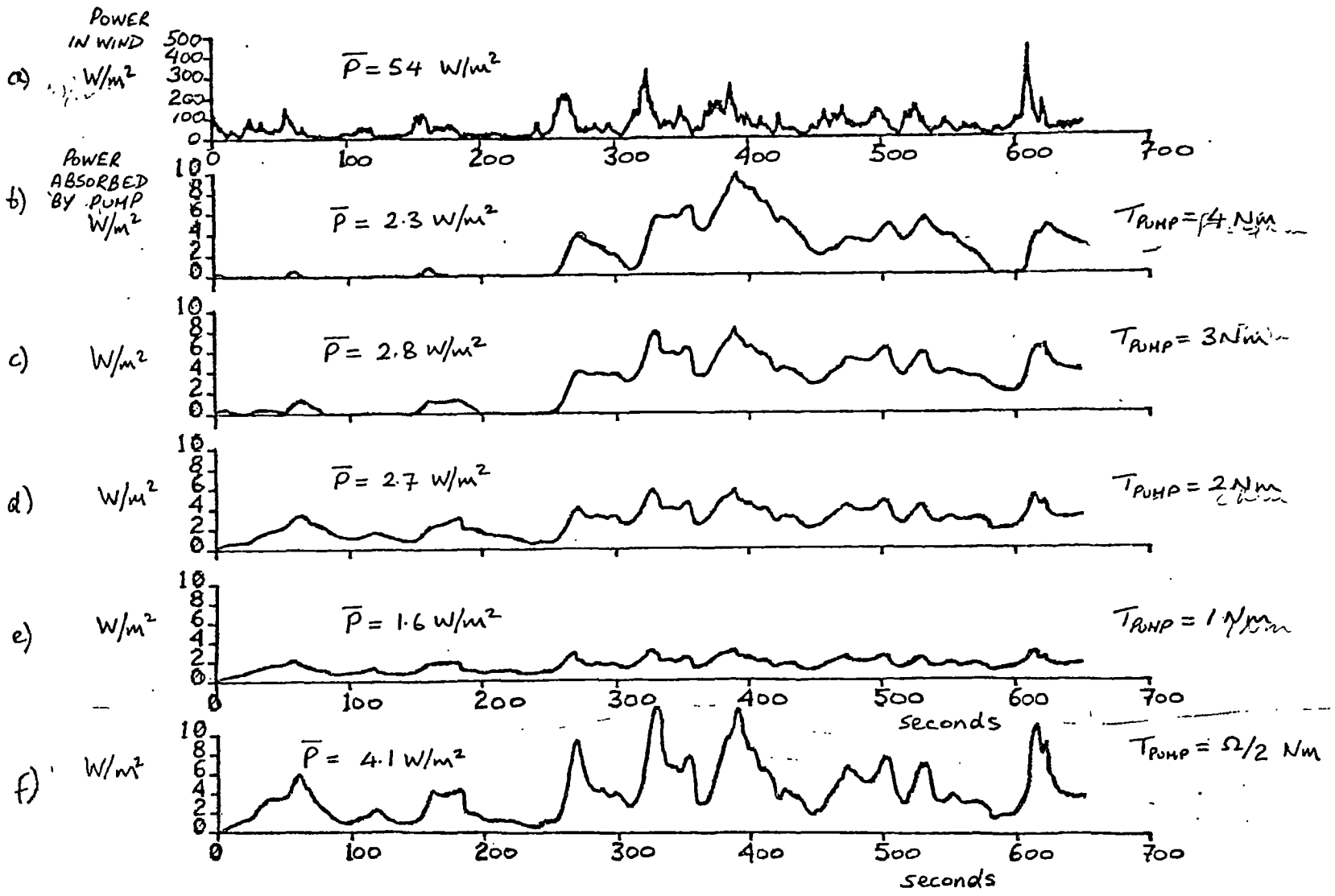

Fig. 7.5. Wind power and power absorbed by various loads vs. time.

7.3. Inertia Flow in Reciprocating Pumps

One approach to improving the torque characteristics of reciprocating pumps is to use the inertia of the water being pumped to increase the volumetric efficiency of the pump with speed. Dixon (1979) has suggested this and some efforts to use this approach are described by Burton (1979) and Burton and Ewens (1980).

Burton and Ewens show two non-dimensional relationships to be of particular interest; A non-dimensional speed δ a non-dimensional flow ξ :

$$\delta = \Omega \sqrt{\frac{L_i R_p A_p}{g A_i H}} \qquad [7.1]$$

$$\xi = \pi Q \sqrt{\frac{L_i}{R_p A_p A_i g H}} = \eta_{VOL} . \delta \qquad [7.2]$$

where R_p is half the stroke length of the pump, A_p is the piston area, L_i is the length of the inertia pipe, A_i is the cross-sectional area of the pipe, H is the total head, Ω is the pump angular velocity, Q is the volumetric flow rate and η_{VOL} is the volumetric efficiency.

As is shown in Appendix 7, a theoretical curve of dimensionless flow against dimensionless speed may be drawn (Fig.7.6). It can be seen that, at high dimensionless speeds, the volumetric efficiency may exceed two.

Reciprocating pumps are normally operated at low dimensionless speeds but suitable choices of the parameters allows inertia flow to occur and higher volumetric efficiencies. For a windpump, the choice of pump size ($R_p A_p$) is fixed by the operating head H and the starting torque provided by the

wind turbine in the chosen starting windspeed. The relationship between the angular speed and the dimensionless speed is then determined by the length and cross-sectional area of the inertia pipe.

The most promising area for application of inertia flow effects seems likely to be in low lift situations, where sufficient torque can be provided by a relatively fast running rotor, allowing high dimensionless speeds to be obtained without excessive lengths of inertia pipe.

7.4. Performance Tests on a Diaphragm Pump

To investigate inertia flow in practice and to measure the performance of a particular pump, some tests on a reciprocating pump were carried out. A diaphragm bilge pump was chosen for the tests as this was readily available in a suitable size, was self priming and could handle dirty water without any problem. The pump used (Henderson, Chimp) is moulded in plastic and uses a neoprene diaphragm. It was mounted so that it could be driven through a crank mechanism with a stroke of 30mm.

The tests were carried out with a 3m suction lift and minimal pressure head. This is a suitable configuration for a low lift application, with a self-priming pump, and minimises the length of the transmission required between the wind turbine and the pump.

7.4.1. Apparatus and Procedure

The test arrangement is illustrated in Fig.7.7. 22mm bore, armoured pvc tubing was used for the inertia pipe, and lengths of 3.9m and 5.9m were tested. A simple test rig was designed and built.(Fig.7.8). This was driven by hand and torque measurement was provided by a tensioner on the drive chain. A continuous recording of torque was made using a chart recorder and average torque was obtained using a time domain analyser with an averaging time of 10s. A static calibration of the torque reading was made; weights being suspended from the drive handle with the crank wheel locked in position. This calibration was then corrected for any dynamic effects and for friction losses in the drive chain, by recording the torque reading obtained, with the crank rod disconnected, over the full speed range. This reading was subtracted from the torque readings subsequently obtained; The test results therefore still include losses occurring in the crank mechanism. The calibration error is thought to be less than 2%.

The average flow rate was determined by weighing the volume of water pumped in a measured time. The error in the flow rate may be 4%. The speed was simply calculated by counting the number of cycles completed in the measured time. A recording run was rejected if the speed varied by more than 5% over the interval.

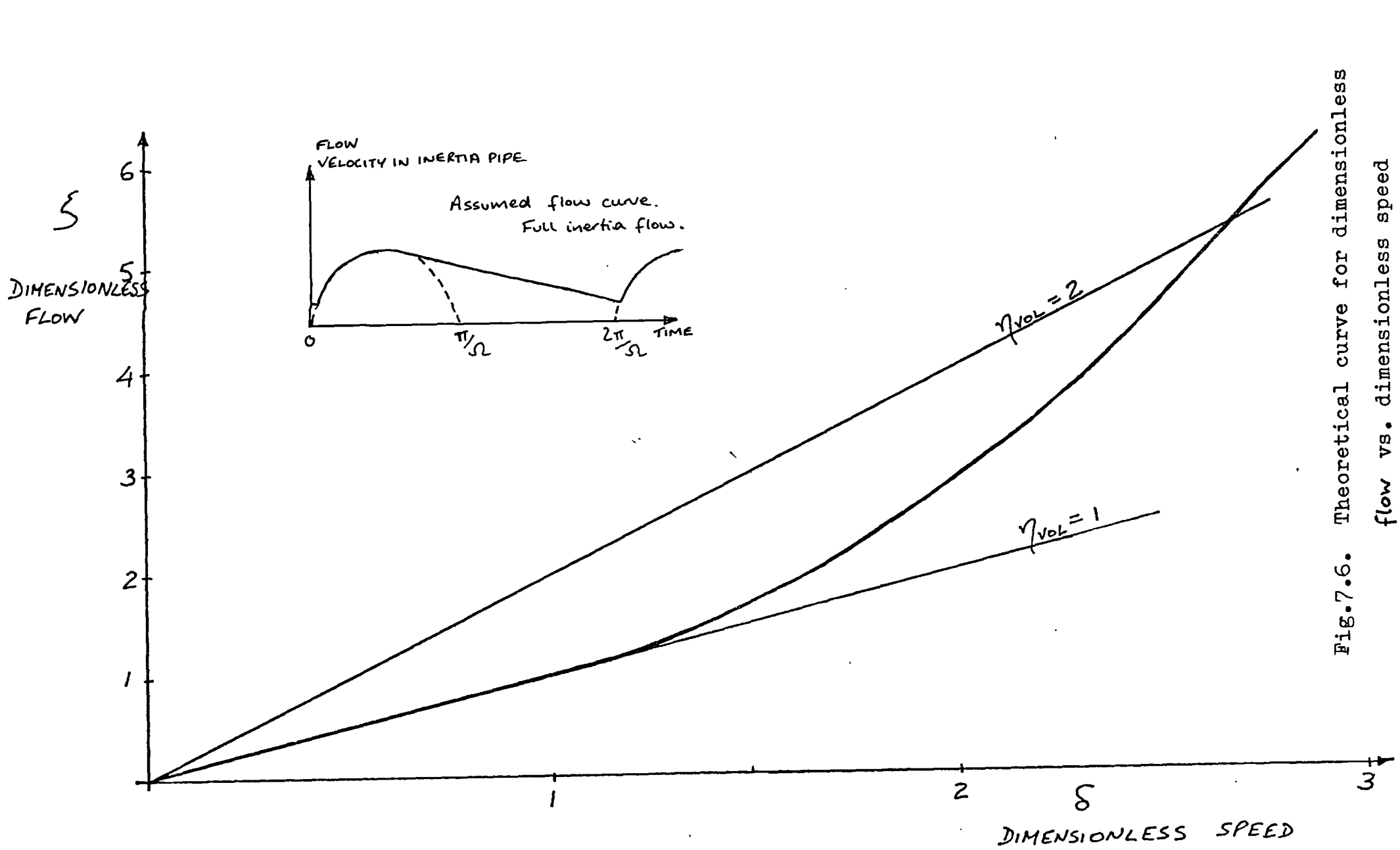

Fig.7.6. Theoretical curve for dimensionless flow vs. dimensionless speed

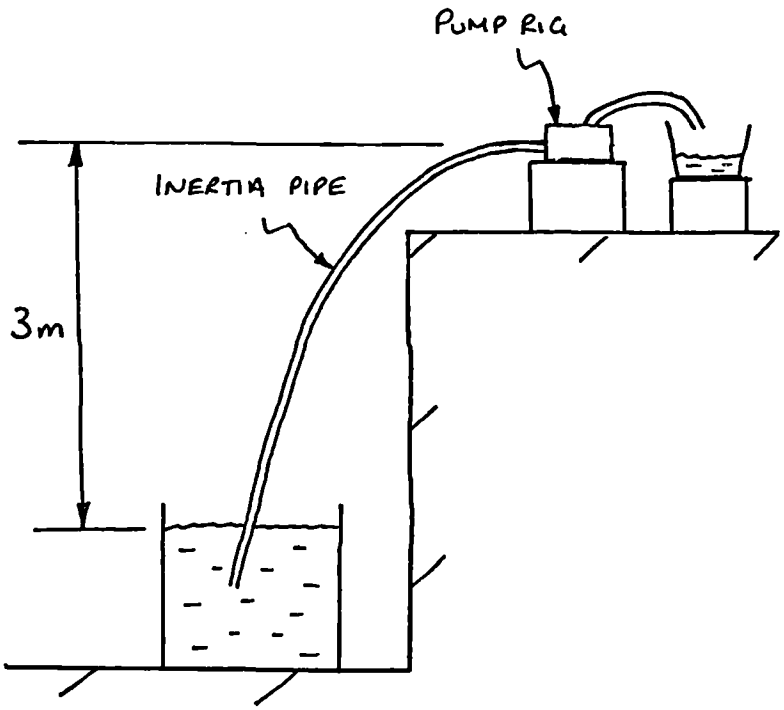

Fig.7.7. Arrangement for pump performance tests

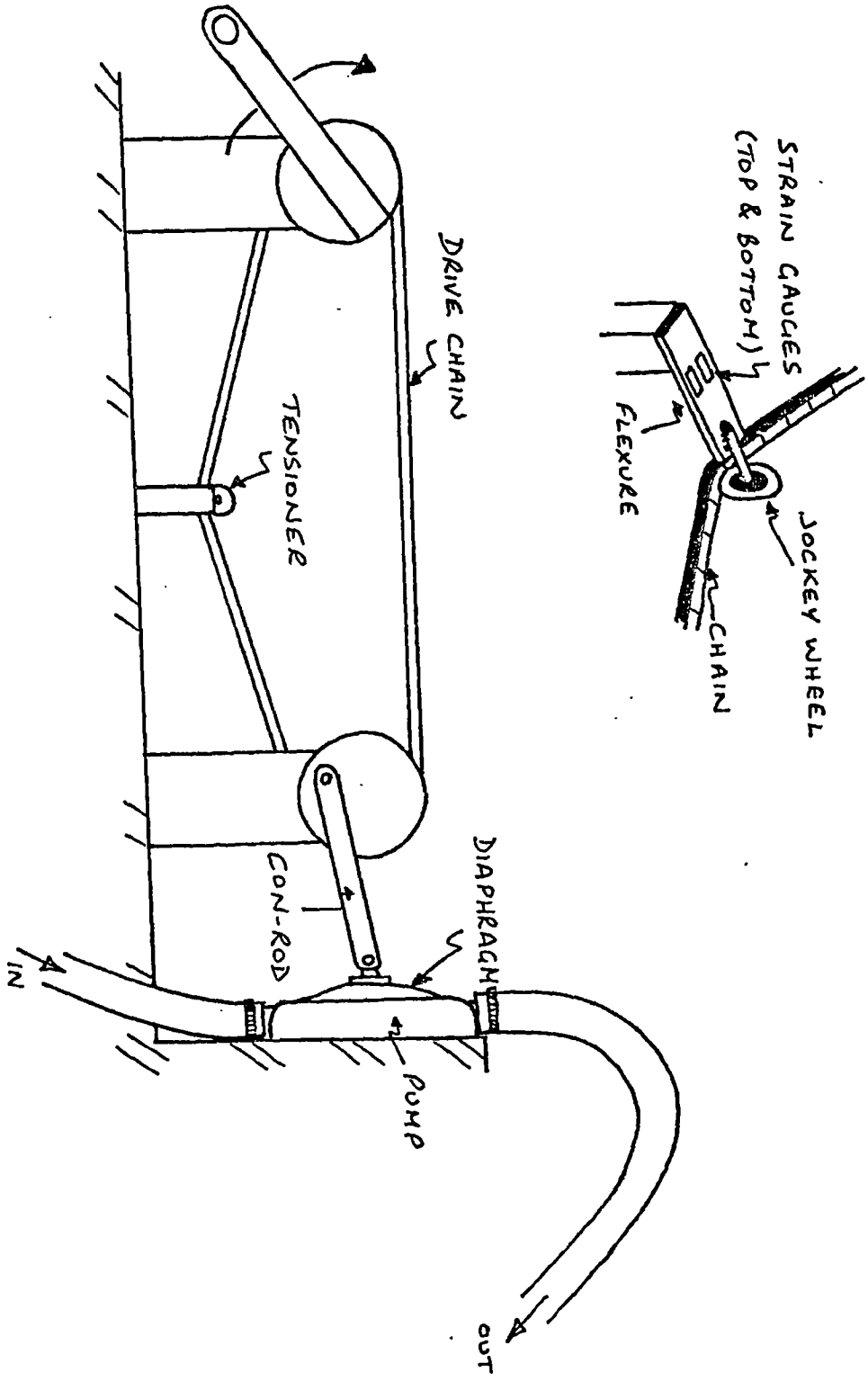

Fig.7.8. Pump test rig and tensioner arrangement.

7.4.2. Results and Discussion

The results are shown in Figs.7.9 to 7.11. To compare the measurements with the theoretical predictions, the dimensionless flow and speed have also been calculated, using eqns.[7.1] and [7.2] (Fig.7.12). With a diaphragm pump, it is not possible to define the piston area A_p except by calculating it from the measured swept volume and the stroke. The effective 'piston' area will be a maximum near the maximum velocity position, causing a higher peak flow velocity than a rigid piston pump with the same swept volume and stroke (Fig.7.13a). This would explain the higher than expected inertia effect at low speeds. It can be seen that the volumetric efficiency did not continue to rise at high dimensionless speeds. This is thought to have been due to the pipe losses which occurred. The torque input rose much faster than would be expected from the rise in the volumetric efficiency. The view that this was due to high pipe losses is supported by the estimate of the losses in Appendix 7 and by the increase in torque which occurred with the increase in pipe length. High pipe losses would of had the effect of retarding the inertia flow (Fig.7.13b). Another factor may have been the reduction in the swept volume occurring at high speeds, due to the distortion of the diaphragm arising under the low pressure in the pump during the suction stroke.

The pipe losses would be reduced by increasing the pipe diameter. However the losses in the pump valves and the pump itself would remain unchanged and these losses appear to have been significant. The present pump was clearly not designed for efficient operation with high fluid velocities.

It should be remembered that, to maintain the same inertia effects, the pipe length must be increased in proportion with the pipe cross-sectional area. This means that increasing the pipe diameter may be expensive.

The peak overall efficiency of 70% seems low, but actually this compares well with the efficiency of "70% reducing to less than 50% at high speeds" reported by Beurskens et al (1980) for a membrane pump. Burton and Ewens give a value of 50% as an average efficiency for short stroke reciprocating pumps.

The starting torque was measured as 2.6Nm, slightly higher than the starting torque predicted from the 3m head and the average piston area of $5.2.10^{-3} m^2$, with the 15mm crank.

Although the volumetric efficiencies obtained were not as high as had been hoped, it appears that this was largely due to pipe losses; these could be greatly reduced by increasing the pipe diameter and re-designing the pump inlet and outlet. It may be that at very high dimensionless speeds, the volumetric efficiency would still be limited by the distortion of the diaphragm reducing the swept volume. As they stand, a pair of such pumps would appear to provide a good load match for the prototype turbine, as can be seen from the torque curves (Fig.7.14). This would seem to provide a suitable load with which to test the prototype turbine in operation as a windpump.

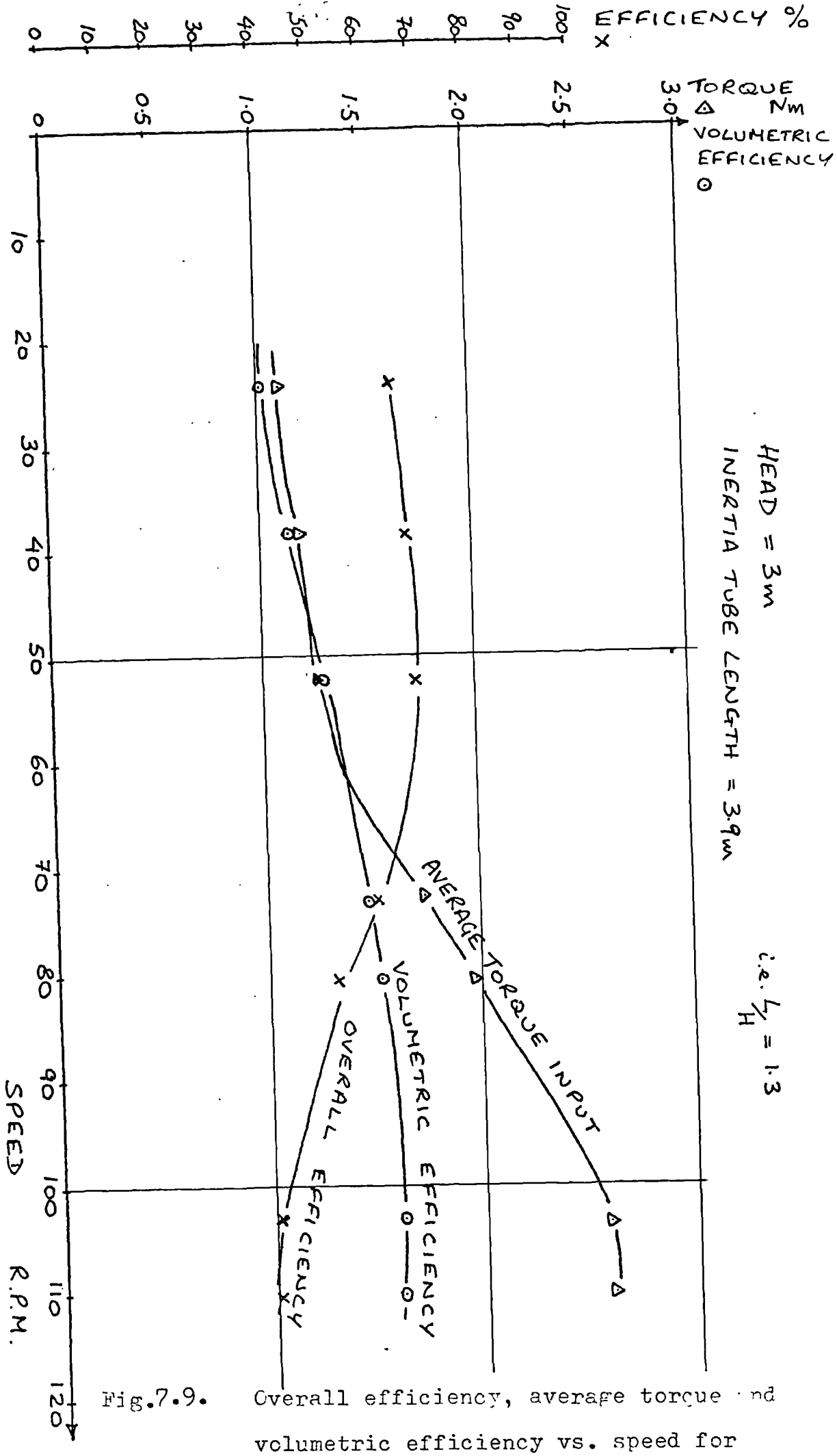

Fig.7.9. Overall efficiency, average torque and volumetric efficiency vs. speed for diaphragm pump.

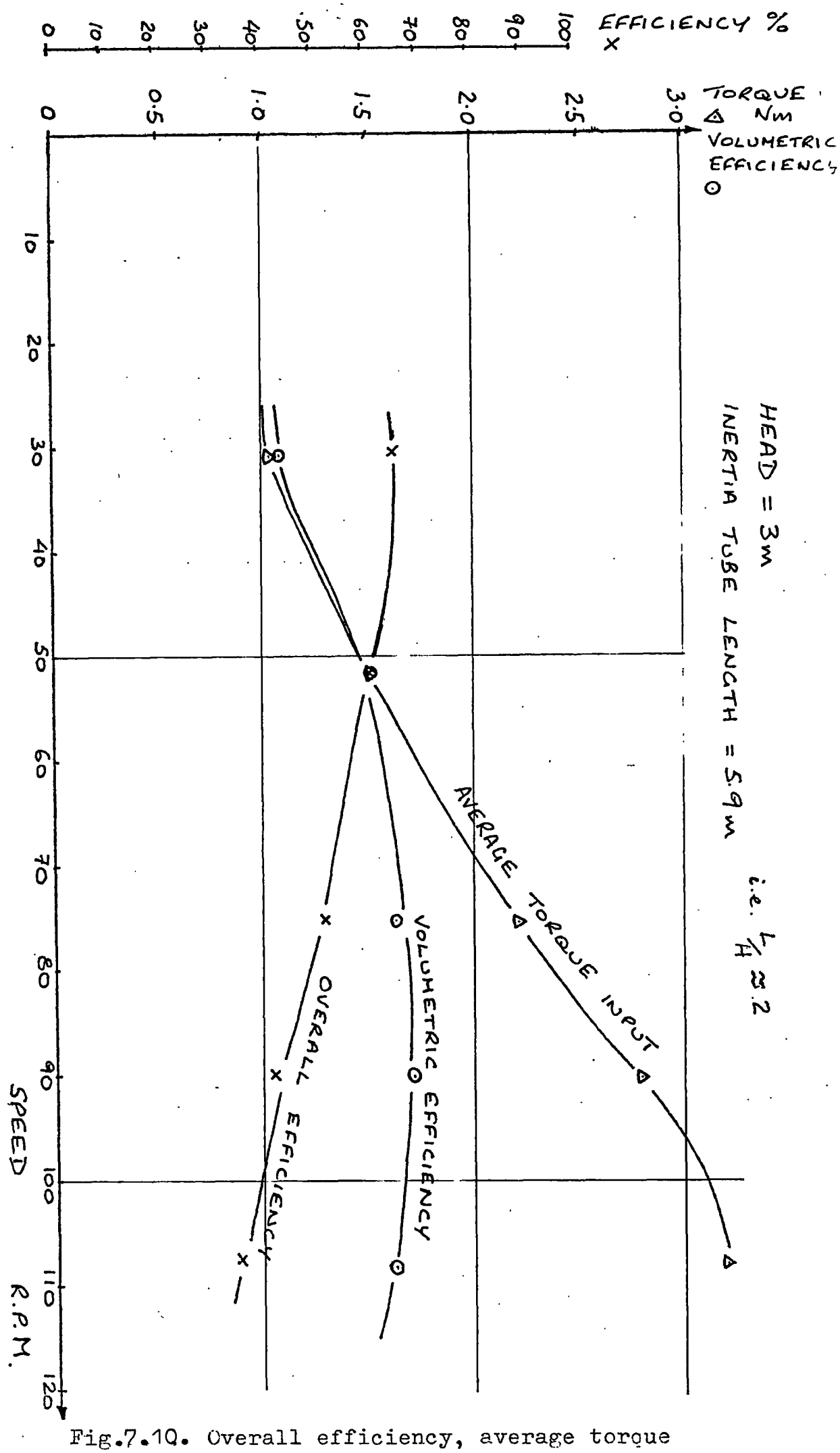

Fig.7.10. Overall efficiency, average torque and volumetric efficiency vs. speed for diaphragm pump.

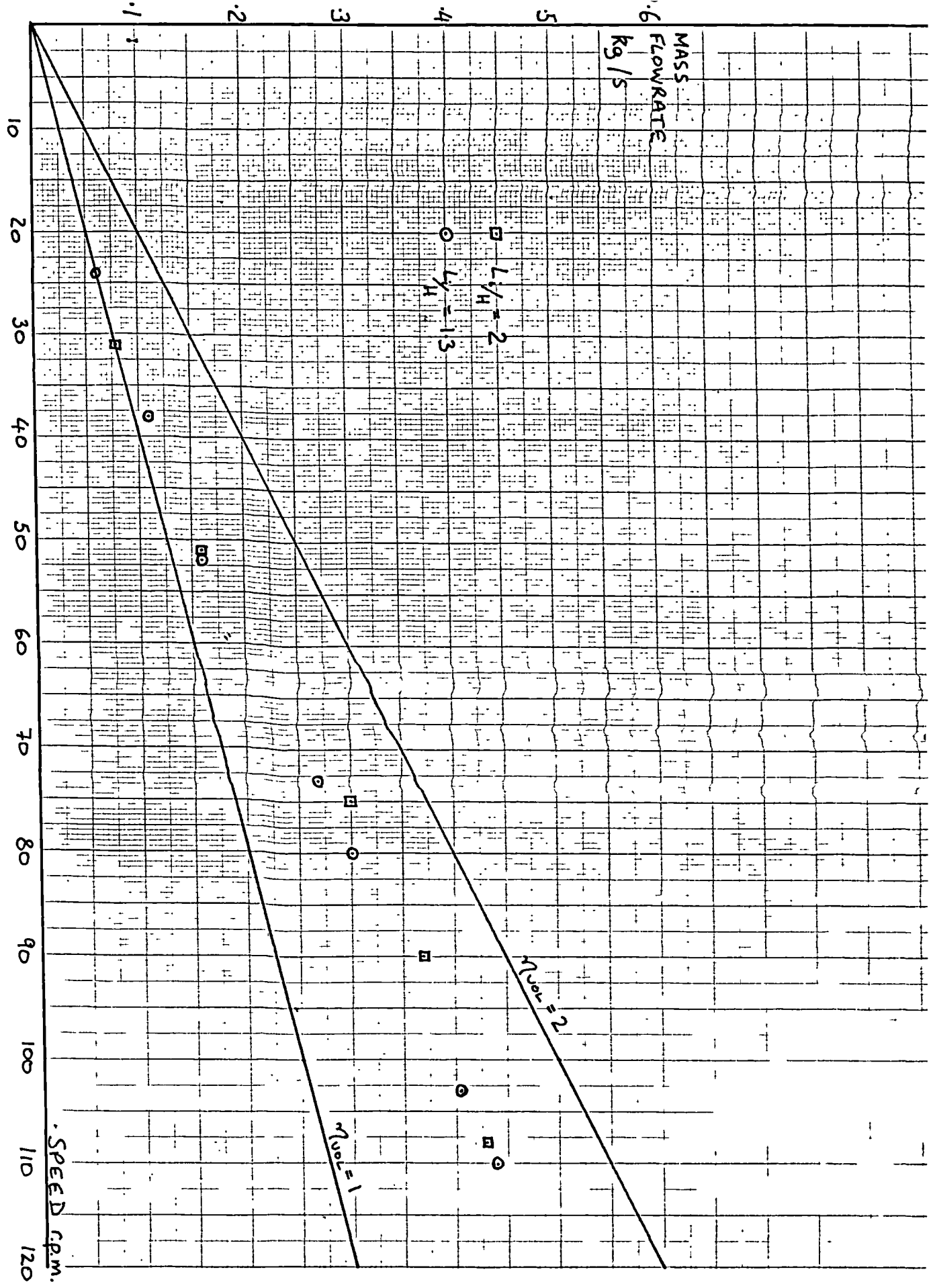

Fig.7.11. Water mass flow rate vs. pump speed.

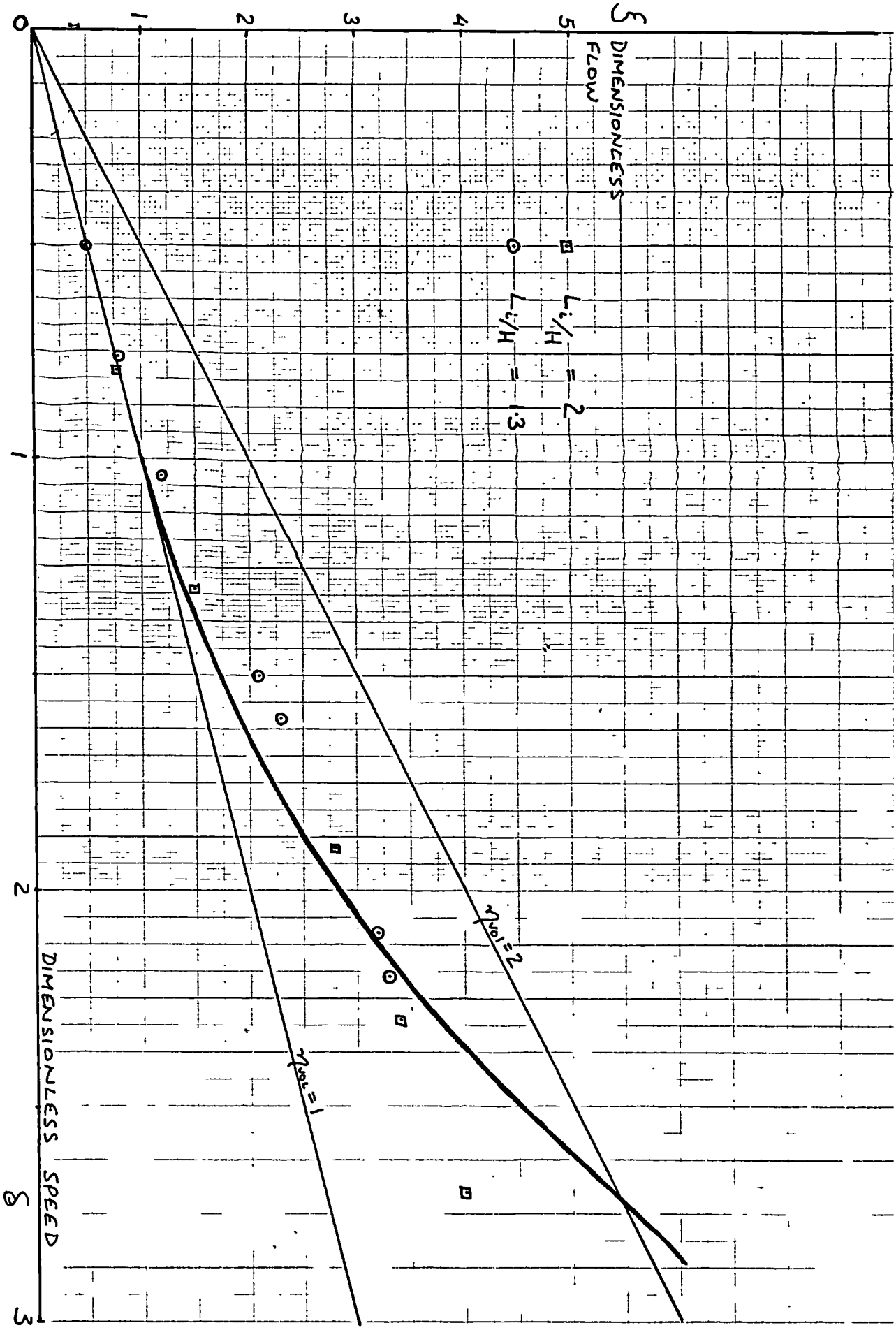

Fig.7.12. Dimensionless flow vs. dimensionless speed -comparison of measurements and theory.

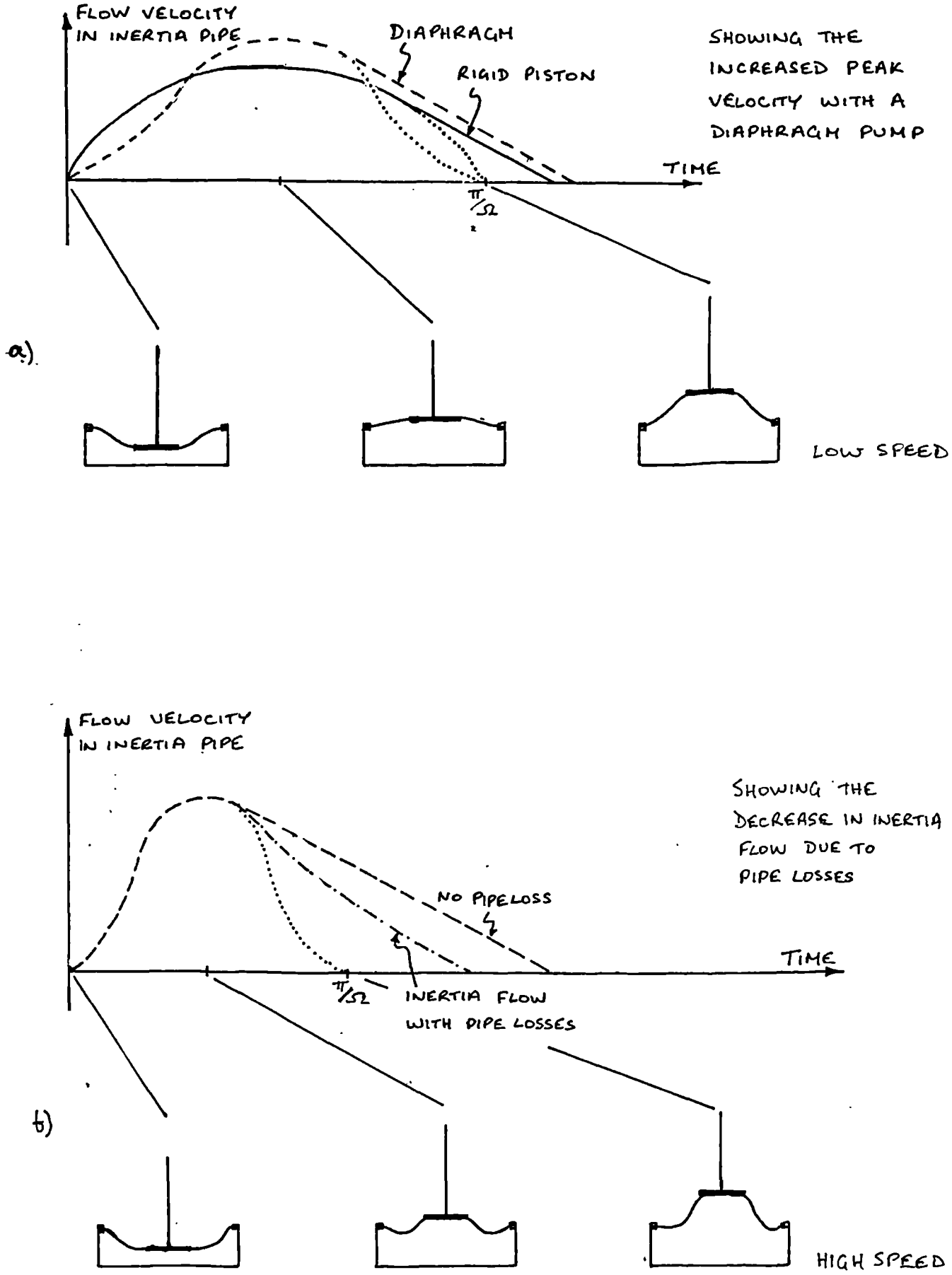

Fig.7.13. Assumed flow velocity curves for a diaphragm pump.

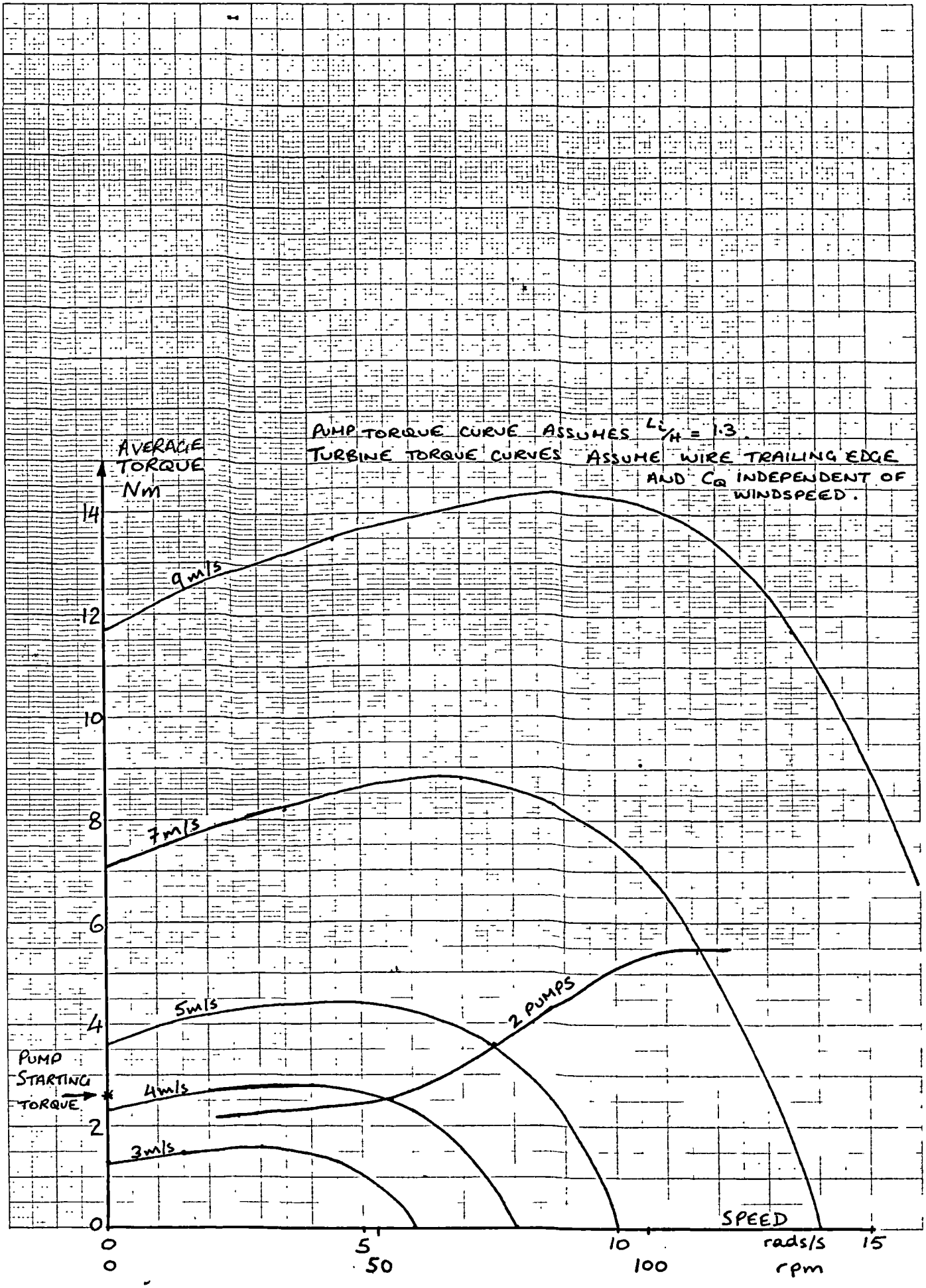

Fig.7.14. Torque vs. speed curves for the turbine and a pair of pumps.

7.5. Testing of the Prototype Turbine under Load

By setting up the prototype turbine to drive a pair of the diaphragm pumps operating on a 3m lift, it was hoped to demonstrate its potential as a power source and to test its behaviour when loaded. The wire trailing edge was fitted.

7.5.1. Arrangement and Predicted Performance

The two pumps were mounted opposite each other on plates attached near the top of the tower. Connecting rods were pivoted on a crank-pin mounted at a 15mm radius on the driveshaft. The driveshaft was coupled directly to the bottom shaft of the turbine, running through another self-aligning bearing (Fig.7.15).

A flexible coupling between the two shafts was originally used, so as to accomodate the inevitable mis-alignment between the three bearings. However, it was found that this allowed excessive deflection of the driveshaft to occur, due to the shock loads in the con-rods at the start of each stroke. The flexible coupling was therefore replaced by a simple rigid connection on the assumption that enough flexibibity existed in the shafts and in the restraint of the top bearing. This arrangement seemed quite satisfactory.

A hole was dug adjacent to the tower, lined with polythene and partly filled with water to give a 3m suction lift. 3.9m of 22mm bore, armoured pvc pipe were used as the inertia pipe for each pump. Pumped water drained back into

the hole.

Using the torque curves of Fig.7.14, and the flow measurements of Fig.7.11, the simple numerical analysis used in section 7.2 has been repeated so as to predict the system performance in a typical wind. The assumptions made in the analysis may be repeated: rotor speed and power absorbed by the pump are calculated at one second intervals, assuming quasi-steady operation at each point, cyclic torque variations are ignored, i.e. mean torque values are always used.

The predicted rotor speed and water flow rate are shown in Fig.7.16. The results predict that a total of 210kg of water would have been pumped over the eleven minute period, giving a useful power output of 2.5 W/m^2 in this 4.1m/s mean windspeed. This can be compared with useful power outputs of between 0.6 W/m^2 and 1.8 W/m^2 obtained in this windspeed by Cretan windmills driving ordinary reciprocating pumps, as described by Fraenkel (1976), and with a useful power output of about 4 W/m^2 measured by Beurskens et al (1980) with their THE-I horizontal axis windmill driving a membrane pump. (Fig.7.16 a/b) This suggests that the prototype turbine could be competitive for low lift pumping, especially if the pumps were run more efficiently.

By using a pair of pumps, half a cycle out of phase, the starting torque remains the same as with a single pump and the difference between the starting and mean running torque is minimised. From the torque curves (Fig.7.14) it appears that starting should occur in winds slightly above 4m/s, gusts of which magnitude occur frequently, even in low

winds.

7.5.2. Tests, Results and Discussion

It was unfortunate that since the previous tests, an oil seed rape crop had been planted in the fields surrounding the test site. This grew to a height of about 1½m, effectively reducing the tower height to just 0.5m and providing a very rough ground surface. These two factors made the wind at the site extremely turbulent during most of the time available for testing. Fig.7.17 shows a typical wind recording made at this time. This turbulence made it difficult to identify the causes of the problems which were encountered and, in fact, aggravated the problems.

Problems occurred with starting and with running in low winds. It was found that self-starting under load did not occur in gusts of less than about 8m/s. In weaker gusts, the turbine was unable to gain enough momentum to keep going. Once the rotor did get going its response appeared to be very slow and it stalled easily when the wind dropped below about 4m/s.

Since the wind frequently did fall below 4m/s, if only for short periods, it was difficult to do any measurements of the actual performance. A few short duration tests were made in which the time taken to collect 13kg (1 bucket) of water was measured. In winds averaging between 4m/s and 5m/s the time taken ranged from 30s to 45s, giving useful power outputs of between $2W/m^2$ and $3W/m^2$.

It was clear that, if any useful test running was going to be obtained, the low speed performance needed to be improved. Some experiments were therefore made with an air snifting device to be attached to the pump body. An air snifter allows the pump to draw in air from the atmosphere when operating at slow speeds, so reducing the torque requirement. At operating speeds no leakage occurs and the pump operates normally. Such a device has been used with a windpump by the Dutch group SWD.

A design of air snifter was developed (Fig.7.18) and it operated satisfactorily. A thin rubber diaphragm was clamped between two, machined brass washers and this formed an insert into a brass fitting which screwed into a mounting made on the pump body. Above a certain speed, the diaphragm sealed alternately against the inlet and outlet to the snifter.

One pump was modified in this way and the behaviour observed. Little leakage occurred at speeds above about 30 rpm. With just this pump connected to the turbine however, the low speed performance still did not appear as good as should have been expected. Unfortunately it was not possible to obtain any recordings of the turbine operating in low winds with this modified pump. Some very short recordings which were made in a strong wind (Fig.7.19 and 7.20) indicate that the performance then fell far short of expectations.

It is suggested that the reason for the poor performance relative to the prediction is the cyclic nature of the torques involved and the consequent non-linear effects.

Since the turbine only had three sets of blades, it was inevitable that the driving torque which it produced should be strongly cyclic. This is clear from the variation of the instantaneous torque coefficient $C_T q^2$ with azimuthal angle for test Ca1p (Fig. 4.1). Thus, both the driving torque and the load torque were cyclic, with periods of $\frac{0.7\pi}{\Omega}$ and $\frac{\pi}{\Omega}$ respectively. Combining this with the rapidly varying windspeed, it is perhaps not surprising that the performance in practice fell below that predicted by the simple analysis with its assumptions of quasi-steady operation and no cyclic torque variations. When stationary, the turbine tended to become locked in a position where it could produce little torque. At higher speeds, the turbine had insufficient inertia for there to be a significant flywheel effect; this may be a general problem with small turbines coupled directly to reciprocating pumps. There would presumably be some improvement with a larger turbine. For a reasonably smooth driving torque to be produced, six sets of turbine blades would be necessary. Another factor in the poor performance may be the loss in performance expected in high winds; this would tend to reduce the effect of gusts.

The running of the turbine would seem likely to be improved if a rotary positive displacement pump or a centrifugal pump were used in place of a reciprocating pump. This would not allow the use of inertia flow effects but a centrifugal pump could provide a good load match and there is no reason why an air snifter could not be used with a rotary pump, to reduce the starting torque. Unfortunately, lack of time did not allow any modifications to the windpump to be tried.

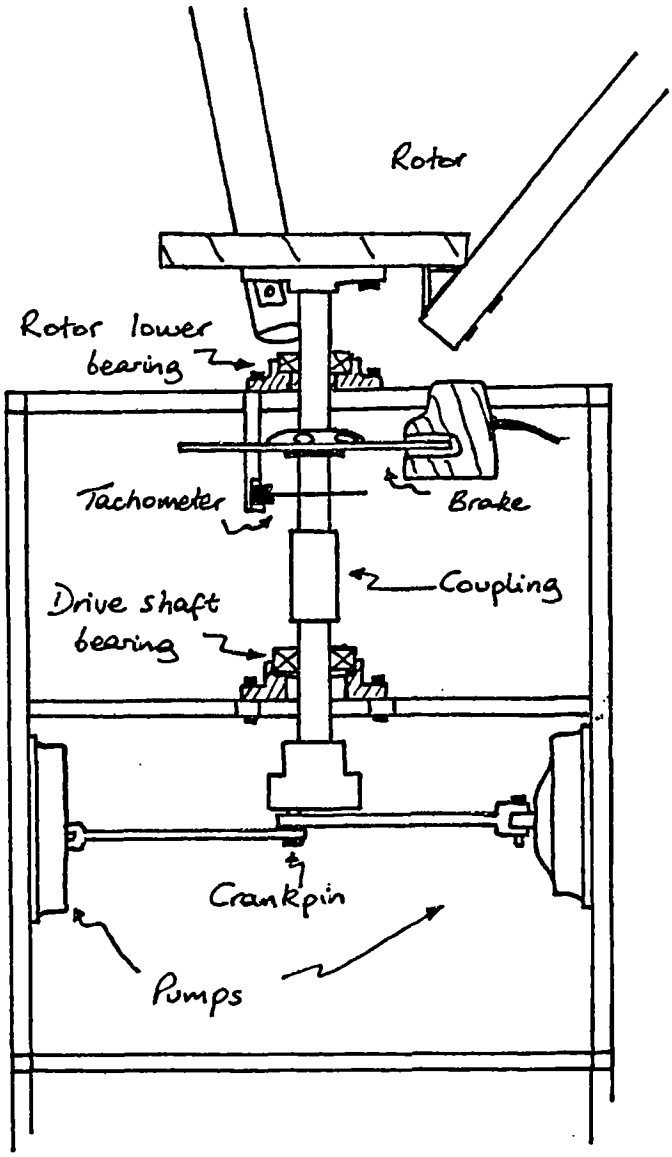

Fig. 7.15. Arrangement of the pump drive shaft.

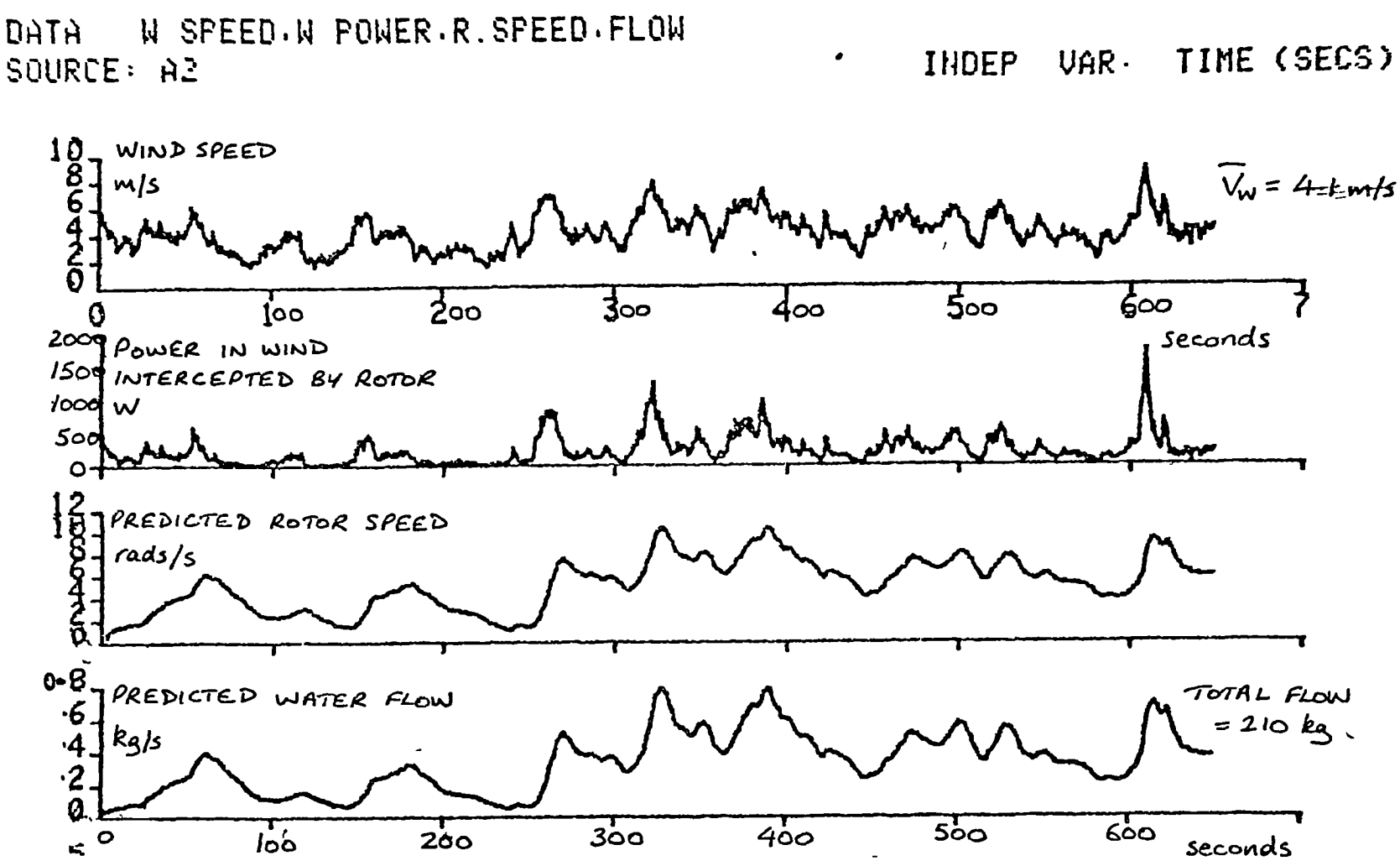

Fig.7.16. Predictions for rotor speed and water flow rate for the prototype wind pump.

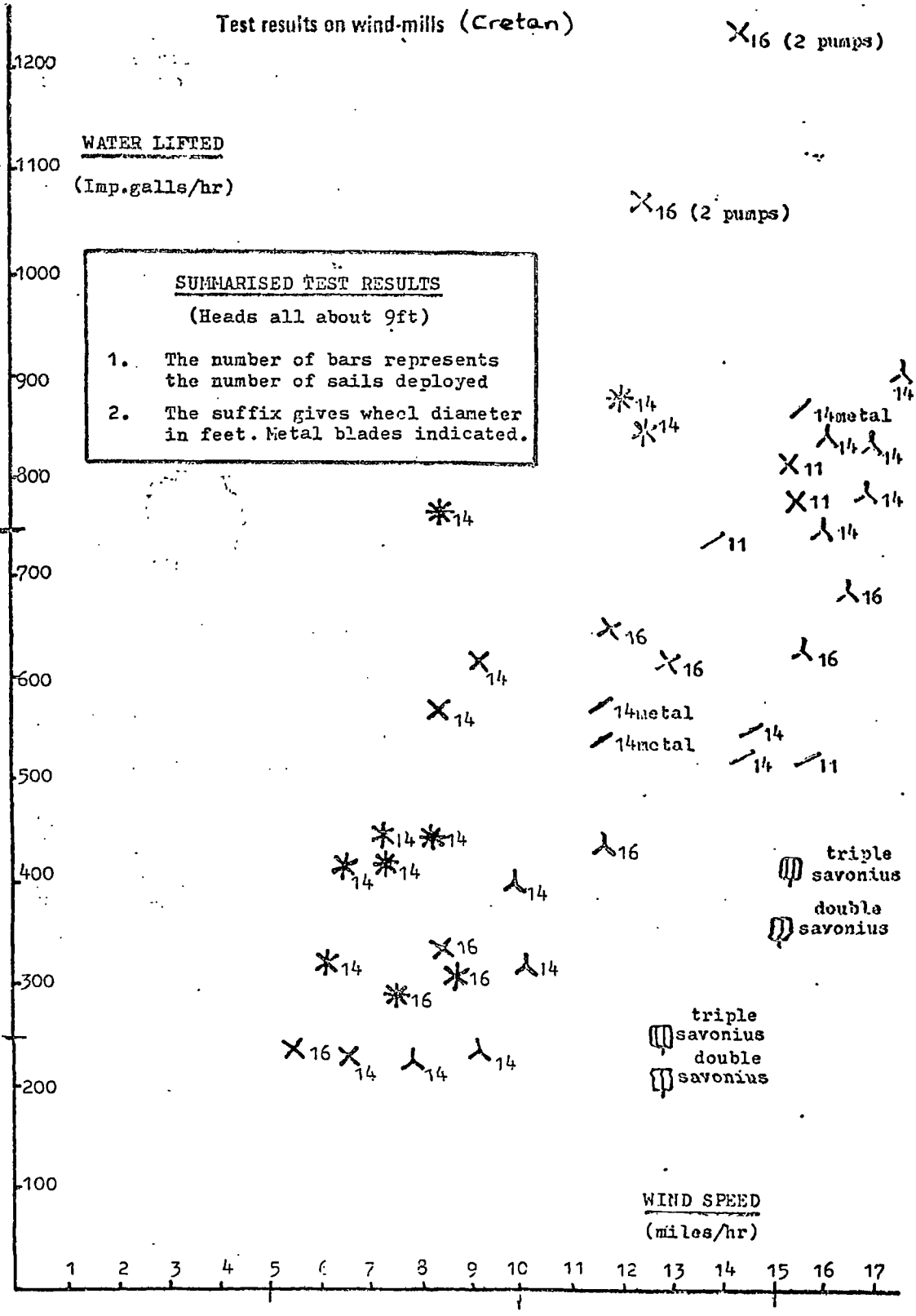

Fig 7.16a. Results from Fraenkel (1976)

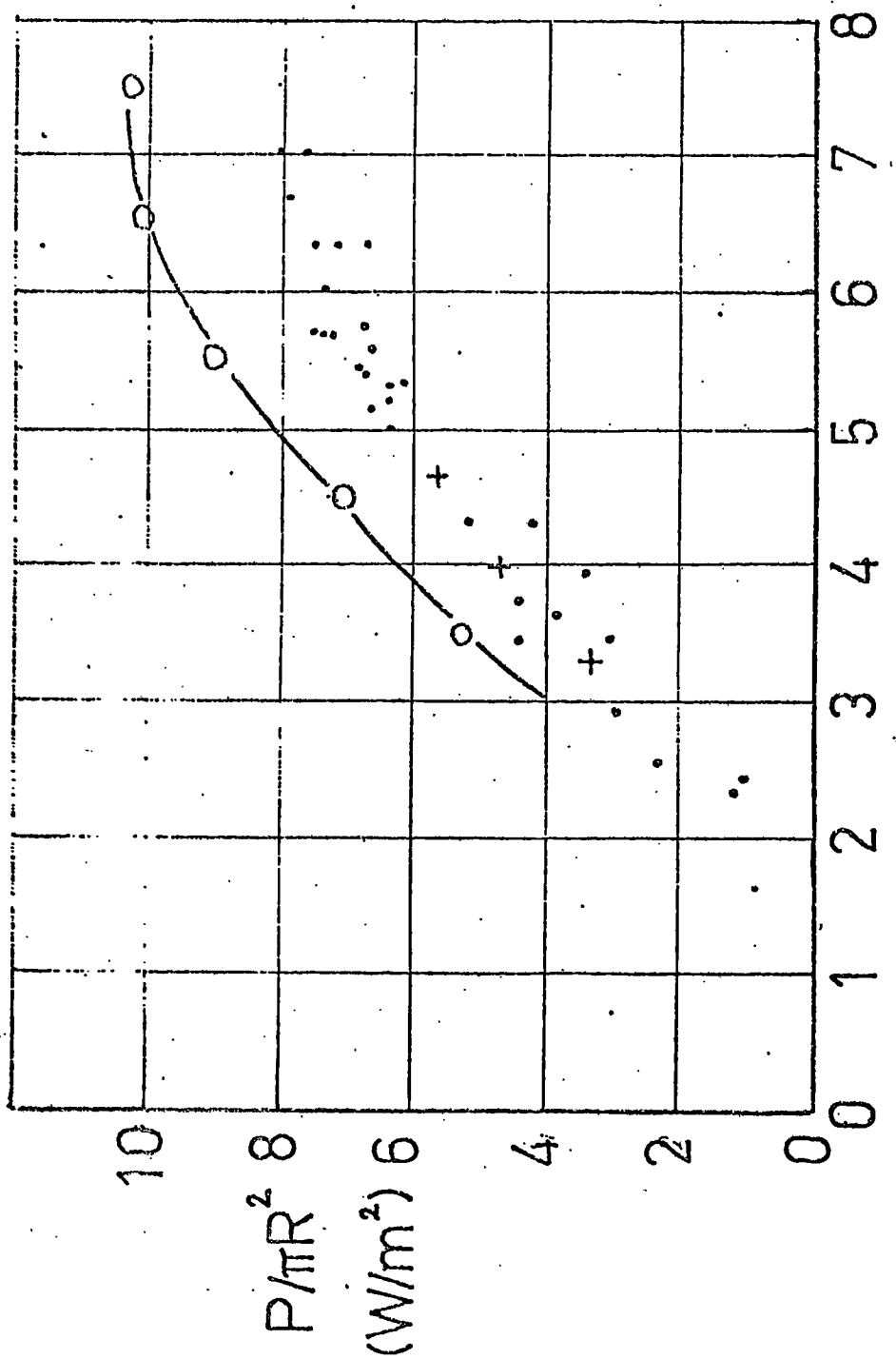

Field measurements of the effective power output (per m^2 swept rotor area) of the THE-I water pumping windmill, with a stroke of 3 cm at a head of 3.5 m. The three field data indicated with "+" are long term measurements of several hours. The curve represents the theoretical output determined with fig. 22.

Fig 7.16 b Results from Beurskens et al (1980)

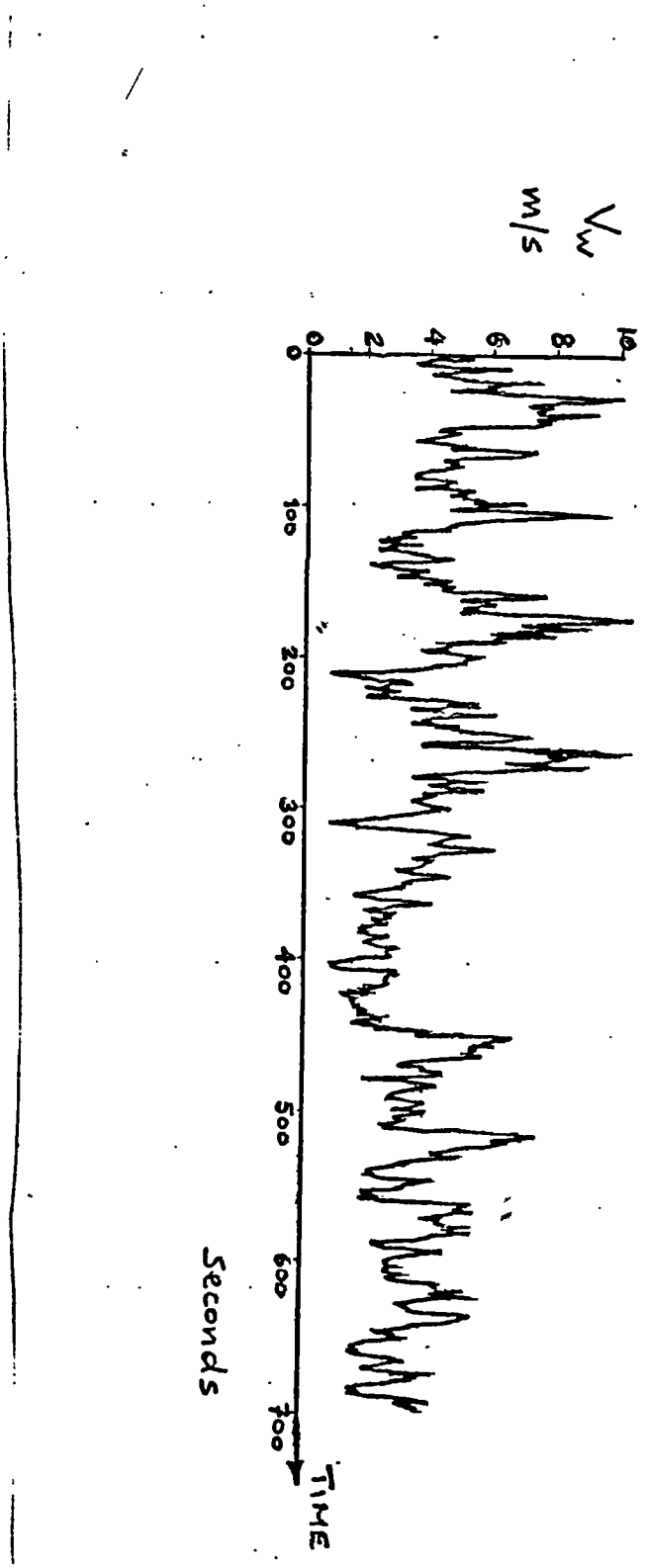

Fig.7.17. A typical recording of turbulent wind.

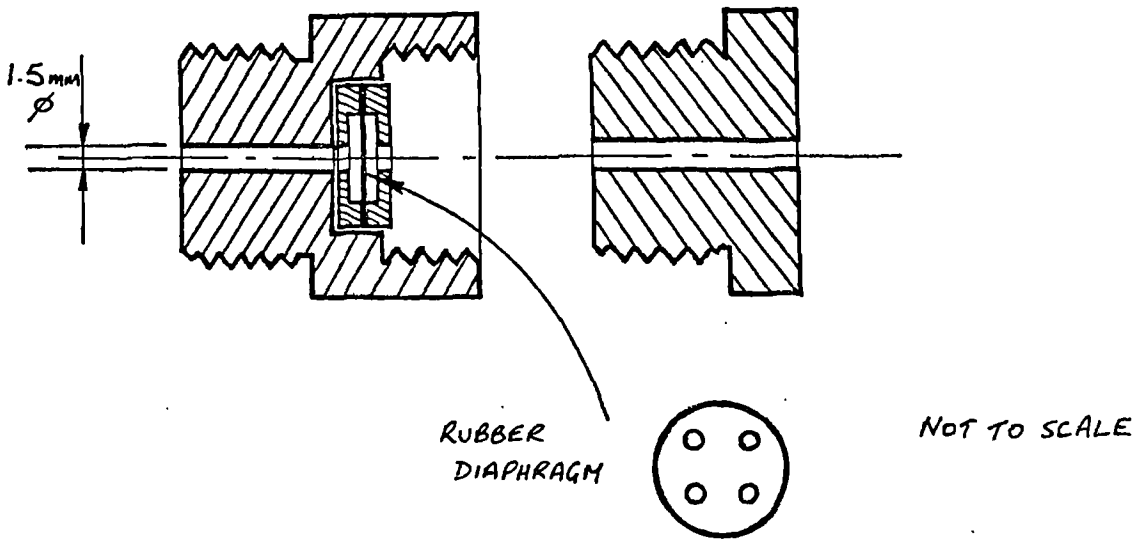

Fig. 7.18. Section through air snifter.

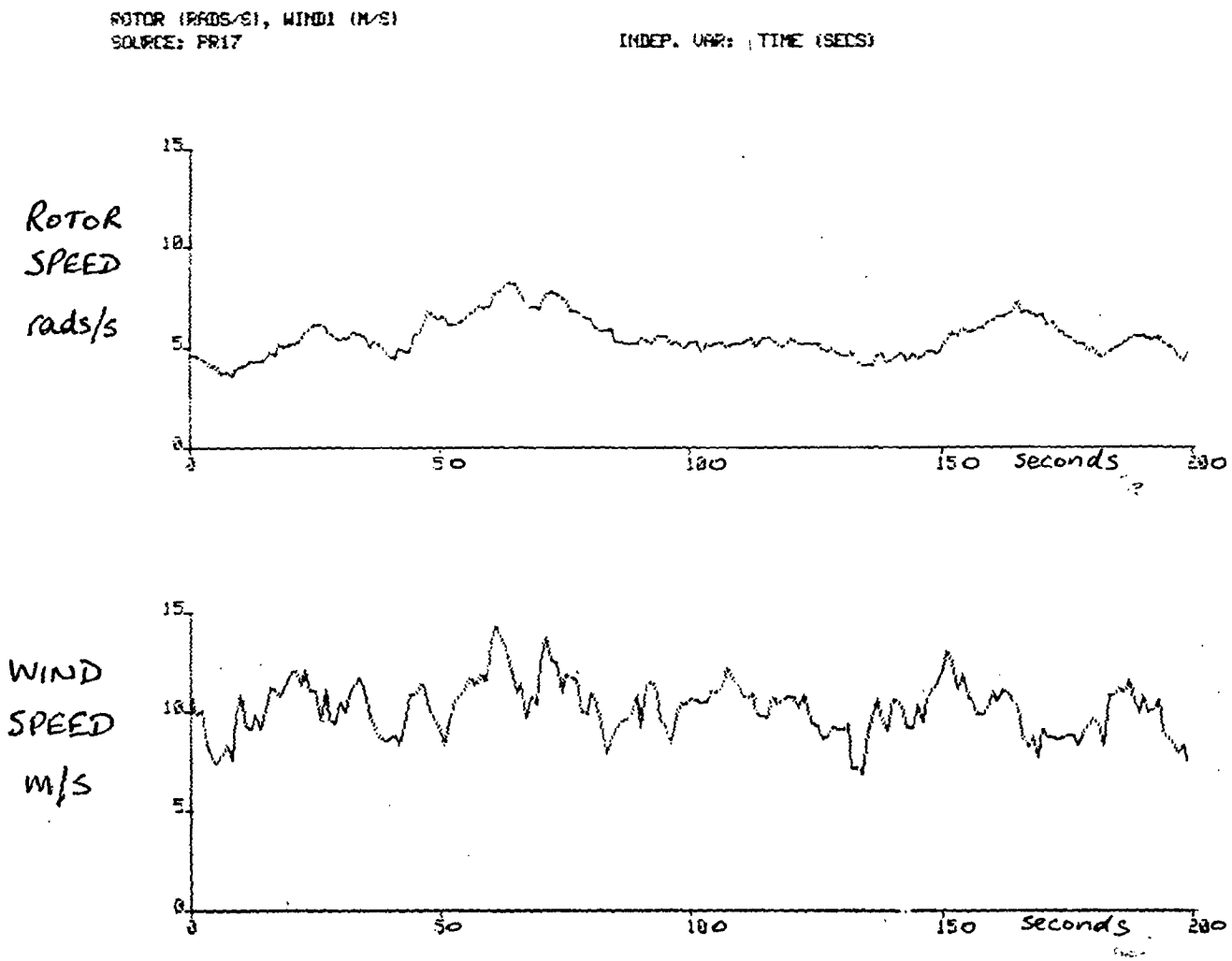

Fig.7.19. Rotor and wind speed vs. time
-two pumps.

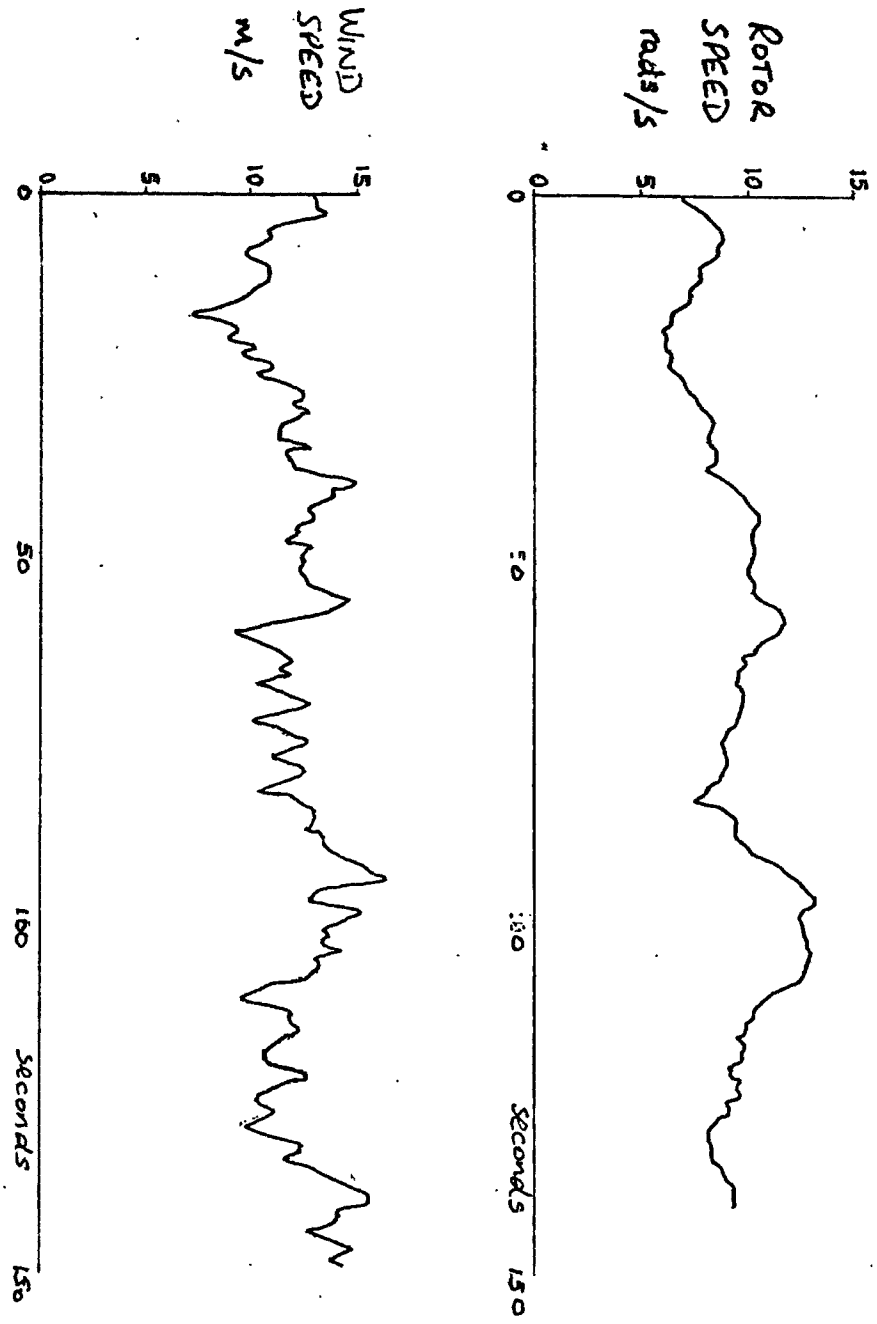

Fig.7.20. Rotor and wind speed vs. time -one pump.

7.6. Conclusions

Measurements at the test site showed that, due to gusts, the energy in the wind was about 20 to 30% greater than would be calculated from the mean windspeed. Small windmills should be able to use a large part of this additional energy and vertical axis turbines would seem to be at an advantage because of the avoidance of yawing losses.

Modifying the torque characteristics of a pump to improve the load matching should allow a significant increase in the system efficiency of a windpump, through improving the utilisation of this 'gust-energy'. The use of inertia effects as a means of improving the torque characteristics of reciprocating pumps seems quite feasible but care will be required in the design so as to minimise the pipe losses that occur. It appears that a diaphragm pump may cause inertia effects at slower speeds than expected, due to the varying 'piston' area.

The potential of the prototype design as a windpump has not been demonstrated. The cyclic driving torque it produced caused problems in driving reciprocating pumps. To operate such pumps, probably six sets of blades would be required, so as to provide a more even driving torque. It is not clear if this would then allow efficient use of 'gust-energy'. It is likely that the prototype would operate better with a rotary positive displacement pump or a centrifugal pump.

DISCUSSION AND CONCLUSIONS

The research work described sought to investigate the possible use of sailwing aerofoils in vertical axis wind turbines. It was anticipated that such a turbine could be suitable as a power source for water pumping in low lift irrigation. Previous attempts to use sailwings in such a turbine appeared to have had limited success, or at least not to have been developed, or demonstrated, as a windpump.

An initial analysis was made to attempt to ascertain the potential theoretical performance of such a turbine. A single streamtube model of the flow was used with existing published aerodynamic data for sailwings. This analysis suggested that high tip speed ratio operation might be possible but that more extensive aerodynamic data was required. It was clear that such a turbine should have much better starting characteristics than solid bladed turbines and that a significant scale effect was likely with small turbines; i.e. increasing the scale would give a significant benefit due to increasing Reynolds number. It was clear that if high tip speed ratio operation did occur then induced drag losses would be a problem and high aspect ratio blades would be essential.

To obtain more aerodynamic data on sailwings, a series of wind tunnel tests were made. A measuring balance was designed which provided readings of the chordwise and normal force components on the aerofoils. The tests investigated the effect of the pre-tension in the sail and the performance of several different fabrics. It was found that performance

was very poor prior to stall, when the pre-tension was a dominant influence; lower pre-tension giving better performance. The elasticity and stiffness of the fabric had no clear influence but porosity appeared detrimental. After stall, it was found that canvas gave higher chordwise force components than other fabrics but no explanation of this was clear. Increased pre-tension gave a general increase in this force component with the canvas being the most sensitive.

The fresh data showed that, with a simple sailwing, such a turbine would be restricted to low tip speed ratios but that the starting torque coefficient would be high. The data showed that the pre-tension coefficient C_{p_T} would be a significant factor in the turbine performance. However, the coefficient is affected more by the tip speed ratio and windspeed than by the pre-tension. A quite high pre-tension would seem to be required if sail instability at high tip speed ratios in higher winds is to be avoided. The canvas sailwings appeared superior to other fabrics as they seemed likely to produce higher starting torque coefficients and performance was predicted to be best in low winds, when least energy is available in the wind.

A two metre diameter prototype turbine was designed and constructed. Three sets of blades were used, with canvas sails, in an inclined blade configuration with a guyed top bearing. This was tested in the open air using an acceleration test method. Quite smooth curves for the averaged torque and power coefficients were obtained and these were in quite good agreement with predictions. The torque coefficient C_Q had a value of about 0.07 on starting and the average value of the peak power coefficient was about 0.1 at a tip speed ratio of 1.4.

It has been argued that a small vertical axis wind turbine should be at an advantage in utilising the 20% to 30% of the energy in the wind which is contained in short gusts. This would require a pump with suitable, speed dependent, torque characteristics. The use of inertia flow effects seems a feasible way of improving the load matching provided by reciprocating pumps but care in the design is necessary to avoid large losses occurring at high flow velocities.

The prototype turbine was not successfully demonstrated as a windpump. Problems were encountered in driving reciprocating pumps, due it appeared to the cyclic driving torque provided by the turbine. Probably six sets of blades would be required in order to drive directly coupled reciprocating pumps successfully. It may be that a pump with a non-cyclic torque requirement would provide a more suitable load for the turbine.

The prototype design may be discussed in comparison with the criteria suggested by Makhijani (1976) for windmill design in the rural Third World (see page two).

1. The material cost of the prototype design was about £200. The material cost of a production design would obviously depend very much on the local cost of materials but the cost seems quite high in view of the low power output. It may be noted that the materials used to construct the prototype would be almost sufficient to construct a six bladed horizontal axis sailwing turbine of twice the diameter.

2. Assuming a power requirement of perhaps 50W to irrigate a small plot (see page 3), and assuming the prototype windpump to be capable of producing the predicted useful power output of $2.5W/m^2$ in a 4.1m/s wind, then a swept area of $20m^2$ would be necessary. This compares with the prototype which had a swept area of $3.5m^2$.

However, the power take off from the prototype turbine was quite straight-foward and the rotary drive would lend itself to driving other equipment.

3. The design is such that use could probably be made of alternative local materials, e.g. bamboo for the leading edge, struts etc.. Fairly sophisticated bearings would always be required. Construction required no particular skill.

4. The design survived some very high winds with only minor damage, which was easily repaired. For unattended operation a production turbine would need some form of speed limiting device. This could be a centrifugally activated brake on the drive shaft.

5. Although the starting torque was quite high on average, its cyclic variation caused starting problems when trying to drive reciprocating pumps. These problems should be overcome by the use of more turbine blades or a rotary or centrifugal pump.

The cost of a vertical axis sailwing turbine would be reduced if a vertical rather than an inclined blade configuration were adopted. This is because the starting torque would be higher and so a lower solidity could be used. Even then, an horizontal axis sailwing turbine seems likely to use less material per unit swept area and would certainly be at least as efficient. The advantages of a vertical axis design are: the simple construction, largely because there is no need for a yawing arrangement; the increased effective swept area, due to the avoidance of yawing losses; and the rotary drive which lends itself to multiple uses.

It is suggested that any future work with vertical axis sailwing turbines should investigate a vertical blade arrangement; structural design may be more difficult and trailing edge deflections will have more influence. Secondly, such a turbine should be demonstrated as a windpump and data on its performance and reliability obtained. A comparison may then be made with alternative designs.

REFERENCES

Beurskens,H. et al,. Low Speed Water Pumping Windmills:Rotor Tests and Overall Performance.Proc.3.Int.Symp. on Wind Energy Conversion Systems,Copenhagen,1980.

Burton,J.,The Matching of Water Pumps to Windmills for use in Developing Countries,ODA Research Scheme Report R3496, 1979.

Burton,J.,& Ewens,M.,Assembly and Testing of a New Water Pump and Windmill Combination,ODA Research Scheme Report R3601,1980.

Critzos,C. et al.,Aerodynamic Characteristcs of NACA0012 Airfoil Section at Angles of Attack from 0 to 180, NACA Tech. Note 3361,1955.

Darrieus,G.,US Patent No. 1,835,018, Dec.,1931.

Dixon,J.,Improving the Mechanical Load Matching of Wind Energy Convertors,Proc.1.BWEA Workshop,April 1979.

Duremberg,C.,Unsteady Aerodynamics of Vertical Axis Wind Turbines,Proc.1.BWEA Workshop,April 1979.

Fanucci,J. & Walters,R.,The Theoretical Performance of a Vertical Axis Wind Turbine,Proc.VAWT Technology Workshop, Sandia Labs.,Albuquerque,1976.

Fraenkel,P.,An International Development Program to Develop a Wind Powered Water Pumping System Suitable for Small Scale Local Manufacture,Proc.2.International Symposium on Wind Energy Systems,Amsterdam,BHRA,1978.

Fraenkel,P.,Food from Windmills,Intermediate Technology Development Group,London,1976.

Dunn,P. & Eisa,T. et al.,Performance Measurements on the Six Metre Diameter Horizontal Axis Windmill,Proc.2.BWEA Workshop,April 1980.

Glauert,H.,The Elements of Aerofoil and Airscrew Theory, Cambridge University Press,1959.

Golding,E.,The Generation of Electricity by Wind Power,Spon, London,1976.

Grylls,W., et al.,A theoretical and Experimental Investigation into the Variable Pitch Vertical Axis Wind Turbine, Proc.2.Int.Symp.WECS,Amsterdam,1978.

Herepath,R. & Woollard,M.,Initial Test Results on the 5m Horizontal Axis Wind Turbine at Swansea,Proc.2.BWEA Workshop,1980.

van der Hoven,I.,Power Spectrum of Horizontal Wind Speed in the Frequency Range from 0.0007 to 900 Cycles per hour, Journal of Meterology,Vol.14,pp160-164,1957.

Hurley,B.,The Vertical Axis Sail Rotor,MSc Thesis,Trinity College,Dublin,1979

Hurley,B.,Report on Meausrements on Five Sail Vertical Axis Rotor,Low Energy Systems,3 Larkfield Gardens,Dublin,1980.

der Kinderen,W. et al.,Effects of Wind Fluctuations on Windmill Behaviour,Wind Engineering,Vol.1,No.2,1977.

Lumley,J. & Panofsky,H.,The Structure of Atmospheric Turbulence, Wiley,New York,1964.

Makhijani,A.,Energy Policy for the Rural Third World,IIED, London,1976.

Maskell,E,,Theory of Blockage Effects on Bluff Bodies and Stalled Wings in a Closed Wind Tunnel,Aeronautical Research Council,R & M No.3400,London,1963.

Massey,B.,Mechanics of Fluids,van Nostrand Reinhold,London,1970.

Mays,I. & Musgrove,P.,Performance of the Variable Geometry Vertical Axis Wind Turbine at High and Low Solidities, Proc,2.Int.Symp.WECS,Amsterdam,1978.

Migliore,P.,A Free Vortex Model With Numerical Solution for the Unsteady Lifting Characteristics of Straight Bladed Darrieus Wind Turbines,West Viginia University, 1978.

Migliore,P. & Wolfe,W.,Some Effects of Flow Curvature on the Performance of Darrieus Wind Turbines,AAIA,17.Aerospace Meeting,New Orleans,1979.

Miller,D.,Internal Flow, A Guide to Losses in Pipe and Duct Systems,BHRA,1971.

Musgrove,P. & Mays,I.,Development of the Variable Geometry Vertical Axis Windmill,Proc.2.Int.Symp.WECS,Amsterdam, 1978.

Needham,J.,Science and Civilisation in China,Vol.4,II, Cambridge University Press,1965.

Newman,B. & Ngabo,T.,The Design and Testing of a Vertical Axis Wind Turbine Using Sails,Energy Conversion,Vol,18, 1978.

Ormiston,R.,Theoretical and Experimental Aerodynamics of the Sailwing,Journal of Aircraft,Vol.8,2,1971.

Read,S. & Sharpe,D.,An Extended Multiple Streamtube Theory for Vertical Axis Wind Turbines,Proc.2.BWEA Workshop, 1980.

Robert,J. & Newman,B.,Lift and Drag of a Sail Aerofoil,Wind Engineering,Vol.3,No.1,1979.

Savonius,S.,The S-Rotor and its Applications,Mechanical Engineering,Vol.53,5,1930.

Shankar,P.,On the Aerodynamic Performance of a Class of Vertical Shaft Windmills,Proc.R.Soc.London A,349,1976.

Sharpe,D.,A Theoretical and Experimental Study of the Darrieus Vertical Wind Turbine,Kingston Polytechnic Research Report,1977.

Sherman,M.,Development of Wind Energy Utilisation in Asia and thePacific,Proc.Expert Working Group on the Use of Solar and Wind Energy,Energy Resources and Development Series No.16,United Nations,1976.

Sherman,M.,The Design and Construction of Low Cost Wind Powered Water Pumping Systems,ibid.

Sherman,M.,A Water Pumping Windmill that Works,Journal of the New Alchemists II,1973.

South,P. & Rangi,R.,Preliminary Tests of a High Speed Windmill, NAE Report LTR/LA74,Ottowa,1971.

Stern,P.,Small Scale Irrigation,ITDG/IIIC,1979.

Stacey,G.& Musgrove,P.,The Effect of a Fixed Pitch Offset on a High Solidity Vertical Axis Windmill,Proc.3.BWEA Workshop,1981.

Strickland,J.,A Performance Prediction Model for the Darrieus Turbine,Proc.1.Int.Symp.WECS,Cambridge,1976.

Templin,R.,Aerodynamic Performance Theory for the NRC Vertical Axis Wind Turbine,NRC Report LTR-LA-160,1974.

Tewari,S.,Economics of Wind Energy Use for Irrigation in India, Science,Vol.202,3,Nov.,1978.

TOOL Foundation,Amsterdam,Private Communication.

United Nations,Small Scale Solar Powered Irrigation Pumping Systems,Phase I Project Report,UNDP GLO/78/004,1981.

Watson,G,,The Self-starting Capabilities of Low Solidity Fixed Pitch Darrieus Rotors,Proc.1.BWEA Workshop,1979.

APPENDIX 1 Derivation of some equations.

Considering Fig.A1.1, and applying the sine rule to the velocity triangle:

$$\frac{V}{\sin\alpha} = \frac{\mu' V}{\sin(\theta-\alpha)} = \frac{V_R}{\sin(180°-\theta)}$$

hence:

$$\mu' \sin\alpha = \sin(\theta-\alpha) = \sin\theta\cos\alpha - \cos\theta\sin\alpha$$

i.e.

$$\mu' = \sin\theta\cot\alpha - \cos\theta$$

$$\frac{\mu'+\cos\theta}{\sin\theta} = \cot\alpha$$

$$\alpha = \operatorname{atan}\frac{\sin\theta}{\mu'+\cos\theta} \qquad [1.9]$$

and:

$$\frac{V_R}{V} = \frac{\sin(180°-\theta)}{\sin\alpha} = \frac{\sin\theta}{\sin\alpha} \qquad [1.14]$$

Also from Fig.A1.1:

$$C_T = C_{T_L} - C_{T_D} = C_L\sin\alpha - C_D\cos\alpha \qquad [1.10]$$

Considering Fig.A1.2:

Instantaneous retarding force on airstream

$$= \tfrac{1}{2}\rho A_B V^2 (C_L\sin(\theta-\alpha) + C_D\cos(\theta-\alpha))$$

Mean retarding force on airstream, per blade

$$= \tfrac{1}{2}\rho A_B V^2 \frac{1}{2\pi}\int_0^{2\pi}(C_L\sin(\theta-\alpha) + C_D\cos(\theta-\alpha))\,d\theta$$

Hence, coefficient of thrust C_F',

$$C_F' = \frac{\tfrac{1}{2}\rho A_B V^2}{\tfrac{1}{2}\rho A V^2}\cdot\frac{1}{2\pi}\int_0^{2\pi}(C_L\sin(\theta-\alpha) + C_D\cos(\theta-\alpha))\,d\theta$$

i.e.

$$C_F' = \frac{\Sigma A_B}{A}\cdot\frac{1}{2\pi}\int_0^{2\pi}(C_L\sin(\theta-\alpha) + C_D\cos(\theta-\alpha))\,d\theta \qquad [1.24]$$

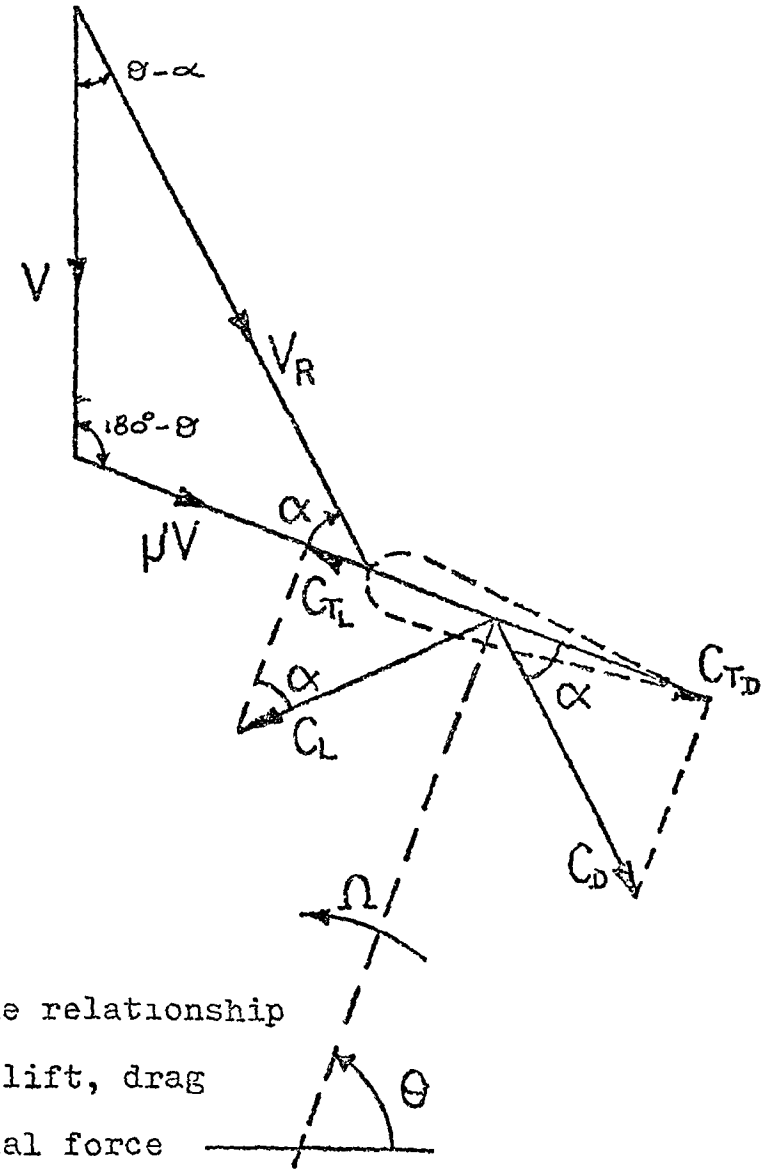

Fig. A1.1 The relationship between the lift, drag and tangential force coefficients.

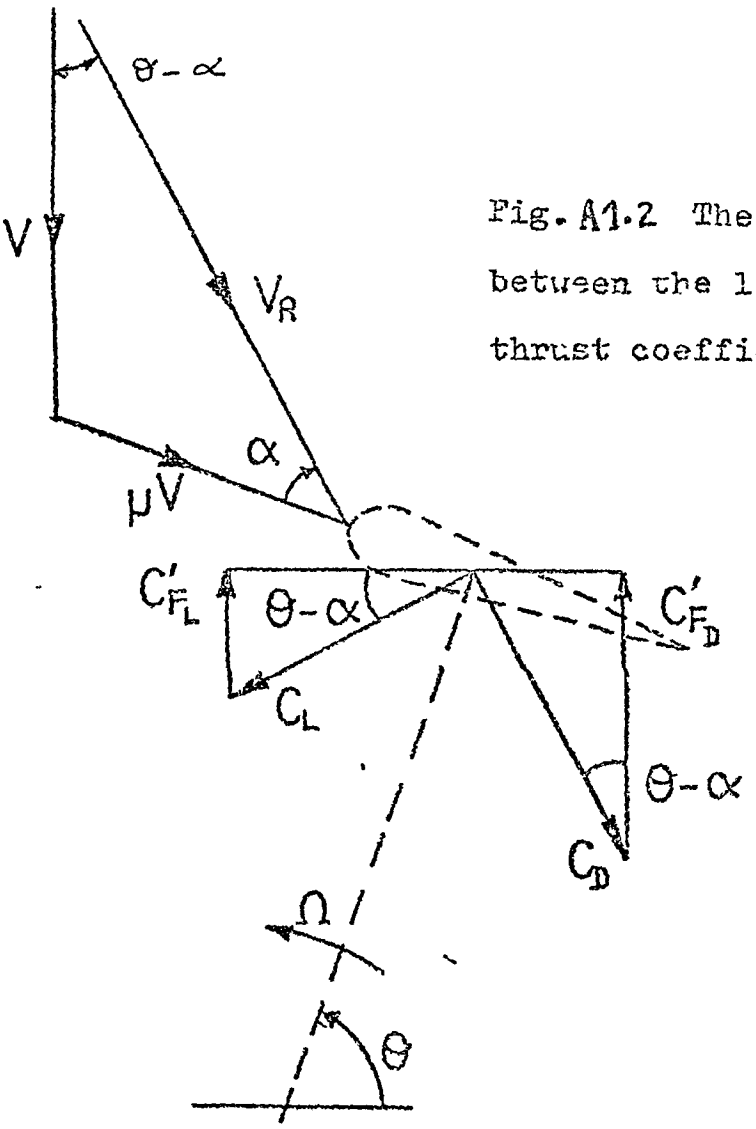

Fig. A1.2 The relationship between the lift, drag and thrust coefficients.

Betz Analysis

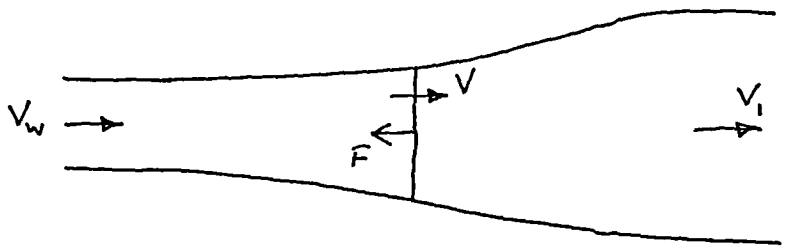

Rate of change of momentum = $\rho A V (V_w - V_1) = F$

Power absorbed = $FV = \rho A V (V_w - V_1) V$ — ①

Rate of change of KE in wind = $\frac{1}{2} \rho A V (V_w^2 - V_1^2)$ — ②

since ① = ② hence $(V_w - V_1) V = \frac{1}{2} (V_w^2 - V_1^2)$

$$\text{and} \qquad \frac{V_w + V_1}{2} = V$$

Power extracted by rotor = $P = \rho A V (V_w - V_1) V$

$$P = \rho A \left(\frac{V_w + V_1}{2} \right)^2 (V_w - V_1)$$

if $\alpha = \frac{V_1}{V_w}$

$$P = \rho \frac{A V_w^3}{4} [(1+\alpha)(1-\alpha^2)]$$

$$\frac{dP}{d\alpha} = \rho \frac{A V_w^3}{4} [1 - 2\alpha - 3\alpha^2] = 0$$

$$\Rightarrow \qquad \alpha = 1/3$$

hence $P_{max} = \rho \frac{A V_w^3}{4} \left(\frac{4}{3} \cdot \frac{8}{9} \right)$

i.e. $P_{max} = \frac{1}{2} \rho A V_w^3 \cdot \frac{16}{27}$

APPENDIX 2

Some Sample Computer Programs Used in the Numerical Analysis of Chapter Two:

1. A single streamtube program.
2. A single streamtube program including allowance for varying Reynolds number and a finite aspect ratio.

```
  100     *RESET FREE
  200           DIMENSION CR(27),CT(27),ALPHA(15,50),ANG(27),CPII(50),
  300          1           THII(50),CP(15,15),TH1(15,15),TH(15,15),VR(15,15),
  301          1            CP1(15,15),VR1(15)
  400           INTEGER R,T,A
  500           REAL MU
  600     C READ IN AEROFOIL DATA (CT) AND (CR)
  700           READ(3,60)((CT(K),CR(K),ANG(K)),K=1,27)
 1000        60 FORMAT(3F8.3)
 1110     C SET AND INCREMENT SOLIDITY (SOLID)
 1120           SOLID=0.0
 1130           DO45N=1,5
 1140           SOLID=SOLID+0.1
 1200     C SET AND INCREMENT VEL.RATIO (MU)
 1300           MU=1.0
 1400           DO40N=1,15
 1500           MU=MU+0.6
 1550           VR1(M)=MU
 1600     C SET AND INCREMENT AZIMUTHAL ANGLE (THETA)
 1700           THETA=0.0
 1800           DO41T=1,50
 1900           THETA=THETA+0.0628
 2000     C CALCULATE EXPECTED ANGLE OF ATTACK (ALPHA)
 2100           ALPHA(M,T)=ATAN(SIN(THETA)/(MU+COS(THETA)))
 2200     C CONVERT A NEGATIVE ALPHA TO POSITIVE FROM 90-180 DEGREES
 2300           IF(ALPHA(M,T).LT.0.0)ALPHA(M,T)=ALPHA(M,T)+3.142
 3100     C FIND FORCE COEFFS. (CT) AND (CR)
 3200        23 IF(ALPHA(M,T).GE.0.0)K=1
 3300           IF(ALPHA(M,T).GE.0.035)K=2
 3400           IF(ALPHA(M,T).GE.0.07)K=3
 3500           IF(ALPHA(M,T).GE.0.105)K=4
 3600           IF(ALPHA(M,T).GE.0.140)K=5
 3700           IF(ALPHA(M,T).GE.0.165)K=6
 3800           IF(ALPHA(M,T).GE.0.209)K=7
 3900           IF(ALPHA(M,T).GE.0.244)K=8
 4000           IF(ALPHA(M,T).GE.0.279)K=9
 4100           IF(ALPHA(M,T).GE.0.314)K=10
 4200           IF(ALPHA(M,T).GE.0.349)K=11
 4300           IF (ALPHA(M,T).GE.0.524)K=12
 4400           IF (ALPHA(M,T).GE.0.698)K=13
 4500           IF(ALPHA(M,T).GE.0.873)K=14
 4600           IF(ALPHA(M,T).GE.1.047)K=15
 4700           IF(ALPHA(M,T).GE.1.222)K=16
 4800           IF(ALPHA(M,T).GE.1.396)K=17
 4900           IF(ALPHA(M,T).GE.1.570)K=18
 5000           IF(ALPHA(M,T).GE.1.745)K=19
 5100           IF(ALPHA(M,T).GE.1.920)K=20
 5200           IF(ALPHA(M,T).GE.2.094)K=21
 5300           IF(ALPHA(M,T).GE.2.269)K=22
 5400           IF(ALPHA(M,T).GE.2.443)K=23
 5500           IF(ALPHA(M,T).GE.2.618)K=24
 5600           IF(ALPHA(M,T).GE.2.793)K=25
 5700           IF(ALPHA(M,T).GE.2.967)K=26
 5800     C IMPROVE VALUES BY INTERPOLATION
 5900           X=0.035
 6000           IF(K.GT.10)X=0.1745
 6100           CTA=CT(K)+(CT(K+1)-CT(K))*(ALPHA(M,T)-ANG(K))/X
 6200           CRA=CR(K)+(CR(K+1)-CR(K))*(ALPHA(M,T)-ANG(K))/X
 6500           Q2=(SIN(THETA)/SIN(ALPHA(M,T)))**2
 6600           CTQ2=CTA*Q2
```

```
6610          CP1I(T)=SOLID*CT02*MU/2
6620          TH1I(1)=SOLID*02*(CRA*SIN(THETA)-CTA*COS(THETA))/2
6640    C INTEGRATE NUMERICALLY
6650          C=0.0
6660          DO10L=2,48
6670          C=C+CP1I(L)
6680       10 CONTINUE
6681          CP1(N,M)=(C+CP1I(1)/2+CP1I(49)/2)/50
6682          E=0.0
6683          DO11L=2,48
6684          E=E+TH1I(L)
6685       11 CONTINUE
6686    C USE ACTUATOR DISK APPROXIMATION TO  CONVERT VALUES
6687    C TO TRUE WINDSPEED
6688          TH1(N,M)=(E+TH1I(1)/2+TH1I(49)/2)/50
6689          CP(N,M)=CP1(N,K)/(1+TH1(N,M)/4)**3
6690          TH(N,M)=TH1(N,M)/(1+TH1(N,M)/4)**2
6691          VR(N,M)=MU/(1+TH1(N,K)/4)
6700       41 CONTINUE
6800       40 CONTINUE
8000          DO43M=1,15
8300          WRITE(6,68)VR1(K),CP1(N,K),TH1(N,M),VR(N,M),CP(N,K),TH(N,K)
8400       68 FORMAT(1X,F4.1,2X,F6.3,3X,F6.3,5X,F5.3,2X,F6.3,2X,F6.3)
8600       43 CONTINUE
8650       45 CONTINUE
8700          END
```

BACHI (01/21/80) 2. A single streamtube program including allowance for varying Reynolds number and finite aspect ratio.

```
      $RESET FREE
            DIMENSIONCL(27,5),CD(27,5),CT02(15,50,10),ALPHA(15,50),
           1 ANG(27),CPI(50),THI(50),CP(15,15),
           1 TH1(15,15),TH(15,15),VR(15,15),CPI(15,15),VRI(15),
           1 ALPHAI(15,50,10),SLORAT(7),B(10)
            INTEGER R,T,A
            REAL MU
      C READ IN AEROFOIL DATA (CL) AND (CD)
            READ(1,60)((CL(K,R),R=1,5),K=1,27)
            READ(2,61)(ANG(K),K=1,27)
            READ(2,60)((CD(K,R),R=1,5),K=1,27)
         60 FORMAT(5F8.3)
         61 FORMAT(8X,F8.3)
      C READ IN ASPECT RATIO CORRECTION FACTORS(SLORAT)
            READ(4,63)(SLORAT(I),I=1,7)
         63 FORMAT(F8.3)
      C SET AND INCREMENT ASPECT RATIO (AR)
            AR=6
            DO46A=1,2
            AR=AR+2
      C SET AND INCREMENT SOLIDITY (SOLID)
            SOLID=0.0
            DO45N=1,5
            SOLID=SOLID+0.1
      C SET AND INCREMENT VEL.RATIO (MU)
            MU=1.0
            DO40M=1,15
            MU=MU+0.6
            VR1(M)=MU
      C SET AND INCREMENT AZIMUTHAL ANGLE (THETA)
            THETA=0.0
            DO41T=1,50
            THETA=THETA+0.0628
      C CALCULATE EXPECTED ANGLE OF ATTACK (ALPHA)
            ALPHA(M,T)=ATAN(SIN(THETA)/(MU+COS(THETA)))
      C CONVERT A NEGATIVE ALPHA TO POSITIVE FROM 90-180 DEGREES
            IF(ALPHA(M,T).LT.0.0)ALPHA(M,T)=ALPHA(M,T)+3.142
      C CALCULATE REYNOLDS NUMBER
            U=10*SIN(THETA)/SIN(ALPHA(M,T))
            IF(U.GT.12.6)R=5
            IF(U.LE.12.6)R=4
            IF(U.LE.9.8)R=3
            IF(U.LE.7.2)R=2
            IF(U.LE.5.1)R=1
            STANG=0.157
            IF(R.GT.3)STANG=0.175
            IF(ALPHA(M,T).LT.STANG)A0=3.4
            IF(ALPHA(M,T).LT.0.0873)A0=8.2
      C FIND CORRECTION FACTOR (SLORAT)
            B(A)=AR/A0
            IF(B(A).GT.1.625)I=7
            IF(B(A).LE.1.625) I=6
            IF(B(A).LE.1.375)I=5
            IF(B(A).LE.1.125)I=4
            IF(B(A).LE..875)I=3
            IF(B(A).LE..625)I=2
            IF(B(A).LE..375)I=1
      C CALCULATE EFFECTIVE ANGLE OF ATTACK (ALPHAI)
            ALPHAI(M,T,A)=ALPHA(M,T)*SLORAT(I)
      C IGNORE  EFFECT OF (AR) ABOVE STALL ANGLE
```

```
2340          IF(ALPHA1(M,T,A),GT,STANG)GO TO 23
2342      C FIND LIFT AND DRAG COEFFS. (CL) AND (CD)
2344          IF(ALPHA1(M,T,A),GE,0,0)K=1
2346          IF(ALPHA1(M,T,A),GE,0,035)K=2
2348          IF(ALPHA1(M,T,A),GE,0,07)K=3
2350          IF(ALPHA1(M,T,A),GE,0,105)K=4
2352          IF(ALPHA1(M,T,A),GE,0,140)K=5
2354          IF(ALPHA1(M,T,A),GE,0,165)K=6
2356          IF(ALPHA1(M,T,A),GE,0,209)K=7
2358      C IMPROVE VALUES BY INTERPOLATION
2360          X=0,035
2362          CLA=CL(K,R)+(CL(K+1,R)-CL(K,R))*(ALPHA1(M,T,A)-ANG(K))/X
2364          CDA=CD(K,R)+(CD(K+1,R)-CD(K,R))*(ALPHA1(M,T,A)-ANG(K))/X
2366      C CALCULATE NEW CD
2368          CDA=CDA+(CLA**2/(AR*3,142))
2370
3005          GO TO 99
3100      C FIND LIFT AND DRAG COEFFS. (CL) AND (CD)
3200       23 IF(ALPHA(M,T),GE,0,0)K=1
3300          IF(ALPHA(M,T),GE,0,035)K=2
3400          IF(ALPHA(M,T),GE,0,07)K=3
3500          IF(ALPHA(M,T),GE,0,105)K=4
3600          IF(ALPHA(M,T),GE,0,140)K=5
3700          IF(ALPHA(M,T),GE,0,165)K=6
3800          IF(ALPHA(M,T),GE,0,209)K=7
3900          IF(ALPHA(M,T),GE,0,244)K=8
4000          IF(ALPHA(M,T),GE,0,279)K=9
4100          IF(ALPHA(M,T),GE,0,314)K=10
4200          IF(ALPHA(M,T),GE,0,349)K=11
4300          IF (ALPHA(M,T),GE,0,524)K=12
4400          IF (ALPHA(M,T),GE,0,698)K=13
4500          IF(ALPHA(M,T),GE,0,873)K=14
4600          IF(ALPHA(M,T),GE,1,047)K=15
4700          IF(ALPHA(M,T),GE,1,222)K=16
4800          IF(ALPHA(M,T),GE,1,396)K=17
4900          IF(ALPHA(M,T),GE,1,570)K=18
5000          IF(ALPHA(M,T),GE,1,745)K=19
5100          IF(ALPHA(M,T),GE,1,920)K=20
5200          IF(ALPHA(M,T),GE,2,094)K=21
5300          IF(ALPHA(M,T),GE,2,269)K=22
5400          IF(ALPHA(M,T),GE,2,443)K=23
5500          IF(ALPHA(M,T),GE,2,618)K=24
5600          IF(ALPHA(M,T),GE,2,793)K=25
5700          IF(ALPHA(M,T),GE,2,967)K=26
5800      C IMPROVE VALUES BY INTERPOLATION
5900          X=0,035
6000          IF(K,GT,10)X=0,1745
6100          CLA=CL(K,R)+(CL(K+1,R)-CL(K,R))*(ALPHA(M,T)-ANG(K))/X
6200          CDA=CD(K,R)+(CD(K+1,R)-CD(K,R))*(ALPHA(M,T)-ANG(K))/X
6300      C CALCULATE (CT)
6400       99 CT=CLA*SIN(ALPHA(M,T))-CDA*COS(ALPHA(M,T))
6500          Q2=(SIN(THETA)/SIN(ALPHA(M,T)))**2
6600          CTQ2(M,T,A)=CT*Q2
6620          TH1I(T)=SOLID*Q2*(CLA*(SIN(THETA)*COS(ALPHA(M,T))-COS(THETA)*
6630         1SIN(ALPHA(M,T)))+CDA*(COS(THETA)*COS(ALPHA(M,T))+SIN(THETA)*
6631         1SIN(ALPHA(M,T))))/2,0
6635       42 CP1I(T)=SOLID*CTQ2(M,T,A)*MU/2
6640      C INTEGRATE NUMERICALLY
6650          C=0,0
6660          DO10L=2,48
6670          C=C+CP1I(L)
6680       10 CONTINUE
6681          CP1(N,M)=(C+CP1I(1)/2+CP1I(49)/2)/50
```

```
6682            E=0.0
6683            DO11L=2,48
6684            E=E+TH1(I)
6685         11 CONTINUE
6686      C USE ACTUATOR DISK APPROXIMATION TO  CONVERT VALUES
6687      C TO TRUE WINDSPEED
6688            TH1(N,M)=(E+TH1(1)/2+TH1(49)/2)/50
6689            CP(N,M)=CP1(N,M)/(1+TH1(N,M)/4)**3
6690            TH(N,M)=TH1(N,M)/(1+TH1(N,M)/4)**2
6691            VR(N,M)=MU/(1+TH1(N,M)/4)
6700         41 CONTINUE
6800         40 CONTINUE
8000            DO43M=1,15
8300            WRITE(6,68)VR1(M),CP1(N,M),TH1(N,M),VR(N,M),CP(N,M),TH(N,M)
8400         68 FORMAT(1X,F4.1,2X,F6.3,3X,F6.3,5X,F5.3,2X,F6.3,2X,F6.3)
8600         43 CONTINUE
8650         45 CONTINUE
8660         46 CONTINUE
8700            END
```

APPENDIX 3

1. Relationship between the tension coefficients C_{P_T} and C_{T_T}.
2. Calibration of the leading edge strain gauges.
3. An additional test with a jib-sail.

1. Relationship between the tension coefficients C_{P_T} and C_{T_T}

For a rectangular sail, length b, with a trailing edge curved in a circular arc with radius s and having a maximum trailing edge hollow x (Fig.3.5); Newman and Ngabo (1978) give: $x = b^2/8s$ for small x/b.

The chordwise tension in the sail per unit length P_T, is related to the tension in the trailing edge by: $P_T = T_T/s$

Hence: $P_T = T_T \cdot \frac{8x}{b^2}$ i.e. $C_{P_T} = \frac{P_T}{\frac{1}{2}\rho V_R^2 c} \approx \frac{T_T \cdot 8x}{\frac{1}{2}\rho V_R^2 A_s b}$

$$= C_{T_T} \cdot 8\frac{x}{b}$$

2. Calibration of the leading edge strain gauges

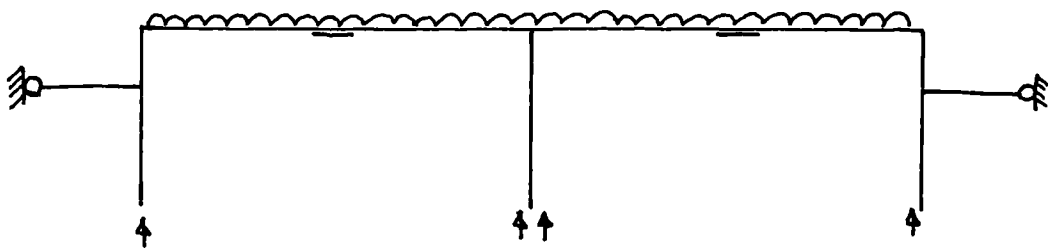

Fig.A3.1. Loads in the sailwing frame due to pre-tension in the sail.

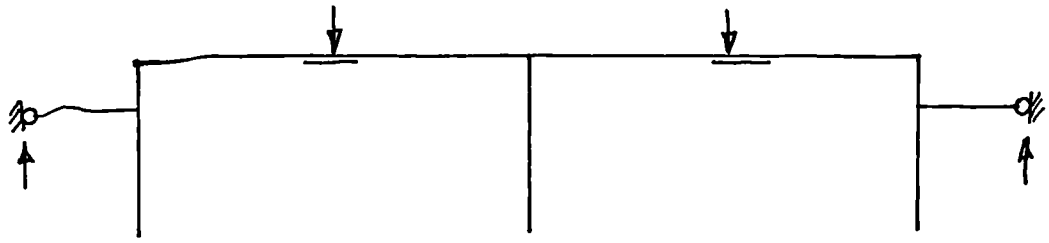

Fig.A3.2. Calibration load.

A standard computer program package (Linear Elastic Analysis of Plane Frames) was used to calculate the relative strain in the leading edge, at the strain gauge position, with the load applied by the tension in the sail and with the calibration loading used.

The uncertainty in the pre-tension values is largely due to the difficulty of applying a perfectly even pre-tension to the fabric.

3. An additional test with a jib-sail

After the tests described in Chapter Three, a test was made in which the effect of a jib-sail in front of the existing sail was observed. It was anticipated that this might give the effect of a slotted wing and improve the aerodynamic performance at low angles of incidence.

The sailwing frame was modified to enable jib-sails to be fitted (Fig.A3.3). The jib chord tapered from 70mm at mid-span to 30mm at the endplates. The jib leading edge was

a taut 1mm stranded steel wire and the trailing edge was the same but slightly slack and with some curvature. Wax proofed canvas was used for the sails.

It was found that the jibs became unstable very easily at angles of incidence below 5 degrees and above 140 degrees. This would obviously not be satisfactory for a turbine. Surprisingly, it was found that the aerodynamic performance was only improved at angles of incidence between about 15 to 30 degrees (Fig.A3.4).

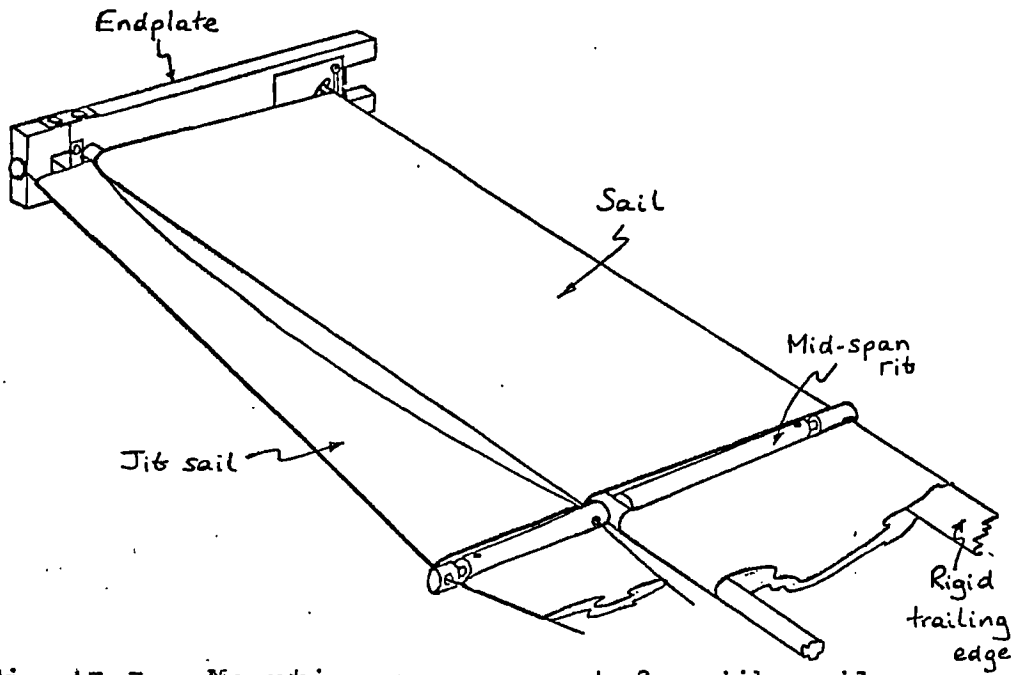

Fig.A3.3. Mounting arrangement for jib sails.

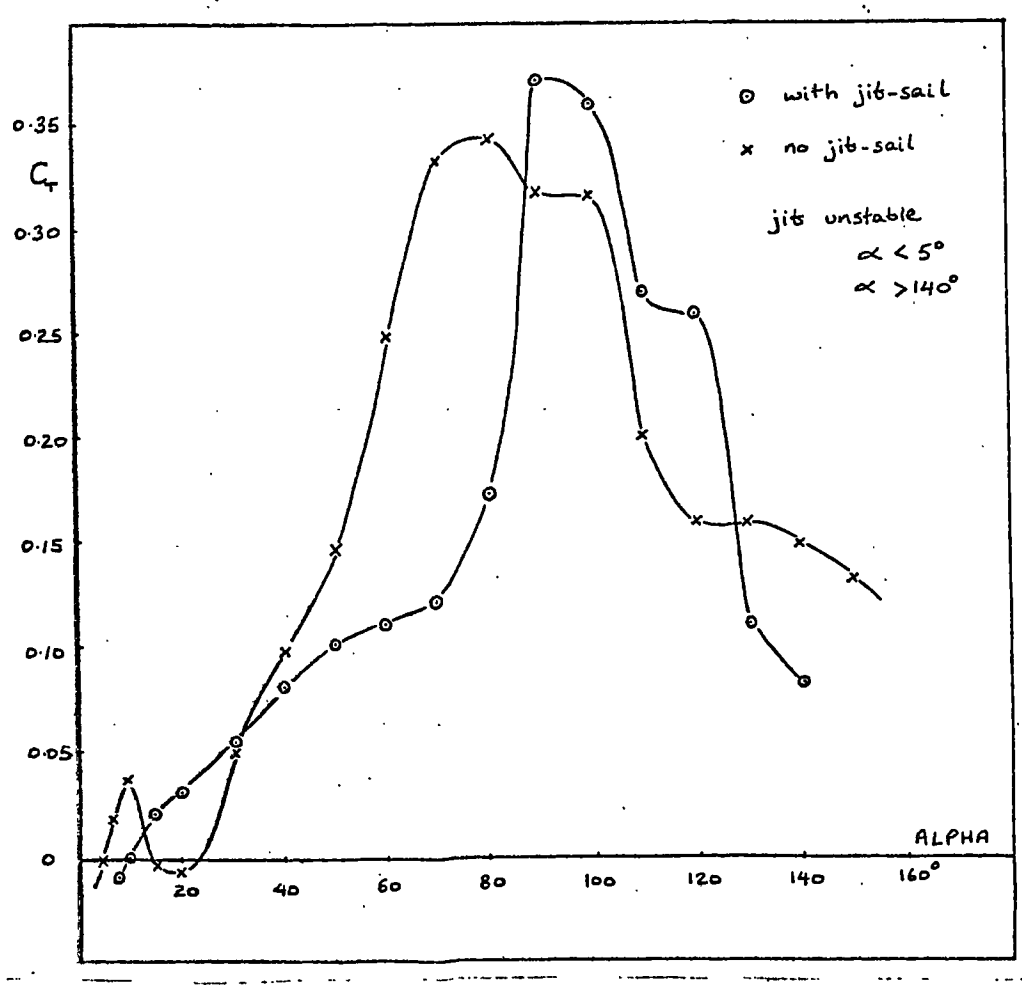

Fig.A3.4. Tangential force coefficient vs. angle of incidence for a canvas sailwing with and without a jib sail.

APPENDIX 5

1. Modified Expressions for an Inclined Blade.
2. The Power Absorbed by a Rotating Strut.

1. Modified Expressions for an Inclined Blade

Consider an inclined blade at angular position θ and consider an element at radius r.

Define $y = \frac{r}{R} = \frac{z}{R\tan\gamma}$ (Fig.A5.1)

where γ is the angle to the vertical made by the unit normal to the blade axis $\hat{e}_n$:

$$\hat{e}_n = -\cos\gamma.\hat{e}_z + \sin\gamma(\cos\theta.\hat{e}_p + \sin\theta.\hat{e}_q)$$

The unit vector along the chord is $\hat{e}_c$:

$$\hat{e}_c = -\sin\theta.\hat{e}_p + \cos\theta.\hat{e}_q$$

The true relative wind velocity at the blade section is V_R':

$$V_R' = -V\hat{e}_q + r\Omega(\sin\theta.\hat{e}_p - \cos\theta.\hat{e}_q)$$

However the windspeed contributing to driving torque is given only by the components in the plane of the blade section:

$$V_R^2 = (V_R'\cdot\hat{e}_n)^2 + (V_R'\cdot\hat{e}_c)^2 = \underline{(V\sin\gamma\sin\theta)^2 + (r\Omega + V\cos\theta)^2}$$

Now $q^2 = \left(\frac{V_R}{V}\right)^2 = \underline{(\sin\gamma\sin\theta)^2 + (\mu' y + \cos\theta)^2}$

where $\mu' = \frac{r\Omega}{V}$

The effective angle of attack at the blade section is α:

$$\alpha = \text{atan}\left(\frac{V_R'\cdot\hat{e}_n}{V_R'\cdot\hat{e}_c}\right) = \underline{\text{atan}\left(\frac{\sin\gamma\sin\theta}{\mu' y + \cos\theta}\right)}$$

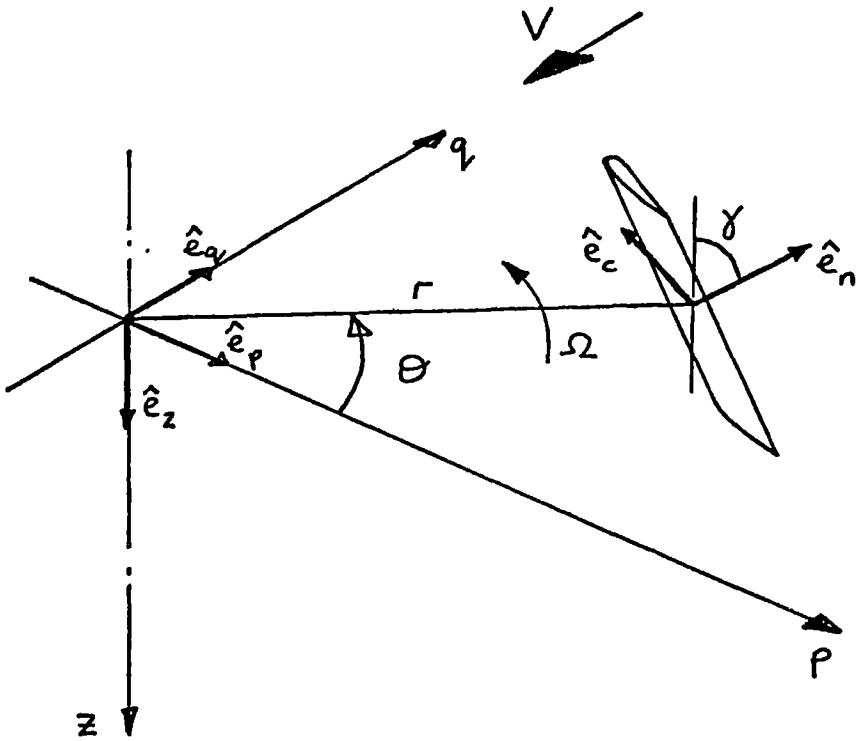

Fig.A5.1. To define the nomenclature used in deriving expressions for an inclined blade.

APPENDIX 5

2. The Power Absorbed by a Rotating Strut

Consider a single strut, length R, chord c. Assume that drag depends solely on the relative flow normal to it and that the drag coefficient C_D is constant and independent of the direction of relative flow.

The work done against drag in one revolution is W:

$$W = \tfrac{1}{2}\rho c C_D 2\int_0^R \left\{ \int_0^{\pi/2} (V\cos\theta + r\Omega)^2 d\theta + \int_{\pi/2}^{\pi} \pm (r\Omega - V\cos\theta)^2 d\theta \right\} r\,dr$$

where the +sign applies when $r\Omega > V\cos\theta$ i.e. $r > \frac{V\cos\theta}{\Omega}$

Integrating with respect to r in two parts

$$0 < r < \frac{V\cos\theta}{\Omega} \quad \& \quad \frac{V\cos\theta}{\Omega} < r < R$$

$$W = \rho c C_D \left\{ \int_0^{\pi/2} \left[\frac{V^2}{2} r^2\cos^2\theta + \frac{r^4\Omega^2}{4} + \frac{2r^3\Omega}{3} V\cos\theta \right]_0^R d\theta \right.$$
$$+ \int_{\pi/2}^{\pi} -\left[\frac{r^4\Omega^2}{4} + \frac{V^2 r^2}{2}\cos^2\theta - \frac{2r^3}{3} V\cos\theta \right]_0^{\frac{V\cos\theta}{\Omega}}$$
$$\left. + \left[\frac{r^4\Omega^2}{4} + \frac{V^2 r^2}{2}\cos^2\theta - \frac{2r^3}{3} V\cos\theta \right]_{\frac{V\cos\theta}{\Omega}}^R d\theta \right\}$$

$$W = \rho c C_D \left\{ \int_0^{\pi/2} \left(\frac{V^2 R^2}{2}\cos^2\theta + \frac{R^4\Omega^2}{4} + \frac{2R^3\Omega}{3} V\cos\theta \right) d\theta \right.$$
$$+ \int_{\pi/2}^{\pi} \left(2\left[-\frac{V^4\cos^4\theta}{4\Omega^2} - \frac{V^4\cos^4\theta}{2\Omega^2} + \frac{2}{3}\frac{V^4\cos^4\theta}{\Omega^2} \right] \right.$$
$$\left. \left. + \left[\frac{R^4\Omega^2}{4} + \frac{V^2 R}{2}\cos^2\theta - \frac{2}{3} R^3\Omega V\cos\theta \right] \right) d\theta \right\}$$

$$W = \rho c C_D \left\{ \frac{4}{3} R^3\Omega V + \frac{R^4\Omega^2\pi}{4} + \frac{V^2 R^2\pi}{4} - \frac{V^4\pi}{32\Omega^2} \right\}$$

Putting $R\Omega = \mu V$

$$W = \rho c C_D R^2 V^2 \left\{ \frac{4}{3}\mu + \frac{\pi}{4}\mu^2 + \frac{\pi}{4} - \frac{\pi}{32\mu^2} \right\}$$

The power absorbed P_{strut} is: $P_{strut} = W.\frac{\Omega}{2\pi}$

$$P_{strut} = \rho c C_D R V^3 \left\{ \frac{2}{3\pi}\mu^2 + \frac{\mu^3}{8} + \frac{\mu}{8} - \frac{1}{64\mu} \right\}$$

and so the change in power coefficient due to drag from the strut ΔC_p is:

$$\Delta C_p = \frac{c C_D R}{A} \left\{ \frac{4}{3\pi}\mu^2 + \frac{\mu^3}{4} + \frac{\mu}{4} - \frac{1}{32\mu} \right\}$$

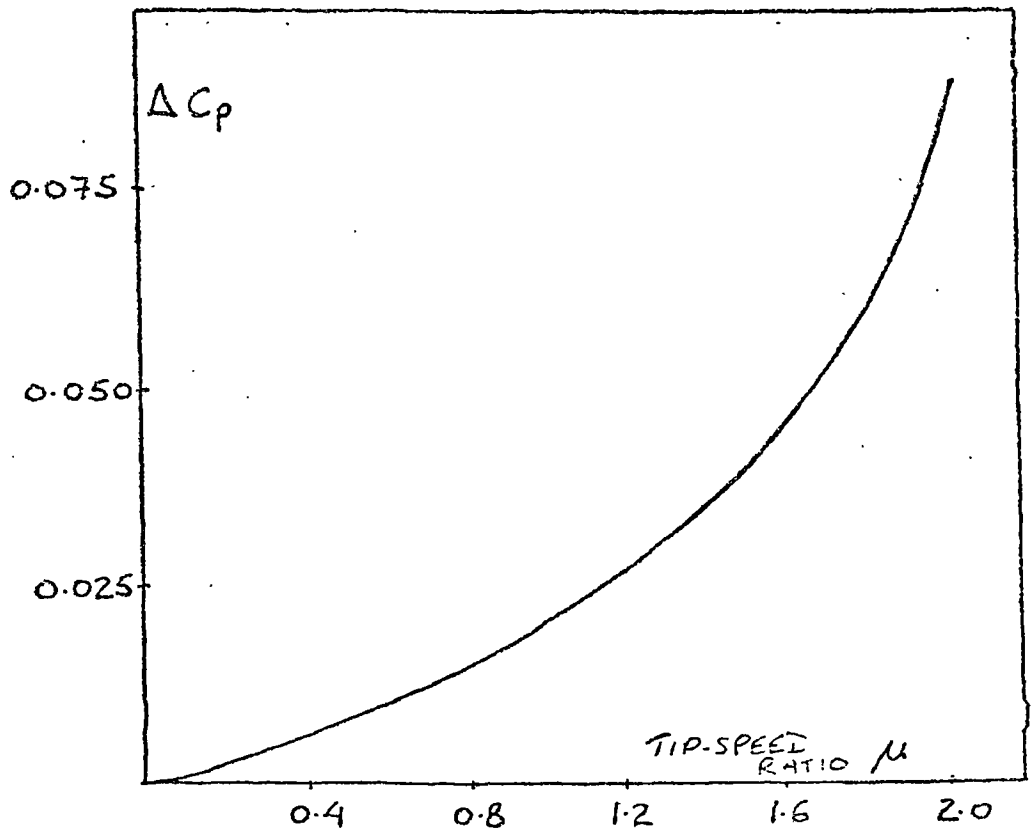

Fig.A5.2. Estimated change in the power coefficient due to the power absorbed by the three struts of the prototype turbine. ($C_D = 1{\cdot}2$, $c = 20\text{mm}$, $R = 1\text{m}$, $A = 3{\cdot}5\text{m}^2$)

APPENDIX 6

Prototype Performance Measurements

1. Tachometer circuit

This circuit (Fig.6.2) is based on a 76810 tachometer chip. This chip contains a Schmitt trigger circuit and produces constant amplitude, constant width pulses at the same frequency as the input signal. A simple filter network on the output was used to produce a voltage proportional to input frequency. The saturation voltage is determined by the timing components (R) and (C) which control the pulse width. Calibration of the circuit showed a linear output up to about 300Hz (Fig.A6.1). At very low frequencies there was a slight ripple in the output. At 5Hz this amounted to 3% of the output voltage, reducing to 0.7% at 10Hz. The slotted disc contained 65 slots; the input frequency was therefore 65 times the turbine frequency.

The slotted opto-isolator was an RS-306-061 with an infra-red light emitting diode. It was found necessary to provide extra shielding from sunlight for the photo-transistor.

The circuit was calibrated using a frequency counter and signal source and is thought to be within 0.5% accuracy.

The slot spacing at the circumference of the disc was 5mm. If the possible random error in theslot spacing was $\pm$10%, then in a 5m/s wind, five slots would pass per second at a tip speed ratio of 0.1. This would cause a random error in the output voltage of $\pm$2% and this would reduce to 0.2% at

a tip speed ratio of 1.0.

2. Anemometers

The anemometers were connected to identical circuits as used for the tachometer. They were calibrated in the wind tunnel (Fig.A6.2). To obtain low windspeeds the tunnel was run in its starting mode. The calibration is thought to be within 1% accuracy. Random errors due to ripple should be negligable as the circuit input frequency was always quite high.

3. Accuracy of the Performance Measurements

Apart from the uncertainty in the estimate of the windspeed experienced by the turbine, and scatter introduced by changes in the turbine performance with windspeed, random errors were introduced by the slight ripple in the tachometer circuit output at very low frequencies and by imperfect spacing of the slots in the slotted discs.

In a 5m/s wind, these errors could combine to give a 5% random error in the voltage output at a tip speed ratio of 0.1, reducing to 0.9% at a tip speed ratio of 1.0. A 5% random error in the speed measurement could cause a 10% error in the acceleration estimate and hence, a 10% error in the values of torque and power coefficients. At a tip speed ratio of 1.0, the random error in the coefficients from this cause will be less than 1.8%.

Systematic errors were introduced by the possible error in measurement of turbine inertia, ±4% (see section 6.2.1) and by calibration errors. If the errors in the tachometer and anemometer calibrations were 0.5% and 1% respectively, then possible systematic errors were as follows: (referring to page 65)

$V_w(t)$ ±1%

$\dot{\vartheta}(t)$ ±0.5%

$\ddot{\vartheta}(t)$ ±0.5%

$T(t)$ ±4.5%

$P(t)$ ±5.0%

μ ±1.5%

$C_Q(t)$ ±6.5%

$C_P(t)$ ±8%

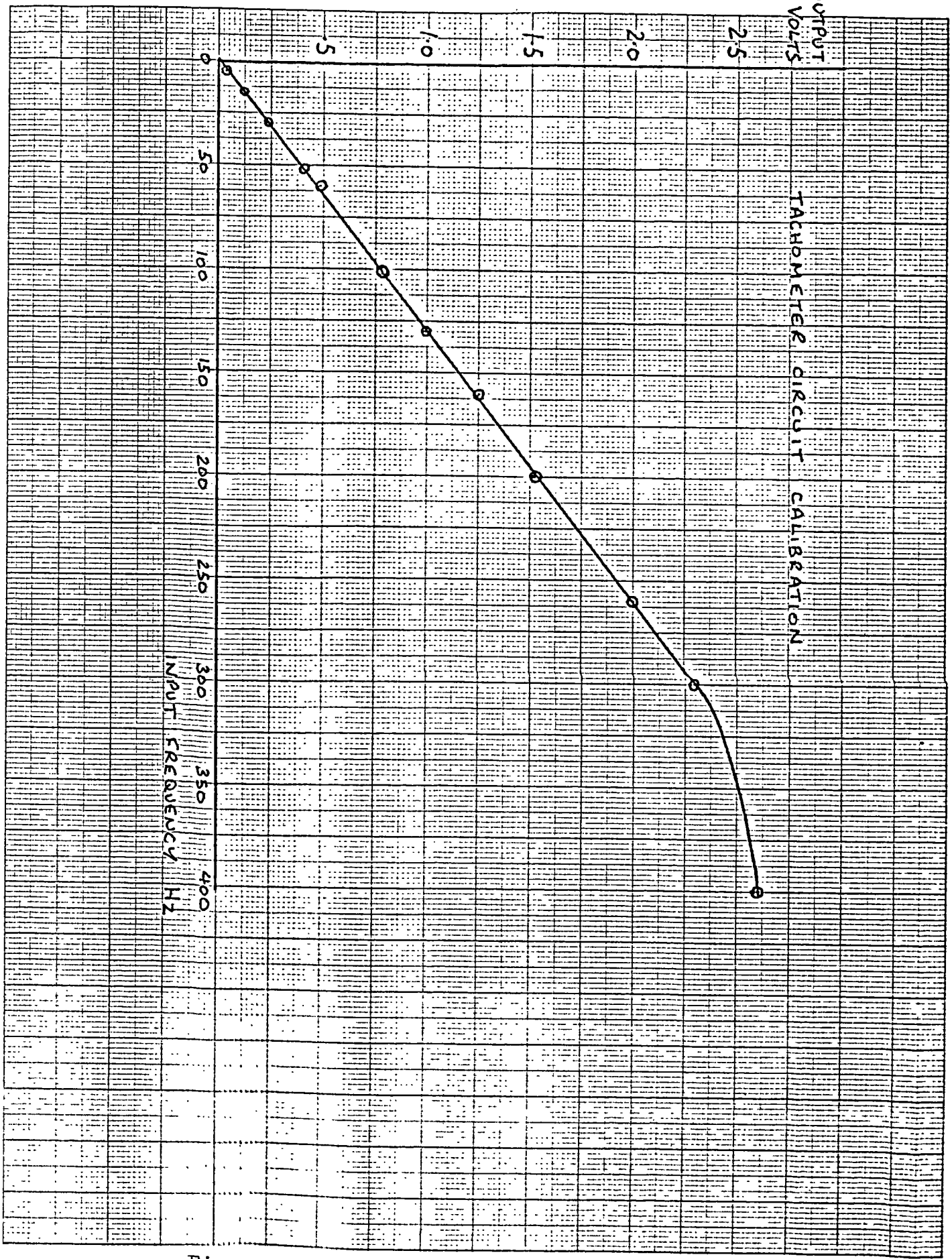

Fig.A6.1. Calibration curve for tachometer circuit.

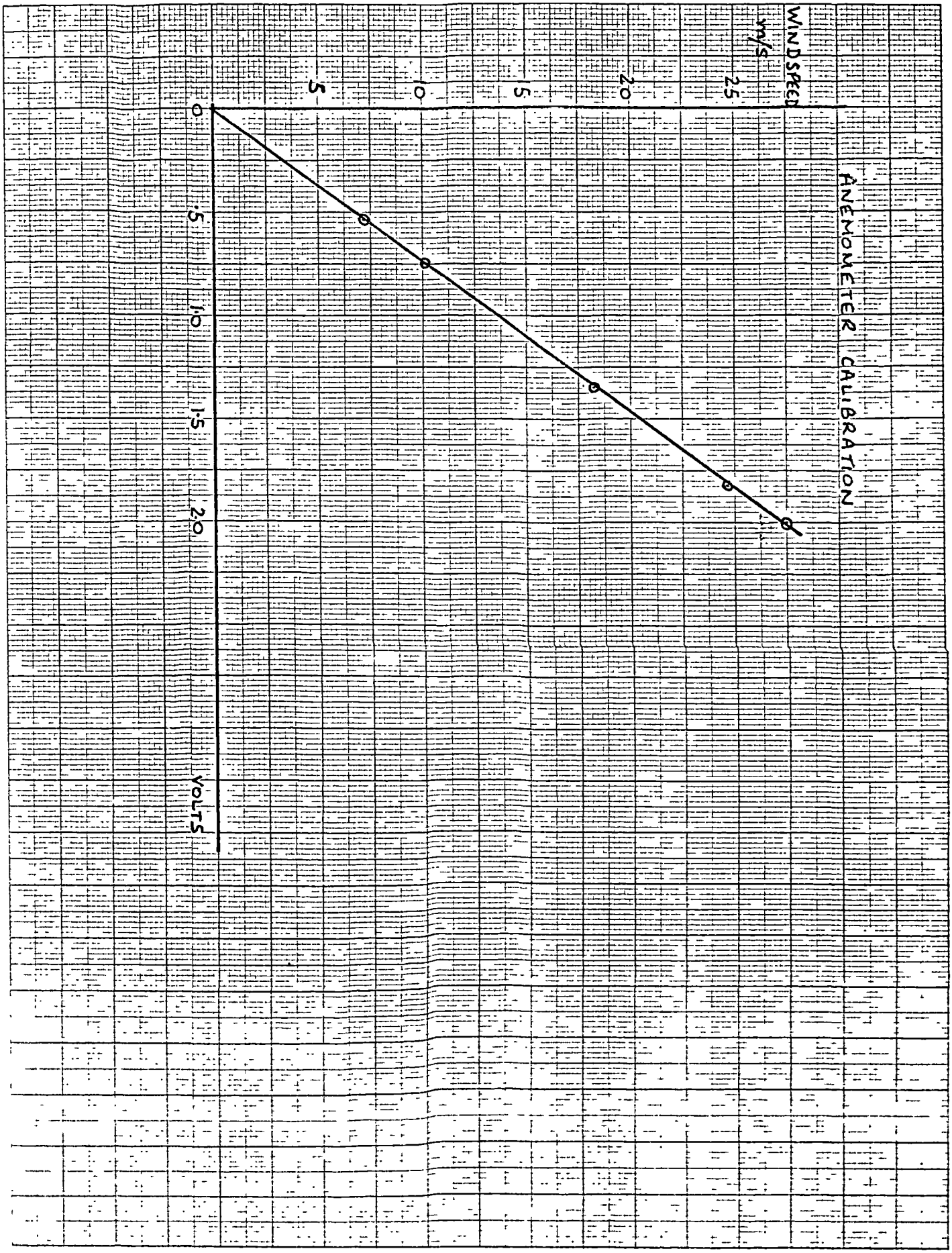

Fig.A6.2. Calibration curve for anemometers.

APPENDIX 7

1. Turbulence in the Wind
2. A Simple Theory for Inertia Flow
3. Pipe Losses in the Pump Performance Tests

1.Turbulence in the Wind

As a random phenomenom, turbulence in the wind may be analysed using the statistical methods of random signal analysis. As was shown in section 7.2, the power in the wind is approximately equal to: $\frac{1}{2}\rho(\bar{V}_w^3 + 3\bar{V}_w\overline{v^2})$ per unit area, where $\bar{V}_w$ is the mean windspeed and $\overline{v^2}$ is its variance.

The autocorrelation function is defined as:

$$R_{ii}(\tau) = \overline{v(t_1)\,v(t_2)}$$

where $\tau = t_2 - t_1$; When $\tau = 0$, it is equal to the variance. This function shows how the windspeed at time t_2 correlates with its value at time t_1.

A power spectral density can be obtained from the autocorrelation function by Fourier analysis:

$$\Phi(\omega) = \frac{1}{2\pi}\int_{-\infty}^{\infty} e^{i\omega\tau} R_{ii}(\tau)\, d\tau$$

where ω is the frequency. This shows the relative contribution made by fluctuations of each frequency to the power content of the fluctuations. The frequency of the fluctuations is characteristic of the eddy size. der Kinderen et al (1977) suggest that a 3.7m diameter turbine is unable to use gust energy in eddies with frequencies above about 0.05 Hz.

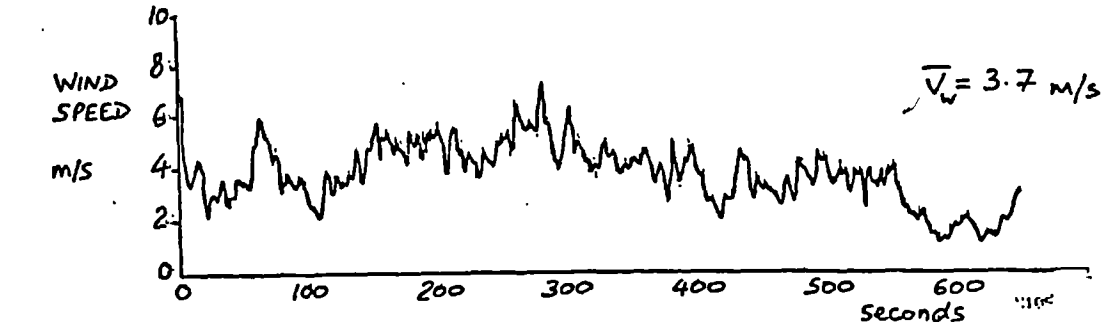

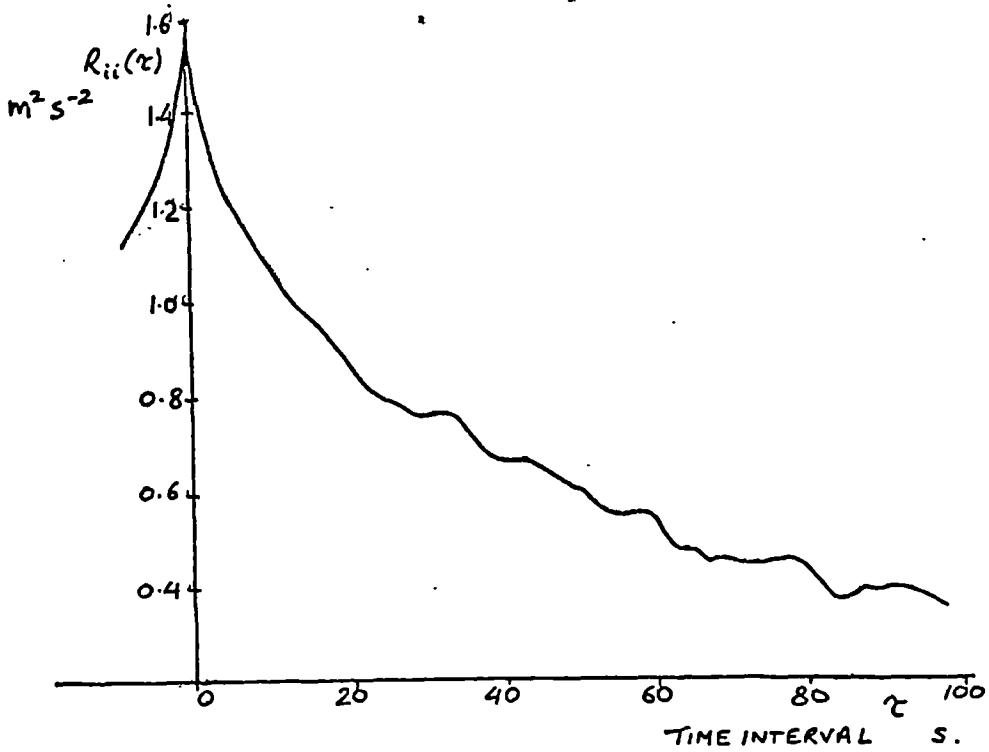

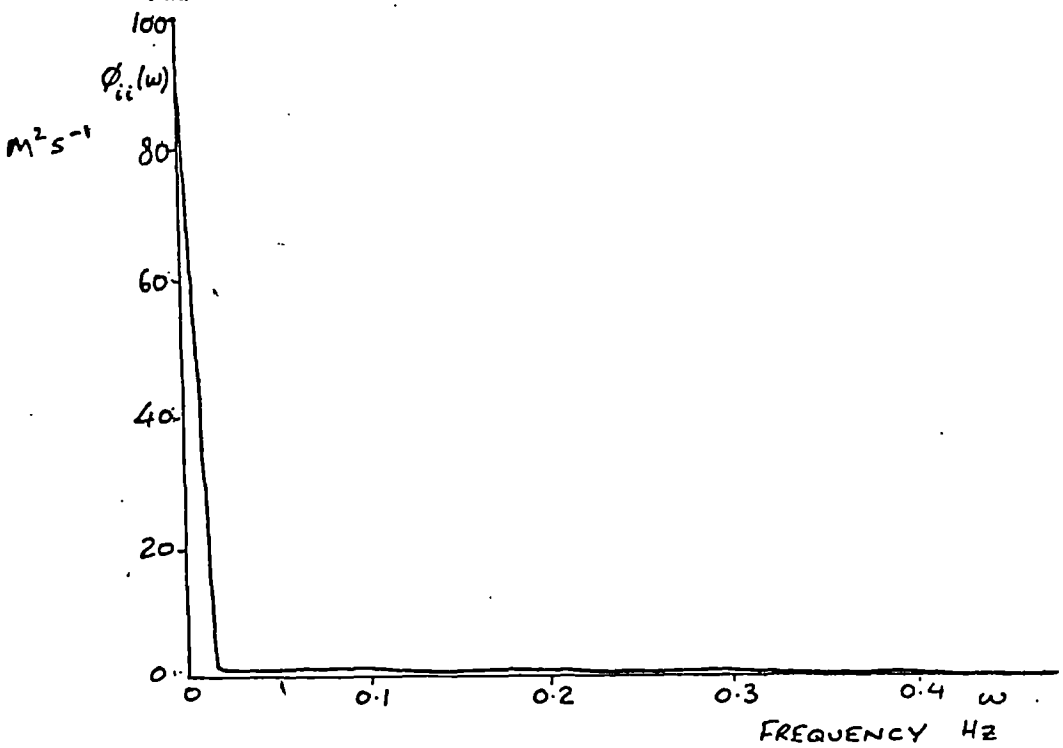

Fig.A7.1. Auto-correlation function and power spectral density for a sample of wind speed.

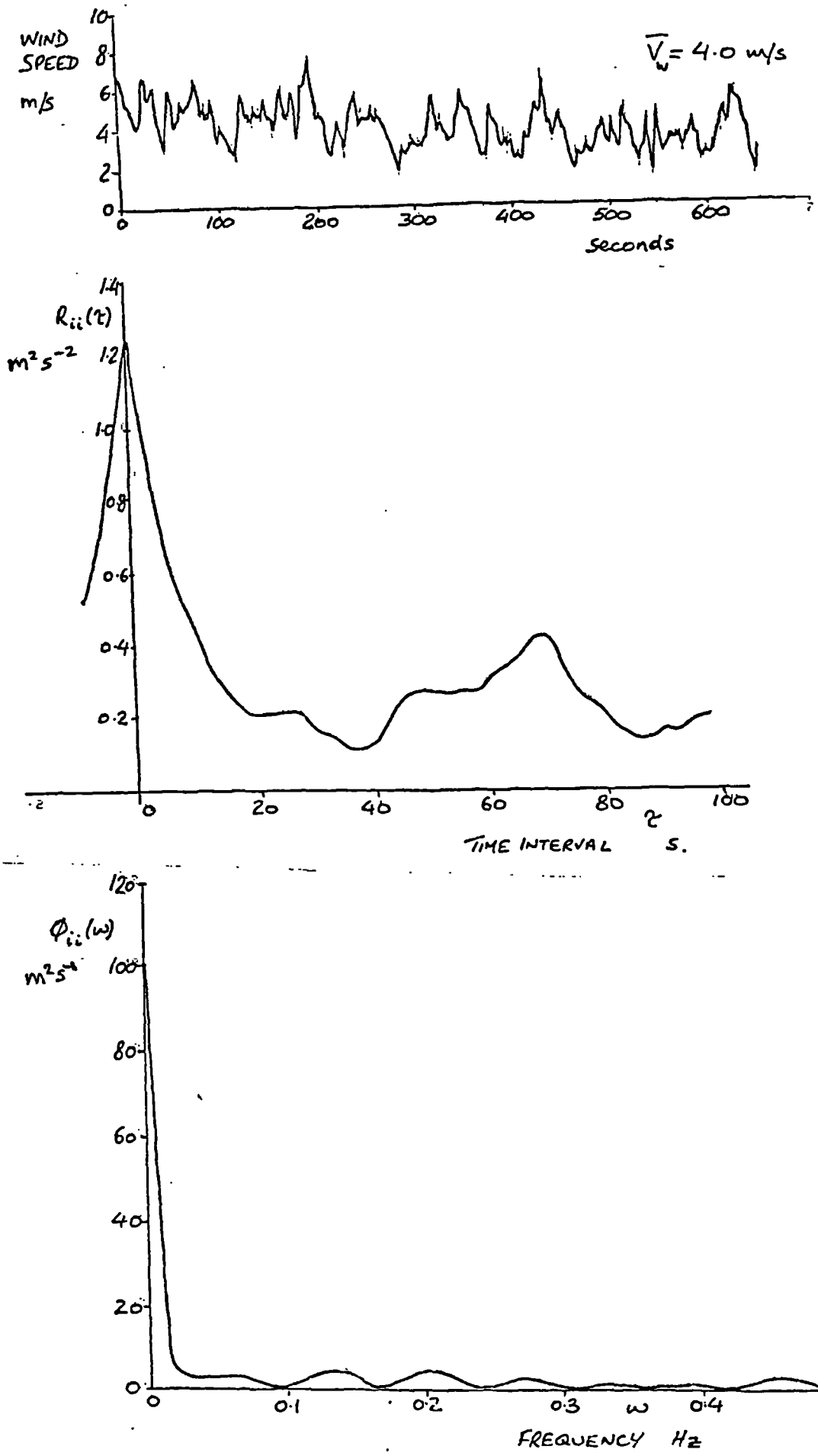
WIND SPEED m/s
$\bar{V}_w$ = 4.0 m/s
seconds
$R_{ii}(\tau)$
$m^2 s^{-2}$
TIME INTERVAL τ s.
$\Phi_{ii}(\omega)$
$m^2 s^{-1}$
FREQUENCY ω Hz

Fig.A7.1. cont.

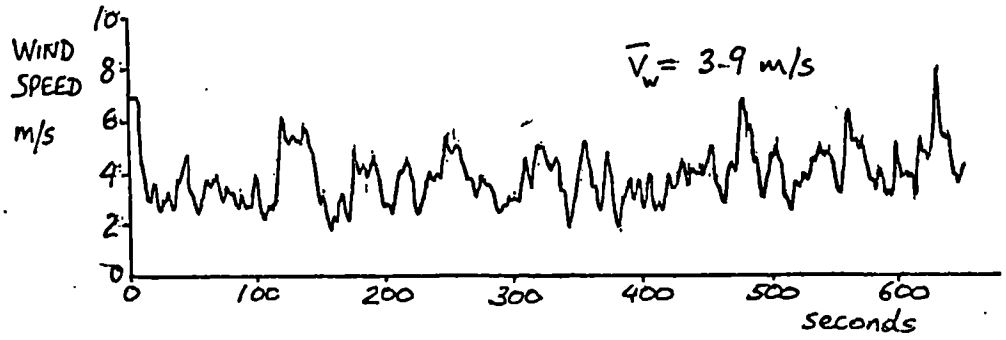

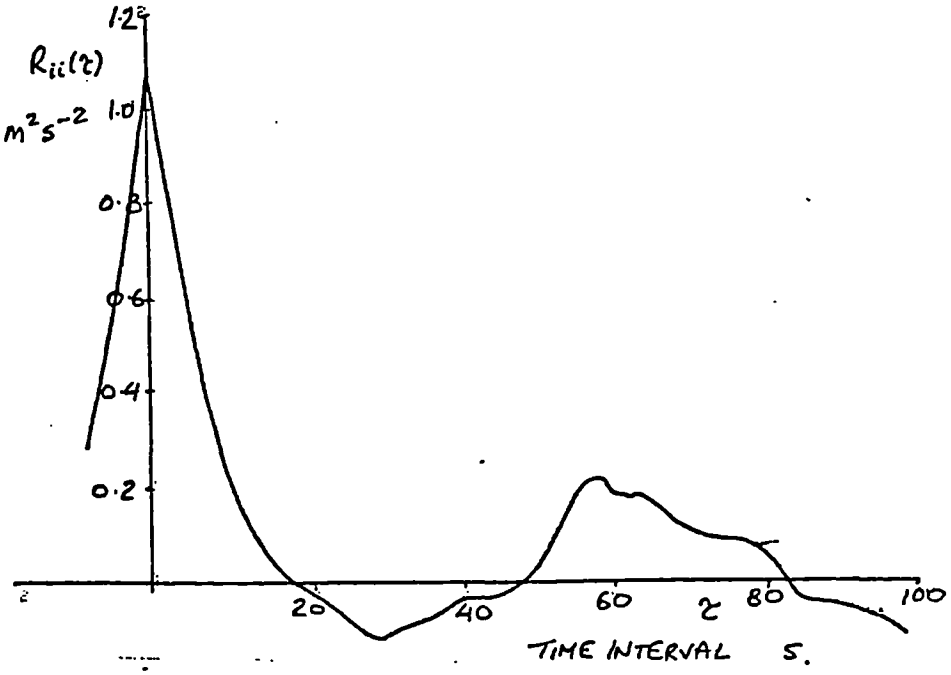

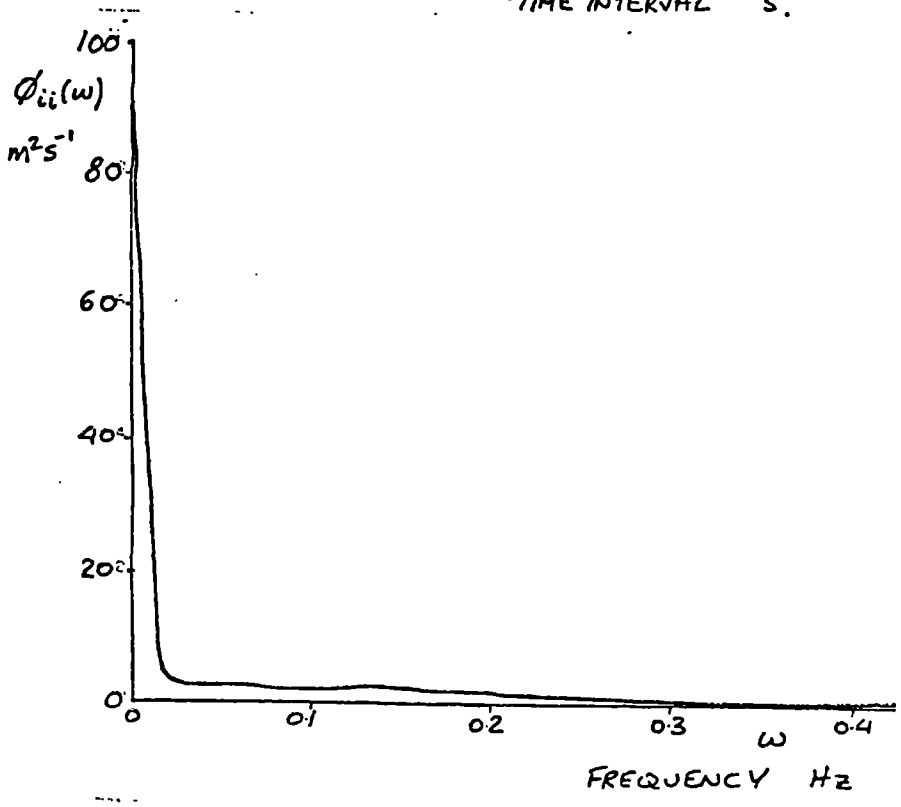

Fig.A7.1. concluded.

Fig.A7.1 shows a number of traces of windspeed, recorded at the test site, together with their autocorrelation functions and power spectral densities.

2. A Simple Theory for Inertia Flow

Burton and Ewens (1980) give the velocity time curve shown in Fig.A7.2.a for full inertia flow. Their description is concerned with a rigid piston pump with the inertia pipe on the discharge side. Here, it is assumed that the inertia pipe is entirely on the suction side but there would not seem to be any reason for the flow to be affected for being pulled of pushed and so the same curve will be used.

When full inertia flow occurs, the inertia of the water keeps itflowing faster than the piston as the piston slows towards top dead centre at time π/Ω. Flow continues even on the delivery stroke of the pump($\pi/\Omega < t < 2\pi/\Omega$) as the water pressure in the inertia pipe remains higher than that in the pump, which hardly rises above atmospheric as there is assumed to be no pressure head.

When partial inertia flow occurs it will be assumed that the velocity time curve is as in Fig.A7.2.b. The difference from the full inertia flow case being that the momentum of the water in the inertia pipe is dissipated some time before the delivery stroke is complete. It is assumed that non-return valves are fitted.

Referring to Fig.A7.2.a, it can be seen that at point a

the slope of the curve is: $-\frac{gH}{L_i} = \Omega^2 \frac{R_\rho A_\rho}{A_i} \cos\lambda$

and that the difference in flow velocity between point b and point a' is:

$$-\frac{gH}{L_i}\left(\frac{2\pi}{\Omega} - \frac{\lambda-\gamma}{\Omega}\right) = \Omega \frac{R_\rho A_\rho}{A_i}(\sin\gamma - \sin\lambda)$$

These give: $$\frac{\sin\gamma - \sin\lambda}{\cos\lambda} = 2\pi - (\lambda - \gamma)$$

Now the volumetric efficiency η_{VOL} is the ratio of the area under the curve aba', to the area under the sine curve for $0 \leq t \leq \frac{\pi}{\Omega}$.

Area under curve aba': $$= \frac{\Omega R_\rho A_\rho}{A_i}\left\{\int_{\gamma/\Omega}^{\lambda/\Omega} \sin\Omega t\, dt + \tfrac{1}{2}(\sin\lambda + \sin\gamma)\left(\tfrac{2\pi}{\Omega} + \tfrac{\gamma}{\Omega} - \tfrac{\lambda}{\Omega}\right)\right\}$$

$$= \frac{R_\rho A_\rho}{A_i}\left\{(\cos\gamma - \cos\lambda) + \tfrac{1}{2}(\sin\lambda + \sin\gamma)(2\pi + \gamma - \lambda)\right\}$$

Area under sine curve : $$\frac{2 R_\rho A_\rho}{A_i}$$

i.e. $$\eta_{VOL} = \tfrac{1}{2}\left\{(\cos\gamma - \cos\lambda) + \tfrac{1}{2}(\sin\lambda + \sin\gamma)(2\pi + \gamma - \lambda)\right\}$$

for full inertia flow.

A similar analysis for partial inertia flow gives:

$$\eta_{VOL} = \tfrac{1}{2}\left\{(1-\cos\lambda) - \tfrac{1}{2}\sin\lambda(2\pi + \gamma - \lambda)\frac{\sin\lambda}{\sin\gamma - \sin\lambda}\right\}$$

Now since dimensionless speed δ and flow ξ are related by eqn. [7.1] : $\xi = \eta_{VOL} \cdot \delta$, solution of the above equations allows a curve of dimensionless flow to be plotted against dimensionless speed (Fig.7.6).

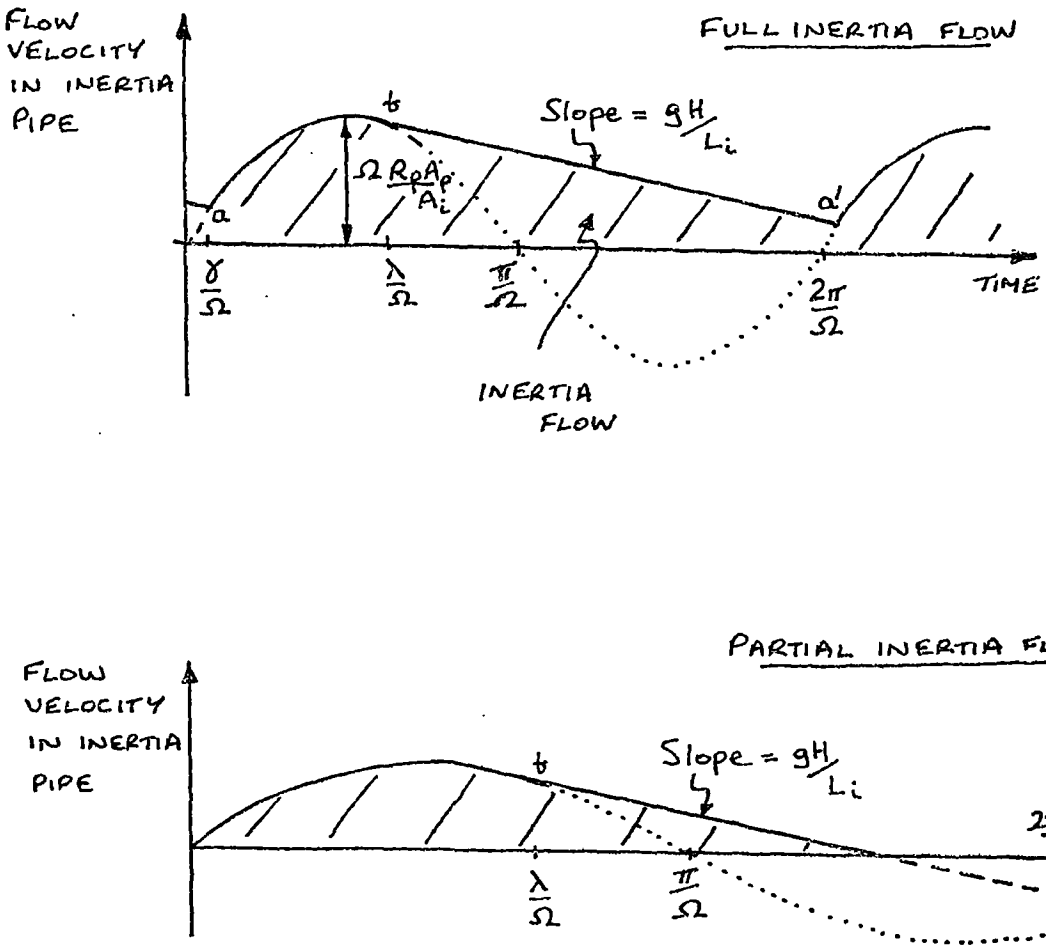

Fig.A7.2. Theoretical flow velocity curves for full and partial inertia flow.

3. Pipe Losses in the Pump Performance Tests

An accurate calculation of the pipe losses occurring in the pump performance tests seems prohibitively difficult in view of the unsteady flow and the uncertain nature of flow velocity variation with the diaphragm pump.

An estimate of the magnitude of the losses has been made as follows:

The estimate will be made for when: $L_i = 3.9\,m$

$\Omega = 10\ rads/s$

$\eta_{VOL} = 1.6$

$\dot{m} = 0.4\ kg/s$

From the volumetric efficiency and average torque input at slow speeds (Fig.7.9), the average torque input expected when $\Omega = 10 rads/s$ would be about 1.8 Nm if there were no losses. The actual torque input measured was 2.5 Nm, giving an average loss torque of 0.7 Nm.

Other relevant values were as follows: $D_i = 22\ mm$

$A_i = 0.38.10^{-3}\ m^2$

$R_p = 15\ mm$

$\overline{R_p A_p} = 0.078.10^{-3}\ m^3$

The mean flow velocity at this speed was therefore:

$$\bar{u} = \frac{\dot{m}}{\rho_w A_i} = \frac{0.4}{0.38} = 1.1\ m/s$$

Defining the Reynolds number for the flow as:

$$Re = \frac{\bar{u} D_i}{\nu}$$

where the kinematic viscosity of water ν, is about 10^{-6} gives a mean Reynolds number of: $Re = 2.4.10^4$

Assuming pre-dominantly turbulent flow, a non-dimensional head loss coefficient may be defined as:

$$K = \frac{h_L}{u^2/2g}$$

where h_L is the head lost in the component and u is the flow velocity.

The following components to the losses are assumed:

1. Inlet to the inertia pipe
2. Pipe friction
3. Right angle bend at inlet to the pump
4. Inlet valve to pump
5. Losses inside the pump
6. Outlet valve from pump
7. Exit kinetic energy of the pumped water

Head loss coefficient values have been taken from Miller (1971).

1. For the inlet: $K_1 = 0.5$
2. The coefficient value for the pipe friction depends on the instantaneous Reynolds number. At the mean Reynolds number and assuming a smooth pipe, the friction factor f is given as 0.025. The head loss coefficient is then: $K_4 = f\frac{L_i}{D_i} = 4.4$
3. Assuming a bend radius equal to twice the pipe diameter: $K_3 = 0.25$
4. The inlet valve was a rubber flap type (Fig.A7.3). For check valves, Miller gives, K = 0.3 to 1.0 or more for when the valve is open or partially closed. Here, an average value will be assumed as: $K_4 = 0.5$
5. Losses inside the pump are due to the sudden enlargement into the pump, losses in eddies generated by the diaphragm (some cavitation may also have occurred at high speeds) and

losses in the sudden contraction into the oulet valve. For the enlargment, K =0.7, for the contraction, K = 0.4. The total loss coefficient for the pump will be taken as: $K_5 = 1.5$

6. The outlet valve was of a 'heart-valve' type (Fig.A7.3). No loss coefficient data for such avalve is known but it is thought that the losses may have been rather high. An average value will be taken as: $K_6 = 2.0$

7. Since the dynamic head is $\frac{u^2}{2g}$ and no diffuser was fitted, the loss coefficient for the exit is: $K_7 = 1.0$

The total average head loss coefficient is therefore estimated as: $\Sigma K = 10.2$

The total instantaneous head loss will be taken as:

$$\Sigma h_L \simeq 10.2 . u^2/2g$$

giving an instantaneous head loss pressure on the diaphragm of:

$$p_i \simeq (10.2 . u^2/2g) . \rho g$$

The force on the diaphragm due to this pressure is:

$$F = [(10.2\, u^2/2g) . \rho g] . A_p$$

and the instantaneous head loss torque is:

$$T_L = [(10.2\, u^2/2g)\rho g] A_p . R_p \sin\Omega t$$

The average head loss torque is therefore:

$$\overline{T_L} = \frac{\Omega}{2\pi} \int_0^{2\pi/\Omega} [(10.2\, u^2/2g)\rho g A_p R_p \sin\Omega t \, dt$$

Evaluation of this integral is difficult for two reasons: Firstly, the 'piston' area A_p is not constant, but will be a maximum when $\sin\Omega t$ is a maximum; use of the average value of $\overline{R_p A_p}$ in the calculation will therefore under-estimate the average torque. Secondly, and because of the above factor, the flow velocity u does not follow a simple

sine curve but, presumably, follows the form shown in Fig.A7.4.

As a lower bound estimate of the losses, the flow velocity may be taken as: $u = \frac{\overline{R_p A_p}}{A_i} \Omega \sin \Omega t \quad 0 \leq t \leq \pi/\Omega$

$$\text{i.e. } u = 2.1 \sin \Omega t \text{ m/s} \quad 0 \leq t \leq \pi/\Omega$$

$$\text{Average head loss torque} = \frac{\Omega}{2\pi} \int_0^{\pi/\Omega} \frac{10.2}{2} (2.1 \sin \Omega t)^2 . \rho . \overline{R_p A_p} \sin \Omega t \, dt \text{ Nm}$$

$$= 2.8 \int_0^{\pi/\Omega} \sin^3 \Omega t \, dt \text{ Nm}$$

$$= 2.8 \left[4/3\Omega \right] = \underline{0.37 \text{ Nm}}$$

As an upper bound estimate of the losses, the flow velocity may be taken as the half-sine curve whose mean value would give the measured mean flow rate.

$$\text{i.e. } u = 3.5 \sin \Omega t \text{ m/s (Fig.A7.5)}$$

Then, the average head loss torque is: $0.37 . \left(\frac{3.5}{2.1} \right)^2 = \underline{1.0 \text{ Nm}}$

These estimates support the assertion that the loss torque was due to pipe losses.

****

If the pipe diameter were doubled, the head loss in the valves and the pump would remain unchanged and, in fact, some extra losses would occur due to the change in diameter between the pipes and the pump inlet and outlet. The pipe friction head loss would be reduced to about 1/8 of its previous value (noting that the pipe length must be

increased four times to maintain the same inertia effect) and other losses would become insignificant. The loss torque would therefore be approximately halved. A further reduction in the losses would require the pump to be re-designed. The present pump was clearly not designed for efficient operation with high fluid velocities.

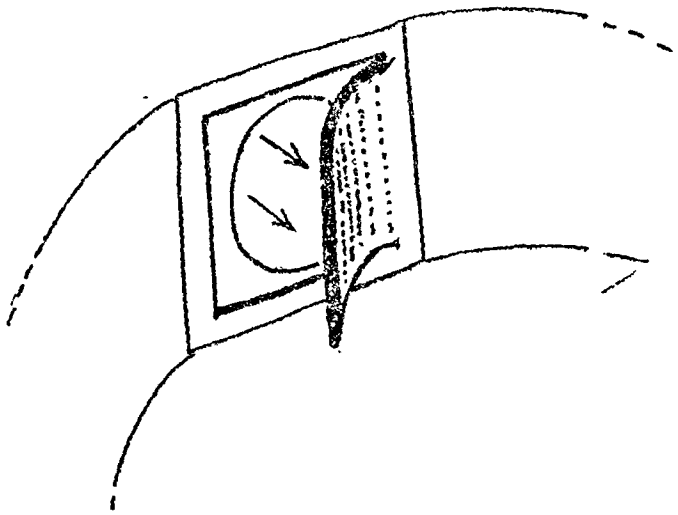

Fig.A7.3. Inlet and outlet valves to the pump

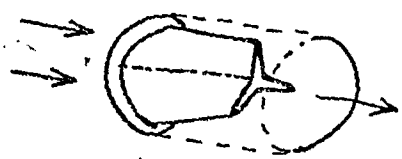

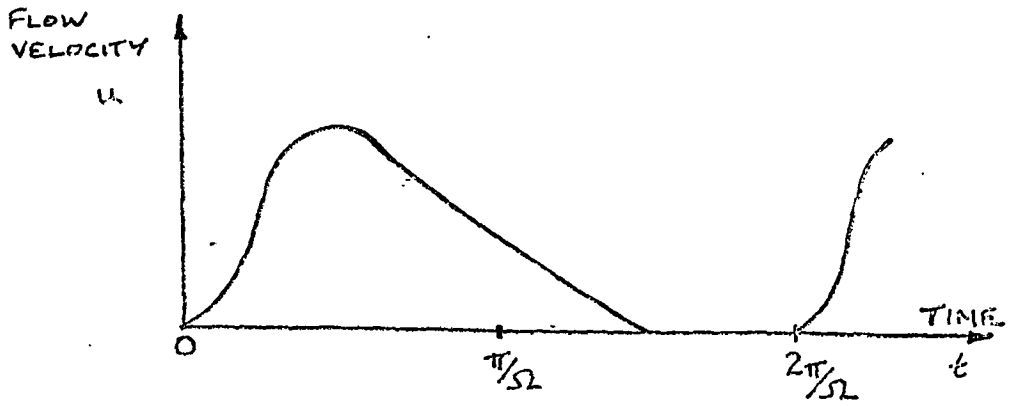

Fig.A7.4. Assumed flow velocity curve for the diaphragm pump

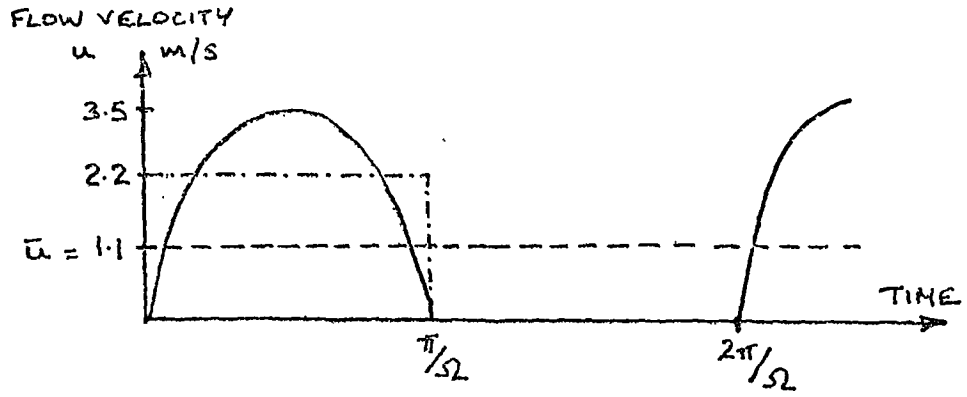

Fig.A7.5. Half-sine curve with mean value giving the measured mean flow rate.